University of Sheffield

Investigating cerebrovascular function in pre-clinical models of health and disease

Beth Eyre

A thesis submitted for the degree of Doctor of Philosophy (PhD)

Department of Psychology

May 2023

Abstract

Background: Alzheimer's disease (AD) is the leading cause of dementia. Over 50 million people are currently living with dementia world-wide, and this is set to increase to over one hundred and thirty-nine million by 2030. However, AD is not a disease that occurs in isolation, with many people experiencing comorbidities, a number of which impact the vasculature, such as atherosclerosis. Yet, studies investigating AD often do not explore the impact of comorbidities on disease pathology. Therefore, I wanted to explore how comorbid disease, namely atherosclerosis, may impact cognitive and vascular function. One study has previously investigated the impact of atherosclerosis on AD. However, they used a mild model of AD and completed the neurovascular assessment under lightly anaesthetised conditions. Therefore, part of my work aimed to extend and replicate this study, by using a more 'severe' model of AD and completing vascular assessments in awake conditions.

Aims: As this research is conducted in awake mice, I firstly needed to investigate the effect of locomotion on sensory-evoked haemodynamic responses (**chapter 2**). My second aim was to investigate cognition in the APP/PS1 mouse model of AD, a model of atherosclerosis, and a mixed model of AD and atherosclerosis (**chapter 3**). My third aim was to investigate neurovascular function (using 2D-OIS) in the APP/PS1 mouse model of AD, a model of atherosclerosis and a mixed model of AD and atherosclerosis (**chapter 3**). My fourth aim was to investigate the effect of mixed disease on amyloid pathology (**chapter 3**). As a result of observations within my initial studies, my fifth aim was to explore the novel phenomenon relating to locomotion and early vascular responses in large draining veins of the brain (**chapter 4**).

Results: I found that the timing of locomotion can significantly impact sensory-evoked haemodynamic responses. This was especially relevant when locomotion occurred prior to or during whisker stimulation. I observed preserved recognition memory in AD, atherosclerosis and mixed disease mice. I observed preserved vascular responses in the APP/PS1 AD mouse model and mixed AD and atherosclerosis model. I found no impact of disease on vascular function when locomotion was ignored. However, I did observe deficits in the evoked-haemodynamic response in the atherosclerosis group, during the least locomotion trials, when locomotion was ranked during the whisker stimulation. I also found no evidence of increased amyloid pathology in mixed disease

mice. Finally, in studies where I assessed vascular responses to spontaneous locomotion, I observed a previously unreported phenomena, whereby the onset of locomotion appeared to cause a large and fast decrease in cerebral blood volume (CBV) within large draining veins.

Conclusions: This work suggests that locomotion should be monitored during awake haemodynamic imaging experiments, as it can significantly impact sensory-evoked haemodynamic responses. Additionally, the work extended and replicated previous findings regarding the presence of vascular dysfunction in an atherosclerosis model. The work further adds to the literature regarding the observation of no vascular deficits in an AD and mixed disease model. Finally, the work suggests that large draining veins of the brain may be important regulators of CBV during locomotion.

Declaration

I Beth Eyre, declare that the work presented in this PhD thesis is that of my own. The work has not previously been submitted at this university or others for the award of a higher degree.

The thesis takes the format of a **publication thesis**. Therefore, some aspects of the thesis have previously been published or are in preparation to be published.

1) **Chapter 1** has not previously been published and was written up for this PhD thesis
2) **Chapter 2** *This paper was published in April 2022 in Scientific Reports. Eyre, B., Shaw, K., Sharp, P., Boorman, L., Lee, L., Shabir, O., Berwick, J. and Howarth, C., 2022. The effects of locomotion on sensory-evoked haemodynamic responses in the cortex of awake mice. Scientific Reports, 12(1), p.6236.*
3) **Chapter 3** has not been published; however, it is in preparation to be submitted to a manuscript. The journal to which it will be submitted has not been decided yet.
4) **Chapter 4** has not yet been published; however, it has been written up in the communications biology format with the plan to submit to this journal in the next few months
5) **Chapter 5** has not previously been published and was written up for this PhD thesis

At the beginning of each chapter (in a publication format) author contributions are clearly defined.

Acknowledgements

It truly does take a village to get you through a PhD. This thesis would not have been possible without the support of a number of people.

Firstly, I would like to thank my phenomenal supervisors. Jason, I can't thank you enough for the patience, time and effort you have put into my development over the past three and a half years. Thank you for your unrelenting honesty – in good times and bad. Thank you for always being passionate and interested in my data. And thank you for believing in me – especially when I didn't believe in myself. You will always be the number one fan of neurovascular coupling.

Clare, you are an incredible role model. Smart, hard-working and most importantly kind. Your unwavering support on this journey has been most appreciated. Whatever you were doing, you always had the time for my constant questions and you never made me feel like my questions were stupid – and for this I am so thankful. From the hours and hours of chats about statistics to the red wine, daily croissants and missing equipment at the Cajal course - it truly has been a blast.

You both have provided me with an environment that has allowed me grow as a scientist. I feel so lucky to have had you both as my supervisors. I couldn't have done any of this without you both. So, thank you. I can't wait to continue to work with you both over the next couple of years – I still have so much to learn and I am so grateful I get to stick around for a while.

A huge thank you to the rest of the Sheffield neurovascular lab, who've made completing my PhD fun, even when it was just a bit grim. Osman, you are just the best, thank you for always being there for me when I needed to vent or moan or just be a bit grumpy. And thank you for being the social secretary of the lab. Llywelyn, my fellow dream team member. Thank you for always being your supportive self and always being there when I needed a pick me up chat.

Thank you to my family, my mum, my brother and my sister. You have always been so supportive of my choices and for that I am truly thankful. Thank you, Elyse and

Lucy, for your unwavering support over the years. Thank you for always being interested in what I do, always asking how it was going – and for always believing in me.

Also, a huge thank you to the northern science gals. Beth, Maria and Laura, my Instagram and now real-life friends. Thank you for always listening and always being my number one fans. I feel so privileged to know such smart, ambitious and phenomenal women.

There is definitely someone who needs a huge mention. Enrico, I'm not even being dramatic when I say I could *not* have done this without you. You have been my rock over the past 5 years, most of which you've had to deal with me and my annoying academic deadlines. Thank you for keeping me fed and watered and bringing me all the glasses of juice a gal could need. Thank you for always believing in me, thank you for making sure I put my mental health first and thank you for being the best life partner anyone could wish for. I am so lucky to have a partner who is so supportive of my goals and ambitions, thank you for being you.

Finally, I want to thank myself. Thank you for persevering when it was really hard. Thank you for never giving up when you really felt like it. And thank you for just being the best. If you can spend 150 days in a dark room collecting all this data, you can do anything.

Table of Contents

List of Figures

List of Abbreviations

20-HETE	20-Hydroxyeicosatetraenoic acid
2D-OIS	Two- dimensional optical imaging spectroscopy
2PM	Two photon microscopy
Aβ	Amyloid Beta
AAV	Adeno-associated viruses
ABC	Avidin-biotin complex
AD	Alzheimer's disease
AMPA	α-amino-3-hyroxy-5-methyl-4-isoxazol epropionic acid
ANOVA	Analysis of variance
APOE4	Apolipoprotein E4
APOEB	Apolipoprotein-B
APP	Amyloid precursor protein
ASL	Arterial spin labelling
ATH	Atherosclerosis
ATP	Adenosine triphosphate
AUC	Area under curve
BACE	Beta-amyloid cleaving enzyme
BBB	Blood brain barrier
BOLD	Blood oxygen level dependent
Ca^{2+}	Calcium
CAA	Cerebral amyloid angiopathy
Cav1	Caveolin 1
CBF	Cerebral blood flow
CBV	Cerebral blood volume
cEC $K_{IR}2.$	Capillary endothelial cell potassium inward rectifying channels
cGMP	Guanosine 3',5—cyclic monophosphate
ChAT	Choline acetyltransferase
CHD	Coronary heart disease
Cl^-	Chloride
$CMRO_2$	Cerebral metabolic rate of oxygen consumption
CO_2	Carbon dioxide
COX	Cyclooxygenase

COX-2	Cyclooxygenase 2
CVD	Cardiovascular disease
DAB	3,3-diaminobenzidine tetrahydrochloride
EET	Epoxyeicosatrienoic acid
eGFP	Enhanced green florescent protein
eNMDAR	Endothelial N-methyl-D-aspartate receptor
eNOS	Endothelial nitric oxide synthase
EOAD	Early onset Alzheimer's disease
FADHC	Familial autosomal dominant hypercholesterolemia
FFPE	Formalin fixed paraffin embedded
fMRI	Functional magnetic resonance imaging
GECI	Genetically encoded calcium indicator
GLUT1	Glucose transporter 1
HbO	Oxygenated haemoglobin
HbR	Deoxygenated haemoglobin
HbT	Total Haemoglobin
ICP	Intracranial pressure
IL-1β	Interleukin 1-beta
K^+	Potassium
LDL	Low-density lipoproteins
LDLR	Low-density lipoprotein Receptor
LFP	Local field potential
LRP1	Low density lipoprotein receptor related protein 1
LRP2	Low density lipoprotein receptor related protein 2
LTM	Long term memory
MCI	Mild cognitive impairment
MCT1	Monocarboxylate transporter 1
mGLUR	Metabotropic glutamate receptors
MIX	Mixed atherosclerosis and Alzheimer's disease
MR	Magnetic resonance
MRI	Magnetic resonance imaging
MRI-PET	Magnetic resonance imaging – positron emission tomography
MUA	Multi-unit activity
NA^+	Sodium

NFT	Neurofibrillary tangles
NMDA	N-methyl-D-aspartate
nNOS	Nitric oxide synthase
NO	Nitric oxide
NOR	Novel object recognition test
NPY	Neuropeptide Y
NVC	Neurovascular coupling
NVU	Neurovascular unit
O_2	Oxygen
PCA	Principal component analysis
PCSK9	Proprotein convertase subtilisin/kexin type 9
PDGF-B	Platelet-derived growth factor B-chain
PGE2	Prostaglandin E2
PGI	Prostacyclin
PLSA	Path length scale algorithm
PMT	Photomultiplier tube
PrP	Prion protein
PSEN1	Presenilin 1
PSEN2	Presenilin 2
PV	Parvalbumin
PWV	Pulse wave velocity
RBC	Red blood cell
rCBV	Relative cerebral blood volume
ROI	Region of interest
ROS	Reactive oxygen species
SEM	Standard error of the mean
SOM	Somatostatin
STD	Standard deviation
STM	Short term memory
Thy-1	Thymocyte differentiation antigen
VCAM1	Vascular cell adhesion molecule 1
VIP	Vasoactive intestinal peptide
VSMC	Vascular smooth muscle cell

WFOM	Wide field optical mapping
WT	Wild type
ZO-1	Zonula occludens-1

Chapter 1: Literature review

Literature review

1.1 What is Neurovascular Coupling?

The brain is a highly metabolic organ, consuming approximately 20% of the oxygen and glucose in the body[1,2]. However, the brain lacks the ability to store reserves of energy – which creates a problem. Continuous cerebral blood flow (CBF) is therefore needed in order to supply the brain with the large volume of nutrients it needs and to remove toxic by-products of metabolism.

Regional increases in neural activity result in a subsequent increase in CBF to that same brain region. This increase in CBF leads to an influx of oxygenated haemoglobin (HbO), increasing the levels of oxygen within that brain region. The relationship between neural activity and an increase in CBF is termed neurovascular coupling (NVC). NVC ensures that the brain receives prompt increases in CBF to activated regions of the brain. This allows for the delivery of oxygen (O_2) and glucose and the removal of waste products such as carbon dioxide (CO_2) and lactate[3]. CBF to neurons is aided by a functional network of cells - the neurovascular unit (NVU)[4,5]. Research indicates that NVC is impaired in many neurological disorders, including Alzheimer's disease[6,7], whereby neurovascular dysfunction occurs, which leads to a discrepancy between neural activity, CBF and the delivery of O_2. Therefore, understanding how NVC may be altered by disease is integral to the development of potential therapies. Further understanding of NVC is also important, as functional magnetic resonance imaging (fMRI) relies heavily on NVC, measuring the blood oxygen level dependent (BOLD) changes and inferring neural activity from these changes. If we fail to fully understand the relationship between CBF and neural activity then we cannot make accurate interpretations of fMRI data.

1.1.2 The Neurovascular Unit

The brain is an immensely vascularised network[8], comprising of approximately 400 miles of arteries, arterioles, capillaries and veins[2]. Blood flows into the brain via the internal carotid arteries and the vertebral arteries, forming the anterior and posterior circulation respectively[9]. Superficial pial arteries envelop the cortex before taking a deep dive into the brain, where they become penetrating arterioles. As penetrating

arterioles delve further into the brain, they become parenchymal arterioles, and eventually branch off into capillaries. CBF throughout the brain is facilitated by a functional network of cells, known as the neurovascular unit (NVU). The NVU is comprised of neurons, interneurons, astrocytes, endothelial cells, vascular smooth muscle cells (VSMCs) and pericytes[5,10]. A vast amount of research has focused on the role of each cell type in the regulation of CBF[11–14], however the specifics of how and what each cell type does has still not been fully elucidated.

1.1.3 NVU and the Blood-brain-barrier

The NVU (Figure 1.1) is integral to the formation and maintenance of the blood-brain barrier (BBB). The BBB is a selectively permeable membrane that limits what can and cannot enter the brain from the blood, with tight junctions and adherens junctions between endothelial cells being 'physically' responsible for BBB integrity[15–17]. Small lipophilic molecules, such as oxygen and CO_2 can easily diffuse across the BBB, however larger hydrophobic molecules cannot. Movement of larger molecules across the BBB occurs via other routes, including transport/carrier proteins and receptor-mediated transcytosis[18,19]. Endothelial cells possess transport/carrier proteins to facilitate the movement of larger molecules, such as glucose transporter 1 (GLUT1), and monocarboxylate transporter 1 (MCT1), which facilitate the transport of glucose and lactate respectively[2,20]. Peptides and proteins, such as insulin and transferrin can be transferred across the BBB via receptor-mediated transcytosis[18]. Lipoproteins such as low density lipoprotein receptor related protein 1 (LRP1) and low density lipoprotein receptor related protein 2 (LRP2) are also expressed in endothelial cells, with LRP1 known to mediate the clearance of proteins associated with Alzheimer's disease - amyloid beta (Aβ)[21,22]. Pericytes and astrocytes are also important cells of the BBB. Pericytes attach to the surface of endothelial cells and astrocytic endfeet associate with endothelial cells via the basal lamina. Pericytes are crucial to the formation and maintenance of the BBB and astrocytes are important for the maintenance of the BBB[18,23,24]. Maintenance of the BBB is important for brain homeostasis, if the BBB becomes too permeable, i.e 'leaky', and subsequent breakdown occurs it can lead to an increase in damaging molecules entering the brain, changes in CBF and impaired clearance of toxins[2,6,25]. For an in-depth review of the BBB see Sweeney et al.,[26].

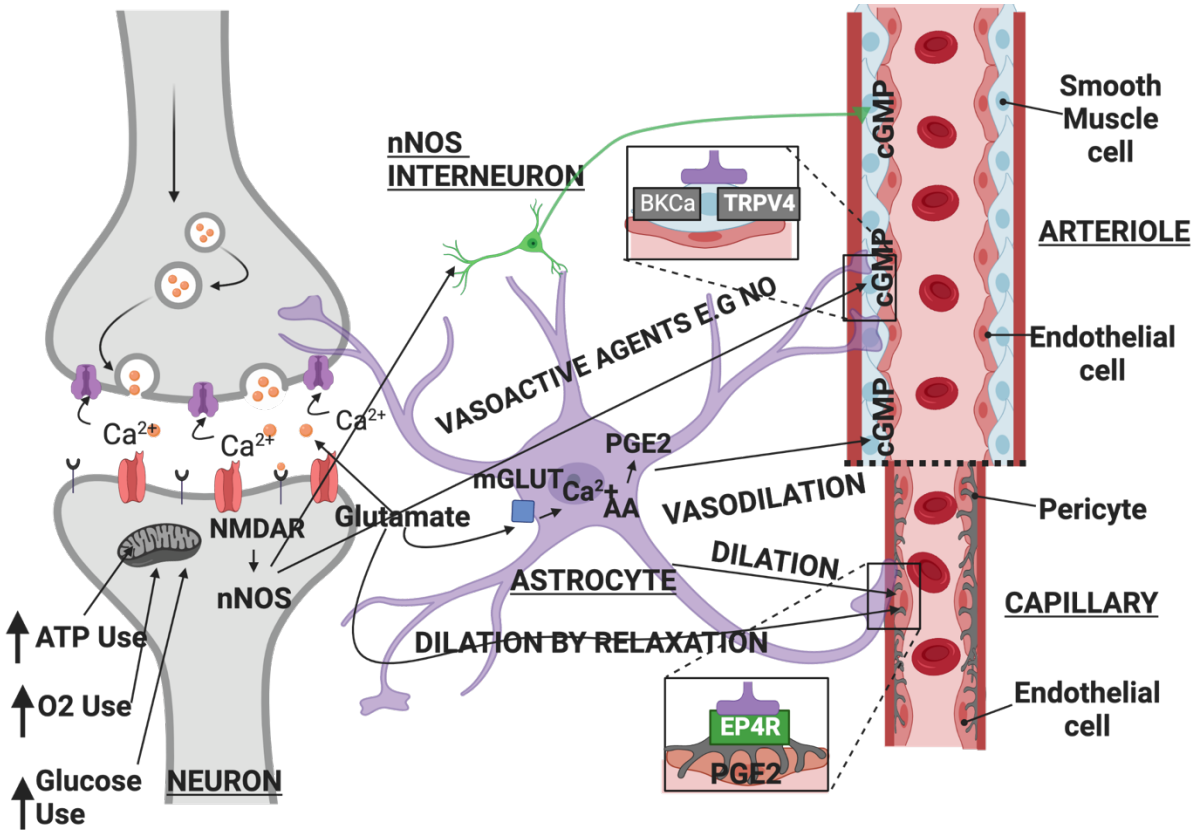

Figure 2.1: overview of the NVU and cellular mediators of NVC adapted from Shabir et al (2018)

NVC is a complex relationship between neural activity and a subsequent increase in blood flow to that same brain region. NVC is mediated by numerous cells within the NVU, including neurons, interneurons, astrocytes, endothelial cells, smooth muscle cells and pericytes (at capillaries). A complex interplay of signalling mechanisms occurs (see sections below) resulting in the relaxation of VSMCs and the subsequent vasodilation of vessels, which leads to an increase in blood flow to the active region of the brain. Figure created with BioRender.com.

1.2 Neurovascular unit: cellular mediators of NVC

1.2.1 Neurons

Excitatory neurons are able to control CBF by producing signals that directly or indirectly act upon blood vessels[4]. For instance, glutamate released following synaptic activity activates post synaptic receptors such as N-methyl-D-aspartate (NMDA) and α-amino-3-hyroxy-5-methyl-4-isoxazol epropionic acid (AMPA) receptors. When glutamate binds to these receptors there are increases in intracellular calcium levels ($[Ca^{2+}]_i$), the increase in $[Ca^{2+}]_i$ activates Ca^{2+} dependent enzymes, including neuronal nitric oxide (NO) synthase (nNOS) and cyclooxygenase 2 (COX-2). These enzymes produce powerful vasodilator products, NO and prostanoid[3,27,28] which act on VSMCs. NO has been shown to produce direct vasodilation in the endothelium, as a result of stimulating guanosine 3',5—cyclic monophosphate (cGMP) in VSMCs, which results in the relaxation of VSMCs, leading to an increase in CBF (Figure 1.1). NO can also lead to indirect dilation of blood vessels via the inhibition of cytochrome P4504A, which is integral in the production of 20-Hydroxyeicosatetraenoic acid (20-HETE), known to be an important vasoconstrictor[29,30]. Neural activity is also known to increase the level of extracellular K^+ ions. At concentrations below 12mM these ions have been shown to have vasodilatory properties[31], indicating that these ionic changes may have the ability to initiate a vascular response.

1.2.2 Interneurons

There are numerous inhibitory interneurons within the cortex, including nitric oxide synthase (NOS)[32], neuropeptide Y (NPY)[33], somatostatin (SOM)[14], vasoactive intestinal peptide (VIP), choline acetyltransferase (ChAT)[34] and parvalbumin (PV)[35]. Interneurons fall into different subtypes dependent on their neurotransmitters, shape, and properties[36]. Ex vivo pharmacology studies have shown that the application of a NPY receptor antagonist eliminated vasoconstriction responses within cortical arterioles, suggesting that NPY-positive interneurons may be important mediators of vasoconstriction[37]. These findings were further supported by in vivo optogenetic studies. Uhlirova et al.,[33] showed that optogenetic stimulation of interneurons produced a response consisting of periods of dilation and constriction, highlighting a potential role for interneurons in the control of CBF. Under glutamatergic blockade only the dilation response occurred, suggesting that the constriction phase of the

haemodynamic response occurred due to the activation of these interneurons. Using an NPY-1 antagonist the constriction phase of the hemodynamic response produced by optogenetic and sensory-evoked stimulation was eliminated - indicating the importance of NPY interneurons in the constriction phase of the haemodynamic response. Other GABA-ergic interneurons are thought to play a role in the cellular production of NVC as they have been shown to innervate local microvessels[38] and can produce both vasodilation and vasoconstriction of vessels[34]. More recently Lee et al.,[14] revealed the role of specific subpopulations of GABAergic neurons, showing that optogenetic stimulation of SST and nNOS interneurons produced a haemodynamic response. These results confirm earlier findings, and provide further evidence that GABAergic neuronal activity can lead to increases in CBF[39,40].

1.2.3 Astrocytes

Astrocytes are in an ideal position to regulate CBF, as their end feet envelop cerebral blood vessels[4,41]. Astrocytes can also release a number of vasoactive mediators, including NO, adenosine and K^+ which can alter the vascular tone of VSMCs[42]. Astrocytes can synthesise vasodilatory messengers, such as epoxyeicosatrienoic acids (EETS) - products of arachidonic acid, produced by cytochrome P450 epoxygenases[43]. In vitro studies show that activation of astrocytes can result in vasodilation. In their research, Zonta et al.,[44] used brain slices and showed that glutamate released from neurons led to $[Ca^{2+}]_i$ increases in astrocytes, resulting in vessel dilation, which was abolished when cyclooxygenase (COX) inhibitors were applied. Thus, supporting the idea that astrocyte mediated vasodilation is dependent on prostanoids - products of the COX pathway. Evidence indicates that prostaglandin E2 (PGE2) is particularly important, as studies have demonstrated that astrocytes can release this dilating agent in response to activation of metabotropic glutamate receptors (mGLUR)[45].

Although there are caveats regarding the use of brain slices for NVC research, the main issue being the lack of CBF, complementary findings have been observed in vivo. Using 2-photon imaging Takano et al.,[46] showed that stimulation of astrocytes generated rapid vasodilation (1-2s delay), with photolysis of Ca^{2+} in astrocytic endfeet being associated with an 18% increase in arterial area, which resembled a 37%

increase in blood flow. However, it has been suggested that these responses were too slow to attribute a role for astrocytes in the regulation of CBF, as astrocytic Ca^{2+} increases have been shown to lag behind the onset of the vascular response[47]. In contrast to this, Lind et al.,[48] observed both slow and fast Ca^{2+} responses in astrocytes. Fast astrocytic Ca^{2+} responses were observed in the somas, processes and end feet, and occurred before local vasodilation. It was suggested that fast Ca^{2+} responses are important for the initiation of the haemodynamic response and slower Ca^{2+} responses may be important in supporting the prolonged haemodynamic response. Other studies have been conducted, using genetically encoded calcium indicators (GECIs) to overcome the caveats of bulk loading of chemical calcium dyes. Otsu et al.,[49] showed that in the olfactory bulb of adult mice, Ca^{2+} responses as a result of odour stimulation were shown to precede increases in local CBF, with these Ca^{2+} increases occurring 1-2s before increases in local CBF. Using both chemical indicators and GECIs, Lind et al.,[50] observed fast Ca^{2+} responses in astrocytic endfeet before vasodilation in both arterioles and capillaries.

Astrocytes clearly play a role in the regulation of CBF. However, their role may differ depending on their location along the cerebrovascular. For example, Mishra et al.,[11] showed that at the level of the capillary, astrocytic Ca^{2+} signals were integral for NVC. However, arteriole dilation was not dependent on astrocytic Ca^{2+} signalling, but reliant on the activation of NMDA receptors and the production of neuronal NO, via neuronal nitric oxide synthase (nNOS).

1.2.4 Vascular smooth muscle cells (VSMCs)

Vascular smooth muscle cells (VSMCs) line blood vessels, and have the ability to contract and relax, due to high levels of alpha-smooth muscle actin[51]. VSMCs relax in response to neural activity in pial and penetrating arterioles[6], dilating the vessels and facilitating an increase in CBF, implicating these cells in the regulation of vascular tone. Substances generated by neurons and astrocytes can directly alter the tone of VSMCs[52]. For instance, NO generated by neurons can hyperpolarise VSMCs, resulting in the relaxation of these cells. Adenosine triphosphate (ATP) and adenosine generated by neurons can also act through different receptors and lead to the constriction and relaxation of VSMCs respectively. Increases in extracellular K^+

(mediated via neurons) can also activate voltage-gated receptors on VSMCs, increase $[Ca^{2+}]_i$ and result in the contraction of VSMCs. Astrocytic calcium increases can lead to the production of vasoactive products, such as EETs and PGE_2, which through different pathways both result in the relaxation of VSMCs[6]. VSMCs allow for the mechanical alteration of the diameter of vessels. In the absence of VSMCs and their contractile elements vessels would not be able to respond to vasodilatory or constricting stimuli. Considering the evidence above, VSMCs are clearly vital for the regulation of CBF.

1.2.5 Pericytes

When arterioles become capillaries in the brain parenchyma, the vessels are no longer covered by VSMC's but are instead replaced with pericytes[53]. Pericytes are known to have a number of roles within the brain, including maintenance of the BBB[54].

Some suggest that pericytes regulate CBF, however, this viewpoint still remains controversial. In vitro studies have shown that pericytes have the capacity to contract and relax when exposed to vasoactive messengers[55,56]. In vivo studies have also demonstrated that pericytes possess contractile properties[12]. Nevertheless, other groups suggest that pericytes do not possess contractile properties and therefore do not regulate CBF[57]. Controversies exist due to difficulties in distinguishing pericytes from other mural cells, as there are no specific pericyte markers available. For example, transgenic mouse models using fluorescent labels (NG2-DsRed or PDGFR-B-tdTomato) can be used to visualise pericytes, with the use of 2-photon microscopy[12,58]. However, both the above 'reporters' label all types of mural cells, including VSMC's and pericytes[59], which may make it difficult to differentiate pericytes from VSMCs in regions where arterioles become capillaries[4]. Antigen markers have also been developed for pericytes. However, these are not specific to pericytes[53].

This controversy is further enhanced by conflicting definitions of pericytes. Some suggest that pericytes can be split into 'contractile' and 'non-contractile' pericytes[60], whereas others suggest that 'contractile' pericytes are actually VSMCs and 'true' pericytes possess no contractile properties[57]. However, it has been suggested that there are actually three distinguishable subtypes of pericytes. These include

ensheathing pericytes; which are thought to possess contractile properties, and reside at the transition of the arteriole and capillary; mesh pericytes, which wrap around the vessel and are located on the capillary and thin strand pericytes, located at the middle section of the capillary[61].

Although there is controversy regarding the definition of pericytes and the lack of specific markers, these cells may be important in CBF regulation. Kisler et al.,[62,63] demonstrated that mice deficient of pericytes had diminished NVC and lower levels of oxygen in brain tissue. This highlights that pericytes are integral for normal NVC and tissue oxygenation. However, neurovascular uncoupling may have occurred due to BBB breakdown which can result in an increase of damaging molecules entering the brain and blood flow alterations. Therefore, the above findings may not be solely due to pericyte regulation of CBF.

1.2.6 Endothelial cells

Endothelial cells line the inside of the endothelium and are vital for the integrity of the BBB. These cells are also associated with a number of substances that can alter vascular tone. For instance, substances can be generated within endothelial cells which can result in the relaxation of VSMCs, including NO and prostacyclin (PGI_2)[64,65]. Additionally, endothelial cells are thought to be important in the backward propagation of vasodilation[66]. When a region is activated deep in the brain the increase in blood flow that accompanies must be able to reach upstream vessels. This response, whereby an increase in blood flow from downstream to upstream vessels occurs is known as retrograde propagation and can travel distances larger than 1mm away from the region where vasodilation originated[67,68], with fMRI studies reporting that blood flow responses first occur in the deep cortex followed by more surface activation[69]. Studies have also demonstrated that selective disruption of a single pial arteriole eliminated the retrograde propagation of blood flow[68].

Additional studies have also suggested an important role for endothelial cells in the control of CBF. Longden et al.,[13] suggested that capillary K^+ release can result in an increase in CBF. They demonstrated that the activation of capillary endothelial cell potassium inward rectifying channels (cEC $K_{IR}2.1$) with K^+ starts a propagating

hyperpolarisation response which leads to the dilation of arterioles upstream. Elimination of endothelial NMDARs (eNMDARs) also diminished haemodynamic responses in response to whisker stimulation[70]. This suggests that these endothelial receptors are important in the regulation of sensory-evoked haemodynamic responses. Most recently, a study investigated the role of caveolae in the control of CBF[71]. Caveolae are common in the arteriole endothelium but very few are present in capillary endothelium. Mice deficient of caveolin-1 ($Cav1^{-/-}$) had reduced arteriolar dilation in response to whisker stimulation. When arteriolar endothelial cells (but not adjacent smooth muscle cells) were ablated, NVC was impaired. Ablation of eNOS and caveolae also stopped NVC, whereas in mice mutant of Cav1 or eNOS only partial impairment of the NVC response occurred, suggesting that the arteriolar endothelial cell response, mediated via caveolae is important in NVC. It was concluded that vasodilation is mediated to a large degree by endothelial cells. The study used awake mice, which is advantageous as anaesthesia can have negative impacts upon NVC (See section 1.4.1). However, $Cav1^{-/-}$ mice have an impaired ability to complete physical tasks, such as swimming[72]. The above study does not mention how locomotion may have impacted their results. Future studies should therefore investigate the impact of a caveolin-1 deficiency, the effects this may have on locomotion and how this may impact NVC.

1.2.7 Concluding remark

No single cell type controls NVC and the regulation of CBF, and although there are controversies regarding the roles of cells within the NVU, it is clear that NVC is the result of an interplay of signals between cells of the NVU - making each cell type integral to NVC. This is evidenced by the observation that when cells within the NVU are damaged, as has been shown in neurodegenerative diseases, this can lead to the breakdown of NVC.

1.3 Imaging techniques to investigate NVC

In order to understand how NVC and the NVU may be affected by disease, visualisations of the brain are crucial. Different neuroimaging techniques can be used to measure brain structure and function from the level of the whole brain, to single vessels and individual cells.

1.3.1 Functional Magnetic Resonance imaging (fMRI) and the BOLD response

fMRI is a non-invasive tool based upon the magnetic resonance (MR) properties of magnetic resonance imaging (MRI). The technique was a huge breakthrough for neuroscientists as it was one of the first imaging methods that gave insight into the intact brain.

T2* relaxation allows researchers to investigate the blood oxygen level dependent (BOLD) response, with T2* being particularly sensitive to concentrations of deoxygenated haemoglobin (HbR)[73]. BOLD fMRI takes advantage of the differing magnetisation properties of oxygenated haemoglobin (HbO) and deoxygenated haemoglobin (HbR). Additionally, the method takes advantage of the discrepancy between an increase in CBF (as a result of neuronal activation) and the cerebral metabolic rate of oxygen consumption ($CMRO_2$), as the local increase in CBF is much greater than needed. The discrepancy between CBF and $CMRO_2$ results in a reduction of HbR, thus altering the T2* signal[74]. Oxygenated blood is diamagnetic, whereas deoxygenated blood is paramagnetic. The exposed iron in deoxygenated blood leads to inhomogeneities in the magnetic field of the scanner, these inhomogeneities lead to a decreased T2* signal, a more rapid signal decay and ultimately a decrease in the BOLD signal in that region[75]. Therefore, when there is a greater ratio of HbO to HbR, there is an increase in the BOLD response and when there is a greater ratio of HbR to HbO, there is a decrease in the BOLD response.

The BOLD response is used as a proxy for neuronal activity, making the BOLD response reliant on NVC[76]. The positive BOLD response has a distinctive shape whereby there is a large increase in HbO, which reaches an initial peak and then slowly decreases below baseline where the response then plateaus. This occurs alongside a large decrease in HbR and an increase in CBV. The positive BOLD response usually occurs around ~500ms after neurons fire, with the peak of the response occurring around ~2-5s after the onset of neural activity[76]. A post-stimulus undershoot is frequently observed, whereby the response decreases below baseline[77,78].

Studies have been conducted to investigate what type of neuronal activity is most associated with the BOLD response. The BOLD response was shown to be better predicted by local field potential (LFP's) as compared with postsynaptic multi-unit activity (MUA). Consequently, the BOLD response is thought to be a reflection of the input of activity, not spiking output activity[79].

Advances in techniques now mean that tissue perfusion and CBF can be assessed using fMRI, using arterial spin labelling (ASL)[80]. The method has been important in establishing the hypoperfusion that is commonly observed in Alzheimer's disease (AD)[81–83]. Additionally, resting state fMRI is also commonly used to assess individuals with AD and could potentially be a biomarker for those at risk of AD[84,85].

1.3.2 Widefield imaging: Two-Dimensional Optical Imaging Spectroscopy (2D-OIS)

2D-optical imaging spectroscopy (also referred to as wide field optical mapping[86] (WFOM)) is a method with superior spatial and temporal resolution to fMRI. This means that the method can be used to investigate specific properties of the BOLD response[76]. 2D-OIS uses different wavelengths of light to produce 2D spatial images of the cortex - by capturing the reemitted light the method can reveal information about the surface vasculature and underlying changes in total haemoglobin (HbT) and oxygen saturation - HbO and HbR. The method relies on the differing absorption properties of HbO and HbR in response to light. Whisker stimulations can be used as a sensory stimulus to activate the somatosensory cortex and produce a haemodynamic response. A thinned cranial window surgery is required to reduce light scattering and specularities. The implementation of a cranial window can also allow for multiple imaging sessions over long periods of time[87,88]. This method can also be used in conjunction with genetically encoded calcium indicators (GECIs – see section 1.3.5) to reveal both changes in haemodynamic and changes in calcium (a proxy for neural activity). As thinned window procedures can be altered in size, the imaging modality can have the potential to reveal information about haemodynamic changes across the entire cortex.

However, this method is constrained to the surface vasculature (pial vessels), hence 2D-OIS cannot give insight regarding blood oxygenation within capillaries of the brain. Nevertheless, using specific algorithms and analysis pipelines, wide-field imaging can produce spatial maps of CBV changes during whisker stimulation. Using this technique, it is therefore possible to delineate the haemodynamic response in different vascular compartments, including in the artery, vein and parenchyma[89–91].

In the subsequent studies of this thesis 2D-OIS will be used to assess haemodynamic responses in surface vessels of the brain. See below for an overview of how the methodology works.

1.3.2.1 The physics of 2D-OIS

The method relies on the fact that the absorption properties of oxygenated (HbO) and deoxygenated haemoglobin (HbR) are different for specific wavelengths of light. The specific wavelengths used in the experiments within this thesis were as follows: 494 ± 20 nm, 560 ± 5 nm, 575 ± 14 nm and 595 ± 5 nm. These pairs of wavelengths are used as they have the greatest differences in absorption coefficients for HbO and HbR, therefore increasing the signal to noise ratio[89].

When white light is shone onto a surface, some light is absorbed and some is remitted. The absorption of light can be calculated, however, if light is scattered this creates issues when calculating the absorption. Importantly, the absorption of light is impacted by the material that the light is shone onto[92]. For example, when using 2D-OIS to investigate changes in haemoglobin levels in the brain, white light is shone onto the cortex. Some of the photons are absorbed, whereas others are remitted. However, when the light is shone onto the cortex the different tissues within the brain result in the scattering of light, this results in one being unable to measure a continuous pathway of photons in the brain tissue. Due to this, a Monte Carlo simulation is applied, that estimates the path length of photons. The pathlength of photons is estimated at different absorption concentrations, with scattering angles of photons also considered. In order to get the estimate of path length, both the angle of scattering and scattering coefficient need to be included.

The scattering angle of photons are calculated using the Henyey-Greenstein probability function[93]. The function creates a weighting factor. The weighting factor is assumed, as 0.85 using in vivo measurements previously recorded[94]. Once calculated, the scattering angle can then be used to calculate the scattering coefficient. The scattering coefficient, alongside the absorption and remittance are all used to gain an estimate of the path length that photons travel[95]. Estimated path lengths were then used in a modified Beer-Lambert law. The modified Beer-Lambert law can be used to establish changes, and create spatial maps of haemoglobin changes across the cortex, by relating the path length to the attenuation of light, absorption coefficients and concentrations of specific chromophores[95]. For the above to be able to estimate changes in haemoglobin concentration within the cortex of the brain, baseline haemoglobin concentration and tissue saturation must be included in the model. A homogeneous tissue model was implemented, which has previously been used to investigate neurovascular function in disease[91,96]. Total blood volume (HbT) is then acquired by summating oxygenated (HbO) and deoxygenated (HbR) values.

1.3.3 Electrophysiology

Electrophysiology is used to investigate the electrical properties of living cells, including neurons and other tissues. At rest neurons have a resting membrane potential of -70mV, due to the concentration of inorganic ions within the cell, including sodium (NA^+), potassium (K^+) and chloride (Cl^-) and due to the extracellular fluid. The intracellular concentration of the different ions is controlled via sodium-potassium ion pumps and the differing permeability of each type of ion. The difference in intracellular and extracellular membrane potential is important in the communication between neurons, as neurons communicate with one another via alterations in membrane potential. Action potentials occur due to a small but rapid rise in Na^+, this rise in Na^+ abolishes the negative resting membrane potential, makes the transmembrane potential positive and thus depolarises the cell[97].

Microelectrodes are used to record the electrical activity of cells within the brain. Recordings can be extracellular or intracellular[97]. Extracellular recordings are more likely to detect action potentials, whereas intracellular recordings are more likely to reveal the small changes that initiate action potentials[98]. Additionally,

electrophysiology can be in vitro, for example in brain slices. Microelectrodes can also record different aspects of neural activity. Local field potential (LFP) is low frequency (usually <300Hz) summated activity from any transmembrane current within the brain, within a certain region, reflecting the input[99]. Whereas multi-unit activity (MUA) is the high frequency component of neural activity and is thought to reflect spiking activity[100]. As previously mentioned, research indicates that the BOLD response reflects the input of activity (LFPs) rather than the output spiking activity (MUA)[79].

Neural activity alone cannot give us a complete insight into NVC. However, electrophysiology can be used concurrently with wide-field imaging to provide further understanding of the relationship between neural activity and the haemodynamic response. Concurrent wide-field imaging and electrophysiology is commonly used to investigate neurovascular function and the role of specific cells in NVC[14,90,96].

1.3.4 Two-Photon microscopy

The development of 2-photon microscopy (2PM) has revolutionised neuroscientific research, as it has allowed for the visualisation of the structure and function of living systems at the cellular and single vessel level[101,102]. 2PM works by exciting fluorophores, leading to the emission of light. In 2PM an infrared pulsed laser is shone into a specimen, focused via a numerical aperture objective lens[103]. Light is shone into the specimen, and two photons are absorbed at the same time. The simultaneous absorption of the two photons excites the fluorophore, leading to the transition from its ground to excited state. Pulsed lasers are utilised to increase the possibility that the two photons are absorbed simultaneously[104]. Excitation of fluorophores occurs in the focal volume and these photons are caught and detected by the photomultiplier tube (PMT), and then used to construct an image[105].

2PM has numerous advantages over some of the earlier imaging methods. This technique allows for the visualisation of different vessels of the vascular tree, for example the method can be used to visualise pial and penetrating vessels, as well as capillaries within the brain[106,107]. 2PM is therefore an ideal method to investigate the vasculature of the brain, especially within mouse models. Fluorescent dyes such as Texas-Red-Dextran can be injected into the vascular system to label blood plasma,

allowing for the visualisation of the vasculature during imaging. Additionally, 2PM can result in less photobleaching of dyes[108], however some disagree with this[109].

Importantly, the device has furthered our understanding of the structure and function of the NVU and has aided our understanding of NVC[12,46,47,50] helped by the tools ability to measure Ca^{2+} changes in numerous cells, a suitable proxy for neural activity. The technique has also enhanced our knowledge of different aspects of blood flow within the brain, as the method can measure red blood cell (RBC) flux and vessel diameter[110–112].

The method can be used for long-term in vivo imaging of the brain[61,102] and is a vital tool to study diseases, such as AD. For example, methoxy-XO4 can be used to stain Aβ plaques[113] which can then be imaged over time[114], this is important to aid our understanding of how Aβ affects the brain and additionally is important for intervention studies, aimed at reducing Aβ[115].

1.3.5 Calcium imaging

Calcium (Ca^{2+}) is an integral intracellular messenger, involved in a multitude of processes both pre and post synaptically[116]. At rest intracellular Ca^{2+} levels are approximately 50-100nm, as a result of an action potential, these levels rise between 10-100x the level observed at rest[117]. The well-established rise in intracellular Ca^{2+} as a result of an action potential has meant that Ca^{2+} can be used as a correlate of neural activity.

The use of Ca^{2+} as an imaging tool has increased in recent years as a result of the development of numerous Ca^{2+} indicators and imaging devices[118]. Most calcium indicators are fluorophores, they exist in a ground and excited state, absorb light of one wavelength and emit light of a differing wavelength. When Ca^{2+} binds to a calcium indicator, it leads to a conformational change, and results in the emittance of a wavelength of light, different to that used to excite the indicator. Recently developed calcium indicators such as GECIs have become invaluable to the neuroscientific field, as they are more specific than earlier chemical dyes, and can be used for long term in vivo imaging [119], as they are less likely to be affected by photobleaching[120]. GECI's

comprised of a single fluorophore include indicators in the GCaMP family, which have become ever more popular in in vivo calcium imaging[121]. GCaMP contain a single fluorophore, enhanced green florescent protein (EGFP), which sits between calmodulin: a calcium binding protein and M13: a calmodulin binding peptide[122]. When calcium binds to calmodulin, a conformational change occurs, leading to an increase in the florescence emitted by EGFP[122]. GECI's can also be expressed in cells using adeno-associated viruses (AAV)[123,124]. To ensure GECI's are expressed solely in the cells of interest cell-type promoters are utilised[125].

1.4 Factors that can affect neurovascular research

1.4.1 Anaesthesia and NVC

Anaesthesia has been used in NVC research for a number of years. Anaesthetic agents produce pain relief and reduce movement artefacts, which can reduce the variability of animal responses, facilitating the comparison of different studies. However, there is evidence to indicate that anaesthesia can negatively impact the underlying aspects of NVC. For a detailed review see Gao et al.,[126].

Not only does anaesthesia dampen neural activity but it can also reduce many aspects of the haemodynamic response - including blood oxygenation, CBF and CBV[127,128]. Anaesthesia can alter the BOLD signal and baseline and stimulus-evoked neural activity - this relationship was especially dependent on the type of anaesthesia used[128]. Anaesthesia can also delay the haemodynamic response[127,129]. In order to reliably infer neural activity from the BOLD response (the premise of fMRI) a valid haemodynamic response is needed. As evidence indicates that anaesthesia can alter the time course of the haemodynamic response, the use of an anaesthetic agent could be problematic.

However, some anaesthetic regimes can produce comparable haemodynamic responses to awake regimes. Sharp et al.,[90] developed a novel anaesthetic regime, using a 'modular' approach of both injectable (fentanyl-fluanisone and midazolam, 0.8 ml/kg,) and inhalation (isoflurane 0.5-0.8%) anaesthetic. The group found no significant differences in the amplitude or onset time of the stimulus-evoked haemodynamic response, when comparing awake and anesthetised mice whilst using

the above anaesthetic protocol under medical air (21% O_2). This study shows that the impacts of anaesthesia can be reduced if certain anaesthetic regimes are used.

As a result of the impact anaesthesia can have upon NVC research, and advances in technology, the NVC field has begun to move away from the use of anaesthesia and started to image awake animals. An important advancement that allowed for the imaging of awake animals was the development of head-fixed devices[130]. These devices allow groups to image animals, whilst preventing head movement, which would inevitably produce artefacts in imaging data. Rodents can easily be trained to accept the head-fixed devices and to become accustomed to other equipment, such as a moving ball that allows animals to walk freely during imaging. Many studies have now used awake animals to investigate NVC and the roles of cells within the NVU.

1.4.2 Locomotion and NVC

Recently more research groups have moved to imaging awake, behaving animals[33,131–133], to avoid some of the confounds related with the effects of anaesthesia. However, awake imaging brings a multitude of new issues – such as the impact of locomotion on haemodynamic responses. Many studies have been conducted assessing how spontaneous locomotion can impact haemodynamic responses within the brain[132,134]. Locomotion can increase CBF within the brain, with CBV in arteries increasing more locally and CBV increases in veins being more spread out[135]. However, few studies have investigated how locomotion may impact sensory-evoked haemodynamic responses, such as those evoked by a whisker stimulation[133]. Whisker stimulations are often used in neurovascular research as the rodent barrel cortex is well defined[136,137] and the stimulations provide a robust way of probing neuronal and vascular relationships within the brain. However, it is important to address how locomotion may affect this response, especially when considering how neurovascular relationships may be altered in disease. If locomotion does have a significant impact on evoked responses, then this could affect conclusions regarding impairments in neurovascular function across disease states. The studies that have been conducted regarding locomotion and the corresponding haemodynamic response have rarely looked at the effects of locomotion on evoked-haemodynamic responses, with most focusing on how locomotion alone impacts CBF[131,132,135].

Therefore, as the work conducted in my PhD will be conducted in awake behaving mice, I will firstly investigate how locomotion may impact whisker-evoked haemodynamic responses, as very few studies have investigated this.

Not only are there unanswered questions regarding the effects of locomotion on evoked-haemodynamic responses, but we still don't fully understand the effects of locomotion alone on different aspects of the vasculature. One component of the vascular network that are often overlooked are cerebral veins. Studies indicate that voluntary locomotion results in more diffuse increases in CBV within veins[135] and that these CBV increase in veins during voluntary locomotion may be somewhat driven by cardiovascular changes[131]. This same group also found that voluntary locomotion resulted in the dilation of pial arteries and veins within both the sensory and visual cortices. Further to this, they also reported that dural vessels constrict in response to locomotion – and propose this may occur due to a 'space saving' mechanism during locomotion[138]. They found that responses to locomotion in dural vessels and veins were delayed, whereas arterial responses to locomotion were more rapid. As cerebral veins are vastly understudied, it would be important to investigate the effects of locomotion on surface veins. Additionally, studies should attempt to replicate the previous findings of Gao et al.,[138] to further add to our understanding of how locomotion impacts cerebral blood flow and neurovascular responses.

During my PhD we observed a novel finding regarding the effects of locomotion on large veins within the surface of the brain. Therefore, the final part of my PhD will be to further investigate this novel observation in more detail.

1.5 Alzheimer's Disease

NVC and cells within the NVU are known to be altered in many neurodegenerative disorders, including Alzheimer's disease. Using the methods above, neurovascular function can be assessed in order to develop our understanding of the mechanisms of Alzheimer's disease and to aid in the identification of potential biomarkers and treatments of the disease.

Alzheimer's disease (AD) is the most prevalent cause of dementia in the elderly population and has now become the leading cause of death in the UK[139]. Alzheimer's

disease (AD) is a neurodegenerative disease, characterised by the accumulation of extracellular amyloid beta (Aβ), which results in the deposition of Aβ plaques in the brain parenchyma as well as along cerebral vessels, known as cerebral amyloid angiopathy (CAA)[140]. AD is also characterised by the presence of neurofibrillary tangles (NFTs) - (comprised of hyperphosphorylated tau) and neuronal loss[141]. These hallmark features occur alongside cognitive impairments, including memory loss[142]. AD is an age-related disease, with age being an important risk factor; however, it is not a normal part of ageing.

Around 10% of all AD cases are familial, with most cases developing before 65 years of age, this is known as early onset Alzheimer's disease (EOAD). EOAD occurs due to autosomal dominant mutations of Presenilin 1, presenilin 2 (PSEN1, PSEN2) and the amyloid precursor protein (APP) genes, with mutations in these genes altering the production of Aβ[143]. There are two pathways that can process APP: the amyloidogenic and the non-amyloidogenic. The amyloidogenic pathway leads to the production of Aβ through the sequential cleavage of APP by β-secretase (Beta-amyloid cleaving enzyme, BACE) and γ-secretase[144,145]. γ-secretase can lead to the production of soluble $A\beta_{40}$ and insoluble $A\beta_{42}$[146]. Mutations to PSEN1/PSEN2 result in the increased formation of $A\beta_{42}$ - the more toxic Aβ peptide[147]. $A\beta_{42}$ fragments form oligomers, which lead to the production of Aβ plaques[148,149]. According to the Aβ cascade hypothesis[150] AD is thought to be caused by soluble Aβ oligomers accumulating in the brain, as a result of an imbalance in Aβ production and/or clearance. This accumulation of Aβ leads to neuroinflammation, oxidative stress, damage to neurons and ultimately leads to the formation of NFT's, which inevitably cause neuronal death[151]. The majority of support for this hypothesis results from the findings regarding the familial mutations in APP, PSEN1 and PSEN2, which lead to the increased production of Aβ.

However, most individuals with AD develop the disease later in life, sporadically, with no inheritable mutations related to APP processing. This suggests that the Aβ cascade hypothesis may not be the only explanation of the cause of AD. Certain vascular risk factors have been associated with the development of sporadic AD: these include diabetes[152,153], obesity[154,155] and hypertension[156,157]. The above cardiovascular disease (CVD) risk factors are thought to predispose individuals to the development

of vascular dementia and AD. Evidence linking CVD risk factors to AD[158] lead to the development of the 'two hit hypothesis' (Figure 1.2). Zlokovic et al.,[2] suggested that vascular risk factors lead to BBB dysfunction and hypoperfusion (hit one). The dysfunction in the BBB and reduction in CBF can lead to the accumulation of toxins, which have been shown to lead to neuronal dysfunction, ultimately leading to neurodegeneration, cognitive decline and eventually dementia, with all of the above occurring independently of Aβ. However, some aspects of the hypothesis are thought to be Aβ dependent. Vascular risk factors such as hypertension can cause vascular injury, this change in the vasculature is thought to impact the clearance of Aβ, and is also postulated to increase the production of the protein and lead to hypoperfusion, ultimately leading to the accumulation of Aβ. This accumulation of Aβ is referred to as 'hit two', and enhances neuronal dysfunction, leading to faster neurodegeneration and eventually the cognitive decline associated with dementia. The hypothesis also proposes that Aβ and/or the reduction in CBF can result in the production of hyperphosphorylated tau, which can later lead to the production of NFTs.

1.5.1 Neurovascular dysfunction in Alzheimer's disease – the two-hit vascular hypothesis

Zlokovic et al.,[2,159] proposed the two-hit vascular hypothesis of neurodegeneration in AD suggesting that neurodegeneration does not just occur as a result of Aβ accumulation but in fact is the result of vascular risk factors making the brain vulnerable to BBB dysfunction and a reduction in blood flow. This can later exacerbate the production and inhibit the clearance of Aβ, thus resulting in enhanced hypoperfusion, Aβ accumulation, phosphorylated tau which can all lead to neuronal dysfunction, neurodegeneration and ultimately the cognitive decline observed in dementia.

NVC is thought to be impaired in AD, with numerous studies revealing cerebral hypoperfusion in a number of brain regions, including the posterior cingulate gyrus and precuneus in individuals with early AD[81,160,161]. Studies have also reported reduced glucose reuptake in these same regions[81,162]. Furthermore, using simultaneous magnetic resonance imaging – positron emission tomography (MRI-

PET), reduced CBF (measured via arterial spin labelling (ASL)) and reduced glucose reuptake in the precuneus has also been reported in individuals with AD[83]. Hypoperfusion is not limited to the above regions, but has also been observed in posterior parietal and prefrontal regions[163]. Hence, cerebral hypoperfusion may be an early indicator of AD, as studies have shown that hypoperfusion in the precuneus and parietal regions occurs before patients transition from mild cognitive impairment (MCI) to AD[164,165]. In support of this, a recent study using young participants demonstrated a reduction in grey matter CBF in apolipoprotein E4 (APOE4) carriers[166]. Additionally, they found that individuals with greater polygenic risk scores had reductions in grey matter CBF in frontal regions. This study highlights a link between a reduction in CBF before any AD pathology - suggesting that hypoperfusion may be an early biomarker of the disease.

Clinical research with AD patients indicates an association between hypoperfusion and cognitive decline[167]. However, studies using murine models have been able to give a greater insight into the neurovascular dysfunction that occurs in AD and how this neurovascular dysfunction can impact NVC and the NVU.

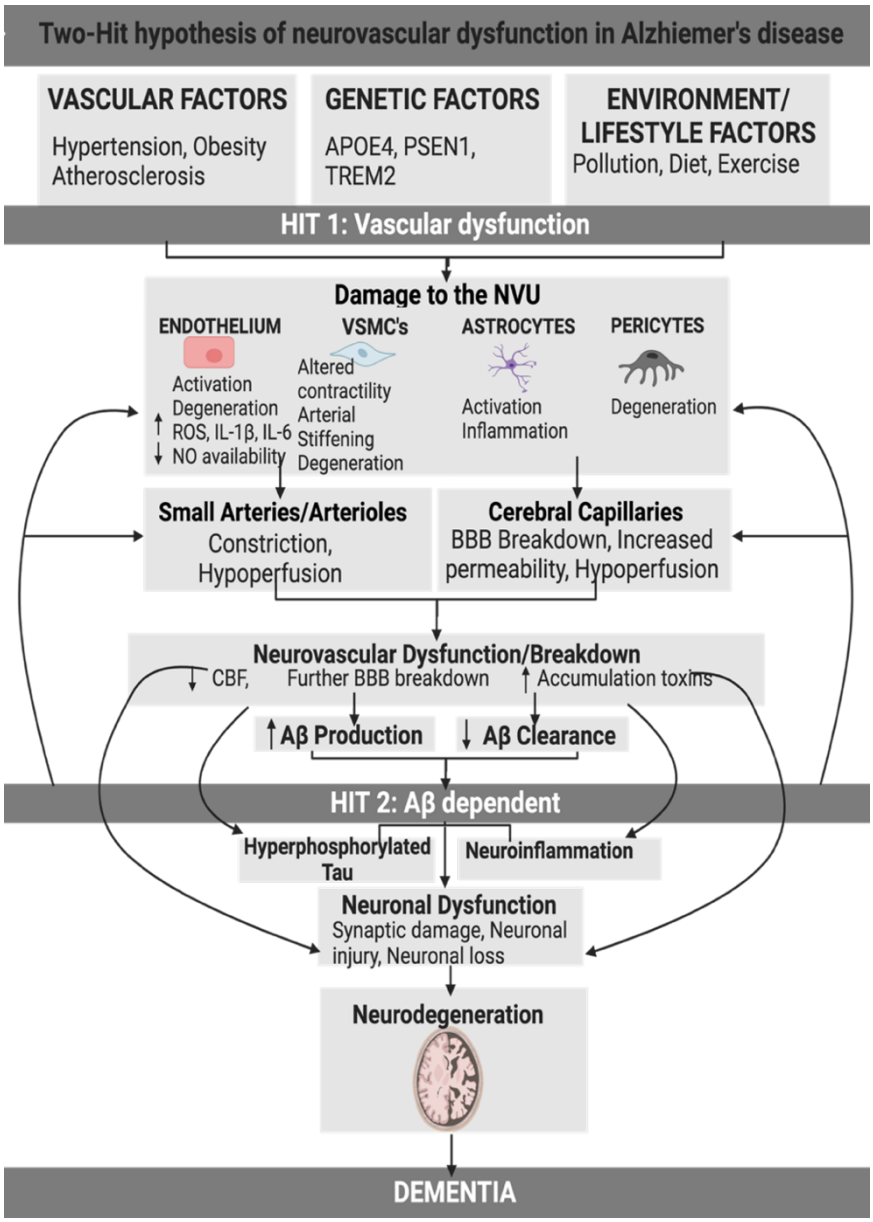

Figure 1.2: A schematic, adapted from Kisler et al., (2017) highlighting the steps and interactions involved in the 'two-hit' hypothesis of Alzheimer's disease.

Vascular, genetic and lifestyle factors can damage the vasculature and impact cells of the NVU. Over time this can result in damage to smaller vessels of the brain, resulting in constriction of vessels and hypoperfusion. Vascular damage can also damage the BBB, resulting in its breakdown. All of the above can result in neurovascular breakdown which can impact the production and clearance of toxins. The amyloid dependent part of the pathway impacts tau phosphorylation and results in neuroinflammation. Again, factors which can impact the production and clearance of proteins such as amyloid. Over time, neurodegeneration occurs resulting in dementia. Figure created with BioRender.com.

1.5.2 Alzheimer's murine models

The symptoms of EOAD and sporadic AD are somewhat similar, especially with regards to the deposition of Aβ. As a method to investigate the development of AD, mouse models have been created, with mutations that increase the production of Aβ. The development of these models has been integral in developing our understanding of AD and invaluable in the search for new treatments.

There are many AD mouse models that can be utilised to study AD[146,168,169]. Nonetheless, there is no singular model which possesses all the features of AD. The models available acquire the clinical and pathological features of the disease to different extents. Therefore, the choice of AD model should always be driven by the research question proposed[169].

AD models exist with mutations in APP only (e.g J20 (hAPP, Tg2576), APP and presenilin (e.g APP/swe/PSEN1dE9, 5xFAD) and APP, presenilin and tau (e.g 3xTg-AD). Most of the APP only and APP and presenilin mutation models acquire memory deficits, alongside Aβ deposits, however they show no tau pathology and most show no neuronal loss. Models with tau mutations show the above pathology and behavioural deficits but also have an increase in hyperphosphorylated tau and often develop NFT's and neuronal loss.

Other factors can also affect the phenotype in AD models - including promoters. Each promotor differs with regards to the timing and expression observed within the brain. The most common promotors used in AD models include thymocyte differentiation antigen (Thy-1), platelet-derived growth factor B-chain (PDGF-B) and the prion protein (PrP)[170,171]. Background strain can also change the phenotype of the AD model. For example, the APPswePSEN1dE9 mice on a C57BL/6J congenic background have been shown to display hyperexcitability and unprovoked seizures, with a mortality rate up to 15%[172]. However, the same mutation on the C57BL/6;C3H background show no evidence of seizures. Additionally, some models possess the retinal degeneration (rd) gene, which leads to retinal degeneration[173]. Homozygous retinal degeneration mice perform more poorly in some cognitive tasks, including the Morris water maze which is frequently used to test cognition in AD models[173]. Therefore, it is integral to

understand the phenotypes related to the background strain used, as to ensure that the strain used does not impact behavioural testing - which is commonly used in AD research.

The model of choice for this PhD is the B6;C3 Tg(APPswe,PSEN1dE9)85Dbo/Mmjax (APP/PS1)[174]. This model was chosen as mice develop amyloid plaques in the hippocampus from approximately 3 months of age[175,176], therefore would already have amyloid plaque deposition between 9 and 12 months (the age point to be used within the subsequent disease studies). This model has also been shown to display cognitive deficits, including non-spatial recognition memory deficits from 7 months of age[177] and deficits in spatial memory at 9 months of age[178,179]. Neurovascular impairments have also been observed[180,181]. It is important to note that the model of choice is an amyloid only model and therefore the experiments to be addressed within this PhD will only be able to assess the impact of amyloid pathology and its subsequent effects on cognitive and neurovascular function.

1.5.4 Neurovascular dysfunction in Alzheimer's disease – clinical and pre-clinical research

Early work using murine models focused on the role of Aβ in AD – with Aβ shown to impact neurovascular function. The application of Aβ-peptides can lead to vasoconstriction of blood vessels and can damage the endothelium, as observed in the rat aorta[182]. Similar findings have been observed in vivo, where the application of $A\beta_{1\text{-}40}$ enhanced the vasoconstrictive effects of a thromboxane analog and led to a reduction in resting CBF[183]. Moreover, impaired resting CBF and impaired cerebral autoregulation has also been observed in transgenic mouse models that overexpress APP[184,185]. In both studies mice were at an age where there were no Aβ plaques or neurodegeneration, suggesting that Aβ can exert its impact early in disease, and alterations in CBF could be a potential biomarker of disease.

Aβ can also alter the structure of microvessels [186,187]. Ahn et al.,[187] showed that in the 5xFAD mouse model mice had damaged blood vessels, evidenced by a 40% reduction in GLUT1, a glucose transporter expressed within the brain - especially within endothelial cells[188].This suggests a structural impairment within the endothelium of

cerebral vessels. There was also a reduction in the expression of zonula occludens-1 (ZO-1), a tight junction protein associated with endothelial cells. The reduction of ZO-1 was also associated with the activation of astrocytes. Again, providing evidence for vascular disruption as a result of APP overexpression.

Neurovascular responses within the brain can be investigated by utilising sensory stimulation and recording the subsequent haemodynamic changes within the brain. Numerous studies have been conducted using AD models to assess how neurovascular function is affected by Alzheimer's pathology. With many transgenic mouse models reported to have deficits in neurovascular responses[189]. For example, studies have shown that in the J20 amyloid model of AD CBF responses to a whisker stimulation are reduced in the cortex from 11 months[190,191] and hippocampus at 6 months[192]. However, not all studies assessing neurovascular function find deficits in AD mouse models. For example, other groups have reported preserved neurovascular responses to whisker stimulation in the same model between 9 and 12 months of age[91,96]. Furthermore, contradictory findings regarding neurovascular function are also found in the APP/PS1 model. For example, between 9-12 months van Veluw et al.,[181] observed neurovascular deficits in awake mice, whereas at 7 months of age Kim et al.,[193] observed augmented responses to a sensory stimulation. As contradictory findings are often reported, this highlights the importance of completing future studies that aim to replicate and extend prior research studies. As a result of this, part of my PhD will aim to extend and replicate the prior observations of Shabir et al.,[96] who demonstrated preserved NVC in the J20 mouse model.

1.5.4.1 BBB breakdown

The BBB is integral to the maintenance of homeostasis within the brain. However, there is evidence that BBB breakdown occurs in AD. Post-mortem studies have shown a loss of tight junctions, leakage of capillaries, endothelial and pericyte impairments and the accumulation of fibrinogen and thrombin within the brain of individuals with AD[194]. Many studies have also shown BBB leakage, as assessed using gadolinium in MCI and early AD, including in the hippocampus[195,196]. Similar alterations in the BBB have been observed in both patients with AD and AD research models. For instance, endothelial tight junctions have been shown to be altered in AD patients[197], and in

response to Aβ application in vitro[198]. The loss of these tight junctions can increase the permeability of the BBB. Animal models with differing AD mutations also show BBB dysfunction[199,200]. Wang et al.,[199] showed altered BBB integrity in the APP/PS1 mouse model at 12m, evidenced by disruption to tight junctions and fewer pericytes. These mice also demonstrated increased BBB permeability, thought to have occurred as a result of the structural changes in the BBB. Using different methods to assess BBB permeability Minogue et al.,[201] similarly observed increased BBB permeability in both 14 and 24 month old APP/PS1 mice. Likewise, increased BBB permeability has also been observed in the 5xFAD mouse model[202]. Mouse models with tau mutations also show BBB impairment. Blair et al.,[200] demonstrated that tau alone could damage the BBB (using the rTg4510 mouse model), however BBB impairment was only observed when vascular tau developed in later life and was not observed early in disease progression despite the presence of neuronal loss and inflammation in this mouse model[203,204]. Interestingly, reducing the levels of tau reversed the BBB impairments.

1.5.4.2 Hypoperfusion

Diminished CBF can lead to an insufficient supply of key nutrients to cells within the NVU, leading to dysfunction and in some cases cell death. Previous studies have shown a reduction in resting CBF and overall hypoperfusion in individuals with AD[160,205] with hypoperfusion also observed early in disease, before AD symptoms or pathology[166,206].

Hypoperfusion may be associated with cognitive decline. Lower whole-brain and parietal CBF has been related to a faster decline in cognition in women with AD[207]. Reduced CBF has also been shown to predict cognitive decline and the progression from MCI to dementia[208,209]. However, both studies had small samples of those that progressed from MCI to dementia, therefore findings may be underpowered. Nevertheless, the above studies suggest reduced CBF may play an important role in the cognitive deficits observed in individuals with AD.

Hypoperfusion has also been reported in AD mouse models. Studies have assessed the direct effects of hypoperfusion in C57 mice to establish the effects of diminished

CBF in the absence of AD pathology. Chronic hypoperfusion in C57 mice led to loss of neurons, cognitive decline, BBB disruption, activated astrocytes and deposition of Aβ[210] - highlighting the negative consequences of cerebral hypoperfusion. What's more, hypoperfusion induced in AD mice can exacerbate pathology. Young APP_{swe}/PS1 mice subjected to severe hypoperfusion were shown to have greater memory impairments and increased deposition of Aβ plaques[211]. Other studies have delved deeper, trying to understand the cellular mechanisms of cortical hypoperfusion in AD[180]. Cruz-Hernandez[180] investigated the mechanism behind hypoperfusion in APP/PS1 and 5xFAD mice. They found that in AD mice there was an increased number of stalled capillaries as compared to WT mice. Stalled capillaries and reduced CBF were suggested to be due to neutrophils attaching to the endothelium in capillaries. Additionally, they revealed that the administration of an antibody for neutrophils (anti-Ly6G) reduced the number of stalled capillaries, rescued blood flow and increased cognitive function. Further investigations showed that anti-Ly6G improved short term memory (STM) in mice from 3 months of age to as old as 15-16 months, yet it failed to improve cognition in mice above 17 months of age. However, at 21-22m old, anti-Ly6G could still reduce stalled capillaries and improve CBF[212]. As no improvement in STM was observed at 21-22m but CBF was increased it suggested that later stages of AD may have other mechanisms, that lead to cognitive deficits observed in AD, not including hypoperfusion. Importantly, Bracko et al.,[212] conducted an imaging session after the application of anti-Ly6G and cognitive testing in old mice (21-22m). This enabled the group to show that anti-Ly6G did reduce the number of stalled capillaries and led to an increase in CBF even though no improvements in cognition were observed at this age point.

1.6 Atherosclerosis

Similar to age being a risk factor for the development of AD, atherosclerosis is also an age-related disease, with symptoms becoming apparent in the mid-to-late 50s. Atherosclerosis is a disease defined by the build-up and hardening of fatty deposits in the intima of the endothelium[213]. The deposition of fat in the endothelium can lead to the narrowing of the lumen, which can progressively impede blood flow and lead to coronary heart disease (CHD), (if in the coronary arteries) or stroke (if atheroma form in the carotid or cerebral arteries). Thus, atherosclerosis plays a major role in two of

the most prominent causes of death worldwide[214]. The pathogenesis of atherosclerosis is complex and multifactorial; however, it is suggested that genetic, environmental, lifestyle and inflammatory factors lead to its development, with a major risk factor being high levels of plasma low-density lipoproteins (LDL)[213,215].

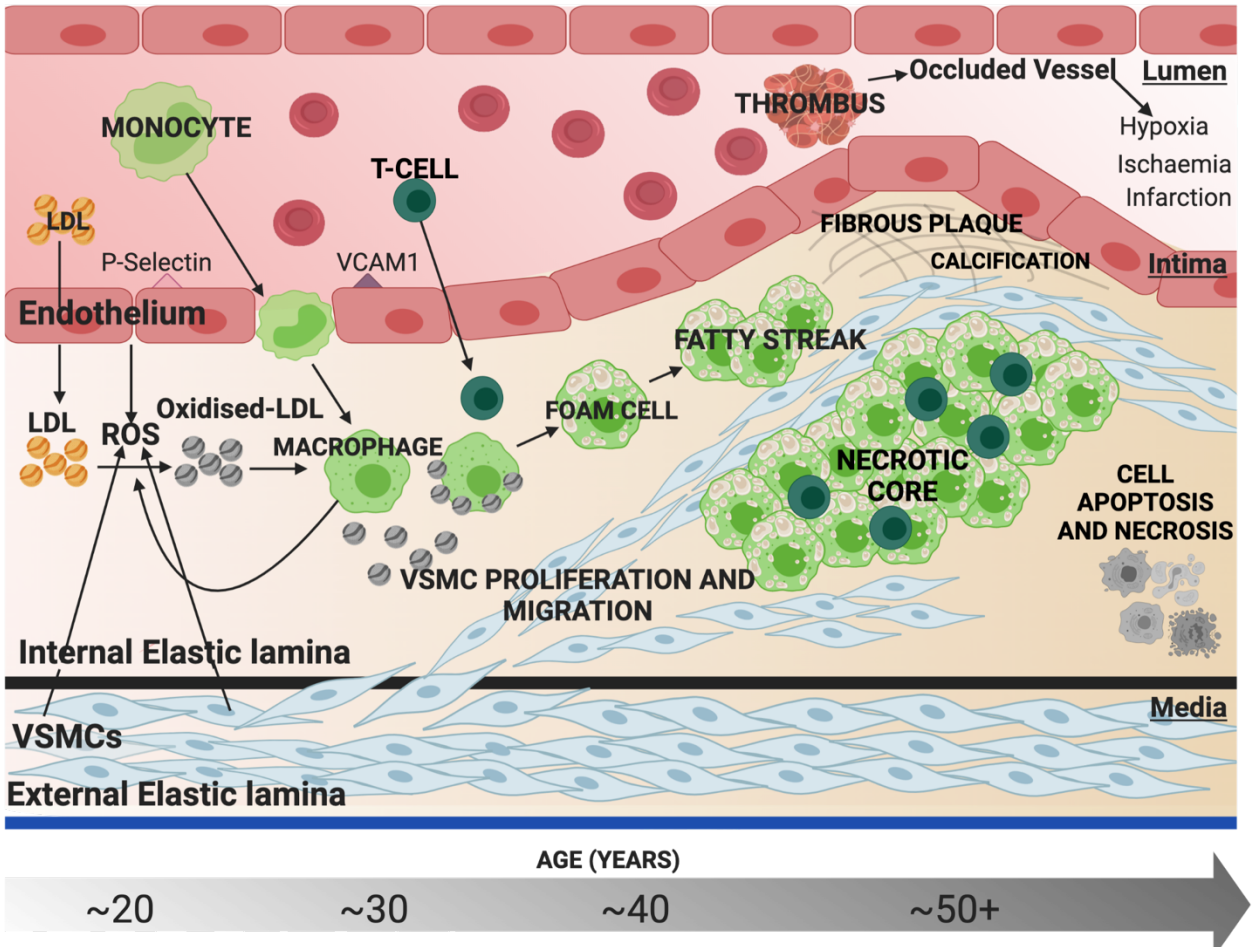

Figure 1.3: A schematic, adapted from Shabir et al., (2018) highlighting how atherosclerosis develops over time

Inflammatory changes, due to the deposition of LDLs within the inside of large arteries is thought to lead to the pathogenesis of atherosclerosis. Once LDLs are deposited in the endothelium, they are oxidised by reactive oxygen species (ROS) – this reaction results in an immune response whereby monocytes are recruited. These monocytes bind to endothelial receptors, including VCAM1 and P-Selectin. Monocytes differentiate into macrophages. Once they invade the endothelium they ingest the oxidised LDLs, this results in the macrophages becoming 'foam cells'. Over time, foam cells converge together, and become 'fatty streaks'. At the same time as this, VSMCs increase in number and move to the intima of the artery. With the aim of trying to stabilise the fatty streaks by forming a ring around the fatty streak. Over time, some of these VSMCs calcify, and harden, which leads to the formation of a solid core inside the endothelium. Over time, this solid core can increase in size and impede blood flow within the lumen of the vessel. The solid core can also rupture, forming a thrombus. Figure created with BioRender.com.

Atherosclerosis is thought to occur as a result of inflammatory changes that transpire due to the deposition of LDLs in the intima of the endothelium[216]. Once LDLs have been deposited in the endothelium, they are oxidised by reactive oxygen species (ROS): subsequently initiating an immune response, involving monocytes and leukocytes[217]. It is believed that the initiation of this immune response starts the disease[218]. Atheroma's are also thought to harden as a consequence of this immune response. When LDLs have been deposited in the intima of the endothelium and subsequently oxidised by ROS, monocytes bind to endothelial receptors, such as P-Selectin and vascular cell adhesion molecule 1 (VCAM1)[219] and subsequently differentiate into macrophages. The invading macrophages then ingest the oxidised LDLs, leading to the conversion of macrophages into 'foam cells': with foam cells comprising of accumulated lipids[220]. As an individual advances in age, foam cells gather together, this clustering leads to the development of 'fatty streaks', which are visible inside the endothelium. Concurrent to the formation of 'fatty streaks', VSMCs multiply and move from the media of the endothelium to the intima, these cells begin to stabilise the plaque by forming a ring around the 'fatty streak'[221]. Some of the VSMCs become calcified and begin to harden next to the atheroma. This process forms a solid core inside the endothelium, with this solid core becoming more substantial over time. The enlarging of the solid core can partially block the lumen of the vessel, leading to the narrowing of the artery[222] - which can impede blood flow. Moreover, the plaque may rupture, and form a thrombus - depending on the location this can lead to both a heart attack or stroke. For a more detailed review of the development of atherosclerosis see the following review papers[213,215,223] (Figure 1.3).

1.6.1 Modelling Atherosclerosis

Just as mouse models can be used to model AD, murine models have also been utilised to try and understand the mechanisms of atherosclerosis. The most extensively used mouse models that have successfully demonstrated atherosclerosis include the $LDLR^{-/-}$ and $ApoE^{-/-}$ models[224,225]. Interestingly, these mouse models not only display atherosclerotic lesions but have also been shown to possess neurovascular changes.

1.6.1.1 Low density lipoprotein receptor knockout ($LDLR^{-/-}$) mice

LDL receptors are located in hepatocytes and are integral in the endocytosis of LDL cholesterol[226], thus, mice deficient of these receptors ($LDLR^{-/-}$) develop amplified levels of overall cholesterol in the plasma. LDLR are also important for the uptake of other lipoproteins, these include apolipoprotein-B (ApoB) and apolipoprotein-E (ApoE). When fed a normal chow diet $LDLR^{-/-}$ develop no atherosclerotic lesions[227] or develop few lesions[228], however when fed a western diet or high fat diet this makes them more likely to develop atherosclerotic lesions[224]. For example, Hartvigsen et al.,[229] showed that $LDLR^{-/-}$ mice fed a western diet developed hypercholesterolemia and larger atherosclerotic lesion burden in the aorta as compared to mice on a high cholesterol diet and no diet at all. However, other studies have demonstrated that $LDLR^{-/-}$ mice do not need the addition of a high fat diet to develop atherosclerosis and develop atherosclerotic lesions on a chow diet at approximately 3m[230].

A recent study using $LDLR^{-/}$ mice has demonstrated that atherosclerosis can result in decreased cerebral tissue oxygenation, reduced capillary diameter and reduced capillary blood flow in old atherosclerotic mice, as compared to young atherosclerotic mice[231]. This group later extended these findings by using the same $LDLR^{-/-}$ mouse model, under awake conditions using a number of optical imaging techniques. They established that old atherosclerotic mice displayed decreased haemodynamic responses to sensory-evoked stimulation, lower tissue oxygenation and structural and functional alterations in penetrating arterioles. Atherosclerosis was also shown to decrease RBC flux within capillaries in old mice. However, capillary dilation was observed in old atherosclerotic mice, suggesting a mechanism to try to compensate for the reduced oxygen supply[232]. Both of the above studies demonstrate that the development of atherosclerosis not only affects the systemic vasculature but can negatively impact the cerebral vasculature and result in neurovascular changes, including deficits in oxygenation.

1.6.1.2 Apolipoprotein E knockout ($ApoE^{-/-}$) mice

ApoE is a glycoprotein produced in the brain and liver. It has many functions including cholesterol homeostasis and dietary absorption of cholesterol[233,234]. Mice deficient in $ApoE^{-/-}$ have a diminished ability to successfully clear plasma lipoproteins, leading to

hypercholesterinaemia even when fed a normal diet[235]. Similar to other mouse models used to investigate atherosclerosis, ApoE$^{-/-}$ mice have also been shown to possess cerebrovascular changes. Chirico et al.,[236] demonstrated that in old ApoE$^{-/-}$ mice fed a high fat, high cholesterol diet, BBB disruption and an increase in brain abnormalities were observed alongside increased inflammation and oxidative stress. Therefore, suggesting that atherosclerosis may result in neurovascular dysfunction. Moreover, these old ApoE$^{-/-}$ mice had an enhanced mortality rate and it was suggested this was the result of the neurovascular changes observed.

1.6.1.3 Proprotein convertase subtilisin/kexin type 9 (PCSK9)

LDLR$^{-/-}$ and ApoE$^{-/-}$ genetically engineered knockout models can be difficult to produce, as creating double knockout models takes a vast amount of time and subsequently can be expensive[237]. A recent alternative to these expensive, genetically modified models has shown that atherosclerosis can be induced with the use of an adeno-associated-virus (AAV). rAAV8 D377Y-mPCSK9 was injected into male C57/BL6 mice and with the addition of a paigen or western diet cholesterol levels quickly increased, and mice developed aortic atherosclerotic lesions after three months[238].

PCSK9 is involved in the metabolism of cholesterol and regulates plasma cholesterol levels by internalising and degrading LDL Receptors (LDLR)[239]. PCSK9 gain-of-function mutations have been linked to familial autosomal dominant hypercholesterolemia (FADHC)[240] - whereby individuals have greater internalisation and degradation of LDLR and thus increased levels of LDL in the blood. Whereas loss-of-function PCSK9 mutations have been associated with the opposite findings, with these individuals appearing to be protected against the development of CHD[241].

Mouse models have been integral in furthering our understanding of the role of PCSK9 and development of atherosclerosis. Maxwell & Breslow[242], showed that overexpression of PCSK9 in C57BL/6 mice resulted in the elevation of plasma cholesterol and levels of LDL. The increases in LDL levels were found to be dependent on LDLR, as mice deficient in LDLR and infected with PCSK9 had no changes in LDL cholesterol levels within the plasma. Additionally, other studies have shown that mice

lacking in PCSK9 have much lower levels of LDL in the plasma and are much less likely to develop atherosclerosis[243,244] - mimicking the findings of humans with loss of function PCSK9 mutations. As mentioned previously, Bjorkland et al.,[238] showed that PCSK9 gain of function could be induced with a single injection of rAAV8 D377Y-mPCSK9. This injection, paired with a paigen or western diet not only induced a rapid increase in cholesterol levels but also produced aortic atherosclerotic lesions within 3 months. Thus, this is a valid method to investigate hypercholesteremia and atherosclerosis without using $ApoE^{-/-}$ or $LDLR^{-/-}$ mice.

One study has assessed neurovascular function in atherosclerotic mice, induced via PCSK9 injection with the addition of a western diet. It was shown that between 9 and 12 months of age systemic atherosclerosis could induce neurovascular changes, whereby a reduction in HbT was observed in response to sensory-evoked stimulation. Immunohistochemistry revealed an increase in amyloid plaque number in the mixed disease mice. Interleukin 1-beta (IL-1β) was also elevated in atherosclerosis mice, suggesting increased neuroinflammation in response to atherosclerotic lesions[96]. This study shows that neurovascular dysfunction can occur as a result of systemic atherosclerosis.

1.6.2 Atherosclerosis and AD

As evidenced in the previous section, common atherosclerotic mouse models possess atherosclerotic pathology with the addition of neurovascular alterations. Coexisting cerebrovascular disease is frequently observed in individuals with AD and is more commonly seen in those with AD as compared to other neurodegenerative diseases[245]. Vascular dysfunction also occurs early in disease, before AD pathology and cognitive symptoms[26,206].

Increasing evidence suggests there is a link between atherosclerosis and AD. For instance, atherosclerosis and AD have overlapping risk factors - including age, hypertension, heart disease and diabetes[246,247] (Figure 1.4). Individuals who possess the above risk factors have been shown to be more likely to develop AD[248]. A recent study also showed that in a sample of 5995 individuals, MCI and dementia was associated with mid-life diabetes, obesity, hypertension and hypercholesteremia[249].

Moreover, individuals with severe atherosclerosis have a 3-fold greater risk of developing AD or vascular dementia[250].

Autopsy studies have also been valuable in identifying a direct link between atherosclerosis and AD. One study found that individuals with AD had more atherosclerotic lesions within the circle of Willis, compared to age-matched individuals without AD[251]. Beach et al.,[252] similarly found that intracranial atherosclerosis, within the circle of Willis was more enhanced in patients diagnosed with AD and vascular dementia as compared to control subjects. Interestingly, the more severe the atherosclerotic lesions, the greater the chances an individual had of being diagnosed with AD or vascular dementia. Additionally, there was an association between atherosclerotic grade and increased plaque density and NFT stage. However, some studies find no association between atherosclerosis and an increased risk of developing AD. Gustavsson et al.,[253] found that systemic atherosclerosis and increased thickening of the intima of the carotid artery was associated with a higher odds ratio of developing vascular dementia, but not AD, at a 20 year follow up. Yet, this study used ultrasound, an indirect measurement of carotid plaques and intima thickness, in comparison to the above studies which were conducted at autopsy. Moreover, Gustavsson et al., did not assess for intracranial atherosclerosis; which could explain why contradictory findings were observed.

Both atherosclerosis and AD can also impair the vasculature. Arterial stiffness - a measure of vascular disease can be measured using pulse wave velocity (PWV), this method is usually used to assess the carotid and femoral arteries. Rivera-Rivera et al.,[254] used 4D flow MRI to evaluate PWV transcranially in individuals with AD, MCI, healthy participants positive for APOE4 and healthy controls. Individuals with AD and MCI had significantly higher PWV ratios as compared with age-matched controls, suggesting vascular stiffness may be implicated in the development of AD. Additionally, they found vascular alterations in healthy adults positive for APOE4.

There is also evidence associating atherosclerosis with Aβ and vice versa. Aβ peptides have been observed in atherosclerotic lesions[255] mainly consisting of the $A\beta_{1\text{-}40}$ peptide[256]. In addition to this, there is a vast amount of literature suggesting $A\beta_{1\text{-}40}$ has

a predisposition for deposition within the vasculature[257]. Increased levels of $A\beta_{1-40}$ have also been associated with aortic stiffness and number of atherosclerotic plaques[258].

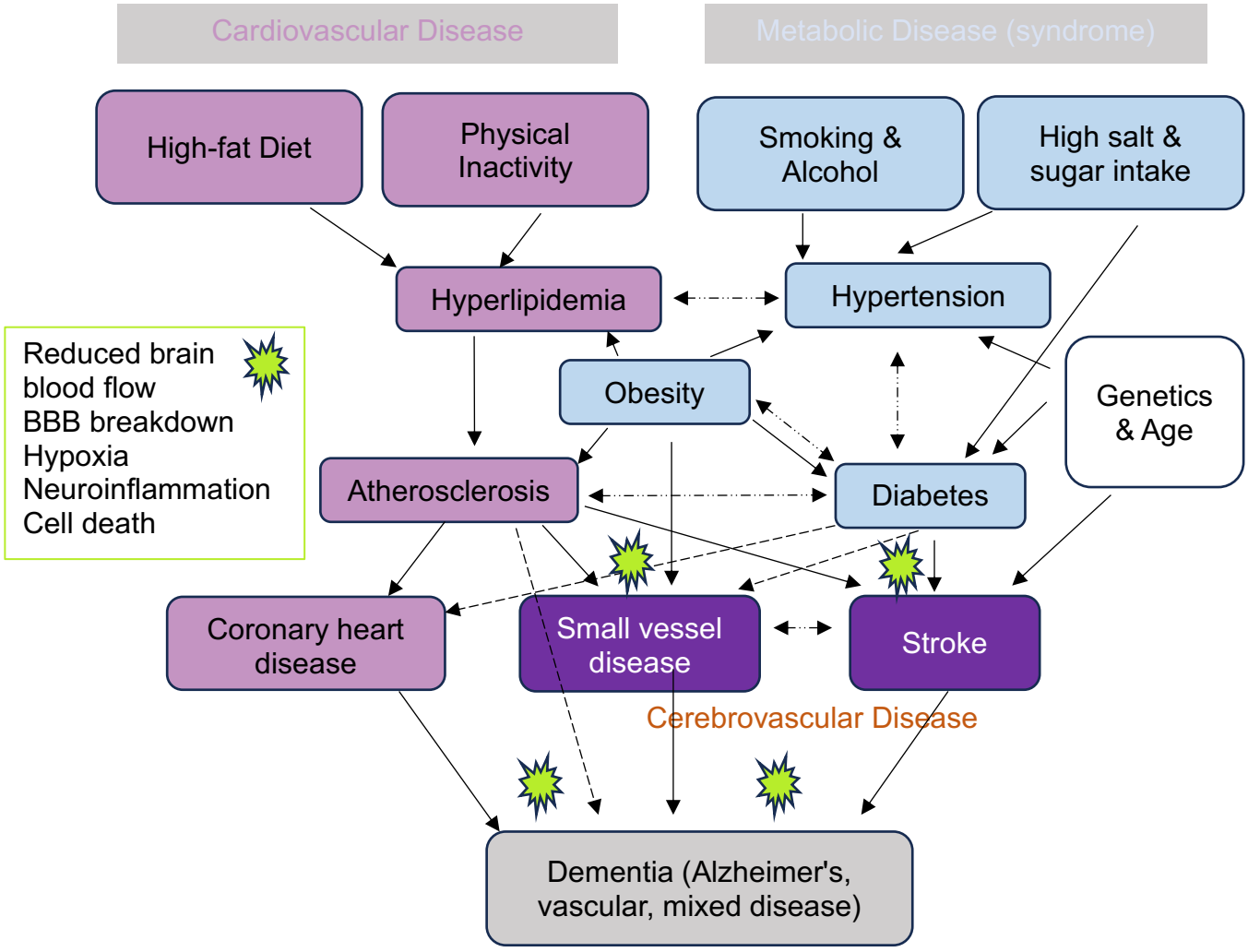

Figure 1.4: A schematic, adapted from Shabir et al., (2020) highlighting links between atherosclerosis (including the causes of atherosclerosis) and dementia

A schematic adapted from Shabir et al., (2020)[259] highlighting the links between cardiovascular disease, metabolic disease and the development of dementia.

It has also been postulated that AD may enhance atherosclerosis. For example, APP overexpressing mice crossed with $ApoE^{-/-}$ mice given a western diet have been observed to develop more enhanced aortic atherosclerotic lesions, accompanied by increased levels of inflammation and evidence of oxidative stress within the

vasculature as compared to ApoE$^{-/-}$ only mice. Furthermore, these mice also showed slightly increased microglia and endothelial cell activation in the brain[260]. This occurred despite no Aβ deposits within the brain, suggesting that there may be overlapping inflammatory mechanisms of atherosclerosis and AD. Moreover, using a different model to induce atherosclerosis in APP overexpressing mice – (partial ligation of the carotid artery) Jung et al.,[261] demonstrated that lesion area and size were significantly increased alongside increased arterial wall thickness. These structural alterations were observed alongside an increase in vascular inflammation as compared to non-AD mice who received partial ligation of the carotid artery. These findings suggest that the overexpression of APP results in enhanced atherogenesis. The above findings are further supported by Van de Parre et al.,[262] who demonstrated that the size of atherosclerotic plaques could be significantly reduced by crossing APP$^{-/-}$ and ApoE$^{-/-}$ mice. These mice had similar cholesterol levels as compared to ApoE$^{-/-}$ only mice, suggesting that the reduced size of atherosclerotic lesions did not occur due to changes in cholesterol levels.

Atherosclerosis can inhibit blood flow within vessels, as a result of narrowing the lumen of arteries. This can lead to hypoperfusion, as less O_2 and glucose are able to travel in the blood. Hypoperfusion can result in the increased production of Aβ, this has been observed in WT and AD mice[210,211]. In addition to this, increased production of Aβ can result in endothelial dysfunction and the release of reactive oxygen species, which itself can promote the development of atherosclerotic plaques[263]. It has also been suggested that atherosclerosis may impair the clearance of Aβ. Research indicates that approximately 50% of Aβ clearance within the brain involves vascular pathways[264]. Hence it is plausible to suggest that as atherosclerosis can impair the vasculature the disease could also impact Aβ clearance.

Hypercholesteremia is a risk factor for both atherosclerosis and AD. The induction of hypercholesteremia in rodents can result in cognitive dysfunction, Aβ deposits and BBB dysfunction[265,266]. Hypercholesteremia has been induced in AD mouse models to assess how high levels of cholesterol may impact AD pathology. Refolo et al.,[267] revealed that a high cholesterol diet could enhance AD pathology in AD mice. The induction of hypercholesteremia was enough to increase the number and size of Aβ

deposits. Moreover, a high cholesterol diet in 3xTg mice was shown to weaken cognition (but not significantly) alongside some alterations in the vasculature, although it did not enhance AD pathology[268]. However, 3xTg mice given a high cholesterol diet did not survive past 14m of age, therefore it could be reasoned that they may have developed enhanced pathology if they had survived longer.

The above studies only induced hypercholesteremia and not atherosclerosis. However, a single injection of rAAV8 D377Y-mPCSK9 with the addition of a western diet can induce both hypercholesteremia and atherosclerosis. This is a convenient way to induce atherosclerosis in an AD mouse model to investigate how atherosclerosis can impact AD pathology. Grames et al.,[269] injected APP/PS1 mice with rAAV8 D377Y-mPCSK9. These mice developed increased cholesterol levels 13 weeks post-injection. Increased Aβ deposits were also observed in the hippocampus although a non-significant increase was found within the cortex. However, the mice were sacrificed at 7m, early in disease, therefore excessive increases in pathology may have occurred later in disease. Unfortunately, the study did not assess atherosclerotic lesions within the aorta, so it cannot be known if these mice developed atherosclerosis. However, one study has previously investigated neurovascular function in AD and atherosclerosis and in a mixed disease model, using the J20 model of AD and the rAAV8 D377Y-mPCSK9 model of atherosclerosis with a western diet. Shabir et al.,[96] reported that haemodynamic responses were impaired in the atherosclerosis group, whereas responses were preserved in the AD and mixed disease mice. Interestingly, they also reported that the mixed disease model had enhanced amyloid plaque pathology, evidenced by an increase in the number of amyloid plaques within the hippocampus compared with the AD alone mice[96]. However, they did not assess cognition and neurovascular experiments were conducted in lightly anesthetised mice. As previously mentioned, anaesthesia can greatly impact neurovascular responses, therefore, it is important for future studies to be conducted without the use of anaesthesia. Moreover, the J20 model they used is a relatively 'mild' model of AD[270].

Therefore, in my PhD I aim to extend and replicate the findings of Shabir et al.,[96]. To facilitate this I will use a more 'severe' model of AD[270], the APP/PS1 model, I will

conduct neurovascular experiments in awake mice and I will also assess cognition using the novel object recognition test (NOR).

1.7 Aims

When investigating AD, the majority of studies have been conducted in 'pure' AD models, however, in life, comorbidities commonly occur with AD, with many individuals possessing vascular risk factors/vascular disorders[271,272]. It is important to investigate how AD and cardiovascular diseases, such as atherosclerosis, may interact as atherosclerosis alone has been associated with cognitive decline, as well as an increased risk of dementia[273]. There is only one study that has investigated neurovascular function in AD, atherosclerotic and mixed disease mice[96]. However, this study used a relatively 'mild' model of AD, did not assess cognition, and neurovascular function studies were completed in lightly anesthetised mice. Therefore, the overarching aim of my PhD is to extend and replicate the findings of Shabir et al.,[96] by using a more 'severe' model of AD, assessing cognition, and completing the assessments of neurovascular function in awake, behaving mice. Additionally, as the studies will be conducted in awake mice, I will assess the effect of locomotion on sensory-evoked haemodynamic responses, as few studies have investigated the impact that locomotion may have on evoked-haemodynamic responses. Furthermore, following the observation of a novel neurovascular response to locomotion within large draining veins of the brain during my PhD, the final part of my PhD will explore this new phenomenon. The specific aims and hypotheses of my research are as follows:

1) To investigate the effect of locomotion on sensory-evoked haemodynamic responses (chapter 2)
2) To investigate cognition in the APP/PS1 mouse model of AD, a model of atherosclerosis and a mixed model of AD and atherosclerosis (chapter 3)
3) To investigate neurovascular function (using 2D-OIS) in the APP/PS1 mouse model of AD, a model of atherosclerosis and a mixed model of AD and atherosclerosis (chapter 3)
4) To investigate the effect of mixed disease on amyloid pathology (chapter 3)
5) To explore the novel phenomenon relating to locomotion and early vascular responses in large draining veins of the brain (chapter 4)

1.8 Hypotheses

1) Locomotion will have the largest effects on evoked haemodynamic responses when it occurs at a similar time to whisker-stimulation (chapter 2)
2) Non-spatial cognition (as assessed using the NOR test) will be impaired in AD, atherosclerosis and mixed disease mice. These groups will have a reduced preference index for the novel object, compared to WT mice (chapter 3)
3) Neurovascular function will be impaired (evidenced by a reduction in the size of the whisker-evoked haemodynamic response) in AD, atherosclerosis and mixed disease mice. With the greatest reduction in amplitude of the haemodynamic response observed in the mixed disease group, as assessed using 2D-OIS (chapter 3)
4) Mixed disease mice will have an increase in amyloid pathology. These mice will have a greater abundance of amyloid plaques in the brain compared to AD only mice (chapter 3)
5) Locomotion will impact CBV responses within the large veins of the brain and there will be an effect of disease on this (chapter 4)

1.9 Links between the literature review and experimental chapters

Research indicates that vascular changes may be important in the development of AD. Therefore, I wanted to investigate how cerebrovascular function was impacted by the development of amyloid plaques in an amyloid model of AD. Additionally, as AD is a disease that occurs later in life, it is often accompanied by other diseases. Few studies have investigated how comorbid disease may affect cerebrovascular function in AD. Of the comorbidities that often accompany AD diseases of the vasculature are common, therefore I also wanted to investigate how comorbid AD and atherosclerosis impacted cerebrovascular function. Previous work in my current research group observed that in the J20 model of AD, haemodynamic responses to a whisker stimulation were preserved, in addition to also being preserved in a comorbid AD and atherosclerosis model. However, they observed that these same responses were impaired in the atherosclerosis alone model. The initial aim of my PhD was to extend and replicate the findings of the above study, using a more ‘severe’ model of AD (the APP/PS1 model) and conducting awake cerebrovascular assessments. As my plan was to conduct neurovascular assessments in an awake preparation I initially needed

to investigate if locomotion had an effect on evoked haemodynamic responses (Chapter 2). As I found an effect of locomotion on evoked-haemodynamic responses this led me to take account of locomotion during whisker stimulation when assessing vascular function across different disease states, to ensure that any vascular responses I observed were not confounded by locomotion (chapter 3). In my initial observations of awake vascular assessments, I noticed that large pial veins had an early vascular response. Therefore, I wanted to investigate how the large cerebral veins responded to locomotion and if this was impacted by disease, which I investigated in chapter 4.

1.10 References

1. *Basic Neurochemistry*. (Lippincott-Raven, 1999).
2. Zlokovic, B. V. Neurovascular pathways to neurodegeneration in Alzheimer's disease and other disorders. *Nat Rev Neurosci* **12**, 723–738 (2011).
3. Attwell, D. *et al.* Glial and neuronal control of brain blood flow. *Nature* **468**, 232–243 (2010).
4. Iadecola, C. The Neurovascular Unit Coming of Age: A Journey through Neurovascular Coupling in Health and Disease. *Neuron* **96**, 17–42 (2017).
5. Schaeffer, S. & Iadecola, C. Revisiting the neurovascular unit. *Nat Neurosci* **24**, 1198–1209 (2021).
6. Kisler, K., Nelson, A. R., Montagne, A. & Zlokovic, B. V. Cerebral blood flow regulation and neurovascular dysfunction in Alzheimer disease. *Nat Rev Neurosci* **18**, 419–434 (2017).
7. Zhu, W. M., Neuhaus, A., Beard, D. J., Sutherland, B. A. & DeLuca, G. C. Neurovascular coupling mechanisms in health and neurovascular uncoupling in Alzheimer's disease. *Brain* **145**, 2276–2292 (2022).
8. Blinder, P. *et al.* The cortical angiome: an interconnected vascular network with noncolumnar patterns of blood flow. *Nat Neurosci* **16**, 889–897 (2013).
9. Purves, D. *et al.* The Blood Supply of the Brain and Spinal Cord. in *Neuroscience. 2nd edition* (Sinauer Associates, 2001).
10. Maki, T. *et al.* Biphasic Mechanisms of Neurovascular Unit Injury and Protection In CNS Diseases. *CNS Neurol Disord Drug Targets* **12**, 302–315 (2013).
11. Mishra, A. *et al.* Astrocytes mediate neurovascular signaling to capillary pericytes but not to arterioles. *Nat Neurosci* **19**, 1619–1627 (2016).
12. Hall, C. N. *et al.* Capillary pericytes regulate cerebral blood flow in health and disease. *Nature* **508**, 55–60 (2014).
13. Longden, T. A. *et al.* Capillary K+-sensing initiates retrograde hyperpolarization to increase local cerebral blood flow. *Nat Neurosci* **20**, 717–726 (2017).
14. Lee, L. *et al.* Key Aspects of Neurovascular Control Mediated by Specific Populations of Inhibitory Cortical Interneurons. *Cerebral Cortex* **30**, 2452–2464 (2020).
15. Reese, T. S. & Karnovsky, M. J. FINE STRUCTURAL LOCALIZATION OF A BLOOD-BRAIN BARRIER TO EXOGENOUS PEROXIDASE. *Journal of Cell Biology* **34**, 207–217 (1967).
16. Hawkins, B. T. & Davis, T. P. The Blood-Brain Barrier/Neurovascular Unit in Health and Disease. *Pharmacol Rev* **57**, 173–185 (2005).
17. Blanchette, M. & Daneman, R. Formation and maintenance of the BBB. *Mechanisms of Development* **138**, 8–16 (2015).
18. Abbott, N. J., Rönnbäck, L. & Hansson, E. Astrocyte–endothelial interactions at the blood–brain barrier. *Nat Rev Neurosci* **7**, 41–53 (2006).

19. Pardridge, W. M. Molecular Biology of the Blood-Brain Barrier. in *The Blood-Brain Barrier: Biology and Research Protocols* (ed. Nag, S.) 385–399 (Humana Press, 2003). doi:10.1385/1-59259-419-0:385.
20. Rothstein, J. D. *et al.* Knockout of Glutamate Transporters Reveals a Major Role for Astroglial Transport in Excitotoxicity and Clearance of Glutamate. *Neuron* **16**, 675–686 (1996).
21. Herz, J. & Strickland, D. K. LRP: a multifunctional scavenger and signaling receptor. https://www.jci.org/articles/view/13992/pdf (2001) doi:10.1172/JCI13992.
22. Storck, S. E. *et al.* Endothelial LRP1 transports amyloid-β(1-42) across the blood-brain barrier. *J Clin Invest* **126**, 123–136 (2016).
23. Armulik, A. *et al.* Pericytes regulate the blood–brain barrier. *Nature* **468**, 557–561 (2010).
24. Daneman, R., Zhou, L., Kebede, A. A. & Barres, B. A. Pericytes are required for blood–brain barrier integrity during embryogenesis. *Nature* **468**, 562–566 (2010).
25. Wong, S. M. *et al.* Blood-brain barrier impairment and hypoperfusion are linked in cerebral small vessel disease. *Neurology* **92**, e1669–e1677 (2019).
26. Sweeney, M. D. *et al.* Vascular dysfunction—The disregarded partner of Alzheimer's disease. *Alzheimer's & Dementia* **15**, 158–167 (2019).
27. Faraci, F. M. & Breese, K. R. Nitric oxide mediates vasodilatation in response to activation of N-methyl-D-aspartate receptors in brain. *Circ Res* **72**, 476–480 (1993).
28. Niwa, K., Araki, E., Morham, S. G., Ross, M. E. & Iadecola, C. Cyclooxygenase-2 Contributes to Functional Hyperemia in Whisker-Barrel Cortex. *J. Neurosci.* **20**, 763–770 (2000).
29. Alonso-Galicia, M., Drummond, H. A., Reddy, K. K., Falck, J. R. & Roman, R. J. Inhibition of 20-HETE Production Contributes to the Vascular Responses to Nitric Oxide. *Hypertension* **29**, 320–325 (1997).
30. Gebremedhin, D. *et al.* Production of 20-HETE and Its Role in Autoregulation of Cerebral Blood Flow. *Circulation Research* **87**, 60–65 (2000).
31. Filosa, J. A., Morrison, H. W., Iddings, J. A., Du, W. & Kim, K. J. Beyond neurovascular coupling, role of astrocytes in the regulation of vascular tone. *Neuroscience* **323**, 96–109 (2016).
32. Echagarruga, C. T., Gheres, K. W., Norwood, J. N. & Drew, P. J. nNOS-expressing interneurons control basal and behaviorally evoked arterial dilation in somatosensory cortex of mice. *eLife* **9**, e60533 (2020).
33. Uhlirova, H. *et al.* Cell type specificity of neurovascular coupling in cerebral cortex. *eLife* **5**, e14315 (2016).
34. Cauli, B. *et al.* Cortical GABA Interneurons in Neurovascular Coupling: Relays for Subcortical Vasoactive Pathways. *J. Neurosci.* **24**, 8940–8949 (2004).
35. Hu, H., Gan, J. & Jonas, P. Fast-spiking, parvalbumin+ GABAergic interneurons: From cellular design to microcircuit function. *Science* **345**, 1255263 (2014).

36. Markram, H. *et al.* Interneurons of the neocortical inhibitory system. *Nat Rev Neurosci* **5**, 793–807 (2004).
37. Perrenoud, Q. *et al.* Activation of cortical 5-HT3 receptor-expressing interneurons induces NO mediated vasodilatations and NPY mediated vasoconstrictions. *Frontiers in Neural Circuits* **6**, (2012).
38. Hamel, E. Perivascular nerves and the regulation of cerebrovascular tone. *Journal of Applied Physiology* **100**, 1059–1064 (2006).
39. Optogenetic Stimulation of GABA Neurons can Decrease Local Neuronal Activity While Increasing Cortical Blood Flow - Eitan Anenberg, Allen W Chan, Yicheng Xie, Jeffrey M LeDue, Timothy H Murphy, 2015. https://journals.sagepub.com/doi/full/10.1038/jcbfm.2015.140.
40. Vazquez, A. L., Fukuda, M. & Kim, S.-G. Inhibitory Neuron Activity Contributions to Hemodynamic Responses and Metabolic Load Examined Using an Inhibitory Optogenetic Mouse Model. *Cerebral Cortex* **28**, 4105–4119 (2018).
41. MacVicar, B. A. & Newman, E. A. Astrocyte Regulation of Blood Flow in the Brain. *Cold Spring Harb Perspect Biol* **7**, a020388 (2015).
42. Iadecola, C. Neurovascular regulation in the normal brain and in Alzheimer's disease. *Nat Rev Neurosci* **5**, 347–360 (2004).
43. Spector, A. A. Arachidonic acid cytochrome P450 epoxygenase pathway. *Journal of Lipid Research* **50**, S52–S56 (2009).
44. Zonta, M. *et al.* Neuron-to-astrocyte signaling is central to the dynamic control of brain microcirculation. *Nat Neurosci* **6**, 43–50 (2003).
45. Bezzi, P. *et al.* Prostaglandins stimulate calcium-dependent glutamate release in astrocytes. *Nature* **391**, 281–285 (1998).
46. Takano, T. *et al.* Astrocyte-mediated control of cerebral blood flow. *Nat Neurosci* **9**, 260–267 (2006).
47. Nizar, K. *et al.* In vivo Stimulus-Induced Vasodilation Occurs without IP3 Receptor Activation and May Precede Astrocytic Calcium Increase. *J. Neurosci.* **33**, 8411–8422 (2013).
48. Lind, B. L., Brazhe, A. R., Jessen, S. B., Tan, F. C. C. & Lauritzen, M. J. Rapid stimulus-evoked astrocyte Ca $^{2+}$ elevations and hemodynamic responses in mouse somatosensory cortex in vivo. *Proc. Natl. Acad. Sci. U.S.A.* **110**, (2013).
49. Otsu, Y. *et al.* Calcium dynamics in astrocyte processes during neurovascular coupling. *Nat Neurosci* **18**, 210–218 (2015).
50. Lind, B. L. *et al.* Fast Ca2+ responses in astrocyte end-feet and neurovascular coupling in mice. *Glia* **66**, 348–358 (2018).
51. Poittevin, M. *et al.* Smooth Muscle Cell Phenotypic Switching in Stroke. *Transl. Stroke Res.* **5**, 377–384 (2014).
52. Cipolla, M. J., Lessov, N., Hammer, E. S. & Curry, A. B. Threshold Duration of Ischemia for Myogenic Tone in Middle Cerebral Arteries. *Stroke* **32**, 1658–1664 (2001).

53. Armulik, A., Genové, G. & Betsholtz, C. Pericytes: Developmental, Physiological, and Pathological Perspectives, Problems, and Promises. *Developmental Cell* **21**, 193–215 (2011).
54. Brown, L. S. *et al.* Pericytes and Neurovascular Function in the Healthy and Diseased Brain. *Frontiers in Cellular Neuroscience* **13**, (2019).
55. Neuhaus, A. A., Couch, Y., Sutherland, B. A. & Buchan, A. M. Novel method to study pericyte contractility and responses to ischaemia in vitro using electrical impedance. *J Cereb Blood Flow Metab* **37**, 2013–2024 (2017).
56. Peppiatt, C. M., Howarth, C., Mobbs, P. & Attwell, D. Bidirectional control of CNS capillary diameter by pericytes. *Nature* **443**, 700–704 (2006).
57. Hill, R. A. *et al.* Regional Blood Flow in the Normal and Ischemic Brain Is Controlled by Arteriolar Smooth Muscle Cell Contractility and Not by Capillary Pericytes. *Neuron* **87**, 95–110 (2015).
58. Hartmann, D. A. *et al.* Pericyte structure and distribution in the cerebral cortex revealed by high-resolution imaging of transgenic mice. *NPh* **2**, 041402 (2015).
59. Jung, B., Arnold, T. D., Raschperger, E., Gaengel, K. & Betsholtz, C. Visualization of vascular mural cells in developing brain using genetically labeled transgenic reporter mice. *J Cereb Blood Flow Metab* **38**, 456–468 (2018).
60. Attwell, D., Mishra, A., Hall, C. N., O'Farrell, F. M. & Dalkara, T. What is a pericyte? *J Cereb Blood Flow Metab* **36**, 451–455 (2016).
61. Berthiaume, A.-A. *et al.* Dynamic Remodeling of Pericytes In Vivo Maintains Capillary Coverage in the Adult Mouse Brain. *Cell Rep* **22**, 8–16 (2018).
62. Kisler, K. *et al.* Pericyte degeneration leads to neurovascular uncoupling and limits oxygen supply to brain. *Nat Neurosci* **20**, 406–416 (2017).
63. Kisler, K. *et al.* Acute Ablation of Cortical Pericytes Leads to Rapid Neurovascular Uncoupling. *Frontiers in Cellular Neuroscience* **14**, (2020).
64. Duffy, S. J. *et al.* Continuous release of vasodilator prostanoids contributes to regulation of resting forearm blood flow in humans. *American Journal of Physiology-Heart and Circulatory Physiology* **274**, H1174–H1183 (1998).
65. Triggle, C. R. *et al.* The endothelium: influencing vascular smooth muscle in many ways. *Can. J. Physiol. Pharmacol.* **90**, 713–738 (2012).
66. Chen, B. R., Bouchard, M. B., McCaslin, A. F. H., Burgess, S. A. & Hillman, E. M. C. High-speed vascular dynamics of the hemodynamic response. *NeuroImage* **54**, 1021–1030 (2011).
67. Iadecola, C. Regulation of the cerebral microcirculation during neural activity: is nitric oxide the missing link? *Trends in Neurosciences* **16**, 206–214 (1993).
68. Chen, B. R., Kozberg, M. G., Bouchard, M. B., Shaik, M. A. & Hillman, E. M. C. A Critical Role for the Vascular Endothelium in Functional Neurovascular Coupling in the Brain. *Journal of the American Heart Association* **3**, e000787.
69. Silva, A. C. & Koretsky, A. P. Laminar specificity of functional MRI onset times during somatosensory stimulation in rat. *Proceedings of the National Academy of Sciences* **99**, 15182–15187 (2002).

70. Hogan-Cann, A. D., Lu, P. & Anderson, C. M. Endothelial NMDA receptors mediate activity-dependent brain hemodynamic responses in mice. *Proceedings of the National Academy of Sciences* **116**, 10229–10231 (2019).
71. Chow, B. W. *et al.* Caveolae in CNS arterioles mediate neurovascular coupling. *Nature* **579**, 106–110 (2020).
72. Drab, M. *et al.* Loss of caveolae, vascular dysfunction, and pulmonary defects in caveolin-1 gene-disrupted mice. *Science* **293**, 2449–2452 (2001).
73. Ogawa, S., Lee, T. M., Kay, A. R. & Tank, D. W. Brain magnetic resonance imaging with contrast dependent on blood oxygenation. *Proceedings of the National Academy of Sciences* **87**, 9868–9872 (1990).
74. Fox, P. T. & Raichle, M. E. Focal physiological uncoupling of cerebral blood flow and oxidative metabolism during somatosensory stimulation in human subjects. *Proceedings of the National Academy of Sciences* **83**, 1140–1144 (1986).
75. Huettel, S. A. *et al.* Linking Hemodynamic and Electrophysiological Measures of Brain Activity: Evidence from Functional MRI and Intracranial Field Potentials. *Cerebral Cortex* **14**, 165–173 (2004).
76. Hillman, E. M. C. Coupling Mechanism and Significance of the BOLD Signal: A Status Report. *Annual Review of Neuroscience* **37**, 161–181 (2014).
77. Kwong, K. K. *et al.* Dynamic magnetic resonance imaging of human brain activity during primary sensory stimulation. *Proceedings of the National Academy of Sciences* **89**, 5675–5679 (1992).
78. Frahm, J., Krüger, G., Merboldt, K.-D. & Kleinschmidt, A. Dynamic uncoupling and recoupling of perfusion and oxidative metabolism during focal brain activation in man. *Magnetic Resonance in Medicine* **35**, 143–148 (1996).
79. Logothetis, N. K., Pauls, J., Augath, M., Trinath, T. & Oeltermann, A. Neurophysiological investigation of the basis of the fMRI signal. *Nature* **412**, 150–157 (2001).
80. Ferré, J.-C. *et al.* Arterial spin labeling (ASL) perfusion: Techniques and clinical use. *Diagnostic and Interventional Imaging* **94**, 1211–1223 (2013).
81. Verclytte, S. *et al.* Cerebral Hypoperfusion and Hypometabolism Detected by Arterial Spin Labeling MRI and FDG-PET in Early-Onset Alzheimer's Disease. *Journal of Neuroimaging* **26**, 207–212 (2016).
82. Du, A. T. *et al.* Hypoperfusion in frontotemporal dementia and Alzheimer disease by arterial spin labeling MRI. *Neurology* **67**, 1215–1220 (2006).
83. Göttler, J. *et al.* Reduced blood oxygenation level dependent connectivity is related to hypoperfusion in Alzheimer's disease. *J Cereb Blood Flow Metab* **39**, 1314–1325 (2019).
84. Sorg, C. *et al.* Selective changes of resting-state networks in individuals at risk for Alzheimer's disease. *Proceedings of the National Academy of Sciences* **104**, 18760–18765 (2007).
85. Hojjati, S. H., Ebrahimzadeh, A. & Babajani-Feremi, A. Identification of the Early Stage of Alzheimer's Disease Using Structural MRI and Resting-State fMRI. *Frontiers in Neurology* **10**, (2019).

86. Ma, Y. *et al.* Wide-field optical mapping of neural activity and brain haemodynamics: considerations and novel approaches. *Philosophical Transactions of the Royal Society B: Biological Sciences* **371**, 20150360 (2016).
87. Yang, G., Pan, F., Parkhurst, C. N., Grutzendler, J. & Gan, W.-B. Thinned-skull cranial window technique for long-term imaging of the cortex in live mice. *Nat Protoc* **5**, 201–208 (2010).
88. Shih, A. Y., Mateo, C., Drew, P. J., Tsai, P. S. & Kleinfeld, D. A Polished and Reinforced Thinned-skull Window for Long-term Imaging of the Mouse Brain. *J Vis Exp* 3742 (2012) doi:10.3791/3742.
89. Berwick, J. *et al.* Neurovascular coupling investigated with two-dimensional optical imaging spectroscopy in rat whisker barrel cortex. *European Journal of Neuroscience* **22**, 1655–1666 (2005).
90. Sharp, P. S. *et al.* Comparison of stimulus-evoked cerebral hemodynamics in the awake mouse and under a novel anesthetic regime. *Sci Rep* **5**, 12621 (2015).
91. Sharp, P. S. *et al.* Neurovascular coupling preserved in a chronic mouse model of Alzheimer's disease: Methodology is critical. *J Cereb Blood Flow Metab* **40**, 2289–2303 (2020).
92. Zee, P. van der, Essenpreis, M. & Delpy, D. T. Optical properties of brain tissue. in *Photon Migration and Imaging in Random Media and Tissues* vol. 1888 454–465 (SPIE, 1993).
93. Henyey, L. G. & Greenstein, J. L. Diffuse radiation in the Galaxy. *The Astrophysical Journal* **93**, 70–83 (1941).
94. Johns, M., Giller, C. A., German, D. C. & Liu, H. Determination of reduced scattering coefficient of biological tissue from a needle-like probe. *Opt. Express, OE* **13**, 4828–4842 (2005).
95. Kennerley, A. J., Mayhew, J. E., Boorman, L., Zheng, Y. & Berwick, J. Is optical imaging spectroscopy a viable measurement technique for the investigation of the negative BOLD phenomenon? A concurrent optical imaging spectroscopy and fMRI study at high field (7T). *NeuroImage* **61**, 10–20 (2012).
96. Shabir, O. *et al.* Assessment of neurovascular coupling and cortical spreading depression in mixed mouse models of atherosclerosis and Alzheimer's disease. *eLife* **11**, e68242 (2022).
97. Carter, M. & Shieh, J. Chapter 4 - Electrophysiology. in *Guide to Research Techniques in Neuroscience (Second Edition)* (eds. Carter, M. & Shieh, J.) 89–115 (Academic Press, 2015). doi:10.1016/B978-0-12-800511-8.00004-6.
98. *Neuroscience, 3rd ed*. xix, 773 (Sinauer Associates, 2004).
99. Buzsáki, G., Anastassiou, C. A. & Koch, C. The origin of extracellular fields and currents — EEG, ECoG, LFP and spikes. *Nat Rev Neurosci* **13**, 407–420 (2012).
100. Buchwald, J. S., Halas, E. S. & Schramm, S. Comparison of Multiple-unit and Electroencephalogram Activity recorded from the same Brain Sites during Behavioural Conditioning. *Nature* **205**, 1012–1014 (1965).
101. Denk, W., Strickler, J. H. & Webb, W. W. Two-Photon Laser Scanning Fluorescence Microscopy. *Science* **248**, 73–76 (1990).

102. Mostany, R., Miquelajauregui, A., Shtrahman, M. & Portera-Cailliau, C. Two-Photon Excitation Microscopy and Its Applications in Neuroscience. *Methods in molecular biology (Clifton, N.J.)* **1251**, 25–42 (2015).
103. Zipfel, W. R., Williams, R. M. & Webb, W. W. Nonlinear magic: multiphoton microscopy in the biosciences. *Nat Biotechnol* **21**, 1369–1377 (2003).
104. Spence, D. E., Kean, P. N. & Sibbett, W. 60-fsec pulse generation from a self-mode-locked Ti:sapphire laser. *Opt. Lett., OL* **16**, 42–44 (1991).
105. Denk, W. *et al.* Anatomical and functional imaging of neurons using 2-photon laser scanning microscopy. *Journal of Neuroscience Methods* **54**, 151–162 (1994).
106. Helmchen, F. & Denk, W. Deep tissue two-photon microscopy. *Nat Methods* **2**, 932–940 (2005).
107. Kobat, D., Horton, N. G. & Xu, C. In vivo two-photon microscopy to 1.6-mm depth in mouse cortex. *JBO* **16**, 106014 (2011).
108. Svoboda, K. & Yasuda, R. Principles of Two-Photon Excitation Microscopy and Its Applications to Neuroscience. *Neuron* **50**, 823–839 (2006).
109. Kalies, S., Kuetemeyer, K. & Heisterkamp, A. Mechanisms of high-order photobleaching and its relationship to intracellular ablation. *Biomed Opt Express* **2**, 805–816 (2011).
110. Kleinfeld, D., Mitra, P. P., Helmchen, F. & Denk, W. Fluctuations and stimulus-induced changes in blood flow observed in individual capillaries in layers 2 through 4 of rat neocortex. *Proceedings of the National Academy of Sciences* **95**, 15741–15746 (1998).
111. Helmchen, F. & Kleinfeld, D. Chapter 10 In Vivo Measurements of Blood Flow and Glial Cell Function with Two-Photon Laser-Scanning Microscopy. in *Methods in Enzymology* vol. 444 231–254 (Academic Press, 2008).
112. Shih, A. Y. *et al.* Two-Photon Microscopy as a Tool to Study Blood Flow and Neurovascular Coupling in the Rodent Brain. *J Cereb Blood Flow Metab* **32**, 1277–1309 (2012).
113. Klunk, W. E. *et al.* Imaging Aβ Plaques in Living Transgenic Mice with Multiphoton Microscopy and Methoxy-X04, a Systemically Administered Congo Red Derivative. *Journal of Neuropathology & Experimental Neurology* **61**, 797–805 (2002).
114. Hefendehl, J. K. *et al.* Long-Term In Vivo Imaging of β-Amyloid Plaque Appearance and Growth in a Mouse Model of Cerebral β-Amyloidosis. *J. Neurosci.* **31**, 624–629 (2011).
115. Poon, C. T. *et al.* Time course of focused ultrasound effects on β-amyloid plaque pathology in the TgCRND8 mouse model of Alzheimer's disease. *Sci Rep* **8**, 14061 (2018).
116. Berridge, M. J., Bootman, M. D. & Roderick, H. L. Calcium signalling: dynamics, homeostasis and remodelling. *Nat Rev Mol Cell Biol* **4**, 517–529 (2003).
117. Berridge, M. J., Lipp, P. & Bootman, M. D. The versatility and universality of calcium signalling. *Nat Rev Mol Cell Biol* **1**, 11–21 (2000).

118. Grienberger, C. & Konnerth, A. Imaging Calcium in Neurons. *Neuron* **73**, 862–885 (2012).
119. Rose, T., Goltstein, P. M., Portugues, R. & Griesbeck, O. Putting a finishing touch on GECIs. *Frontiers in Molecular Neuroscience* **7**, (2014).
120. Niswender, K. D., Blackman, S. M., Rohde, L., Magnuson, M. A. & Piston, D. W. Quantitative imaging of green fluorescent protein in cultured cells: Comparison of microscopic techniques, use in fusion proteins and detection limits. *Journal of Microscopy* **180**, 109–116 (1995).
121. Wang, J. W., Wong, A. M., Flores, J., Vosshall, L. B. & Axel, R. Two-Photon Calcium Imaging Reveals an Odor-Evoked Map of Activity in the Fly Brain. *Cell* **112**, 271–282 (2003).
122. Nakai, J., Ohkura, M. & Imoto, K. A high signal-to-noise Ca2+ probe composed of a single green fluorescent protein. *Nat Biotechnol* **19**, 137–141 (2001).
123. Barson, D. *et al.* Simultaneous mesoscopic and two-photon imaging of neuronal activity in cortical circuits. *Nat Methods* **17**, 107–113 (2020).
124. Grødem, S. *et al.* An updated suite of viral vectors for in vivo calcium imaging using intracerebral and retro-orbital injections in male mice. *Nat Commun* **14**, 608 (2023).
125. Shevtsova, Z., Malik, J. M. I., Michel, U., Bähr, M. & Kügler, S. Promoters and serotypes: targeting of adeno-associated virus vectors for gene transfer in the rat central nervous system in vitro and in vivo. *Experimental Physiology* **90**, 53–59 (2005).
126. Gao, Y.-R. *et al.* Time to wake up: Studying neurovascular coupling and brain-wide circuit function in the un-anesthetized animal. *NeuroImage* **153**, 382–398 (2017).
127. Pisauro, M. A., Dhruv, N. T., Carandini, M. & Benucci, A. Fast Hemodynamic Responses in the Visual Cortex of the Awake Mouse. *J. Neurosci.* **33**, 18343–18351 (2013).
128. Aksenov, D. P., Li, L., Miller, M. J., Iordanescu, G. & Wyrwicz, A. M. Effects of anesthesia on BOLD signal and neuronal activity in the somatosensory cortex. *J Cereb Blood Flow Metab* **35**, 1819–1826 (2015).
129. Handwerker, D. A., Ollinger, J. M. & D'Esposito, M. Variation of BOLD hemodynamic responses across subjects and brain regions and their effects on statistical analyses. *NeuroImage* **21**, 1639–1651 (2004).
130. Kleinfeld, D. & Griesbeck, O. From Art to Engineering? The Rise of In Vivo Mammalian Electrophysiology via Genetically Targeted Labeling and Nonlinear Imaging. *PLoS Biol* **3**, e355 (2005).
131. Huo, B.-X., Greene, S. E. & Drew, P. J. Venous cerebral blood volume increase during voluntary locomotion reflects cardiovascular changes. *Neuroimage* **118**, 301–312 (2015).
132. Huo, B.-X., Smith, J. B. & Drew, P. J. Neurovascular Coupling and Decoupling in the Cortex during Voluntary Locomotion. *J. Neurosci.* **34**, 10975–10981 (2014).

133. Tran, C. H. T., Peringod, G. & Gordon, G. R. Astrocytes Integrate Behavioral State and Vascular Signals during Functional Hyperemia. *Neuron* **100**, 1133-1148.e3 (2018).
134. Winder, A. T., Echagarruga, C., Zhang, Q. & Drew, P. J. Weak correlations between hemodynamic signals and ongoing neural activity during the resting state. *Nat Neurosci* **20**, 1761–1769 (2017).
135. Huo, B.-X., Gao, Y.-R. & Drew, P. J. Quantitative separation of arterial and venous cerebral blood volume increases during voluntary locomotion. *NeuroImage* **105**, 369–379 (2015).
136. Lecrux, C. & Hamel, E. Neuronal networks and mediators of cortical neurovascular coupling responses in normal and altered brain states. *Philosophical Transactions of the Royal Society B: Biological Sciences* **371**, 20150350 (2016).
137. Petersen, C. C. H. Sensorimotor processing in the rodent barrel cortex. *Nat Rev Neurosci* **20**, 533–546 (2019).
138. Gao, Y.-R. & Drew, P. J. Effects of Voluntary Locomotion and Calcitonin Gene-Related Peptide on the Dynamics of Single Dural Vessels in Awake Mice. *J. Neurosci.* **36**, 2503–2516 (2016).
139. Prince, M. *et al.* Dementia UK: Update (Second edition). 137.
140. Greenberg, S. M. *et al.* Cerebral amyloid angiopathy and Alzheimer disease — one peptide, two pathways. *Nat Rev Neurol* **16**, 30–42 (2020).
141. Hardy, J. A. & Higgins, G. A. Alzheimer's Disease: The Amyloid Cascade Hypothesis. *Science* **256**, 184–185 (1992).
142. Masters, C. L. *et al.* Alzheimer's disease. *Nat Rev Dis Primers* **1**, 15056 (2015).
143. Campion, D. *et al.* Early-Onset Autosomal Dominant Alzheimer Disease: Prevalence, Genetic Heterogeneity, and Mutation Spectrum. *The American Journal of Human Genetics* **65**, 664–670 (1999).
144. Steiner, H., Fukumori, A., Tagami, S. & Okochi, M. Making the final cut: pathogenic amyloid-β peptide generation by γ-secretase. *Cell Stress* **2**, 292–310.
145. Edbauer, D. *et al.* Reconstitution of γ-secretase activity. *Nat Cell Biol* **5**, 486–488 (2003).
146. Hall, A. M. & Roberson, E. D. Mouse Models of Alzheimer's Disease. *Brain Res Bull* **88**, 3–12 (2012).
147. McGowan, E. *et al.* Abeta42 is essential for parenchymal and vascular amyloid deposition in mice. *Neuron* **47**, 191–199 (2005).
148. Suzuki, N. *et al.* An Increased Percentage of Long Amyloid β Protein Secreted by Familial Amyloid β Protein Precursor (βApp717) Mutants. *Science* **264**, 1336–1340 (1994).
149. Citron, M. *et al.* Mutation of the β-amyloid precursor protein in familial Alzheimer's disease increases β-protein production. *Nature* **360**, 672–674 (1992).
150. Hardy, J. A. & Higgins, G. A. Alzheimer's Disease: The Amyloid Cascade Hypothesis. *Science* **256**, 184–185 (1992).

151. Selkoe, D. J. Toward a Comprehensive Theory for Alzheimer's Disease. Hypothesis: Alzheimer's Disease Is Caused by the Cerebral Accumulation and Cytotoxicity of Amyloid β-Protein. *Annals of the New York Academy of Sciences* **924**, 17–25 (2000).
152. Luchsinger, J. A. *et al.* Relation of Diabetes to Mild Cognitive Impairment. *Archives of Neurology* **64**, 570–575 (2007).
153. Chatterjee, S. & Mudher, A. Alzheimer's Disease and Type 2 Diabetes: A Critical Assessment of the Shared Pathological Traits. *Frontiers in Neuroscience* **12**, (2018).
154. Whitmer, R. A. *et al.* Central obesity and increased risk of dementia more than three decades later. *Neurology* **71**, 1057–1064 (2008).
155. Flores-Cordero, J. A. *et al.* Obesity as a Risk Factor for Dementia and Alzheimer's Disease: The Role of Leptin. *Int J Mol Sci* **23**, 5202 (2022).
156. Iadecola, C. & Davisson, R. L. Hypertension and Cerebrovascular Dysfunction. *Cell Metab* **7**, 476–484 (2008).
157. Lennon, M. J., Makkar, S. R., Crawford, J. D. & Sachdev, P. S. Midlife Hypertension and Alzheimer's Disease: A Systematic Review and Meta-Analysis. *JAD* **71**, 307–316 (2019).
158. Jellinger, K. A. Prevalence and Impact of Cerebrovascular Lesions in Alzheimer and Lewy Body Diseases. *Neurodegenerative Diseases* **7**, 112–115 (2010).
159. Zlokovic, B. V. Neurovascular mechanisms of Alzheimer's neurodegeneration. *Trends in Neurosciences* **28**, 202–208 (2005).
160. Kogure, D. *et al.* Longitudinal Evaluation of Early Alzheimer's Disease Using Brain Perfusion SPECT. *Journal of Nuclear Medicine* **41**, 1155–1162 (2000).
161. Huang, C., Wahlund, L.-O., Svensson, L., Winblad, B. & Julin, P. Cingulate cortex hypoperfusion predicts Alzheimer's disease in mild cognitive impairment. *BMC Neurol* **2**, 9 (2002).
162. Mosconi, L. *et al.* MCI conversion to dementia and the APOE genotype: a prediction study with FDG-PET. *Neurology* **63**, 2332–2340 (2004).
163. Ferrando, R., Pascovich, C., Langhain, M., Gómez, A. & Silveira, A. Regional cerebral blood flow differences in early and late onset Alzheimer's disease. *Journal of Nuclear Medicine* **56**, 1599–1599 (2015).
164. Borroni, B., Di Luca, M. & Padovani, A. Predicting Alzheimer dementia in mild cognitive impairment patients. *European Journal of Pharmacology* **545**, 73–80 (2006).
165. Hirao, K. *et al.* The prediction of rapid conversion to Alzheimer's disease in mild cognitive impairment using regional cerebral blood flow SPECT. *NeuroImage* **28**, 1014–1021 (2005).
166. Chandler, H. L. *et al.* Polygenic impact of common genetic risk loci for Alzheimer's disease on cerebral blood flow in young individuals. *Sci Rep* **9**, 467 (2019).
167. Ruitenberg, A. *et al.* Cerebral hypoperfusion and clinical onset of dementia: The Rotterdam study. *Annals of Neurology* **57**, 789–794 (2005).

168. Webster, S. J., Bachstetter, A. D., Nelson, P. T., Schmitt, F. A. & Van Eldik, L. J. Using mice to model Alzheimer's dementia: an overview of the clinical disease and the preclinical behavioral changes in 10 mouse models. *Frontiers in Genetics* **5**, (2014).
169. Jankowsky, J. L. & Zheng, H. Practical considerations for choosing a mouse model of Alzheimer's disease. *Molecular Neurodegeneration* **12**, 89 (2017).
170. Caroni, P. Overexpression of growth-associated proteins in the neurons of adult transgenic mice. *Journal of Neuroscience Methods* **71**, 3–9 (1997).
171. Sasahara, M. *et al.* PDGF B-chain in neurons of the central nervous system, posterior pituitary, and in a transgenic model. *Cell* **64**, 217–227 (1991).
172. Minkeviciene, R. *et al.* Amyloid β-Induced Neuronal Hyperexcitability Triggers Progressive Epilepsy. *J. Neurosci.* **29**, 3453–3462 (2009).
173. Garcia, M. F. *et al.* The retinal degeneration (rd) gene seriously impairs spatial cognitive performance in normal and Alzheimer's transgenic mice: *NeuroReport* **15**, 73–77 (2004).
174. Jankowsky, J. L. *et al.* Mutant presenilins specifically elevate the levels of the 42 residue β-amyloid peptide in vivo: evidence for augmentation of a 42-specific γ secretase. *Human Molecular Genetics* **13**, 159–170 (2004).
175. Georgevsky, D., Retsas, S., Raoufi, N., Shimoni, O. & Golzan, S. M. A longitudinal assessment of retinal function and structure in the APP/PS1 transgenic mouse model of Alzheimer's disease. *Translational Neurodegeneration* **8**, 30 (2019).
176. Zhu, S. *et al.* The role of neuroinflammation and amyloid in cognitive impairment in an APP/PS1 transgenic mouse model of Alzheimer's disease. *CNS Neuroscience & Therapeutics* **23**, 310–320 (2017).
177. Shen, L. *et al.* Amelioration of cognitive impairments in APPswe/PS1dE9 mice is associated with metabolites alteration induced by total salvianolic acid. *PLoS One* **12**, e0174763 (2017).
178. Hulshof, L. A. *et al.* Both male and female APPswe/PSEN1dE9 mice are impaired in spatial memory and cognitive flexibility at 9 months of age. *Neurobiology of Aging* **113**, 28–38 (2022).
179. Zhou, W. *et al.* DL0410 ameliorates cognitive deficits in APP/PS1 transgenic mice by promoting synaptic transmission and reducing neuronal loss. *Acta Pharmacol Sin* **41**, 599–611 (2020).
180. Cruz Hernández, J. C. *et al.* Neutrophil adhesion in brain capillaries reduces cortical blood flow and impairs memory function in Alzheimer's disease mouse models. *Nat Neurosci* **22**, 413–420 (2019).
181. van Veluw, S. J. *et al.* Vasomotion as a Driving Force for Paravascular Clearance in the Awake Mouse Brain. *Neuron* **105**, 549-561.e5 (2020).
182. Thomas, T., Thomas, G., McLendon, C., Sutton, T. & Mullan, M. β-Amyloid-mediated vasoactivity and vascular endothelial damage. *Nature* **380**, 168–171 (1996).

183. Niwa, K. *et al.* Aβ-peptides enhance vasoconstriction in cerebral circulation. *American Journal of Physiology-Heart and Circulatory Physiology* **281**, H2417–H2424 (2001).
184. Niwa, K., Kazama, K., Younkin, S. G., Carlson, G. A. & Iadecola, C. Alterations in Cerebral Blood Flow and Glucose Utilization in Mice Overexpressing the Amyloid Precursor Protein. *Neurobiology of Disease* **9**, 61–68 (2002).
185. Niwa, K. *et al.* Cerebrovascular autoregulation is profoundly impaired in mice overexpressing amyloid precursor protein. *American Journal of Physiology-Heart and Circulatory Physiology* **283**, H315–H323 (2002).
186. Dorr, A. *et al.* Amyloid-β-dependent compromise of microvascular structure and function in a model of Alzheimer's disease. *Brain* **135**, 3039–3050 (2012).
187. Ahn, K.-C. *et al.* Characterization of Impaired Cerebrovascular Structure in APP/PS1 Mouse Brains. *Neuroscience* **385**, 246–254 (2018).
188. Wu, W.-Z. & Bai, Y.-P. Endothelial GLUTs and vascular biology. *Biomedicine & Pharmacotherapy* **158**, 114151 (2023).
189. Nicolakakis, N. & Hamel, E. Neurovascular function in Alzheimer's disease patients and experimental models. *J Cereb Blood Flow Metab* **31**, 1354–1370 (2011).
190. Tong, X.-K. *et al.* Simvastatin improves cerebrovascular function and counters soluble amyloid-beta, inflammation and oxidative stress in aged APP mice. *Neurobiology of Disease* **35**, 406–414 (2009).
191. Lacoste, B., Tong, X.-K., Lahjouji, K., Couture, R. & Hamel, E. Cognitive and cerebrovascular improvements following kinin B1 receptor blockade in Alzheimer's disease mice. *Journal of Neuroinflammation* **10**, 850 (2013).
192. Li, L. *et al.* Impaired Hippocampal Neurovascular Coupling in a Mouse Model of Alzheimer's Disease. *Front Physiol* **12**, 715446 (2021).
193. Kim, J. & Jeong, Y. Augmentation of Sensory-Evoked Hemodynamic Response in an Early Alzheimer's Disease Mouse Model. *Journal of Alzheimer's disease : JAD* **37**, (2013).
194. Nelson, A. R., Sweeney, M. D., Sagare, A. P. & Zlokovic, B. V. Neurovascular dysfunction and neurodegeneration in dementia and Alzheimer's disease. *Biochimica et Biophysica Acta (BBA) - Molecular Basis of Disease* **1862**, 887–900 (2016).
195. Montagne, A. *et al.* Blood-Brain Barrier Breakdown in the Aging Human Hippocampus. *Neuron* **85**, 296–302 (2015).
196. van de Haar, H. J. *et al.* Blood-Brain Barrier Leakage in Patients with Early Alzheimer Disease. *Radiology* **281**, 527–535 (2016).
197. Yamazaki, Y., Zhao, N., Caulfield, T. R., Liu, C.-C. & Bu, G. Apolipoprotein E and Alzheimer disease: pathobiology and targeting strategies. *Nat Rev Neurol* **15**, 501–518 (2019).
198. Marco, S. & Skaper, S. D. Amyloid β-peptide1–42 alters tight junction protein distribution and expression in brain microvessel endothelial cells. *Neuroscience Letters* **401**, 219–224 (2006).

199. Wang, Y., Liu, J., Zhang, Z., Wang, X. & Zhang, C. Structure and permeability changes of the blood-brain barrier in APP/PS1 mice: an Alzheimer's disease animal model. *Neurochem. J.* **5**, 220–222 (2011).
200. Blair, L. J. *et al.* Tau depletion prevents progressive blood-brain barrier damage in a mouse model of tauopathy. *Acta Neuropathol Commun* **3**, 8 (2015).
201. Minogue, A. M. *et al.* Age-associated dysregulation of microglial activation is coupled with enhanced blood-brain barrier permeability and pathology in APP/PS1 mice. *Neurobiology of Aging* **35**, 1442–1452 (2014).
202. Park, J.-C. *et al.* Annexin A1 restores Aβ1-42-induced blood–brain barrier disruption through the inhibition of RhoA-ROCK signaling pathway. *Aging Cell* **16**, 149–161 (2017).
203. Spires, T. L. *et al.* Region-specific Dissociation of Neuronal Loss and Neurofibrillary Pathology in a Mouse Model of Tauopathy. *The American Journal of Pathology* **168**, 1598–1607 (2006).
204. Wes, P. D. *et al.* Tau Overexpression Impacts a Neuroinflammation Gene Expression Network Perturbed in Alzheimer's Disease. *PLOS ONE* **9**, e106050 (2014).
205. Roher, A. E. *et al.* Cerebral blood flow in Alzheimer's disease. *Vasc Health Risk Manag* **8**, 599–611 (2012).
206. The Alzheimer's Disease Neuroimaging Initiative *et al.* Early role of vascular dysregulation on late-onset Alzheimer's disease based on multifactorial data-driven analysis. *Nat Commun* **7**, 11934 (2016).
207. Benedictus, M. R. *et al.* Lower cerebral blood flow is associated with faster cognitive decline in Alzheimer's disease. *Eur Radiol* **27**, 1169–1175 (2017).
208. Caroli, A. *et al.* Cerebral perfusion correlates of conversion to Alzheimer's disease in amnestic mild cognitive impairment. *Journal of neurology* **254**, 1698–707 (2008).
209. Chao, L. L. *et al.* ASL Perfusion MRI Predicts Cognitive Decline and Conversion From MCI to Dementia. *Alzheimer Dis Assoc Disord* **24**, 19–27 (2010).
210. Wang, L. *et al.* Chronic cerebral hypoperfusion induces memory deficits and facilitates Aβ generation in C57BL/6J mice. *Experimental Neurology* **283**, 353–364 (2016).
211. Bordeleau, M., ElAli, A. & Rivest, S. Severe chronic cerebral hypoperfusion induces microglial dysfunction leading to memory loss in APPswe/PS1 mice. *Oncotarget* **7**, 11864–11880 (2016).
212. Bracko, O. *et al.* Increasing cerebral blood flow improves cognition into late stages in Alzheimer's disease mice. *J Cereb Blood Flow Metab* **40**, 1441–1452 (2020).
213. Libby, P. *et al.* Atherosclerosis. *Nat Rev Dis Primers* **5**, 1–18 (2019).
214. The top 10 causes of death. https://www.who.int/news-room/fact-sheets/detail/the-top-10-causes-of-death.
215. Lusis, A. J. Atherosclerosis. *Nature* **407**, 233–241 (2000).

216. Tabas, I., García-Cardeña, G. & Owens, G. K. Recent insights into the cellular biology of atherosclerosis. *Journal of Cell Biology* **209**, 13–22 (2015).
217. Tabas, I., Williams, K. J. & Borén, J. Subendothelial Lipoprotein Retention as the Initiating Process in Atherosclerosis. *Circulation* **116**, 1832–1844 (2007).
218. Hansson, G. K. & Hermansson, A. The immune system in atherosclerosis. *Nat Immunol* **12**, 204–212 (2011).
219. Frostegård, J. *et al.* Cytokine expression in advanced human atherosclerotic plaques: dominance of pro-inflammatory (Th1) and macrophage-stimulating cytokines. *Atherosclerosis* **145**, 33–43 (1999).
220. Spann, N. J. *et al.* Regulated Accumulation of Desmosterol Integrates Macrophage Lipid Metabolism and Inflammatory Responses. *Cell* **151**, 138–152 (2012).
221. Alexander, M. R. & Owens, G. K. Epigenetic Control of Smooth Muscle Cell Differentiation and Phenotypic Switching in Vascular Development and Disease. *Annual Review of Physiology* **74**, 13–40 (2012).
222. Glagov, S., Weisenberg, E., Zarins, C. K., Stankunavicius, R. & Kolettis, G. J. Compensatory Enlargement of Human Atherosclerotic Coronary Arteries. *N Engl J Med* **316**, 1371–1375 (1987).
223. Shabir, O., Berwick, J. & Francis, S. E. Neurovascular dysfunction in vascular dementia, Alzheimer's and atherosclerosis. *BMC Neurosci* **19**, 62 (2018).
224. Getz, G. S. & Reardon, C. A. Animal Models of Atherosclerosis. *Arterioscler Thromb Vasc Biol* **32**, 1104–1115 (2012).
225. Stylianou, I. M., Bauer, R. C., Reilly, M. P. & Rader, D. J. Genetic Basis of Atherosclerosis: Insights from Mice and Humans. *Circ Res* **110**, 337–355 (2012).
226. Feingold, K. R. Introduction to Lipids and Lipoproteins. in *Endotext* (eds. Feingold, K. R. et al.) (MDText.com, Inc., 2000).
227. Ishibashi, S., Goldstein, J. L., Brown, M. S., Herz, J. & Burns, D. K. Massive xanthomatosis and atherosclerosis in cholesterol-fed low density lipoprotein receptor-negative mice. *J. Clin. Invest.* **93**, 1885–1893 (1994).
228. Getz, G. S. & Reardon, C. A. Diet and murine atherosclerosis. *Arterioscler Thromb Vasc Biol* **26**, 242–249 (2006).
229. Hartvigsen, K. *et al.* A Diet-Induced Hypercholesterolemic Murine Model to Study Atherogenesis Without Obesity and Metabolic Syndrome. *Arteriosclerosis, Thrombosis, and Vascular Biology* **27**, 878–885 (2007).
230. Sanan, D. A. *et al.* Low density lipoprotein receptor-negative mice expressing human apolipoprotein B-100 develop complex atherosclerotic lesions on a chow diet: No accentuation by apolipoprotein(a). *Proceedings of the National Academy of Sciences* **95**, 4544–4549 (1998).
231. Li, B. *et al.* Atherosclerosis is associated with a decrease in cerebral microvascular blood flow and tissue oxygenation. *PLOS ONE* **14**, e0221547 (2019).

232. Lu, Y. *et al.* Impact of atherosclerotic disease on cerebral microvasculature and tissue oxygenation in awake LDLR−/−hApoB+/+ transgenic mice. *Neurophotonics* **6**, 045003 (2019).
233. Mahley, R. W. Apolipoprotein E: Cholesterol Transport Protein with Expanding Role in Cell Biology. *Science* **240**, 622–630 (1988).
234. Sehayek, E. *et al.* Apolipoprotein E regulates dietary cholesterol absorption and biliary cholesterol excretion: Studies in C57BL/6 apolipoprotein E knockout mice. *Proceedings of the National Academy of Sciences* **97**, 3433–3437 (2000).
235. Plump, A. S. & Breslow, J. L. Apolipoprotein E and the Apolipoprotein E-Deficient Mouse. *Annual Review of Nutrition* **15**, 495–518 (1995).
236. Chirico, E. N. *et al.* Magnetic resonance imaging biomarkers of exercise-induced improvement of oxidative stress and inflammation in the brain of old high-fat-fed ApoE−/− mice. *The Journal of Physiology* **594**, 6969–6985 (2016).
237. Kumar, S., Kang, D.-W., Rezvan, A. & Jo, H. Accelerated atherosclerosis development in C57Bl6 mice by overexpressing AAV-mediated PCSK9 and partial carotid ligation. *Lab Invest* **97**, 935–945 (2017).
238. Bjørklund, M. M. *et al.* Induction of Atherosclerosis in Mice and Hamsters Without Germline Genetic Engineering. *Circulation Research* **114**, 1684–1689 (2014).
239. Poirier, S. *et al.* The Proprotein Convertase PCSK9 Induces the Degradation of Low Density Lipoprotein Receptor (LDLR) and Its Closest Family Members VLDLR and ApoER2 *. *Journal of Biological Chemistry* **283**, 2363–2372 (2008).
240. Abifadel, M. *et al.* Mutations in PCSK9 cause autosomal dominant hypercholesterolemia. *Nat Genet* **34**, 154–156 (2003).
241. Cohen, J. C., Boerwinkle, E., Mosley, T. H. & Hobbs, H. H. Sequence variations in PCSK9, low LDL, and protection against coronary heart disease. *N Engl J Med* **354**, 1264–1272 (2006).
242. Maxwell, K. N. & Breslow, J. L. Adenoviral-mediated expression of Pcsk9 in mice results in a low-density lipoprotein receptor knockout phenotype. *Proceedings of the National Academy of Sciences* **101**, 7100–7105 (2004).
243. Le May, C. *et al.* Proprotein Convertase Subtilisin Kexin Type 9 Null Mice Are Protected From Postprandial Triglyceridemia. *Arteriosclerosis, Thrombosis, and Vascular Biology* **29**, 684–690 (2009).
244. Creemers, J. W. M. & Khatib, A.-M. Knock-out mouse models of proprotein convertases: unique functions or redundancy? *FBL* **13**, 4960–4971 (2008).
245. Toledo, J. B. *et al.* Contribution of cerebrovascular disease in autopsy confirmed neurodegenerative disease cases in the National Alzheimer's Coordinating Centre. *Brain* **136**, 2697–2706 (2013).
246. Breteler, M. M. B. Vascular risk factors for Alzheimer's disease:: An epidemiologic perspective. *Neurobiology of Aging* **21**, 153–160 (2000).
247. Casserly, I. P. & Topol, E. J. Convergence of Atherosclerosis and Alzheimer's Disease: Cholesterol, Inflammation, and Misfolded Proteins. *Discovery Medicine* (2009).

248. Luchsinger, J. *et al.* Aggregation of Vascular Risk Factors and Risk of Incident Alzheimer's Disease. *Neurology* **65**, 545–551 (2005).
249. Knopman, D. S. *et al.* Midlife vascular risk factors and midlife cognitive status in relation to prevalence of mild cognitive impairment and dementia in later life: The Atherosclerosis Risk in Communities Study. *Alzheimers Dement* **14**, 1406–1415 (2018).
250. Hofman, A. *et al.* Atherosclerosis, apolipoprotein E, and prevalence of dementia and Alzheimer's disease in the Rotterdam Study. *The Lancet* **349**, 151–154 (1997).
251. Roher, A. E. *et al.* Circle of Willis Atherosclerosis Is a Risk Factor for Sporadic Alzheimer's Disease. *Arteriosclerosis, Thrombosis, and Vascular Biology* **23**, 2055–2062 (2003).
252. Beach, T. G. *et al.* Circle of Willis atherosclerosis: association with Alzheimer's disease, neuritic plaques and neurofibrillary tangles. *Acta Neuropathol* **113**, 13–21 (2007).
253. Gustavsson, A.-M. *et al.* Midlife Atherosclerosis and Development of Alzheimer or Vascular Dementia. *Annals of Neurology* **87**, 52–62 (2020).
254. Rivera-Rivera, L. A. *et al.* Assessment of vascular stiffness in the internal carotid artery proximal to the carotid canal in Alzheimer's disease using pulse wave velocity from low rank reconstructed 4D flow MRI. *J Cereb Blood Flow Metab* **41**, 298–311 (2021).
255. De Meyer, G. *et al.* Platelet phagocytosis and processing of beta-amyloid precursor protein as a mechanism of macrophage activation in atherosclerosis. *Circulation research* **90**, 1197–204 (2002).
256. Kokjohn, T. A. *et al.* Chemical characterization of pro-inflammatory amyloid-beta peptides in human atherosclerotic lesions and platelets. *Biochimica et Biophysica Acta (BBA) - Molecular Basis of Disease* **1812**, 1508–1514 (2011).
257. Stakos, D. A. *et al.* The Alzheimer's Disease Amyloid-Beta Hypothesis in Cardiovascular Aging and Disease: JACC Focus Seminar. *J Am Coll Cardiol* **75**, 952–967 (2020).
258. Stamatelopoulos, K. *et al.* Amyloid-beta (1-40) and the risk of death from cardiovascular causes in patients with coronary heart disease. *J Am Coll Cardiol* **65**, 904–916 (2015).
259. Shabir, O. *et al.* Preclinical models of disease and multimorbidity with focus upon cardiovascular disease and dementia. *Mechanisms of Ageing and Development* **192**, 111361 (2020).
260. Tibolla, G. *et al.* Increased atherosclerosis and vascular inflammation in APP transgenic mice with apolipoprotein E deficiency. *Atherosclerosis* **210**, 78–87 (2010).
261. Jung, Y. Y. *et al.* Atherosclerosis is exacerbated by chitinase-3-like-1 in amyloid precursor protein transgenic mice. *Theranostics* **8**, 749 (2018).

262. Van De Parre, T. J. L. *et al.* Attenuated atherogenesis in apolipoprotein E-deficient mice lacking amyloid precursor protein. *Atherosclerosis* **216**, 54–58 (2011).
263. Gupta, A. & Iadecola, C. Impaired Aβ clearance: a potential link between atherosclerosis and Alzheimer's disease. *Frontiers in Aging Neuroscience* **7**, (2015).
264. Roberts, K. F. *et al.* Amyloid-β efflux from the CNS into the plasma. *Ann Neurol* **76**, 837–844 (2014).
265. Ghribi, O., Larsen, B., Schrag, M. & Herman, M. M. High cholesterol content in neurons increases BACE, beta-amyloid, and phosphorylated tau levels in rabbit hippocampus. *Exp Neurol* **200**, 460–467 (2006).
266. Thirumangalakudi, L. *et al.* High cholesterol-induced neuroinflammation and amyloid precursor protein processing correlate with loss of working memory in mice. *J Neurochem* **106**, 475–485 (2008).
267. Refolo, L. M. *et al.* Hypercholesterolemia accelerates the Alzheimer's amyloid pathology in a transgenic mouse model. *Neurobiol Dis* **7**, 321–331 (2000).
268. Hohsfield, L. A., Daschil, N., Orädd, G., Strömberg, I. & Humpel, C. Vascular pathology of 20-month-old hypercholesterolemia mice in comparison to triple-transgenic and APPSwDI Alzheimer's disease mouse models. *Molecular and Cellular Neuroscience* **63**, 83–95 (2014).
269. Grames, M. S. *et al.* Gene Transfer Induced Hypercholesterolemia in Amyloid Mice. *Journal of Alzheimer's Disease* **65**, 1079–1086 (2018).
270. Whitesell, J. D. *et al.* Whole brain imaging reveals distinct spatial patterns of amyloid beta deposition in three mouse models of Alzheimer's disease. *J Comp Neurol* **527**, 2122–2145 (2019).
271. Santiago, J. A. & Potashkin, J. A. The Impact of Disease Comorbidities in Alzheimer's Disease. *Front Aging Neurosci* **13**, 631770 (2021).
272. Duthie, A., Chew, D. & Soiza, R. L. Non-psychiatric comorbidity associated with Alzheimer's disease. *QJM: An International Journal of Medicine* **104**, 913–920 (2011).
273. Bos, D. *et al.* Atherosclerotic calcification is related to a higher risk of dementia and cognitive decline. *Alzheimer's & Dementia* **11**, 639-647.e1 (2015).

Chapter 2: The effects of locomotion on sensory-evoked haemodynamic responses in the cortex of awake mice

This manuscript was published in Scientific Reports in April 2022

Eyre, B., Shaw, K., Sharp, P., Boorman, L., Lee, L., Shabir, O., ... & Howarth, C. (2022). The effects of locomotion on sensory-evoked haemodynamic responses in the cortex of awake mice. Scientific Reports, 12(1), 6236.

The effects of locomotion on sensory-evoked haemodynamic responses in the cortex of awake mice

Beth Eyre[1,2,3^*], Kira Shaw[1,5^], Paul Sharp[1,6], Luke Boorman[1], Llywelyn Lee[1,2,3], Osman Shabir[1,2,3,4], Jason Berwick[1,2,3+], Clare Howarth[1,2,3+]

[1]Sheffield Neurovascular Lab, Department of Psychology, University of Sheffield, Alfred Denny Building, Western Bank, Sheffield, S10 2TN (United Kingdom)
[2]Neuroscience Institute, University of Sheffield, Sheffield, S10 2TN (United Kingdom)
[3]Healthy lifespan Institute, University of Sheffield, Sheffield, S10 2TN (United Kingdom)
[4]Department of Infection, Immunity & Cardiovascular Disease (IICD), University of Sheffield Medical School, Royal Hallamshire Hospital, Beech Hill Road, Sheffield, S10 2RX (United Kingdom)
[5]School of Psychology and Sussex Neuroscience, University of Sussex, Falmer, Brighton, United Kingdom
[6]Medicines Discovery Catapult, Mereside, Alderley Park, Alderley Edge, SK10 4TG
[^]These authors contributed equally. [+]These authors contributed equally. * Corresponding author.

I Beth Eyre am a joint first author on this published research paper. I completed data analysis, statistical tests and wrote up the manuscript.

Kira Shaw completed surgeries and imaging experiments. Paul Sharp completed surgeries and imaging experiments. Myself, Clare Howarth and Jason Berwick analysed the data. Luke Boorman, Kira Shaw, myself, Clare Howarth and Jason Berwick wrote code for the analysis. Myself, Kira Shaw, Llywelyn Lee, Osman Shabir, Clare Howarth and Jason Berwick edited and proofread the manuscript.

2.1 Abstract

Investigating neurovascular coupling in awake rodents is becoming ever more popular due, in part, to our increasing knowledge of the profound impacts that anaesthesia can have upon brain physiology. Although awake imaging brings with it many advantages, we still do not fully understand how voluntary locomotion during imaging affects sensory-evoked haemodynamic responses. In this study we investigated how evoked haemodynamic responses can be affected by the amount and timing of locomotion. Using an awake imaging set up, we used 2D-Optical Imaging Spectroscopy (2D-OIS) to measure changes in cerebral haemodynamics within the sensory cortex of the brain during either 2 s whisker stimulation or spontaneous (no whisker stimulation) experiments, whilst animals could walk on a spherical treadmill. We show that locomotion alters haemodynamic responses. The amount and timing of locomotion relative to whisker stimulation is important, and can significantly impact sensory-evoked haemodynamic responses. If locomotion occurred before or during whisker stimulation, the amplitude of the stimulus-evoked haemodynamic response was significantly altered. Therefore, monitoring of locomotion during awake imaging is necessary to ensure that conclusions based on comparisons of evoked haemodynamic responses (e.g., between control and disease groups) are not confounded by the effects of locomotion.

2.2 Introduction

When neurons fire, there follows a localised increase in blood flow to that same brain region. This relationship between neuronal firing and an increase in blood flow is known as neurovascular coupling (NVC), and underpins the principles of blood oxygen level dependent functional magnetic resonance imaging (BOLD fMRI). NVC ensures that the brain receives prompt increases in cerebral blood flow (CBF) to activated regions of the brain, allowing for the rapid delivery of essential nutrients such as O2 and glucose and the removal of waste products such as CO_2 and lactate[1]. This mechanism is important for healthy brain function; accumulating evidence suggests that NVC is impaired in several neurological disorders, including Alzheimer's disease[2–5]. Therefore, understanding how NVC may be altered by disease is integral to furthering our understanding of the onset and progression of such diseases.

Over the last 50 years, the neurovascular field has been revolutionised by the advent of new scientific methods. The development of techniques such as wide-field optical imaging[6,7] and two-photon microscopy[8], alongside advances in the development of genetically-encoded calcium indicators such as GCAMP[9], have been vital in furthering our knowledge of the inner workings of the brain. Just considering the last twenty years, we have discovered the potential role of pericytes[10–12] astrocytes[13–15] and even caveolae[16] in NVC. Many studies investigating NVC, including several of those previously mentioned were conducted under anaesthesia. The use of anaesthesia has allowed the field to gain an in-depth insight into neural activity and the subsequent haemodynamic response in a controlled environment. However, anaesthesia is not without its pitfalls[17]. Not only does anaesthesia dampen neural activity but it can also reduce many aspects of the haemodynamic response—including blood oxygenation, CBF and cerebral blood volume (CBV)[18,19] in addition to delaying the time-course of the haemodynamic response[18].

To mitigate these effects, several groups, including our own, have developed anaesthetic regimes that produce stable haemodynamic responses, of similar timing and magnitude to those in the awake preparation[20–22]—these regimes can produce stable responses without the confounds of behaviour. Despite this, many groups have begun to move away from the use of anaesthesia. A growing number of studies have used awake, moving animals to investigate NVC and the roles of cells within the neurovascular unit (NVU)[16,23,24].

Studies using electrophysiology, two-photon microscopy and intrinsic optical signal (IOS) imaging have shown that locomotion can generate robust increases in neural activity, vessel diameter, and CBV, respectively[23,25,26]. While these studies focused on how locomotion itself impacts brain haemodynamics (within surface vessels of the brain), Tran et al. explored how locomotion may affect sensory-evoked haemodynamic responses. No significant differences in peak amplitude dilation of arterioles were reported when mice were continuously running during whisker stimulation, went from quiet to running in response to whisker stimulation, or when they remained quiet prior to and after whisker stimulation[24]—suggesting that locomotion did not have an impact on sensory-evoked haemodynamic responses. However, the study focused on dilation

changes in penetrating arterioles, and locomotion may affect sensory-evoked haemodynamic responses within the surface vessels of the brain to a different extent, as it has been shown that the narrowing of the Virchow-Robin space may restrict dilations within penetrating arterioles[27].

It is critical to characterise how sensory-evoked haemodynamic responses may be impacted by locomotion for a number of reasons. If sensory-evoked haemodynamic responses are affected by locomotion and locomotion is not monitored, when comparing responses (for example when comparing a disease group to a wild-type (WT) group), differences in neurovascular function could be erroneously assumed to be a consequence of disease, rather than a consequence of differential locomotion.
Therefore, to improve our understanding of how locomotion may impact sensory-evoked haemodynamic responses we used two-dimensional optical imaging spectroscopy (2D-OIS) to investigate changes in cortical blood oxygenation in C57BL/6J mice. We hypothesised that locomotion would increase the amplitude of evoked haemodynamic responses within the cerebral cortex of the brain, as previous research suggests that locomotion leads to greater dilations within surface vessels as compared to penetrating vessels[27]. Additionally, we hypothesised that the time at which locomotion occurred (in relation to the 2 s whisker stimulation) would also impact evoked haemodynamic responses, with locomotion occurring closer to the stimulation onset being expected to increase the amplitude of the evoked haemodynamic response.

2.3 Methods

2.3.1 Animals

Adult (3–12 m; 24–40 g) female C57/BL6J mice (n = 4) were used in the experiment. Food and water were available ad-libitum and mice were housed on a 12 h dark/light cycle. All animal procedures were approved by the UK Home Office and in agreement with the guidelines and scientific regulations of the Animals (Scientific Procedures) Act 1986 with additional approval received from the University of Sheffield licensing committee and ethical review board. The following study is reported in accordance with the ARRIVE guidelines.

2.3.2 Surgery

Induction of anaesthesia was achieved with a combination of fentanyl-fluanisone (Hypnorm, Vetapharm Ltd), midazolam (Hypnovel, Roche Ltd) and sterile water in the ratio 1:1:2 (1 ml/kg i.p). Surgical anaesthetic plane was maintained using isoflurane (0.25–0.8%) in 100% oxygen. Body temperature was monitored and maintained throughout surgery via a rectal thermometer and a homeothermic blanket respectively (Harvard Apparatus). Eyes were protected using Viscotears (Novartis). A scalpel was used to shave the head prior to the mouse being positioned in a stereotaxic frame (Kopf Instruments). Iodine was applied to the scalp and the scalp was removed. Using a dental drill, the bone covering the right somatosensory cortex was thinned to translucency to create the thinned optical window (~ 3 mm2). Cyanoacrylate glue was thinly applied across the window to strengthen the window and reduce optical specularities. Dental cement (Superbond C & B; Sun Medical) was applied to the bone on the contralateral side of the cranial window and a well was built up around the window to allow for a metal head plate to be attached for chronic imaging. Following surgery, mice were housed individually and given at least one week to recover before any imaging commenced.

2.3.3 Awake imaging

Prior to imaging, mice were gradually habituated to the experimenter, imaging room, spherical treadmill and head-fixation. To achieve this, training sessions were completed with a reward at the end of each session (toffee popcorn, Sunkist). The first session lasted approximately 10 min. The experimenter handled the mice and allowed the mice to explore the spherical treadmill without head fixation. The second session was a repeat of the first session. Session three involved head-fixing the mice for approximately 10 min whilst the lights were on. This was followed by ~ 20 min with the lights off. Session three was repeated daily until mice learned how to move on the spherical treadmill and displayed grooming behaviours (approximately 2–3 sessions). The whisker stimulator was introduced during the final two training sessions.

2.3.4 Whisker stimulation

Whiskers were mechanically stimulated using a plastic T-bar at 5 Hz. Each experiment lasted 1475 s and comprised of 59 25 s trials. During whisker stimulation trials whisker deflection lasted 2 s, occurring every 25 s. Spontaneous experiments were also

conducted using the same timings as 2 s whisker stimulation experiments, however the motor controlling the whisker stimulator was switched off, ensuring whiskers were not stimulated.

2.3.5 Locomotion data collection and analysis

Locomotion data was collected from a spherical treadmill with an optical motion sensor attached, to quantify locomotion. Locomotion data was analysed using in-house created scripts in MATLAB (MathWorks). The optical motion sensor recorded the movement of the treadmill and produced a file comprised of: locomotion data (a vector which showed the rotation of the treadmill, integers were used to quantify the displacement of the treadmill, with stationary periods reflected by 0, the quicker the spherical treadmill moved, the higher the integer; plotted as distance (arbitrary unit, AU)); the time vector (which allowed locomotion to be measured across time (s)); and the trigger points (these indicated the timing of the whisker stimulation, across trials, this enabled locomotion data to be matched with the timing of the haemodynamic data). To establish if locomotion did impact evoked-haemodynamic responses, 2 s whisker stimulation trials were ranked by voluntary locomotion across the entire trial (25 s) and across different 5 s time windows within the stimulation period (− 5 to 0 s, 0–5 s, 5–10 s, 10–15 s, 15–20 s). For each session, evoked haemodynamic time series were created from the top and bottom 10% of ranked trials, these top and bottom 10% of ranked trials were averaged together across sessions and corresponded to trials in which the most and least locomotion occurred (21 sessions from 4 animals, n = 6 top & n = 6 bottom trials per session (an average of the top and bottom ranked trials was taken for each session and used in the visualisation/analysis)). In Fig. 2.5 (Column 2), HbT spatial maps for spontaneous locomotion were created as followed. Locomotion events from spontaneous trials were selected and a spectroscopy file was created to assess how locomotion alone impacts the spatial spread of HbT within the surface vasculature.

2.3.6 2D-Optical Imaging Spectroscopy (2D-OIS)

2D-OIS uses light to measure cortical haemodynamic signals by estimating concentration changes in oxygenated haemoglobin (HbO), deoxygenated haemoglobin (HbR) and total haemoglobin (HbT). In order to measure changes in cortical haemodynamics a Lambda DG-4 high-speed galvanometer (Sutter Instrument

Company, USA) was used to illuminate the right somatosensory cortex with 4 wavelengths of light (494 ± 20 nm, 560 ± 5 nm, 575 ± 14 nm and 595 ± 5 nm). A Dalsa 1M60 CCD camera was used to capture remitted light at 184 × 184 pixels, at a 32 Hz frame rate, this provided a resolution of ~ 75 μm.

To produce 2D images of micromolar changes in HbO, HbR and HbT, spectral analysis (based on the path length scale algorithm (PLSA)) was conducted[28,29]. This algorithm uses a modified Beer Lambert Law, with a path-length correction factor and predicted absorption values of HbO, HbR and HbT. The relative concentration estimates of HbO, HbR and HbT were gathered from baseline values, whereby haemoglobin tissue concentration was estimated as 100 μM, with tissue saturation of oxygen estimated at 80%.

2.3.7 Regions of Interest (ROI) overlying the whisker barrels from 2D spatial maps

MATLAB (MathWorks) was used to select ROI for time series analysis. Custom-made in-house scripts were used to select ROIs from the 2D spatial maps produced using 2D-OIS. The whisker ROI was selected using the HbT spatial map taken from the 2 s whisker stimulation experiments; this was completed for each of the 21 sessions. Pixels were included in the 'active' region if they were > 1.5 × STD across the entire spatial map, hence the whisker ROI (red ROI, Fig. 2.5, Column 1) was the area of cortex with the greatest haemodynamic response for HbT. The following time series analyses included in the study (Figs. 2.2, 2.3 and 2.4) were conducted for the whisker region.

2.3.8 Statistical analysis

Statistical tests were conducted in SPSS (v26) and figures were created in MATLAB and RStudio. P values of < 0.05 were deemed to be significant. Outliers were assessed using box plots, with values greater than 1.5 box lengths from the edge of the box classified as outliers—outliers were kept in the data set. Normality was assessed using the Shapiro Wilk test. If outliers were observed and/or data was non-normal, non-parametric tests were used (if available). For distance travelled calculations, the total distance (AU) from each session for experiments with and without whisker stimulation were used—with the total sum of distance travelled taken

for each experiment during each of the 21 sessions. A sign test was used to assess if there was a statistically significant difference in distance travelled during experiments. Non-parametric Sign tests (HbT and HbO) and the Wilcoxon signed ranks test (HbR) were used to assess if there were significant differences in HbO, HbR and HbT peaks during the 2 s whisker stimulation when comparing trials with the greatest and least amount of locomotion (when locomotion was ranked across the entire 25 s). The peak amplitude of HbT, HbO and HbR were computed as the time point with the greatest change in the concentration of haemoglobin from baseline[20] between 0 and 5 s during the ranked trials where the most and least locomotion occurred. Sign tests (HbT and HbR) and the Wilcoxon signed ranks test (HbO) were used to establish if there were significant differences in the return to baseline of HbT, HbO and HbR, when comparing trials in which the most and least locomotion occurred during a 2 s whisker stimulation—mean HbT, HbO and HbR values were taken at the end of the 25 s stimulation period (mean values between 15 and 20 s). Six, two-way repeated measures ANOVAs were completed to assess if there was an effect of the amount (factors: most & least) and timing (factors: − 5 to 0 s, 0–5 s, 5–10 s, 10–15 s, 15–20 s) of locomotion on the peak of the haemodynamic response (dependent variables: HbT, HbO, HbR) to the 2 s whisker stimulation (peak occurring between 0–5 s). The presence of outliers was assessed using studentised residuals, where values greater than ± 3 were deemed to be outliers. Outliers were observed and were kept in the data set. Normality was assessed by the Shapiro Wilk test, and sphericity was assessed using the Mauchly's test of sphericity. For the two-way ANOVAs, a number of variables were not normally distributed (see Supplementary Statistics Table S9). If Mauchly's sphericity was violated ($p < 0.05$) Greenhouse Geiser correction was used. The use of the Greenhouse Geiser correction can be observed if there is an epsilon (ε) value when reporting ANOVA results. As there is no non-parametric alternative for a two-way ANOVA if variables were not normally distributed and outliers were present, a two-way ANOVA was still completed, as ANOVAs are robust to slight deviations from normality. Data were not transformed as transforming the data results in difficulties comparing the means across different groups[30]. If an interaction effect was found, to assess the simple main effects, one-way ANOVAs were completed and pairwise comparisons with a Bonferroni correction were completed. Data are reported as means ± standard error of the mean (SEM), unless otherwise stated. Individual dots

on violin plots and bar charts represent individual mean data points. Data was visualised as a bar plot when statistical tests compared the mean, whereas violin plots were used when statistical tests compared the median. Detailed statistical outputs can be found in the “Supplementary tables”. Apriori power calculations were not conducted for the study as the dataset had already been collected. However, a post-hoc power calculation was run to assess whether the sample size used in the study was adequately powered. Using an alpha value of α=0.05, and a total sample size of 21, a Cohens f effect size of 0.816 was calculated (using the n^2 value = .400 of a two-way ANOVA for the interaction result for HbT responses (timing: 5 factors and walking: 2 factors). This resulted in a power of 1, suggesting the sample sizes used in the study provided adequate power for the above tests. Additionally, effect sizes were calculated for the two-way repeated measures ANOVAs and can be found in the supplementary tables.

2.4 Results

2.4.1 Locomotion alters the sensory-evoked haemodynamic response

Animals received a thinned cranial window surgery to allow 2D-OIS to measure changes in cerebral haemodynamics (Fig. 2.1 a,b)—specifically changes in oxygenated haemoglobin (HbO), deoxygenated haemoglobin (HbR) and total haemoglobin (HbT). During imaging, animals could move on a spherical treadmill whilst whiskers could be stimulated with a mechanical T-bar (Fig. 2.1 a). The treadmill was attached to an optical motion sensor, which allowed us to assess the impact that the amount and timing of locomotion (in isolation and also relative to whisker stimulation) had on the haemodynamic response. Twenty-one individual recording sessions, each with 59 trials, made up the 2 s whisker stimulation data set. For each session, trials were ranked by voluntary locomotion occurring at different time points relative to the whisker stimulation. Evoked haemodynamic time series were generated from the top (n = 6 trials per session) and bottom (n = 6 trials per session) 10% of locomotion-ranked trials, corresponding to trials in which the most and least locomotion occurred, and were averaged across the 21 sessions. All-time series analyses were conducted on the whisker ROI (Fig. 2.1 b, and Fig. 2.5 column 1).

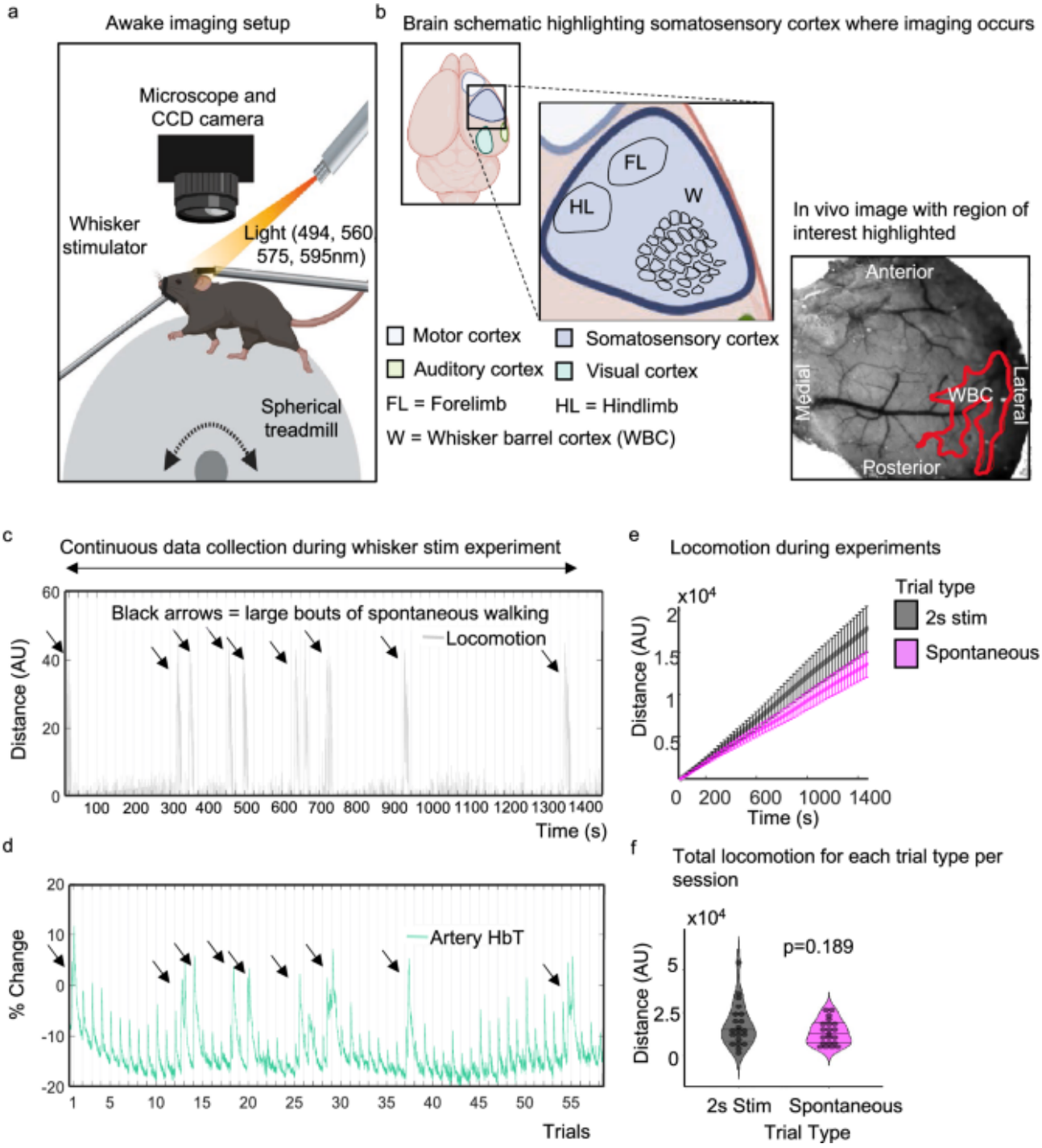

Figure 2.1: Awake imaging experimental set up

(a) Animals were head fixed and could run on a spherical treadmill Locomotion data was collected using an optical motion sensor (attached to the ball—not shown). Light (495, 559, 575, 587 nm) was shone onto the thinned cranial window, and haemodynamic responses were collected during 2 s whisker stimulation trials and during spontaneous (no whisker stimulation) trials. (b) Shows a schematic of the

mouse brain, zooming in on the somatosensory cortex where imaging occurs, a representative in vivo image with the whisker ROI is also shown. (c) and (d) show representative plots of the distance travelled (grey) and percentage change in HbT (green, taken from an artery within the whisker ROI (see in vivo image (b)) across the 2 s whisker experiment (continuous data recording of the 59 whisker-stimulation trials taken from one representative animal/session, black lines on x axis mark individual 25 s stimulation trials) respectively. Black arrows show large bouts of spontaneous walking. (e) shows total distance travelled during whisker stimulation trials (black/grey) compared to spontaneous trials (pink) averaged for all 21 sessions. Error bars represent ± SEM. (f) shows a violin plot with individual points to show the distance travelled during each session for the different trial types (2 s whisker stimulation and spontaneous trials with no whisker stimulation) (Sign test p = 0.189). Black lines on violin plot represent interquartile range and median. Awake imaging experimental figure (a) and (b) created with BioRender.com. (b) ((in vivo image) also used in Sharp et al.,[20] , see Fig. 2.4B).

A representative locomotion and HbT response is shown in Fig. 2.1 c,d. Throughout the stimulations (marked on the x-axis), HbT responses to individual whisker stimulation trials can be observed. Large increases in HbT can be seen that coincide with spontaneous walking events (black arrowheads).

First, we checked whether the presence of whisker stimulation changes the amount of locomotion (Fig. 2.1 e,f). A sign test with continuity correction revealed there was no statistically significant difference in the median distance travelled (Median ± SEM: − 1517 ± 2065) in experiments with a 2 s whisker stimulation (Median ± SEM: 14,894 ± 2732), compared to experiments without whisker stimulation (Median ± SEM: 12,360 ± 1532, z = 1.309, p = 0.189).

We then looked at whether locomotion alters the evoked haemodynamic response. To do this we examined the effects of locomotion across the entire 25 s trial period for the top and bottom 10% of trials ranked by locomotion. We examined how the greatest amount of locomotion influenced the evoked haemodynamic response as compared to the evoked haemodynamic response when the animals moved the least (Fig. 2.2

a–c). Sign tests with continuity correction revealed there were no statistically significant median differences in HbT peak (during a 2 s whisker stimulation) (Median ± SEM: 0.003 ± 0.007) and HbO peak (Median ± SEM: − 0.0004 ± 0.008) during trials with the greatest locomotion (Median ± SEM: HbT: 1.038 ± 0.007, HbO: 1.057 ± 0.009), as compared to when a stimulation occurred during trials with the least locomotion (Median ± SEM: HbT: 1.028 ± 0.003, $z = -0.873$, $p = 0.383$, HbO: 1.049 ± 0.005, $z = 0.000$, $p = 1.000$) (Fig. 2.2 b–e). Additionally, a Wilcoxon signed ranks test revealed no significant median difference in HbR peak (during a 2 s whisker stimulation) (Median ± SEM: − 0.0004 ± 0.005) during trials with the greatest locomotion (Median ± SEM: 0.948 ± 0.006), as compared to when a stimulation occurred during trials with the least locomotion (Median ± SEM: 0.945 ± 0.005, $z = -0.330$, $p = 0.741$) (Fig. 2.2 b,c,f).

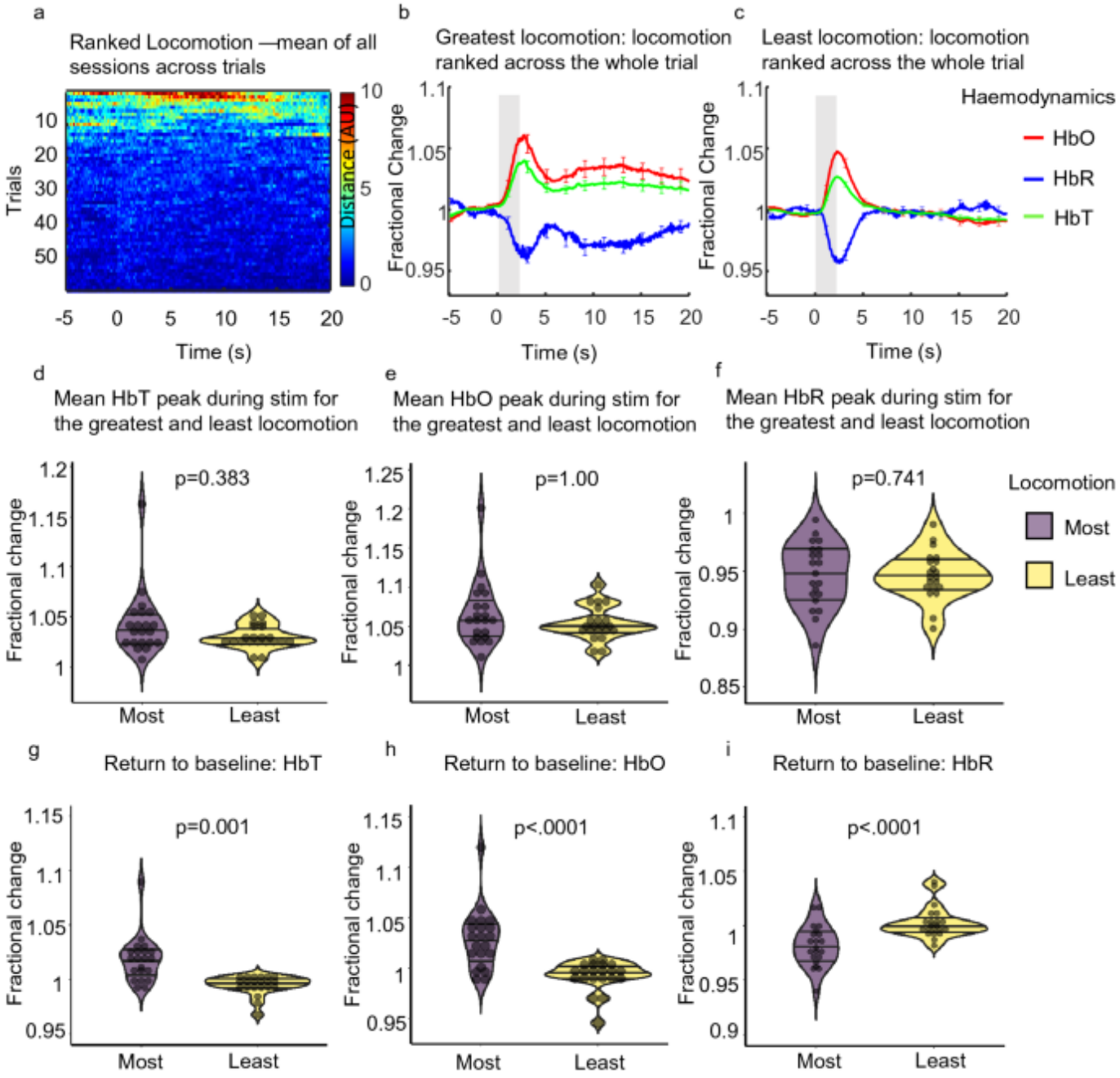

Figure 2.2: Mean sensory evoked haemodynamic responses in the whisker ROI *(Fig. 2.5 column 1) for trials ranked with the greatest and least locomotion across the entire 25 s trial. (a) Heat map showing locomotion traces for the 59 whisker-stimulation trials ranked by locomotion (across the whole 25 s trial), (b) and (c) show mean fractional changes from baseline in HbO, HbR and HbT during a 2 s whisker stimulation (grey shaded bar) when locomotion was ranked across the whole trial*

(between − 5 and 20 s). 'Greatest locomotion' (left) represents the top 10% of these ranked trials, which correspond to trials with the most locomotion during the entire 25 s trial recording (− 5 to 20 s) (21 sessions from 4 animals; per session n = 6 top trials (an average of the top ranked trials was taken for each session)). 'Least locomotion' (right) represents the bottom 10% of ranked trials, which correspond to trials in which the least amount of locomotion occurred during the 25 s recording (21 sessions from 4 animals; per session n = 6 bottom trials (an average of the bottom ranked trials was taken for each session). Error bars represent mean ± SEM between the total 126 trials. (d–f) show mean sensory-evoked peak values for HbT, HbO and HbR respectively, for trials in which the most and least locomotion occurred when locomotion was ranked across the entire trial (25 s). Violin plots show individual mean values overlaid. Black horizontal lines indicate interquartile range and median. p values are from Sign tests for HbT and HbO and from Wilcoxon Signed Ranks test for HbR. (g–i) show the mean return to baseline values (mean values taken between 15 and 20 s) for HbT, HbO and HbR respectively, for trials in which the most and least locomotion occurred when locomotion was ranked across the entire trial (25 s). p values from Sign tests for HbT and HbR and Wilcoxon Signed ranks test for HbO. Black horizontal lines on violin plots indicate interquartile range and median.

However, in trials where the greatest locomotion occurred (Fig. 2.2 b) a slower return to baseline for HbT, HbO and HbR was observed (as compared to trials where the least locomotion occurred). We took mean values of HbT, HbO and HbR between 15 and 20 s to assess the return to baseline differences across the two behaviours. Sign tests with continuity correction revealed a statistically significant median increase in HbT (Median ± SEM: 0.024 ± 0.005) and a median decrease in HbR (Median ± SEM: − 0.021 ± 0.005) at the end of the 25 s stimulation period during trials with the greatest locomotion (Median ± SEM: HbT: 1.019 ± 0.005, HbR: 0.980 ± 0.004) compared to trials where the least locomotion occurred (Median ± SEM: HbT: 0.997 ± 0.002, $z = -3.055$, $p = 0.001$, HbR: 0.999 ± 0.003, $z = 3.491$, $p < 0.0001$). A Wilcoxon signed ranks test revealed a statistically significant median increase in HbO (Median ± SEM: 0.032 ± 0.007) at the end of the 25 s stimulation period during trials with the greatest locomotion (Median ± SEM: 1.030 ± 0.006) compared to trials where the least locomotion occurred (Median ± SEM: 0.994 ± 0.003, $z = -3.702$, $p < 0.0001$) (Fig. 2.2 b,c,g–i).

The above results reveal that when locomotion is ranked across the entire trial, the evoked-haemodynamic responses are similar when comparing greatest and least locomotion trials. However, for the greatest locomotion trials the return to baseline is prolonged.

2.4.2 The timing of locomotion (relative to whisker stimulation) impacts the sensory-evoked haemodynamic response

As we have shown that locomotion across the whole trial can alter the return to baseline of the sensory-evoked haemodynamic response we wanted to investigate in more detail how the timing of locomotion (relative to whisker stimulation) impacted the sensory-evoked response.

To do this, trials taken during the 2 s whisker stimulation experiment were ranked by the amount of voluntary locomotion occurring across different 5 s time windows (pre-stim: − 5 to 0 s, mid-stim: 0–5 s, post-stim: 5–10 s, 10–15 s, 15–20 s; Fig. 2.3, Column 1). Evoked haemodynamic time series were created from the top and bottom 10% of ranked trials, these top and bottom 10% of ranked trials were averaged across sessions and corresponded to trials in which the most and least locomotion occurred

(21 sessions; n = 6 top & n = 6 bottom per session (an average of the top and bottom ranked trials was taken for each session and used in the visualisation/analysis)) during the different 5 s time windows (Fig. 2.3). All mean peak values were taken between 0 and 5 s and are referred to as occurring during the whisker stimulation.

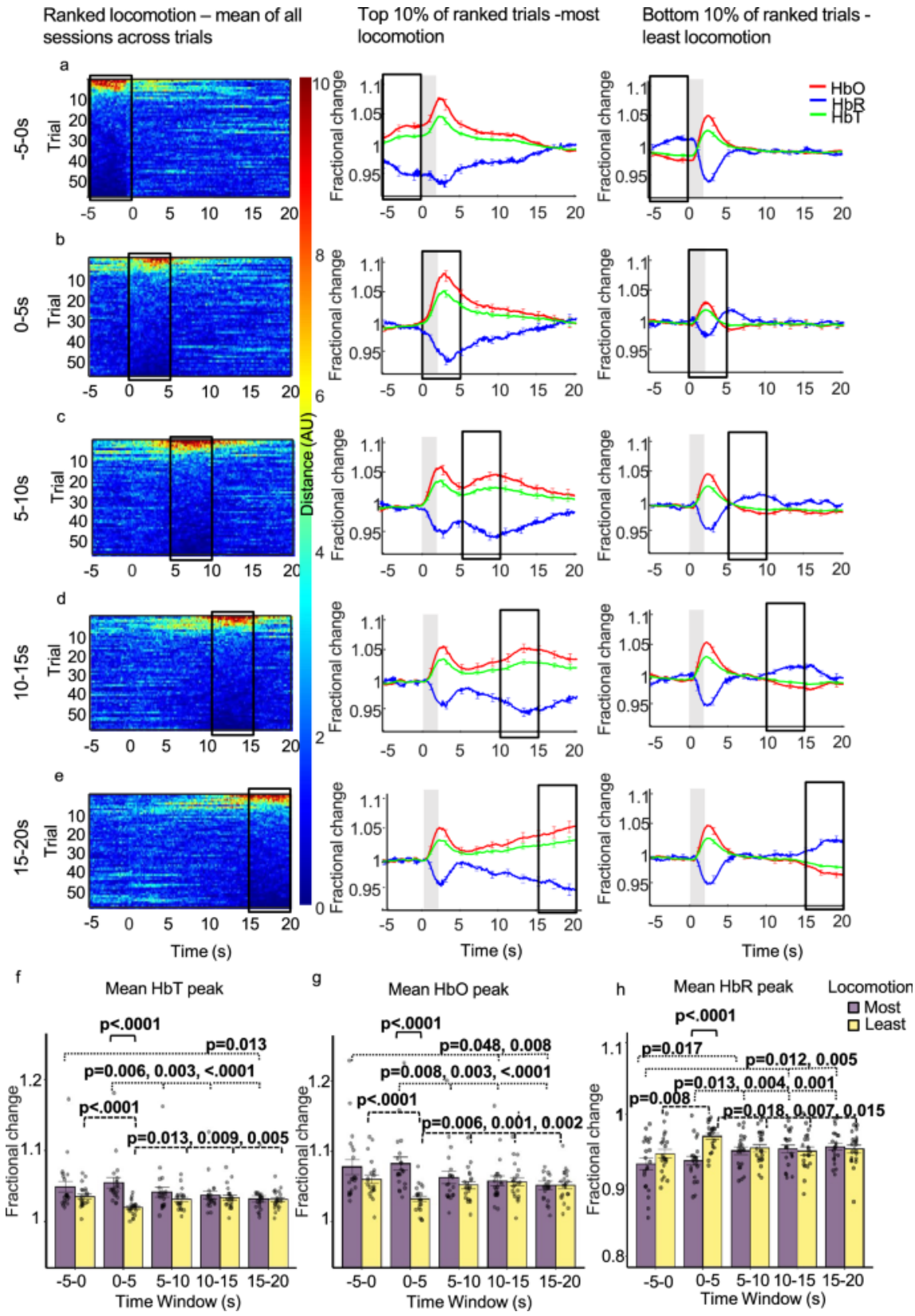

Figure 2.3: Mean sensory-evoked haemodynamic responses for the whisker ROI (Fig. 2.5 column 1) during trials where the most and least locomotion occurred with locomotion ranked at different time windows throughout the 25 s trial

Whisker stimulation between 0 and 2 s (grey bar in centre and right columns). Column one: heat maps showing locomotion traces for the 59 whisker-stimulation trials, with locomotion ranked at different 5 s time windows during the 25 s trial (each ranked trial was averaged across 21 sessions/4 animals). The different 5 s windows during the 25 s trial where locomotion was ranked are: before (a: − 5 to 0 s), during (b: 0–5 s) and after whisker stimulation (c: 5–10 s, d: 10–15 s, e: 15–20 s). Trials were ranked according to locomotion in these 5 s periods and presented in descending order. Colour bar indicates amount of locomotion, red pixels indicate more and dark blue indicate less locomotion. Column two: mean fractional changes from baseline in stimulation-dependent HbT, HbO and HbR taken from the top 10% of ranked locomotion trials across the different 5 s time windows (21 sessions/4 animals; n = 6 top per session (mean of top trials taken for each session, mean of all sessions used in the visualisation/analysis). Column three: mean fractional changes in stimulation-dependent HbT, HbO and HbR for the bottom 10% of locomotion trials ranked across the 5 s time windows throughout the trial (21 sessions/4 animals; n = 6 bottom per session (mean of bottom trials taken for each session, mean of all sessions used in the visualisation/analysis). Black boxes indicate the 5 s time window locomotion was ranked. Data show mean across the total 126 trials ± SEM. (f–h) show mean ± SEM between groups and individual mean peak values per session for HbT, HbO and HbR. Two-way repeated measures ANOVA's were completed for HbT, HbO and HbR. Significant interactions were found and simple effects run (time and locomotion) for each haemodynamic measure. p values from pairwise comparisons (Bonferroni correction) are reported. Black solid brackets indicate comparison between most and least locomotion, dotted brackets reveal comparisons for most locomotion across different time windows and dashed brackets show comparisons for least locomotion across different time windows.

Three two-way repeated measures ANOVAs for HbT, HbO and HbR respectively, revealed that there was a significant interaction between the amount of locomotion (factors: most & least) and the time at which locomotion was ranked (factors: − 5 to 0 s, 0–5 s, 5–10 s, 10–15 s, 15–20 s) on the peak of the haemodynamic response to the 2 s whisker stimulation (peak occurring between 0–5 s):- HbT: $F(2.58, 51.57) = 13.35$, $p < 0.0001$, $\varepsilon = 0.645$; HbO: $F(2.89, 57.88) = 13.32$, $p < 0.0001$, $\varepsilon = 0.723$; HbR: $F(2.53, 50.52) = 8.712$, $p < 0.0001$, $\varepsilon = 0.632$), indicating that the effect of locomotion was dependent on the timing of locomotion.

To dissect how the timing of locomotion during the trial impacted the sensory-evoked haemodynamic response (HbT, HbO or HbR peak detected between 0 and 5 s), simple main effects were run to assess how ranked-locomotion during the five different time windows impacted the sensory-evoked haemodynamic response.

2.4.2.1 Most Locomotion trials:

Simple main effects revealed that for the trials in which the most locomotion occurred (Fig. 2.3, Column 2), the time at which locomotion was ranked had a significant effect on the mean peak of HbT ($F(2.52, 50.41) = 12.99$, $p < 0.0001$, $\varepsilon = 0.630$), HbO ($F(2.66, 53.19) = 12.79$, $p = < 0.0001$ $\varepsilon = 0.665$), and HbR ($F(2.69, 53.78) = 11.50$, $p < 0.0001$, $\varepsilon = 0.672$) during the 2 s whisker stimulation. Pairwise comparisons with a Bonferroni correction revealed significant differences when locomotion occurred before (− 5 to 0 s) and during the stimulation (0–5 s), as discussed in detail below (Table 1).

There were notable differences in the mean peaks of HbT, HbO and HbR during the 2 s whisker stimulation (as assessed by pairwise comparisons with a Bonferroni correction). When locomotion was ranked before the stimulation (− 5 to 0 s), mean HbO peak during the 2 s stimulation was greater than when locomotion was ranked at 10–15 and 15–20 s and mean HbT peak during the 2 s stimulation was greater than when locomotion was ranked at 15–20 s (Fig. 2.3 f,g). Additionally, when locomotion was ranked before the stimulation (− 5 to 0) mean HbR peak during the 2 s stimulation was less than when locomotion was ranked at all time windows after the stimulation (5–10 s, 10–15 s and 15–20 s) (Fig. 2.3 h)—indicating a larger HbR washout occurs when locomotion is ranked before the whisker stimulation as compared to after the whisker stimulation (Table 1).

Additionally, when locomotion was ranked at the stimulation onset (0–5 s) mean HbT and HbO peak responses during the 2 s stimulation were greater than when locomotion was ranked at all time windows after the stimulation (Fig. 2.3 f,g). For HbR when locomotion was ranked at stimulation onset (0–5 s) mean HbR peak during the 2 s whisker stimulation was less than when locomotion was ranked at all time windows after the stimulation (Fig. 2.3 h)—indicating a larger HbR washout when locomotion was ranked at stimulation onset as compared to when it occurred after the whisker stimulation (Table 1).

Generally, the above results show that increased locomotion amplified the size of the haemodynamic response when it occurred before and during stimulation onset.

2.4.2.2 Least locomotion trials

Simple main effects revealed that for the trials in which the least locomotion occurred (Fig. 2.3, Column 3), the time at which locomotion was ranked also had a significant effect on the mean peak of HbT ($F(2.94, 58.79) = 8.93$, $p < 0.0001$, $\varepsilon = 0.735$), HbO ($F(4, 80) = 9.94$, $p < 0.0001$) & HbR ($F(4, 80) = 6.83$, $p < 0.0001$) during the 2 s whisker stimulation. Pairwise comparisons with a Bonferroni correction revealed that significant differences were observed when locomotion was ranked before the stimulation (− 5 to 0 s) and at the stimulation onset (0–5 s) vs the post-stimulation ranked locomotion conditions (5–10 s, 10–15 s, 15–20 s).

When locomotion was ranked before the stimulation (− 5 to 0 s), the mean HbT and HbO peak responses were greater than when locomotion was ranked at stimulation onset (0–5 s) (Fig. 2.3 f,g). Additionally, mean HbR peak when locomotion was ranked before the stimulation (− 5 to 0 s) was less than when locomotion was ranked at stimulation onset (0–5 s) (Fig. 3h)—indicating a larger HbR washout when locomotion was ranked before the stimulation, as compared to when ranked during the stimulation (Table 1).

When locomotion was ranked at the stimulation onset (0–5 s) mean HbT and mean HbO peaks during the 2 s whisker stimulation were less than when locomotion was ranked at all time windows after the stimulation (Fig. 2.3 f,g). Whereas mean HbR peak during whisker stimulation when locomotion was ranked at stimulation onset (0–

5 s) was greater than when locomotion was ranked at all time windows after the stimulation (Fig. 2.3 h)—indicating a smaller HbR washout when locomotion was ranked at stimulation onset compared to when ranked after the stimulation (Table 1).

The above results show that for trials in which the least locomotion occurred, when locomotion was ranked before the stimulation the haemodynamic response was larger than when ranked at stimulation onset. However, when the least locomotion occurred during stimulation onset the haemodynamic response was reduced in size compared to when locomotion was ranked after the stimulation.

Table 1 Comparisons between 5 s time windows for HbT, HbO and HbR peaks during whisker stimulation for most and least locomotion conditions.

Time Window			Most Locomotion			Least Locomotion		
Locomotion ranked	Compared to	Haem Measure	Mean diff	SEM	p	Mean diff	SEM	p
-5-0	0-5	HbT	-.006	.003	1.000	.016	.003	.000*
		HbO	-.005	.006	1.000	.028	.005	.000*
		HbR	-.004	.006	1.000	-.025	.006	.008*
	5-10	HbT	.008	.003	.194	.004	.002	.769
		HbO	.015	.005	.065	.008	.004	.356
		HbR	-.018	.005	.017*	-.008	.004	.546
	10-15	HbT	.012	.004	.100	.001	.003	1.000
		HbO	.020	.006	.048*	.004	.005	1.000
		HbR	-.021	.006	.012*	-.004	.005	1.000
	15-20	HbT	.017	.005	.013*	.004	.003	1.000
		HbO	.026	.007	.008*	.009	.006	1.000
		HbR	-.024	.006	.005*	-.007	.007	1.000
0-5	5-10	HbT	.013	.003	.006*	-.011	.003	.013*
		HbO	.020	.005	.008*	-.020	.005	.006*
		HbR	-.014	.004	.013*	.017	.005	.018*
	10-15	HbT	.017	.004	.003*	-.014	.004	.009*
		HbO	.025	.006	.003*	-.024	.005	.001*
		HbR	-.017	.004	.004*	.021	.005	.007*
	15-20	HbT	.023	.004	.000*	-.011	.003	.005*
		HbO	.031	.006	.000*	-.019	.004	.002*
		HbR	-.020	.004	.001*	.018	.005	.015*
5-10	10-15	HbT	.004	.002	.933	-.003	.002	1.000
		HbO	.005	.003	1.000	-.005	.003	1.000
		HbR	-.003	.003	1.000	.004	.004	1.000
	15-20	HbT	.010	.004	.158	.000	.003	1.000
		HbO	.011	.005	.346	.000	.005	1.000
		HbR	-.006	.004	1.000	.001	.005	1.000
10-15	15-20	HbT	.005	.002	.232	.003	.003	1.000
		HbO	.006	.003	.344	.005	.005	1.000
		HbR	-.003	.003	1.000	-.003	.005	1.000

*Mean diff = mean difference. Pairwise comparisons with a Bonferonni correction reported. SEM is standard error of the mean. * indicates a significant difference between the means.*

2.4.3 The amount of locomotion impacts the sensory-evoked haemodynamic response only when locomotion is ranked at specific time windows

Having previously shown that there is a significant interaction between the amount of locomotion (factors: most & least) and the time at which locomotion was ranked (factors: − 5 to 0 s, 0–5 s, 5–10 s, 10–15 s, 15–20 s) on the peak of the haemodynamic response to the 2 s whisker stimulation (peak occurring between 0 and 5 s), as well as highlighting at which time windows ranked-locomotion impacted the sensory-evoked haemodynamic response, we now wanted to reveal how the amount of locomotion at these five time windows impacted the sensory-evoked response.

Simple main effects with a Bonferroni correction revealed that mean whisker stimulation-evoked HbT peak was greater for trials in which the most locomotion occurred as compared to trials in which the least locomotion occurred when locomotion was ranked at stimulation onset (0–5 s; $F(1,20) = 19.68$, $p < 0.0001$, mean ± SEM: 1.054 ± 0.007 vs 1.020 ± 0.002) (Fig. 2.3 a,b, Columns 2 and 3). No significant differences were found when comparing the effect of locomotion on the mean whisker stimulation-evoked HbT peak when locomotion was ranked before the stimulation (− 5 to 0) and at 5–10 s, 10–15 s and 15–20 s. This indicates that the amount of locomotion only effects the HbT element of the evoked-haemodynamic response when locomotion occurs during the stimulation.

Simple main effects with a Bonferroni correction indicated that mean whisker stimulation-evoked HbO peak was also greater for trials in which the most locomotion occurred as compared to trials in which the least locomotion occurred when locomotion was ranked at stimulation onset (0–5 s; $F(1,20) = 24.83$, $p < 0.0001$, mean ± SEM: 1.083 ± 0.009 vs 1.033 ± 0.004) (Fig. 2.3 a,b, Columns 2 and 3). No significant differences were found when comparing the effect of locomotion on the mean whisker stimulation-evoked HbO peak when locomotion was ranked before the stimulation (− 5 to 0) and when ranked at 5–10 s, 10–15 s and 15–20 s. Indicating that the amount of locomotion only effects the HbO element of the evoked-haemodynamic response when locomotion occurs during the stimulation.

Simple main effects with a Bonferroni correction revealed that mean whisker stimulation-evoked HbR peak was less for trials in which the most locomotion occurred

as compared to trials in which the least locomotion occurred when locomotion was ranked at stimulation onset (0–5 s; $F(1,20) = 38.75$, $p < 0.0001$, mean ± SEM: 0.934 ± 0.006 vs 0.969 ± 0.004)—indicating a larger HbR washout when the animal moved more (Fig. 2.3 a,b, Columns 2 and 3). No significant differences were found when comparing the effect of locomotion on the mean whisker stimulation-evoked HbR peak for trials in which locomotion was ranked before the stimulation (− 5 to 0) and when ranked at 5–10 s, 10–15 s and 15–20 s. This indicates that the amount of locomotion only effects the HbR element of the evoked-haemodynamic response when locomotion occurs during the stimulation.

The above results show that the amount of locomotion only affected the size of the haemodynamic response when locomotion was ranked at the stimulation onset—with a larger haemodynamic response observed when more locomotion occurred at stimulation onset.

2.4.4. Sensory- and locomotion-evoked haemodynamic responses sum in a linear manner

Overall, the results show that locomotion affects the evoked-haemodynamic response when locomotion occurs before or during stimulation onset. To assess whether this was a linear addition of locomotion-evoked haemodynamic responses on top of whisker stimulation-evoked responses, we performed identical analysis on the spontaneous data set (i.e. locomotion with no whisker stimulation, Supplementary Fig. 2.2.1) and subtracted these responses from the whisker stimulation data (Fig. 2.3). Figure 2.4 column 1 shows the differential locomotion heat map—which revealed that the majority of locomotion was removed when a linear subtraction was performed. Therefore, the expectation would be that the majority of the whisker stimulation differences would also be removed.

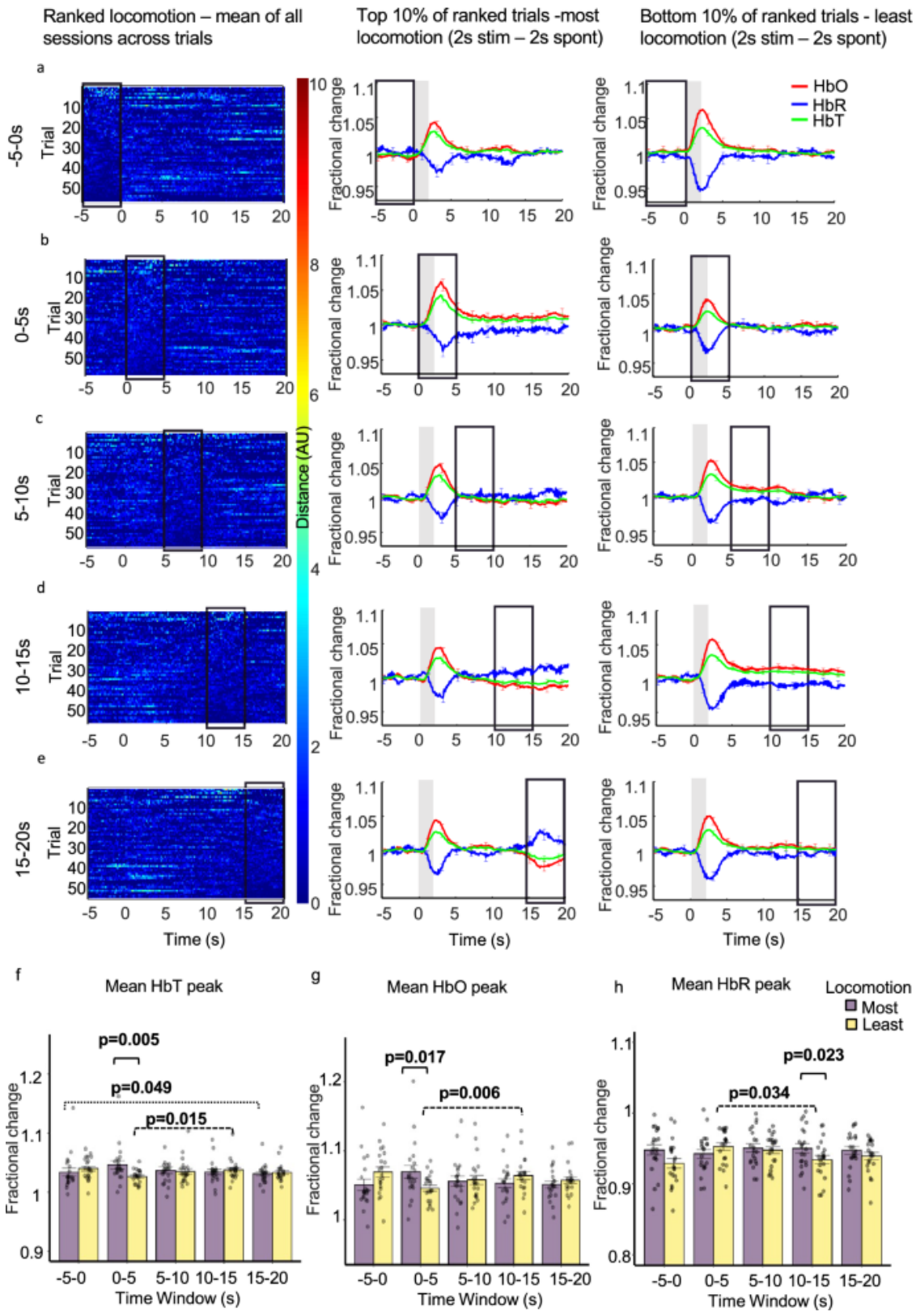

Figure 2.4: Linear subtraction of spontaneous haemodynamic responses from mean sensory-evoked haemodynamic responses for the whisker ROI

(Fig. 2.5 column 1) during trials where the most and least locomotion occurred with locomotion ranked at different time windows throughout the 25 s trial. Haemodynamic responses from spontaneous trials (no whisker stimulation) were subtracted from trials with a 2 s whisker stimulation. Whisker stimulation between 0 and 2 s (grey bar in centre and right columns) Column one: heat maps reveal differential locomotion traces for the 59 trials, with locomotion ranked at different 5 s time windows during the 25 s trial (each ranked trial was averaged across 21 sessions/4 animals). Locomotion was ranked: before (a: − 5 to 0 s), during (b: 0–5 s) and after whisker stimulation (c: 5–10 s, d: 10–15 s, e: 15–20 s). Colour bar indicates amount of locomotion, red pixels indicate more locomotion and dark blue indicate less locomotion. Column two: mean fractional changes from baseline in stimulation-dependent HbT, HbO and HbR taken from the top 10% of ranked locomotion trials across the different 5 s time windows (21 sessions/4 animals; n = 6 top per session (mean of top trials taken for each session, mean of all sessions used in the visualisation/analysis). Column three: mean fractional changes in stimulation-dependent HbT, HbO and HbR for the bottom 10% of locomotion trials ranked across the 5 s time windows throughout the trial (21 sessions/4 animals; n = 6 bottom per session (mean of bottom trials taken for each session, mean of all sessions used in the visualisation/analysis). Black boxes indicate the 5 s time window locomotion was ranked. Data show mean across the total 126 trials ± SEM. (f–h) show mean ± SEM between groups and individual mean peak values per session for HbT, HbO and HbR. Two-way repeated measures ANOVA's were completed for HbT, HbO and HbR. Significant interactions were found and simple effects run (time and locomotion) for each of the haemodynamic measures. p values from pairwise comparisons (Bonferroni correction) are reported. Black solid brackets: comparison between most and least locomotion, dotted brackets: comparisons for most locomotion across different time windows and dashed brackets: comparisons for least locomotion across different time windows.

Three two-way repeated measures ANOVAs were conducted on the mean peaks of HbT, HbO and HbR. Significant interactions were still observed between the amount of locomotion (factors: most & least) and the time at which locomotion was ranked (factors: − 5 to 0 s, 0–5 s, 5–10 s, 10–15 s, 15–20 s) on the peak of the haemodynamic response to the 2 s whisker stimulation (peak occurring between 0 and 5 s) for

HbT: $F(2.59,51.98) = 5.29$, $p = 0.004$, $\varepsilon = 0.650$; HbO: $F(2.87, 57.56) = 5.24$, $p = 0.003$, $\varepsilon = 0.720$ and HbR: $F(4,80) = 3.12$, $p = 0.019$).

However, many of the previous significant effects were removed. Simple main effects with a Bonferroni correction revealed that only 6 (of the previous 30) significant effects remained. For trials in which the most locomotion occurred, the time at which locomotion was ranked still had a significant effect on the mean peak of HbT ($F(2.71, 54.34) = 3.915$, $p = 0.016$, $\varepsilon = 0.679$) and HbO ($F(2.83,56.64) = 2.89$, $p = 0.046$ $\varepsilon = 0.708$) during the 2 s whisker stimulation. When locomotion was ranked at stimulation onset mean HbT peak responses during the 2 s stimulation were still greater than when locomotion was ranked at 15–20 s (Fig. 2.4 f, and Supplementary Table 21).

For trials in which the least locomotion occurred, the time at which locomotion was ranked still had a significant effect on the mean peak of HbT ($F(2.37, 47.46) = 3.75$, $p = 0.024$, $\varepsilon = 0.593$), HbO ($F(4, 80) = 4.17$, $p = 0.004$) & HbR ($F(4, 80) = 4.92$, $p = 0.001$) during the 2 s whisker stimulation. When locomotion was ranked at the stimulation onset (0–5 s) both mean HbT and HbO peaks during the 2 s whisker stimulation were less than when locomotion was ranked at 10–15 s (Fig. 2.4 f,g). Mean HbR peak during whisker stimulation when locomotion was ranked at stimulation onset (0–5 s) was greater than when locomotion was ranked at 10–15 s (Fig. 2.4 h). Finally, simple main effects with a Bonferroni correction revealed that when locomotion was ranked at stimulation onset (0–5 s), mean whisker stimulation evoked responses for HbT ($F(1,20) = 10.04$, $p = 0.005$, mean ± SEM: 1.046 ± 0.007 vs 1.026 ± 0.003) and HbO ($F(1,20) = 6.79$, $p = 0.017$, mean ± SEM: 1.070 ± 0.009 vs 1.046 ± 0.004) were still greater for trials in which the most locomotion occurred as compared to the least (Fig. 2.4 f,g).

Interestingly, the linear subtraction resulted in one additional significant effect: when locomotion was ranked at 10–15 s, mean whisker stimulation evoked responses for HbR ($F(1,20) = 6.06$, $p = 0.023$, mean ± SEM: 0.950 ± 0.006 vs 0.934 ± 0.006) were greater for trials in which the most locomotion occurred as compared to the least—this was not observed in the whisker stimulation analysis (Fig. 2.4 h).

2.4.5 Locomotion impacts the spatial spread of HbT across the surface vasculature

Representative spatial maps from each animal show HbT activation—revealing fractional change in HbT within the surface vasculature, during locomotion occurring with and without a 2 s whisker stimulation (activation between 0 and 5 s with whisker stimulation and 5–10 s without whisker stimulation) (Fig. 2.5). Red pixels indicate increased activation and blue pixels decreased activation. Figure 2.5 (Column 2) was generated from spontaneous trials (with no stimulation). Column 2 shows that during locomotion, a more global activation can be observed which is not restricted to the whisker region alone (red ROIs, Column 1) as per when a whisker-stimulation occurs concurrently with limited locomotion (see Column 4, 'least' locomotion). Figure 2.5 (Columns 3 & 4) shows representative spatial maps for each animal for the trials in which the most and least locomotion occurred during the 2 s whisker stimulation. Increased activation can be observed within the whisker region (red outline, Fig. 2.5, Column 1) for trials in which the most locomotion occurred during the 2 s whisker stimulation (Fig. 2.5, Column 3). Increased activation within the whisker region can also be observed in trials where animals moved the least during a whisker stimulation. However, a decrease in activation (blue pixels in a region adjacent to the whisker region within red outline) can also be seen, which suggests a reduction in HbT within a region anterior to the whisker area (Fig. 2.5, Column 4).

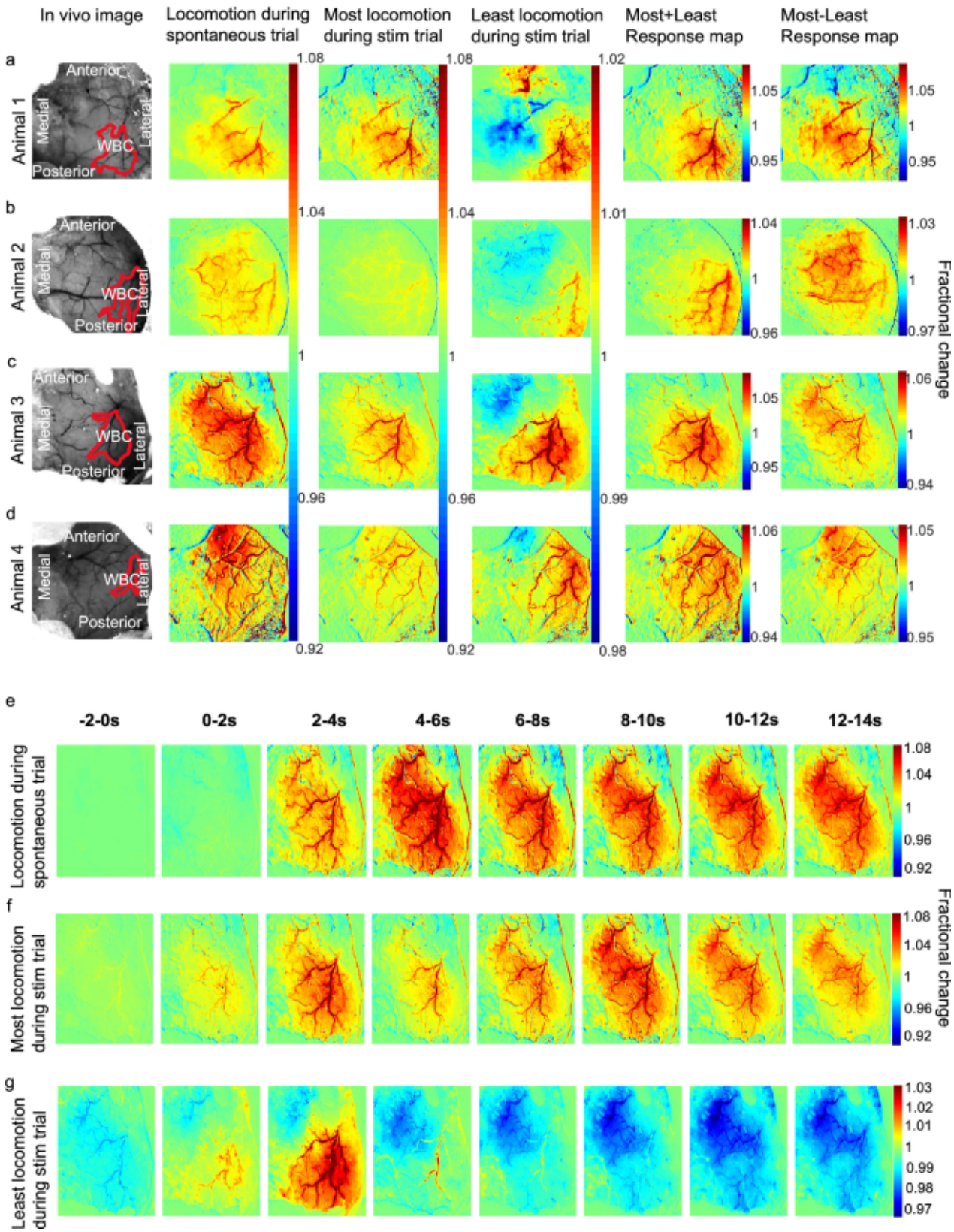

Figure 2.5: Representative HbT spatial maps during locomotion and spatial montage

Spatial maps from each animal included in the analysis (a–d) showing the surface vasculature in the somatosensory cortex as recorded during locomotion alone (left centre, spontaneous recordings), and during trials with the most (right centre) and least (right) locomotion occurring during the 2 s whisker stimulation (from the 0 to 5 s time window, see Fig. 2.3 b). Column one: in vivo images of the thinned cranial window with the automatically generated whisker region highlighted in red. Column two: spatial maps showing fractional changes in HbT generated from spontaneous trials (with no whisker stimulation) during 25 s bouts of continuous locomotion. Column three & four: HbT spatial maps of trials in which the most (right centre) and least (right) locomotion occurred during a 2 s whisker stimulation. This map reveals the spatial location of the whisker region (red pixels, which corresponds to the automatically generated whisker region in red ROI of Column 1), as well as revealing an area with a decrease in fractional change of HbT (blue pixels). Colour bar represents fractional change in HbT, with red indicating an increase in fractional change and blue indicating a decrease. Column five: HbT spatial maps of columns 3 and 4 added together, reveals haemodynamic response predominantly within whisker barrel cortex. Column six: HbT spatial maps of column 3 minus column 4 reveals a spatial response similar to that for spontaneous locomotion (column 2). (e–g) HbT spatial montage revealing how HbT responses change over time from a representative animal. Each spatial image is the average of 2 s starting at the time indicated with whisker stim occurring at 0 s. (e) reveals the HbT spatial map evoked by spontaneous locomotion, with locomotion occurring from 0 s. (f) HbT spatial map over time when the most locomotion occurs during the whisker stimulation. (g) HbT spatial map in response to the least amount of locomotion during a whisker stimulation. Column 1, (b) ((in vivo image animal 2) also used in Sharp et al.[20], see Fig. 2.4B).

To further illustrate this, we added the spatial maps of haemodynamic responses for the most and least locomotion (during the 2 s whisker stimulation) together (Fig. 2.5, columns 3 and 4, respectively). This summation essentially removed the locomotion effect in the spatial image (Fig. 2.5, column 5), revealing responses which are mostly restricted to the whisker sensory region. We also subtracted the spatial maps for least locomotion (during the 2 s whisker stim) from those with most locomotion to provide a map of locomotion-evoked haemodynamic response (under the assumption that whisker-evoked responses are the same size). The resulting map (Fig. 2.5, column 6) is similar to that seen in the case of locomotion alone (Fig. 2.5, column 2). These spatial data support the time series results showing that, in general, locomotion and whisker stimulation are adding in a linear manner to produce the haemodynamic response measured.

The dynamic changes in responses over time can be seen in a montage of images from one animal for locomotion and whisker stimulation with most and least locomotion (Fig. 2.5 e–g). Whisker stimulation or spontaneous locomotion occurred at 0 s and the corresponding change in HbT can be observed over 14 s. In response to the onset of the whisker stimulation a large increase in activation can be observed within the whisker region (Fig. 2.5 f,g), with a slightly larger spatial spread of increased activation observed for spontaneous locomotion (Fig. 2.5 e). Interestingly, for the montage of the least locomotion during the 2 s whisker stimulation, 2 s prior to whisker stimulation a decrease in activation can be observed, with this decrease in activation dominating from 4 to 14 s post stimulation (Fig. 2.5 g).

2.5 Discussion

The present study measured spontaneous (Fig. 2.5) and sensory-evoked (Figs. 2.1, 2.3, 2.4, 2.5) haemodynamic responses from the cerebral cortex in head-fixed, awake mice, whilst locomotion was concurrently monitored. The novel aspect of our approach was to investigate the impact of the amount and timing of locomotion events on sensory-evoked haemodynamic responses. Our experiments revealed that sensory-evoked haemodynamic responses are altered by the presence of locomotion, which was dependent on the timing (relative to whisker stimulation) that the locomotion occurred. Our findings suggest there is a relationship between the time at which

locomotion occurs (in 5 s time windows relative to the whisker stimulation) and the amount of summed locomotion, and that this affects the evoked haemodynamic response, with locomotion appearing to have the largest effects when it occurred before the stimulation (− 5 to 0 s) and during (0–5 s) the stimulation. During the analysis conducted on the 2 s whisker stimulation trials there were 30 significant events when investigating how the amount and timing of locomotion impacted the sensory evoked haemodynamic response—with locomotion having the greatest effect when it occurred before or during whisker stimulation. However, when we subtracted the spontaneous trials from the 2 s whisker stimulation trials, the number of significant events was reduced to only 7—with only 6 of the previous 30 significant effects remaining. This suggests it would be advantageous to collect parallel datasets with no sensory stimulation during experimental data collection to allow locomotion induced differences to be removed.

Previous studies have shown that certain behaviours, including body movements and whisking can enhance CBV in awake, head-fixed mice[31]. It has also been reported that locomotion, in the absence of sensory stimulation, increases cortical CBV[23], and rapidly dilates arteries[25]. However, the above studies did not explore how locomotion may specifically affect sensory-evoked haemodynamic responses, making our findings novel.

Of the few papers that have investigated the impact of locomotion on evoked haemodynamic responses, Tran et al.[24] explored whether the behaviour of an animal during whisker stimulation had an effect on penetrating arteriole dilation. They showed that the behaviour of the animal did not alter the peak amplitude of arteriole dilation. In comparison, our data suggests that the animal's behaviour does impact the peak amplitude of arteriole dilation. Our opposing findings could be explained by the different methods used in the two studies. Tran et al. used two-photon microscopy to investigate haemodynamic responses, focusing on penetrating vessel dilation. In contrast, our study used 2D-OIS to measure changes in blood oxygenation from the surface of the cerebral cortex. It is conceivable that locomotion and the time at which locomotion occurs relative to whisker stimulation may have a differing impact on evoked haemodynamic responses depending on the type and location of blood

vessels investigated. In support of this explanation, Gao et al.[27] found that locomotion impacted surface vessels to a greater extent than penetrating vessels, with locomotion leading to surface vessel dilations that were almost three times the size of intracortical vessel dilation. However, the study did not investigate how locomotion affected sensory-evoked haemodynamic responses. Future studies using two-photon microscopy are still warranted[32] to explore how sensory-evoked haemodynamic responses are impacted by locomotion, as well as to assess if our results can be replicated using other methods.

Our study was not without limitations, the behavioural set up only monitored locomotion behaviours and did not monitor whisking behaviours or pupil dilations in the animals. It has been reported that whisking occurs when an animal moves[33]. Therefore, there may also be a relationship between locomotion, whisking and sensory-evoked haemodynamic responses. It is likely that the animal also whisked during locomotion and this is reflected in the large spatial area revealed by spontaneous locomotion. Simultaneous monitoring of whiskers and locomotion would be required to confirm this. Future studies may therefore benefit from monitoring both locomotion and whisking[24] to assess if there are interactions between these behaviours and the impact this may have on the evoked haemodynamic response—as voluntary whisking has been reported to increase CBV[31]. However, the purpose of our paper was to focus on the effects of locomotion on sensory-evoked haemodynamic responses.

Additionally, neural activity was not measured during the study, it would have been informative to observe how neural activity was affected by the amount and timing of locomotion. Other studies have recorded neural activity alongside CBV during voluntary locomotion and found that voluntary locomotion does indeed increase neural activity[23,34]. Measuring simultaneous haemodynamics in awake animals combined with genetically encoded calcium indicators (such as GCAMP6)[7] to measure spontaneous and evoked neuronal activity will provide additional information on how brain activity is modulated by the interaction of locomotion and sensory stimulation.
Our paper demonstrates the importance of monitoring behaviour—especially locomotion—during awake haemodynamic imaging. As our study shows that the

amount and timing of locomotion (relative to whisker stimulation) can impact the amplitude of an evoked haemodynamic response we suggest that, where possible, groups should monitor locomotion in their awake imaging experiments—particularly when using sensory stimulation. If locomotion behaviours cannot be monitored, other methods could be used to limit locomotion behaviours, such as training animals to remain stationary[35]. Monitoring locomotion is especially important to consider when comparing different disease groups, in which locomotion may differ[36]—if locomotion behaviour is not monitored (or excluded), misleading conclusions could potentially be made.

2.6 Data availability

Data sets used/analysed in the current study are available in the DRYAD repository, https://doi.org/10.5061/dryad.v41ns1rxs.

2.7 References

1. Attwell, D. *et al.* Glial and neuronal control of brain blood flow. *Nature* **468**, 232–243 (2010).
2. Zlokovic, B. V. Neurovascular pathways to neurodegeneration in Alzheimer's disease and other disorders. *Nat Rev Neurosci* **12**, 723–738 (2011).
3. Kisler, K., Nelson, A. R., Montagne, A. & Zlokovic, B. V. Cerebral blood flow regulation and neurovascular dysfunction in Alzheimer disease. *Nat Rev Neurosci* **18**, 419–434 (2017).
4. Kotliar, K. *et al.* Altered neurovascular coupling as measured by optical imaging: a biomarker for Alzheimer's disease. *Sci Rep* **7**, 12906 (2017).
5. Tarantini, S., Tran, C. H. T., Gordon, G. R., Ungvari, Z. & Csiszar, A. Impaired neurovascular coupling in aging and Alzheimer's disease: Contribution of astrocyte dysfunction and endothelial impairment to cognitive decline. *Experimental Gerontology* **94**, 52–58 (2017).
6. Orbach, H., Cohen, L. & Grinvald, A. Optical mapping of electrical activity in rat somatosensory and visual cortex. *J. Neurosci.* **5**, 1886–1895 (1985).
7. Ma, Y. *et al.* Wide-field optical mapping of neural activity and brain haemodynamics: considerations and novel approaches. *Philosophical Transactions of the Royal Society B: Biological Sciences* **371**, 20150360 (2016).
8. Denk, W., Strickler, J. H. & Webb, W. W. Two-Photon Laser Scanning Fluorescence Microscopy. *Science* **248**, 73–76 (1990).
9. Nakai, J., Ohkura, M. & Imoto, K. A high signal-to-noise Ca2+ probe composed of a single green fluorescent protein. *Nat Biotechnol* **19**, 137–141 (2001).
10. Peppiatt, C. M., Howarth, C., Mobbs, P. & Attwell, D. Bidirectional control of CNS capillary diameter by pericytes. *Nature* **443**, 700–704 (2006).
11. Hall, C. N. *et al.* Capillary pericytes regulate cerebral blood flow in health and disease. *Nature* **508**, 55–60 (2014).
12. Kisler, K. *et al.* Pericyte degeneration leads to neurovascular uncoupling and limits oxygen supply to brain. *Nat Neurosci* **20**, 406–416 (2017).
13. Zonta, M. *et al.* Neuron-to-astrocyte signaling is central to the dynamic control of brain microcirculation. *Nat Neurosci* **6**, 43–50 (2003).
14. Lind, B. L., Brazhe, A. R., Jessen, S. B., Tan, F. C. C. & Lauritzen, M. J. Rapid stimulus-evoked astrocyte Ca^{2+} elevations and hemodynamic responses in mouse somatosensory cortex in vivo. *Proc. Natl. Acad. Sci. U.S.A.* **110**, (2013).
15. Mishra, A. *et al.* Astrocytes mediate neurovascular signaling to capillary pericytes but not to arterioles. *Nat Neurosci* **19**, 1619–1627 (2016).
16. Chow, B. W. *et al.* Caveolae in CNS arterioles mediate neurovascular coupling. *Nature* **579**, 106–110 (2020).
17. Gao, Y.-R. *et al.* Time to wake up: Studying neurovascular coupling and brain-wide circuit function in the un-anesthetized animal. *NeuroImage* **153**, 382–398 (2017).

18. Pisauro, M. A., Dhruv, N. T., Carandini, M. & Benucci, A. Fast Hemodynamic Responses in the Visual Cortex of the Awake Mouse. *J. Neurosci.* **33**, 18343–18351 (2013).
19. Aksenov, D. P., Li, L., Miller, M. J., Iordanescu, G. & Wyrwicz, A. M. Effects of anesthesia on BOLD signal and neuronal activity in the somatosensory cortex. *J Cereb Blood Flow Metab* **35**, 1819–1826 (2015).
20. Sharp, P. S. *et al.* Comparison of stimulus-evoked cerebral hemodynamics in the awake mouse and under a novel anesthetic regime. *Sci Rep* **5**, 12621 (2015).
21. Lee, J. *et al.* Opposed hemodynamic responses following increased excitation and parvalbumin-based inhibition. *J Cereb Blood Flow Metab* **41**, 841–856 (2021).
22. Uhlirova, H. *et al.* Cell type specificity of neurovascular coupling in cerebral cortex. *eLife* **5**, e14315 (2016).
23. Huo, B.-X., Smith, J. B. & Drew, P. J. Neurovascular Coupling and Decoupling in the Cortex during Voluntary Locomotion. *J. Neurosci.* **34**, 10975–10981 (2014).
24. Tran, C. H. T., Peringod, G. & Gordon, G. R. Astrocytes Integrate Behavioral State and Vascular Signals during Functional Hyperemia. *Neuron* **100**, 1133-1148.e3 (2018).
25. Huo, B.-X., Gao, Y.-R. & Drew, P. J. Quantitative separation of arterial and venous cerebral blood volume increases during voluntary locomotion. *NeuroImage* **105**, 369–379 (2015).
26. Huo, B.-X., Greene, S. E. & Drew, P. J. Venous cerebral blood volume increase during voluntary locomotion reflects cardiovascular changes. *Neuroimage* **118**, 301–312 (2015).
27. Gao, Y.-R., Greene, S. E. & Drew, P. J. Mechanical restriction of intracortical vessel dilation by brain tissue sculpts the hemodynamic response. *NeuroImage* **115**, 162–176 (2015).
28. Mayhew, J. *et al.* Spectroscopic Analysis of Changes in Remitted Illumination: The Response to Increased Neural Activity in Brain. *NeuroImage* **10**, 304–326 (1999).
29. Berwick, J. *et al.* Neurovascular coupling investigated with two-dimensional optical imaging spectroscopy in rat whisker barrel cortex. *European Journal of Neuroscience* **22**, 1655–1666 (2005).
30. FENG, C. *et al.* Log-transformation and its implications for data analysis. *Shanghai Arch Psychiatry* **26**, 105–109 (2014).
31. Winder, A. T., Echagarruga, C., Zhang, Q. & Drew, P. J. Weak correlations between hemodynamic signals and ongoing neural activity during the resting state. *Nat Neurosci* **20**, 1761–1769 (2017).
32. Peringod, G., Yu, L., Murari, K. & Gordon, G. R. *Spatiotemporal components of sustained functional hyperemia are differentially modulated by locomotion and silenced with vascular chemogenetics*. http://biorxiv.org/lookup/doi/10.1101/2021.09.15.460557 (2021) doi:10.1101/2021.09.15.460557.

33. Sofroniew, N. J., Cohen, J. D., Lee, A. K. & Svoboda, K. Natural Whisker-Guided Behavior by Head-Fixed Mice in Tactile Virtual Reality. *J. Neurosci.* **34**, 9537–9550 (2014).
34. Dombeck, D. A., Khabbaz, A. N., Collman, F., Adelman, T. L. & Tank, D. W. Imaging Large-Scale Neural Activity with Cellular Resolution in Awake, Mobile Mice. *Neuron* **56**, 43–57 (2007).
35. Rungta, R. L. *et al.* Diversity of neurovascular coupling dynamics along vascular arbors in layer II/III somatosensory cortex. *Commun Biol* **4**, 1–11 (2021).
36. Walker, J. M. *et al.* Spatial learning and memory impairment and increased locomotion in a transgenic amyloid precursor protein mouse model of Alzheimer's disease. *Behavioural Brain Research* **222**, 169–175 (2011).

2.8 Acknowledgements

BE would like to thank the Battelle—Dr Jeff Wadsworth studentship for funding her PhD. OS is funded by a British Heart Foundation (BHF) project Grant (PG/20/10010). CH is funded by a Sir Henry Dale Fellowship jointly funded by the Wellcome Trust and the Royal Society. This research was funded in whole, or in part, by the Wellcome Trust [Grant number 105586/Z/14/Z]. For the purpose of Open Access, the author has applied a CC BY public copyright licence to any Author Accepted Manuscript version arising from this submission. We also would like to thank Michael Port for building and maintaining the whisker stimulation device and 2D-OIS imaging equipment. Awake imaging experimental figure created with BioRender.com.

2.9 Author information

These authors contributed equally: Beth Eyre and Kira Shaw. These authors jointly supervised this work: Jason Berwick and Clare Howarth.

2.10 Authors and Affiliations

Sheffield Neurovascular Lab, Department of Psychology, University of Sheffield, Alfred Denny Building, Western Bank, Sheffield, S10 2TN, UK

Beth Eyre, Kira Shaw, Paul Sharp, Luke Boorman, Llywelyn Lee, Osman Shabir, Jason Berwick & Clare Howarth

Neuroscience Institute, University of Sheffield, Sheffield, S10 2TN, UK

Beth Eyre, Llywelyn Lee, Osman Shabir, Jason Berwick & Clare Howarth

Healthy Lifespan Institute, University of Sheffield, Sheffield, S10 2TN, UK

Beth Eyre, Llywelyn Lee, Osman Shabir, Jason Berwick & Clare Howarth

Department of Infection, Immunity & Cardiovascular Disease (IICD), University of Sheffield Medical School, Royal Hallamshire Hospital, Beech Hill Road, Sheffield, S10 2RX, UK
Osman Shabir

School of Psychology and Sussex Neuroscience, University of Sussex, Falmer, Brighton, UK
Kira Shaw

Medicines Discovery Catapult, Alderley Edge, Mereside, Alderley Park, Cheshire, SK10 4TG, UK
Paul Sharp

2.11 Contributions

B.E wrote the main manuscript. C.H and J.B conceived research ideas. K.S and P.S completed surgeries and imaging experiments. B.E, J.B and C.H analysed the data. L.B, K.S., B.E., C.H & J.B. wrote the code for analysis. B.E, K.S, L.L, O.S, C.H, and J.B edited and proofread the manuscript. B.E and K.S contributed equally. J.B and C.H contributed equally.

2.12 Supplementary figures

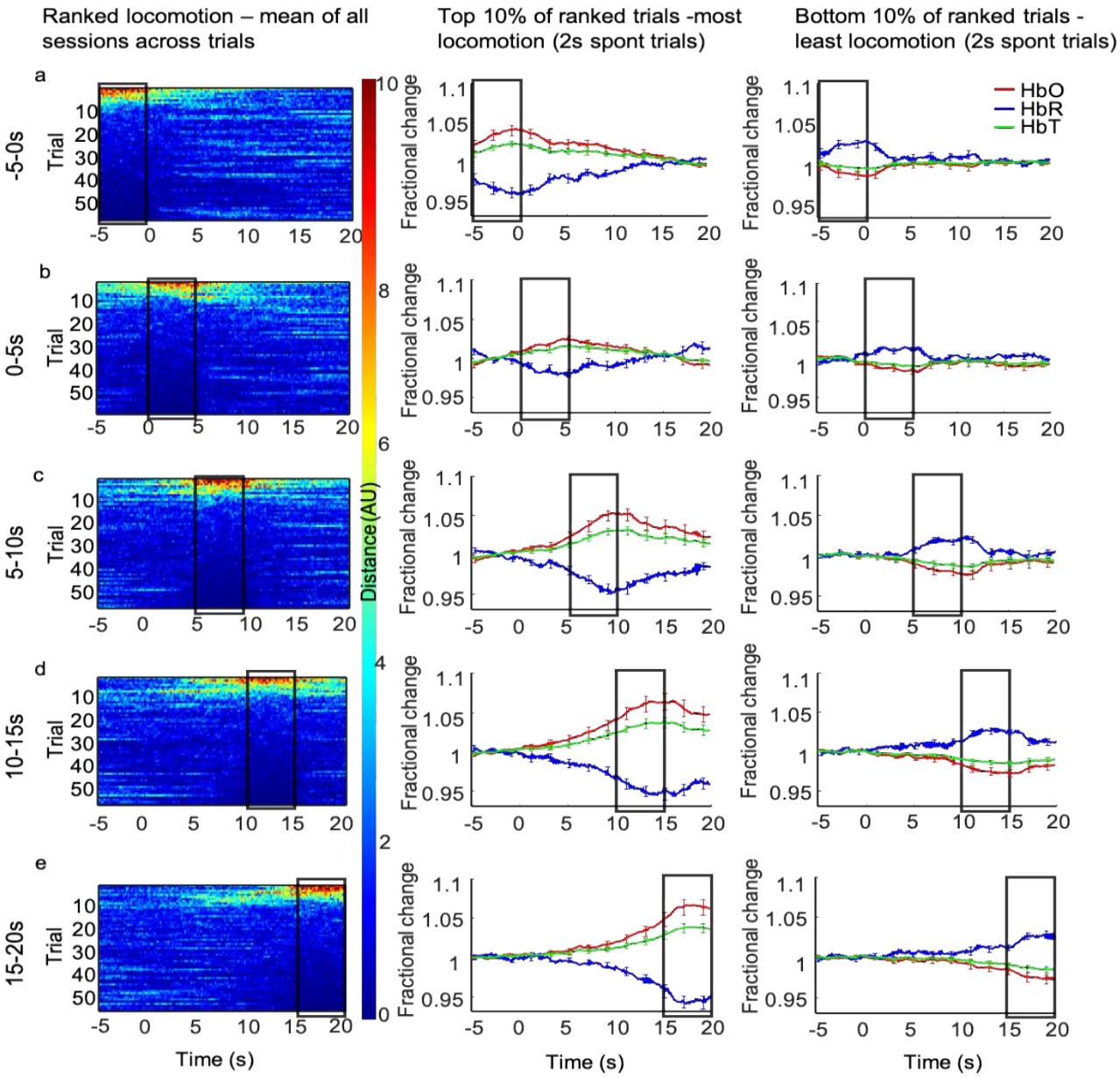

Supplementary figure 1: *Mean locomotion induced haemodynamic responses for the whisker ROI (Fig. 2.5 column 1) during trials where the most and least locomotion occurred with locomotion ranked at different time windows throughout a 25s time period. Column one: heat maps show locomotion traces for the 59 whisker-stimulation trials, with spontaneous locomotion ranked at different 5s time windows during a 25s time period (each ranked trial was averaged across 21 sessions/4 animals). The different 5s windows during the 25s time period where locomotion was ranked are: before (a: -5-0s), during (b: 0-5s) and after whisker stimulation (c: 5-10s, d: 10-15s, e:*

15-20s). Trials were ranked according to locomotion in these 5s periods and presented in descending order. Colour bar indicates amount of locomotion, red pixels indicate more locomotion and dark blue indicate less locomotion. Column two: mean fractional changes from baseline in HbT, HbO and HbR taken from the top 10% of ranked locomotion trials across the different 5s time windows (21 sessions/4 animals; n=6 top per session (mean of top trials taken for each session, mean of all sessions used in the visualisation/analysis). Column three: mean fractional changes in HbT, HbO and HbR for the bottom 10% of locomotion trials ranked across the 5s time windows throughout the trial (21 sessions/4 animals; n=6 bottom per session (mean of bottom trials taken for each session, mean of all sessions used in the visualisation/analysis). Black boxes indicate the 5s time window locomotion was ranked. Data show mean across the total 126 trials +/- SEM

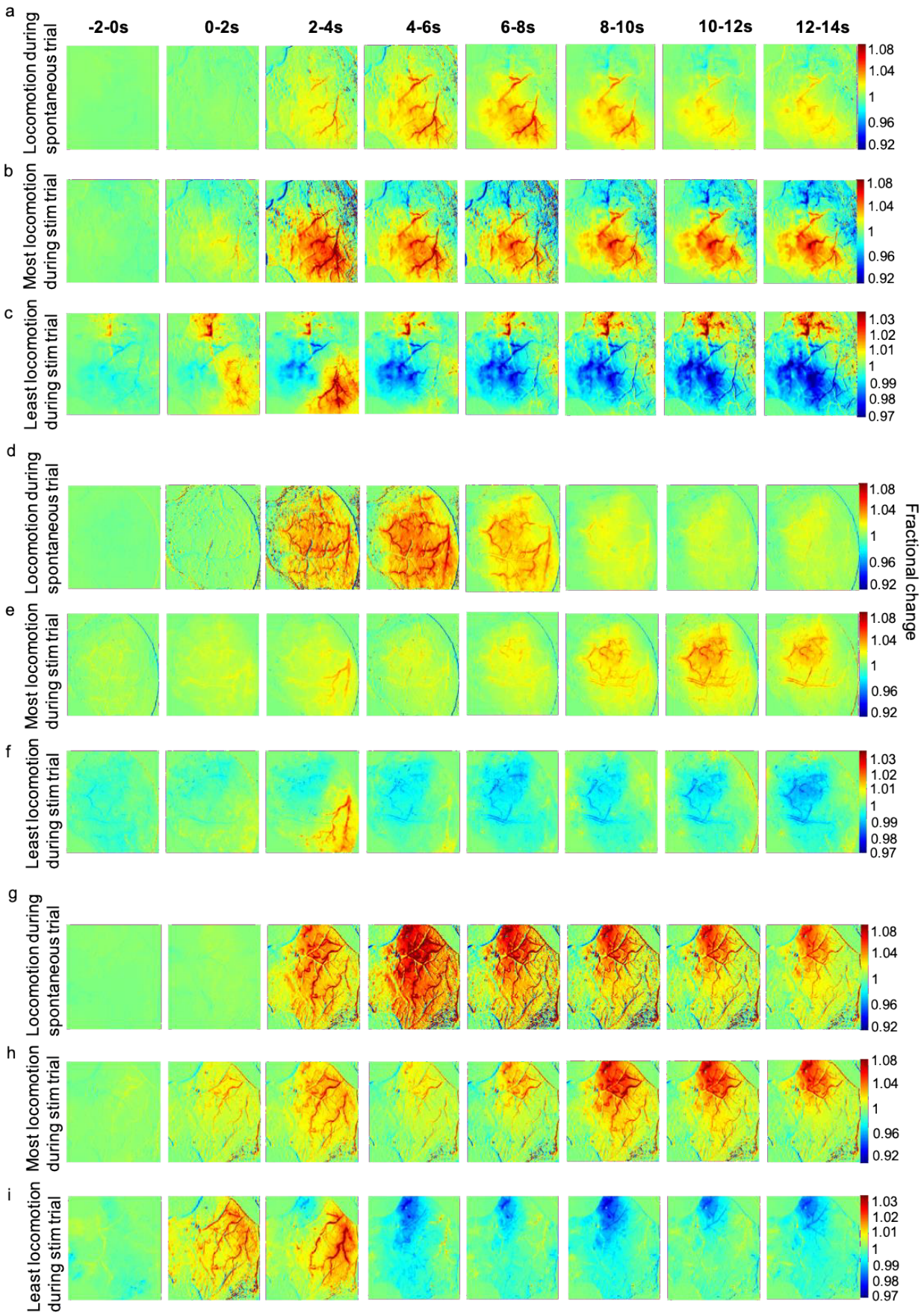
a
Locomotion during spontaneous trial
-2-0s
0-2s
2-4s
4-6s
6-8s
8-10s
10-12s
12-14s
1.08
1.04
1
0.96
0.92
b
Most locomotion during stim trial
1.08
1.04
1
0.96
0.92
c
Least locomotion during stim trial
1.03
1.02
1.01
1
0.99
0.98
0.97
d
Locomotion during spontaneous trial
1.08
1.04
1
0.96
0.92
Fractional change
e
Most locomotion during stim trial
1.08
1.04
1
0.96
0.92
f
Least locomotion during stim trial
1.03
1.02
1.01
1
0.99
0.98
0.97
g
Locomotion during spontaneous trial
1.08
1.04
1
0.96
0.92
h
Most locomotion during stim trial
1.08
1.04
1
0.96
0.92
i
Least locomotion during stim trial
1.03
1.02
1.01
1
0.99
0.98
0.97

Supplementary figure 2: HbT spatial montages for each animal during spontaneous locomotion and most and least locomotion during a 2s whisker stimulation. *HbT spatial maps reveal fractional change in HbT across the vasculature over time, starting 2s prior to whisker stimulation (or locomotion) to 14s post stimulation. Each spatial image is an average of 2s of data. Whisker stim/spontaneous locomotion occur at 0s. Red pixels indicate an increase in activation and blue pixels indicate a decrease in activation.* ***(a-c)*** *show spatial HbT maps for animal 1 for spontaneous locomotion* ***(a),*** *most locomotion during a 2s whisker stim* ***(b)*** *and least locomotion during a 2s whisker stim* ***(c)****.* ***(d-f)*** *show the HbT spatial responses for animal 3 for spontaneous locomotion* ***(d),*** *most locomotion during a 2s whisker stim* ***(e)*** *and least locomotion during a 2s whisker stim* ***(f). (g-i)*** *show the HbT spatial responses for animal 4 for spontaneous locomotion* ***(g),*** *most locomotion during a 2s whisker stim* ***(h)*** *and least locomotion during a 2s whisker stim* ***(i)****.*

2.13 Supplementary tables for statistics outputs

All data values were included in the statistical analysis even if outliers were found as there was no scientific reason to remove them from the data set. Data used in the analysis can be found in the DRYAD repository, doi:10.5061/dryad.v41ns1rxs

Distance travelled

Supplementary table S1: Shapiro Wilk test of normality for distanced travelled during spontaneous and whisker stimulation trials

Distance travelled	Statistic	df	p
Spontaneous vs Whisker stim	.691	21	.000

Normality was assessed using a difference variable comparing distanced travelled during spontaneous trials with distance travelled during whisker stimulation trials

Supplementary table S2: Sign test result for distance travelled during spontaneous and whisker stimulation trials

Type of trial	N	Mean	Median	SEM	z	p
Spontaneous	21	13610	12360	1532	-	-
2s whisker stim	21	17802	14894	2732	-	-
Difference	21	-4192	-1517	2065	1.309	.189

Greatest vs Least locomotion

Supplementary table S3: Shapiro Wilk test of normality for greatest vs least locomotion (where locomotion ranked across the entire 25s trial)

	Greatest Locomotion vs Least Locomotion		
Haemodynamic Measure	**Statistic**	**df**	**p**
HbT	.568	21	.000
HbO	.695	21	.000
HbR	.923	21	.100

Supplementary table S4: Wilcoxon signed ranks result for HbR greatest vs least locomotion (where locomotion is ranked across the entire 25s trial)

	N	Mean	Median	SEM	z	p
HbR peak greatest locomotion	21	0.947	0.948	.006	-	-
HbR peak least locomotion	21	0.947	0.945	.005	-	-
Difference most vs least HbR	21	0.000	-.0004	.005	-.330	.741

Supplementary table S5: Sign test result for HbT and HbO greatest vs least locomotion (where locomotion is ranked across the entire 25s trial)

	N	Mean	Median	SEM	z	p
HbT peak greatest locomotion	21	1.043	1.038	.007	-	-
HbT peak least locomotion	21	1.030	1.028	.003	-	-
Difference most vs least HbT	21	.013	.003	.007	-.873	.383
HbO peak greatest locomotion	21	1.065	1.057	.009	-	-
HbO peak least locomotion	21	1.053	1.049	.005	-	-
Difference most vs least HbO	21	.012	-.0004	.008	.000	1.000

Return to baseline

Supplementary table S6: Shapiro Wilk test of normality for baseline statistics (mean values taken from last 5s of the 2s whisker stimulation trial (between 15-20s)

Haemodynamic Measure	Statistic	df	p
HbT	.877	21	.013
HbO	.932	21	.152
HbR	.885	21	.018

Supplementary table S7: Sign test result for HbT and HbR return to baseline (HbT/HbR mean values between 15-20s for trials with the most locomotion compared with the mean values between 15-20s for trials with the least locomotion)

	N	Mean	Median	SEM	z	p
HbT most locomotion	21	1.018	1.019	.005	-	-
HbT least locomotion	21	0.995	0.997	.002	-	-
Difference HbT most vs least	21	.024	.024	.005	-3.055	.001
HbR most locomotion	21	0.982	0.980	.004	-	-
HbR least locomotion	21	1.000	0.999	.003	-	-
Difference HbR most vs least	21	-.022	-.021	.005	3.491	.000

Supplementary table S8: Wilcoxon Signed Ranks test for HbO return to baseline (HbO mean value between 15-20s for trials with the most locomotion compared with the mean value between 15-20s for trials with the least locomotion)

	N	Mean	Median	SEM	z	p
HbO most locomotion	21	1.028	1.030	.006	-	-
HbO least locomotion	21	0.992	0.994	.003	-	-
Difference HbO most vs least	21	.036	.032	.007	-3.702	.000

Two-way Repeated measures ANOVAs for 2s whisker simulation trials

Supplementary table S9: Shapiro Wilk test of normality for each time window, amount of locomotion and haemodynamic measures

	Most Locomotion						Least Locomotion					
	HbT		HbO		HbR		HbT		HbO		HbR	
Time window	df	p	df	p	df	p	df	p	df	p	df	p
-5-0	21	.000*	21	.001*	21	.518	21	.380	21	.174	21	.867
0-5	21	.000*	21	.001*	21	.654	21	.872	21	.680	21	.186
5-10	21	.000*	21	.000*	21	.429	21	.172	21	.234	21	.649
10-15	21	.000*	21	.001*	21	.316	21	.123	21	.496	21	.991
15-20	21	.000*	21	.005*	21	.843	21	.926	21	.739	21	.046*

*Performed on studentised residuals. Time window is the time window in which locomotion was calculated for ranking purposes. *Indicates normality is violated*

Supplementary table S10: Sphericity Results for the two-way repeated measures ANOVAs (Mauchly's test)

	HbT				HbO				HbR			
Factor	X^2	df	p	ε	X^2	df	p	ε	X^2	df	p	ε
Time	20.297	9	.017	.731	15.859	9	.071	.753	5.798	9	.761	.883
Time * Locomotion	24.286	9	.004	.645	17.771	9	.039	.723	20.637	9	.015	.632

ε indicates Greenhouse Geiser value. X^2 Chi–squared value. Values <.05 sphericity violated

Supplementary table S11: Two-Way Repeated ANOVA outputs for HbT, HbO and HbR investigating the interaction between the amount of locomotion (factors: most & least) and the time at which locomotion occurred (factors: -5-0s, 0-5s, 5-10s, 10-15s, 15-20s)

	HbT				HbO				HbR			
Factor	df	F	p	η_p^2	df	F	p	η_p^2	df	F	p	η_p^2
Time	2.925, 58.492	7.849	.000	.282	4, 80	8.435	.000	.297	4, 80	9.134	.000	.314
Locomotion	1, 20	6.032	.023	.232	1, 20	4.868	.039	.196	1, 20	3.723	.068	.157
Time * Locomotion	2.578, 51.566	13.351	.000	.400	2.894, 57.876	13.317	.000	.400	2.526, 50.521	8.712	.000	.303

η_p^2 partial eta squared values are used for effect size estimates. Small effect = 0.01, medium effect = 0.06, large effect = 0.14.

Supplementary table S12: Sphericity Results (Mauchly's test) for simple main effects (One-way ANOVAs) investigating the effects of timing of locomotion on sensory- evoked hemodynamic responses for the most and least locomotion

	HbT				HbO				HbR			
	X^2	df	p	ε	X^2	df	p	ε	X^2	df	p	ε
Most												
Time	29.923	9	.000	.630	30.653	9	.000	.665	19.251	9	.024	.672
Least												
Time	17.153	9	.047	.735	11.929	9	.219	.772	13.192	9	.156	.729

ε indicates Greenhouse Geiser value. Most refers to most locomotion, least refers to least locomotion

Supplementary table S13: Simple main effects to investigate the interaction between the amount and timing of locomotion and the effect on the haemodynamic response

Factor: Time	**HbT**				**HbO**				**HbR**			
	df	F	p	η_p^2	df	F	p	η_p^2	df	F	p	η_p^2
Most Locomotion	2.520, 50.409	12.998	.000	.394	2.660, 53.192	12.788	.000	.390	2.689, 53.781	11.504	.000	.365
Least Locomotion	2.940, 58.791	8.933	.000	.309	4, 80	9.939	.000	.332	4, 80	6.829	.000	.255

*One-way ANOVAs were use to assess simple main effects

η_p^2 partial eta squared values are used for effect size estimates. Small effect = 0.01, medium effect = 0.06, large effect = 0.14.

Supplementary table S14: Notable comparisons between 5s time windows for HbT, HbO and HbR peaks during whisker stimulation during most or least locomotion conditions

Haemodynamic Measure	Time window for ranking locomotion and time window compared to	P value
Most Locomotion		
HbT	-5-0 > 15-20	.013
	0-5 > 5-10	.006
	0-5 > 10-15	.003
	0-5 > 15-20	.000
HbO	-5-0 > 10-15	.048
	-5-0 > 15-20	.008
	0-5 > 5-10	.008
	0-5 > 10-15	.003
	0-5 > 15-20	.000
HbR	-5-0 < 5-10	.017
	-5-0 < 10-15	.012
	-5-0 < 15-20	.005
	0-5 < 5-10	.013
	0-5 < 10-15	.004
	0-5 < 15-20	.001
Least Locomotion		
HbT	-5-0 > 0-5	.000
	0-5 < 5-10	.013
	0-5 < 10-15	.009
	0-5 < 15-20	.005
HbO	-5-0 > 0-5	.000
	0-5 < 5-10	.006
	0-5 < 10-15	.001
	0-5 < 15-20	.002
HbR	-5-0 < 0-5	.008
	0-5 > 5-10	.018
	0-5 > 10-15	.007
	0-5 > 15-20	.015

> Indicates greater than and < indicates less than

Supplementary table S15: Pairwise comparisons with a Bonferroni correction comparing mean peaks for trials in which most and least locomotion occurred during the different time windows

		Most Locomotion		Least Locomotion					
Time window	Measure	*M*	*SEM*	*M*	*SEM*	*df*	*F*	*p*	η_p^2
-5-0	HbT	1.049	± .008	1.035	± .003	1, 20	3.466	.077	.148
	HbO	1.078	± .011	1.061	± .006	1, 20	2.401	.137	.107
	HbR	0.930	± .008	0.944	± .006	1, 20	2.149	.158	.097
0-5	HbT	1.054	± .007	1.020	± .002	1, 20	19.676	.000*	.496
	HbO	1.083	± .009	1.033	± .004	1, 20	24.825	.000*	.554
	HbR	0.934	± .006	0.969	± .004	1, 20	38.753	.000*	.660
5-10	HbT	1.041	± .007	1.031	± .003	1, 20	3.144	.091	.136
	HbO	1.063	± .009	1.052	± .005	1, 20	1.702	.207	.078
	HbR	0.948	± .005	0.952	± .005	1, 20	.486	.494	.024
10-15	HbT	1.037	± .005	1.034	± .004	1, 20	.756	.395	.036
	HbO	1.058	± .007	1.057	± .006	1, 20	.057	.814	.003
	HbR	0.951	± .005	0.948	± .006	1, 20	.316	.580	.016
15-20	HbT	1.032	± .004	1.031	± .003	1, 20	.058	.812	.003
	HbO	1.052	± .006	1.052	± .005	1, 20	.000	.995	.000
	HbR	0.954	± .005	0.951	± .005	1, 20	.219	.645	.011

**Indicates a significant difference between the mean peak of the haemodynamic measure when comparing most and least locomotion, with Bonferroni adjustment applied. M indicates mean and SEM indicates standard error of the mean*

η_p^2 partial eta squared values are used for effect size estimates. Small effect = 0.01, medium effect = 0.06, large effect = 0.14.

Two-way Repeated measures ANOVAs for linear subtraction of spontaneous trials from 2s whisker stimulation trials

Supplementary table S16: Shapiro Wilk test of normality for each time window, amount of locomotion and haemodynamic measures

	Most Locomotion						Least Locomotion					
	HbT		**HbO**		**HbR**		**HbT**		**HbO**		**HbR**	
Time window	df	p	df	p	df	p	df	p	df	p	df	p
-5-0	21	.000*	21	.005*	21	.150	21	.742	21	.999	21	.923
0-5	21	.000*	21	.014*	21	.618	21	.665	21	.625	21	.036*
5-10	21	.007*	21	.374	21	.663	21	.003*	21	.030*	21	.132
10-15	21	.013*	21	.721	21	.832	21	.002*	21	.336	21	.402
15-20	21	.024*	21	.945	21	.410	21	.006*	21	.021*	21	.054

*Performed on studentised residuals. Time window is the time window in which locomotion was calculated for ranking purposes. *Indicates normality is violated*

Supplementary table S17: Sphericity Results for the two-way repeated measures ANOVAs (Mauchly's test)

	HbT				HbO				HbR			
Factor	X^2	df	p	ε	X^2	df	p	ε	X^2	df	p	ε
Time	15.667	9	.075	.707	14.081	9	.121	.733	8.073	9	.529	.798
Time * Locomotion	24.965	9	.003	.650	17.410	9	.043	.720	14.000	9	.124	.793

ε indicates Greenhouse Geiser value. X^2 Chi–squared value. Values <.05 sphericity violated

Supplementary table S18: Two-Way Repeated ANOVA outputs for HbT, HbO and HbR investigating the interaction between the amount of locomotion (factors: most & least) and the time at which locomotion occurred (factors: -5-0s, 0-5s, 5-10s, 10-15s, 15-20s)

	HbT				HbO				HbR			
Factor	df	F	p	η_p^2	df	F	p	η_p^2	df	F	p	η_p^2
Time	4,80	1.241	.300	.058	4,80	0.622	.648	.030	4,80	2.563	.045	.114
Locomotion	1,20	0.426	.522	.021	1,20	0.417	.526	.020	1,20	2.030	.170	.092
Time * Locomotion	2.599,51.984	5.290	.004*	.209	2.878, 57.562	5.248	.003	.208	4,80	3.123	.019	.135

η_p^2 partial eta squared values are used for effect size estimates. Small effect = 0.01, medium effect = 0.06, large effect = 0.14.

Supplementary table S19: Sphericity Results (Mauchly's test) for simple main effects (One-way ANOVAs) investigating the effects of timing of locomotion on sensory- evoked hemodynamic responses for the most and least locomotion

	HbT				HbO				HbR			
	X^2	df	p	ε	X^2	df	p	ε	X^2	df	p	ε
Most												
Time	23.435	9	.005	.679	19.677	9	.020	.708	15.675	9	.075	.687
Least												
Time	24.856	9	.003	.593	16.553	9	.057	.682	6.793	9	.660	.857

ε indicates Greenhouse Geiser value. Most refers to most locomotion, least refers to least locomotion

Supplementary table S20: Simple main effects to investigate the interaction between the amount and timing of locomotion and the effect on the haemodynamic response

Factor: Time	**HbT**				**HbO**				**HbR**			
	df	F	p	η_p^2	df	F	p	η_p^2	df	F	p	η_p^2
Most Locomotion	2.717, 54.340	3.915	.016	.164	2.832, 56.646	2.891	.046	.126	4,80	0.601	.663	.029
Least Locomotion	2.373, 47.461	3.754	.024	.158	4,80	4.179	.004	.173	4,80	4.925	.001	.198

*One-way ANOVAs were used to assess simple main effects

η_p^2 partial eta squared values are used for effect size estimates. Small effect = 0.01, medium effect = 0.06, large effect = 0.14.

Supplementary table S21: Notable comparisons between 5s time windows for HbT, HbO and HbR peaks during whisker stimulation during most or least locomotion conditions

Haemodynamic Measure	Time window for ranking locomotion and time window compared to	P value
Most Locomotion		
HbT	0-5 > 15-20	.049
Least Locomotion		
HbT	0-5 < 10-15	.015
HbO	0-5 < 10-15	.006
HbR	0-5 > 10-15	.034

> Indicates greater than and < indicates less than

Supplementary table S22: Pairwise comparisons with a Bonferroni correction comparing mean peaks for trials in which most and least locomotion occurred during the different time windows

		Most Locomotion		Least Locomotion					
Time window	Measure	*M*	*SEM*	*M*	*SEM*	*df*	*F*	*p*	η_p^2
-5-0	HbT	1.034	± .007	1.040	± .004	1, 20	0.777	.388	.037
	HbO	1.051	± .008	1.069	± .007	1, 20	3.198	.089	.138
	HbR	0.948	± .007	0.929	± .007	1, 20	3.558	.074	.151
0-5	HbT	1.046	± .007	1.026	± .003	1, 20	10.049	.005*	.334
	HbO	1.070	± .009	1.046	± .004	1, 20	6.790	.017*	.253
	HbR	0.943	± .006	0.953	± .005	1, 20	1.757	.200	.081
5-10	HbT	1.037	± .006	1.035	± .005	1, 20	0.225	.640	.011
	HbO	1.056	± .008	1.058	± .007	1, 20	0.090	.767	.004
	HbR	0.951	± .006	0.948	± .005	1, 20	0.171	.683	.008
10-15	HbT	1.034	± .004	1.038	± .004	1, 20	1.217	.283	.057
	HbO	1.053	± .006	1.065	± .006	1, 20	3.969	.060	.166
	HbR	0.950	± .006	0.934	± .006	1, 20	6.060	.023*	.233
15-20	HbT	1.031	± .003	1.033	± .003	1, 20	0.735	.402	.035
	HbO	1.051	± .005	1.058	± .005	1, 20	1.324	.263	.062
	HbR	0.947	± .006	0.939	± .005	1, 20	1.334	.262	.063

**Indicates a significant difference between the mean peak of the haemodynamic measure when comparing most and least locomotion, with Bonferroni adjustment applied. M indicates mean and SEM indicates standard error of the mean*

η_p^2 partial eta squared values are used for effect size estimates. Small effect = 0.01, medium effect = 0.06, large effect = 0.14.

Chapter 3: Characterising vascular function in mouse models of Alzheimer's disease, atherosclerosis and mixed Alzheimer's and atherosclerosis

This manuscript has been prepared for submission to a journal

Characterising vascular function in mouse models of Alzheimer's disease, atherosclerosis and mixed Alzheimer's and atherosclerosis

Beth Eyre[1,2,3]*, Dave Drew[,2,3,4], Alexandra Rayson[3,4], Osman Shabir[1,2,3,4], Llywelyn Lee[1,2,3], Rahul Sidhu[1,2,3], Sheila Francis[2,3,4], Jason Berwick[1,2,3+], Clare Howarth[1,2,3+]

[1]Sheffield Neurovascular Lab, Department of Psychology, University of Sheffield, Alfred Denny Building, Western Bank, Sheffield, S10 2TN (United Kingdom)
[2]Neuroscience Institute, University of Sheffield, Sheffield, S10 2TN (United Kingdom)
[3]Healthy lifespan Institute, University of Sheffield, Sheffield, S10 2TN (United Kingdom)
[4]Department of Infection, Immunity & Cardiovascular Disease (IICD), University of Sheffield Medical School, Royal Hallamshire Hospital, Beech Hill Road, Sheffield, S10 2RX (United Kingdom)
[^]These authors contributed equally. [+]These authors contributed equally. * Corresponding author.

I Beth Eyre am sole first author on this manuscript. I completed surgeries, cognitive and haemodynamic imaging data collection. Some immunohistochemistry experiment data collection, data analysis, statistical tests and wrote up the manuscript.

Dave Drew taught and assisted with immunohistochemistry staining of brain slices. Alexandra Rayson, taught and assisted with the aortic dissection and staining. Osman Shabir and Llywelyn Lee assisted with some perfusions. Rahul Sidhu performed one run of immunohistochemistry staining. Myself, Clare Howarth and Jason Berwick analysed the data. Myself, Clare Howarth and Jason Berwick wrote code for the analysis. Sheila Francis provided the expertise on the atherosclerosis side of the project. Myself, Clare Howarth and Jason Berwick edited and proofread the manuscript.

3.1 Abstract

Alzheimer's disease is an increasing issue within society, with vascular changes occurring early in disease. However, Alzheimer's disease does not occur in isolation and there are many comorbidities associated with the disease – especially diseases of the vasculature. Atherosclerosis is a known risk factor for the subsequent development of Alzheimer's disease, therefore understanding how both diseases interact will provide a greater understanding of co-morbid disease progression and aid the development of potential new treatments. The current study used APP/PS1 Alzheimer's mice, atherosclerosis mice (induced using a viral injection of a gain-of-function mutation of PCSK9 and a western diet) and a mixed disease group (APP/PS1 & atherosclerosis) between the ages of 9 and 12 months. Recognition memory was assessed using the novel object recognition test. Cerebrovascular function was assessed in awake mice using 2D-Optical imaging spectroscopy (2D-OIS) to assess whisker-evoked haemodynamic responses. Immunohistochemistry was used to assess amyloid pathology. We found no effect of disease on non-spatial recognition memory. We found no effect of disease on evoked-haemodynamic responses when locomotion was ignored, or ranked across the whole trial. However, we did find that when locomotion was ranked during the whisker stimulation (5-10 seconds) during the least locomotion trials, the atherosclerosis group had reduced haemodynamic responses compared to wild-type mice. We observed preserved vascular responses in Alzheimer's and mixed disease mice and found no difference in amyloid pathology between Alzheimer's and mixed disease mice. These findings suggest that systemic atherosclerosis may impact cerebrovascular function. Our results also reveal that there may be different mechanisms that are impaired in atherosclerosis, as locomotion-induced coupling was preserved whereas whisker-evoked coupling was impaired.

3.2 Introduction

Dementia is one of the most pressing health issues of our time. Globally, there are over fifty-five million people living with dementia, with this set to increase to over one hundred and thirty-nine million by 2030[1]. Alzheimer's disease is the most common cause of dementia, with hallmark features including the accumulation of proteins, such as amyloid beta plaques[2] and hyperphosphorylated tau tangles[3]. Accumulating

evidence suggests that neurovascular dysfunction may be important in the pathogenesis of Alzheimer's disease; with vascular changes being observed as one of the first pathological changes in the disease[4]. According to the two-hit vascular hypothesis[5] vascular risk factors, such as diabetes, hypertension, cardiovascular disease and/or cerebrovascular damage result in damage to the blood-brain-barrier (BBB)[6,7], resulting in hypoperfusion[8]. This damage to the BBB and reduction in blood flow to the brain alters the production and clearance of proteins, such as amyloid beta in the brain. Resulting in an overproduction and an impairment in clearance of these proteins[9,10]. This increased accumulation of proteins can be damaging to neurons, resulting in neuronal dysfunction, neurodegenerative changes and ultimately neuronal loss, leading to the cognitive impairment observed in Alzheimer's disease.

Alzheimer's disease is not a disease that occurs in isolation. As age is the greatest risk factor of the disease, many individuals possess comorbidities[11]. Individuals who possess a greater number of comorbidities have poorer outcomes[12]. AD and diseases of the vasculature share common risk factors, such as diabetes, hypertension and hypercholesterinaemia[13,14] and the presence of vascular risk factors in mid-life has been linked to an increase in the risk of developing dementia[15,16]. However, research assessing how vascular comorbidities impact neurovascular function are lacking. It is important to assess how comorbid disease may affect neurovascular function, especially within preclinical research as this could potentially explain why many animal studies assessing drug treatments for Alzheimer's disease are unable to translate to humans[17–19].

Atherosclerosis is the second biggest killer in the UK[20], (with dementia and Alzheimer's disease being the leading cause of death). It is an inflammatory disease caused by an excess of lipids within the blood. Over time this results in the deposition of fat within the intima of arteries within the body[21]. Atherosclerosis can result in reduced perfusion, due to the occlusion of arteries. Over time, atherosclerotic plaques can detach and form thrombi which can result in heart attacks and strokes[21,22]. Worldwide, the disease may affect up to 28% of people aged between 28-79[23]. Many studies have observed associations between atherosclerosis and AD[24–26].

Atherosclerosis can be modelled in a number of ways[27]. For example, atherosclerosis genetic knockout mouse models such as the LDLR$^{-/-}$[28] or APOE$^{-/-}$[29] can be used. Neurovascular deficits have previously been reported in the LDLR$^{-/-}$ model of atherosclerosis. Lu et al.,[30] reported weaker evoked-haemodynamic responses to a whisker stimulation in this model – as well as hypoxic pockets in cortical tissue and microvascular changes in capillaries at 12 months of age. This group further observed that in the cortex of atherosclerotic mice at 12 months of age tissue oxygenation was reduced, as well as slower red blood cell velocity and flux, in addition to observing smaller capillary diameters, as compared to younger mice[31]. However, breeding genetically modified mice can be time consuming and expensive, especially when wanting to model atherosclerosis with other diseases, due to the greater number of back crosses needed. Recently, other ways of inducing atherosclerosis have been employed, via the use of viral vectors[32–34]. Injecting a gain-of function mutation of PCSK9 via a viral vector (in addition to a western diet) can increase cholesterol levels[32,33] and over time result in atherosclerotic lesions. PCSK9 is a protein within the liver, where it's role is to internalise and degrade LDL receptors[35]. A gain of function mutation results in an increased amount of PCSK9 and therefore fewer LDL receptors, therefore leading to enhanced LDL within the blood[36]. Recently, research has investigated whether atherosclerosis alone and in the presence of amyloid overexpression can impact neurovascular function[34]. In a lightly anesthetised preparation, Shabir et al.,[34] observed that the presence of atherosclerosis resulted in a reduction in the size of the peak haemodynamic response to a 2s whisker stimulation. However, they observed no effect of AD alone or mixed Alzheimer's and atherosclerosis on evoked-haemodynamic responses.

In this study we chose to model comorbid Alzheimer's and atherosclerosis using an APP/PS1 mouse model in addition to a viral injection of a gain-of-function mutation of PCSK9 (with a western diet) to model atherosclerosis in an Alzheimer's disease model. We are aware of a previous study that has used this same method to induce hypercholesteremia in the APP/PS1 model of AD[33]. However, they only investigated the impact of mixed disease on amyloid plaque number in the hippocampus. Therefore, in this study we aimed to assess how AD alone, atherosclerosis alone and mixed AD and atherosclerosis impact recognition memory, sensory-induced vascular

function and amyloid pathology. As previously mentioned, Shabir et al., investigated the effect of atherosclerosis alone (using a gain-of function mutation of PCSK9) and mixed atherosclerosis and Alzheimer's disease on neurovascular function, however they used a 'mild' model of AD that develop fewer plaques[37,38] in addition to completing the neurovascular experiments in a lightly anesthetised state[34]. Therefore, in this study we aimed to replicate and further extend the findings of the above study by using a more 'severe' model of AD, in which mice develop plaques from an earlier age, in addition to completing the vascular imaging experiments in an awake preparation to avoid the confounds of anaesthesia[39].

Based on previous research, we hypothesised that AD mice would have impaired recognition memory[40,41], as assessed by the novel object recognition test. We also hypothesised that vascular function would be impaired in the APP/PS1 model[42,43], the atherosclerosis model[34] and the mixed model, which would be evidenced by these groups having a smaller whisker-evoked haemodynamic response to a 2s stimulation compared to the WT control group.

3.3 Methods

3.3.1 Animals

All mice were aged between 9-12m during the study. The following groups of mice were used: APP/PS1 (B6.C3-Tg(APPswe,PSEN1dE9)85Dbo/Mmjax #34829)[33,3444] Alzheimer's model (male and female), WT littermates (male and female), an atherosclerosis model (male only): WT-littermates injected with rAAV8-mPCSK9-D377Y (6 × 10^{12} virus molecules/ml) (Vector Core, Chapel Hill, NC) at 11 weeks of age (i/v or i/p + a western diet at 12 weeks (21% fat, 0.15% cholesterol, 0.03% cholate, 0.296% sodium; #829100, Special Diet Services UK) and a mixed disease group (male only): APP/PS1 mice injected with rAAV8-mPCSK9-D377Y (6 × 10^{12} virus molecules/ml) (Vector Core, Chapel Hill, NC) at 11 weeks of age (i/v or i/p + a western diet at 12 weeks). Western diet was begun at 12 weeks and continued until the end of the study. Mice were housed in litters where possible, however some were singly house for welfare reasons or if there were no available littermates. Post-surgery all mice were singly housed. A 12hr dark/light cycle (lights on 06:00-18:00) was implemented. Food and water were accessible ad-libitum with the western diet limited

to 5g per day per mouse. Experiments were completed during the light cycle, between the hours of 8am and 4pm. Procedures used in the study were approved by the UK Home Office and in agreement with the guidelines and scientific regulations of the Animals (Scientific Procedures) Act 1986. Further approval was also granted by the University of Sheffield licensing committee and ethical review board. The following study is reported in accordance with the ARRIVE guidelines. Mice selection from the colony was randomised. The experimenter was blinded from disease group where possible. The experimenter conducted the analysis in a blinded manner.

3.3.2 Novel object recognition test

At 9 months of age non-spatial recognition memory was assessed using the novel object recognition (NOR) test. A 2-day protocol was used based upon the protocol developed by Lupetow et al[45]. On day 1 the habituation phase took place. Mice were placed into a square open field arena (40x40x40cm) for 10 minutes and behaviour was recorded using a camera placed above the arena. Day 2 consisted of the training and testing phases. In the training phase mice were placed into the open field arena with two identical objects (either two glass beakers or two duplo tower blocks – these were counterbalanced across mice). Objects were placed diagonally from each other; positioning of objects was also counterbalanced across mice. After 10 minutes mice were removed from the arena. After a 1-hour retention period mice were placed back into the arena (Figure 3.1 a). However, one of the familiar objects had been replaced with the novel object. Mice were handled for approximately 7 days prior to cognitive testing to reduce experimental stress. The arena and objects were cleaned with 70% ethanol between mice. At least 30 minutes before cognitive testing mice were moved to the experimental room to habituate them to the new room and to reduce stress. Time spent with each of the objects was measured using EthoVision software (EthoVision XT 15, Noldus). Mice were deemed to be exploring an object if their nose was <2cm away from the object. However, climbing on top of objects was not considered exploration and was not included as exploration of objects. Distance travelled and velocity during training and testing was also recorded. Exploration of individual objects allowed for the calculation of the preference index. Preference index was calculated by dividing the time spent with the novel object with the total exploration of both objects multiplied by one-hundred (during the testing phase).

$$\frac{Time\ spent\ with\ novel\ object\ (s)}{Total\ exploration\ of\ both\ objects\ (s)}\ x\ 100$$

This produced a percentage score of preference for the novel object, with a score of 50% suggesting no preference for the novel object, a score >50% indicating a preference for the novel object and a score <50% indicating a preference for the familiar object. In order to be included in the analysis mice had to explore both familiar objects (in the training phase) for a minimum of 20s each. Two mice were excluded from the final analysis as they didn't reach the minimum exploration criteria. And one mouse was excluded as the video recording of the experiment did not work.

3.3.3 Surgery

Anaesthesia was induced using a cocktail of ketamine (50mg/kg) and medetomidine (0.65mg/kg) (subcutaneously, s/c). The surgical plane of anaesthesia was maintained with the addition of isoflurane (0.5-0.8% in 100% oxygen). Carprofen (10mg/kg, s/c) was administered prior to removal of hair from the head. Animals were placed in a stereotaxic frame (Kopf Instruments) and ophthalmic gel was administered (Viscotears, Novartis). Body temperature was constantly monitored and sustained using a rectal thermometer and a homeothermic blanket (Harvard Apparatus). Iodine and bupivacaine (50-100mcL at 0.025%) were applied prior to exposing the skull. Suture lines were covered with cyanoacrylate glue and a dental scraper scored the contralateral side of the skull. The bone overlying the right somatosensory cortex was thinned to translucency (~4mm^2) using a dental drill. Saline was administered throughout to cool the area and to assist with the visualisation of the pial vasculature. Cyanoacrylate glue was applied to the thinned region. A metal headplate was attached using dental cement (Superbond C & B; Sun Medical). Atipamezole (2mg/kg in 0.3ml warm sterile saline s/c) was administered at the end of the procedure to reverse the effects of medetomidine. Following surgery, mice were placed in an incubator (29 degrees) and monitored. Mice were housed individually and given at least one week to recover, prior to habituation and awake imaging. Mice were closely observed for weight loss and signs of pain for 3-days after surgery and administered carprofen jelly (10mg/kg) for at least 1-day post-surgery.

3.3.4 Awake Imaging

The awake imaging set up was previously described in Eyre et., al 2022[46], however a modified habituation and imaging procedure was used in the current study. Briefly, one week after surgery mice were habituated to the awake imaging spherical treadmill set up. Over 5 days, mice were familiarised to the experimental room, experimenter and awake imaging apparatus. On day one, mice were placed on the spherical treadmill for 10 minutes, the room light was kept on, and mice were not head-fixed. Day 2, mice were head-fixed and placed on the spherical treadmill, lights were turned off and 2s whisker stimulations were conducted using a mechanical plastic T-bar. Mice were on the ball for approximately 20 minutes. Day 3 was the same as day 2, with a supplementary experiment conducted; a 'spontaneous' experiment was completed, where haemodynamic measurements were collected but no whisker stimulation applied. Mice were on the ball for approximately 30 minutes. Day 4 followed the same procedure as the preceding two days; however, an additional 16s whisker stimulation experiment was conducted. Mice were on the ball for approximately 45 minutes to 1 hour. Day 5 followed the exact same procedure as day 4. Mice received a reward of sunflower seeds following each experimental imaging day. Haemodynamic data was collected on all days where mice were head-fixed and used in the subsequent analysis. Only 2s whisker stimulation experiments were analysed in the current study. Mice were briefly anaesthetised using isoflurane (3-4%) prior to being placed on the awake imaging apparatus.

3.3.5 Locomotion data collection and analysis

Locomotion tracking was conducted in the same way as described in Eyre et al., 2022[46]. Locomotion behaviours were gathered using a spherical treadmill with an optical motion sensor. In house Matlab scripts (MathWorks, 2019b) were used to analyse the locomotion data. The optical motion sensor logged treadmill movement during all experiments. Locomotion data files were composed of: the locomotion data; (this was a vector which matched the rotation of the treadmill. When the mouse was still this value was 0, when the treadmill moved integers greater than 0 signified this, the faster the treadmill moved the larger the integer, this was plotted as distance (arbitrary unit, AU). A time vector was also included; this meant locomotion data could be measured across time (in seconds). The trigger points were also contained within

the file; these points specified the explicit timing of whisker stimulations during the different trials. This meant we could match locomotion to the precise timing of the corresponding haemodynamic responses (when we examined whisker stimulation evoked haemodynamic responses).

3.3.6 2D-Optical imaging spectroscopy (2D-OIS)

Changes in haemoglobin concentration to a 2s whisker stimulation were investigated in the surface vasculature using widefield imaging. Two-dimensional optical imaging (2D-OIS) uses four wavelengths of light to measure changes in oxygenated (HbO), deoxygenated (HbR) and total levels of haemoglobin (HbT). Cortical haemodynamics were investigated using 4 differential wavelengths of light (494 ± 20 nm, 560 ± 5 nm, 575 ± 14 nm and 595 ± 5 nm). These wavelengths illuminated the thinned window region of the cortex, using a Lambda DG-4 high-speed galvanometer (Sutter Instrument Company, USA). A Dalsa 1M60 CCD camera was implemented to capture remitted light at 184×184 pixels, at a 32 Hz frame rate, providing a resolution of ~ 75 µm. 2-D spatial maps of micromolar changes in HbO, HbR and HbT, were collected using 2D-OIS. Spatial maps can reveal changes in haemoglobin concentrations in the surface vasculature, within differential vascular compartments (arteries, veins, parenchyma). This is accomplished by implementing a path length scale algorithm (PLSA) to complete a spectral analysis. The PLSA uses the modified Beer Lambert Law, with a path-length correction factor, in addition to predicted absorption values of HbT, HbO and HbR[34,47,48]. Relative concentration estimates of the above were obtained from baseline values, where the haemoglobin concentration within the tissue was estimated as 100 µM, and tissue saturation of oxygen within the whisker region estimated at 70%.

3.3.7 Regions of Interest (ROI) derived from 2D spatial maps

ROIs were generated from the previously described 2D spatial maps, using in-house MATLAB scripts[34,47,48]. A whisker region was made using code that found the region of the cortex with the greatest change in HbT to a 2s whisker stimulation. Pixels were considered ‘active’ if they had a value that was >1.5 standard deviation (STD) across the entire spatial map of the surface vasculature. The whisker ROI was therefore the region of the cortex in which there was the largest increase in HbT in response to a 2s

whisker stimulation. ROIs for a whisker artery (an artery within the previously generated whisker region), whisker vein (a vein within the previously generated whisker region) and parenchyma (brain tissue that did not have an artery or vein in it within the previously generated whisker region) were also manually selected within the whisker region. ROIs were generated for each imaging session. Care was taken to select the same whisker artery, veins and parenchyma across imaging sessions for the same mice. Time series analyses in the current study were conducted on the whisker region.

3.3.8 Haemodynamic data analysis

Analysis of haemodynamic data was conducted in Matlab (R2019b) using in-house scripts. Imaging sessions were not included in the final analysis if there was visible motion, denoted by shadows around vessels on 2D spatial maps. Two-second whisker stimulation trials were conducted at 5Hz, with an interstimulus interval (ISI) of 25s (30 trials per experimental session, 750s of continuous data collection, stimulation at 5-7 seconds). Concurrent haemodynamic and locomotion data were collected during each imaging session. An average of the all 30 trials was taken from each imaging session and included in the group average. Spontaneous trials were also conducted, whereby continuous haemodynamic activity (changes in haemoglobin levels) and concurrent locomotion were collected for 750 seconds (without any whisker stimulation). Spontaneous trial haemodynamic data were not used within the current study. However, it was used and analysed in chapter 4. Peak HbT, HbO and HbR responses were used to assess whether there were differences in evoked-haemodynamic responses across groups. Peak responses were generated by taking the maximum (HbT and HbO) and minimum (HbR) peak responses per trial between 5-12 seconds (with the whisker stimulation occurring between 5-7 seconds). An average was then taken across the individual 30 peak responses per imaging session, then included in the group average.

3.3.9 Histology and immunohistochemistry

At the end of the final experiment mice were euthanised with pentobarbital (100 mg/kg, Euthatal, Merial Animal Health Ltd). Cardiac perfusions were completed using saline (0.9%). A subset of mice were also perfused with formalin (10%). Brains were

dissected and the whole brain (or half) was either placed in formalin (10%) or snap frozen in isopentane and stored in a -80 freezer. Formalin fixed brains were paraffin embedded (FFPE) and were cut into coronal slices (5-7um) using a vibratome. Coronal sections were mounted onto slides for subsequent immunohistochemistry.

3.3.10 Amyloid plaque burden immunohistochemistry

An avidin-biotin complex (ABC) method was used to stain and quantify amyloid plaque burden. Briefly, slides were dewaxed with xylene and rehydrated using ethanol (100%, 100%, 95%, 70%). Slides were put in the above ethanol baths for 5 minutes. Peroxidase activity was inhibited in a bath of 3% H_2O_2/12ml methanol for 20 minutes. Following this, slides were placed in 70% formic acid for 10 minutes. Antigen retrieval was completed using a microwave oven in a buffer of trisodium citrate (PH6) for 10 minutes. After antigen retrieval, slides were place in a bath of dH_2O for 10 minutes. Slides were washed in PBS (for 5 minutes x2). Slides were then incubated with 1.5% normal serum for 30 minutes at room temperature and then incubated with the primary antibody (Amyloid Beta Rabbit Monoclonal – 1:500, Abcam, ab201060) for 24 hours. Slides were again washed in PBS (for 5 minutes x2) and the secondary antibody was applied for 30 minutes at room temperature. Slides were then washed with PBS (for 5 minutes x2). A horseradish peroxidase avidin-biotin complex (Vectastain Elite Kit, Vector Laboratories, UK) was then applied and left at room temperature for 30 minutes. A final wash in PBS (for 5 minutes x2) was completed and then 3,3-diaminobenzidine tetrahydrochloride (DAB) (Vector Laboratories, UK) was applied to help visualise the antibody (left for 3 minutes). Slides were rinsed with dH_2O for 3-5 minutes and counterstained with haematoxylin. Finally, slides were dehydrated using baths of ethanol (70%, 90%, 100%, 100%) for 30 seconds each and placed in xylene for 2-3 minutes. Following dehydration, slices were mounted with coverslips using DPX.

Stained slides were scanned using a slide scanner (Axio Imager.Z2) at a 20x magnification and converted into TIFFs (ZEN Blue Edition). Plaque burden was assessed in the hippocampus using ImageJ. Plaque burden quantification was based upon an already published technique[49]. Briefly, images were opened in ImageJ. The polygon tool was used to draw around the hippocampus (the ROI) and the area of this

was measured. Colour images were converted to 8-bit greyscale images. A threshold was applied to identify amyloid positively stained areas. The threshold applied ranged between 70-100 due to differences in background staining of slides. Slides from the same subject always had the same threshold value. By using a threshold, pixels within the image were converted into a binary format, with black pixels indicating positive staining and white pixels revealing no positive staining. Amyloid burden was quantified using the ROI area, percentage area and area (of black pixels) within the ROI. The percentage area of positive staining was used as a measure of amyloid burden. Between 1 and 4 slices were used per mouse, and an average was taken for each subject (if applicable).

3.3.11 Identification and quantification of atherosclerosis

After cardiac perfusion, the heart and aorta were also dissected for atherosclerotic and mixed disease mice. The heart and aorta were blunt dissected and placed in formalin for a minimum of 24 hours before being placed in PBS. They remained in PBS until they were stained and embedded into wax filled petri dishes. Visible fat was removed from the aorta under a dissecting microscope and the aorta was cut from the heart at the aortic root. Dissecting scissors were used to cut the aorta down the middle to open up the aortic arch. This allowed the aorta to be laid flat and pinned to wax in a petri dish post-staining. Oil red O (Sigma, O0625-100G) was used to stain for natural triglycerides and lipids within the aortic arch. A solution of Oil red O (60% solution) was made using distilled water and isopropanol. Once the aorta had been cut it was stained. Briefly, the aorta was placed into distilled water (10 seconds) then isopropanol (2 minutes) and then into the Oil Red O solution (6 minutes). It was then placed in isopropanol (2 minutes) and finally rinsed in distilled water. Following staining, petri dishes were filled with wax. Once the wax had partially hardened 1mm insect pins (Fine Science Tools, FST) were used to pin the edges of the aorta into the wax. A 12MP camera, placed 10 cm above the samples was used to take images of stained aortas. ImageJ was used to quantify the presence of atherosclerotic plaque burden. The polygon tool was used to draw around the aortic arch (the ROI) and the area of this was measured. Images were converted to 8-bit greyscale images. Similarly, to the amyloid analysis, a threshold was applied to identify positively stained oil red o areas. A threshold of 150 was applied to all samples. Aortic arch plaque burden was

quantified using the ROI area, percentage area and area (of black pixels) within the ROI. The percentage area of positive staining was used as a measure of atherosclerotic burden.

3.3.12 Statistical tests

Appropriate statistical tests were conducted within SPSS (Version 26). Figures were generated in both Matlab (R2019b) and GraphPad Prism (Version 9). Assumptions of statistical tests were tested, if assumptions were not met appropriate non-parametric tests were conducted (if available). Normality was assessed using Shapiro Wilks. Outliers were assessed using box plots (outliers were defined as being 1.5 standard deviations away from the box plot). All outliers were kept within the data set. $P<.05$ was denoted as significant, if initial tests found significant differences, post hoc tests with a Bonferroni correction or Dunns correction, as appropriate, were completed. Kruskal Wallis tests were used to assess whether there were significant differences in preference index scores, distance travelled and velocity in the NOR test across different disease groups. Kruskal Wallis tests were also implemented to assess if there were significant differences in evoked-haemodynamic peak responses across groups. These tests were conducted to assess whether there were differences in peak HbT, HbO and HbR whisker-evoked responses across disease groups when locomotion was ignored, ranked across the whole 25s trial and when ranked during the whisker-stimulation (between 5-10s). Kruskal Wallis tests were also used to assess whether there were significant differences across disease groups for the summed locomotion responses (distanced travelled: assessed by AUC). A Mann Whitney U test was used to assess if there were significant differences in atherosclerotic plaque burden within the aortic arch of atherosclerotic and mixed disease mice. Finally, an independent sample t-test was used to assess if there were significant differences in hippocampal amyloid plaque burden between AD and Mixed disease groups. Descriptive statistics and detailed statistical outputs can be found in the supplementary tables. Apriori power calculations were not conducted for this study. A post-hoc power calculation was run to assess whether the sample size of groups used in the study was large enough to provide adequately powered results. Using an alpha value of α=0.05, and a total sample size of 31 (WT = 6, AD = 9, Athero = 10, Mixed = 6), an effect size (Cohens f) 3.00 was calculated with a power of 1, using the mean preference index values for

each group. This suggests that the above sample sizes provided adequate power for the NOR measure of non-spatial recognition memory. The overall effect is well powered; however, any subtle differences (between groups) may need a larger sample size to detect these, as sample sizes across groups were uneven. Additionally, effect sizes for the statistical tests conducted can be found in the supplementary tables.

3.4 Results

3.4.1 No effect of disease on recognition memory as assessed by the novel object recognition test

We used the novel object recognition test (NOR) to assess recognition memory across groups. Mice were placed into an open field area and could explore two of the same objects (training phase). After a one-hour delay, they were placed back into the same arena, however this time one of the previous objects had been replaced with a novel object (testing) (Figure 3.1 a). Mice have an innate preference for novelty, so therefore should want to spend more time with the novel object. Behavioural software was used to assess the time spent with each object, in order to assess the preference index across groups, (calculated by dividing the time spent with the novel object by the total exploration time of both objects, multiplied by one-hundred). A higher preference index score indicates a greater preference for the novel object. We found no significant differences in the preference index score across disease groups (Kruskal Wallis test; H (3 n=31) = 1.399, p=.706 (median preference index scores: WT=58.15, AD=55.50, ATH=61.28, MIX=60.24) (Figure 3.1 b). This suggests that there were no significant differences in the preference that mice had for the novel object – indicating that recognition memory may still be intact in AD, Atherosclerosis and Mixed disease mice at 9m of age, with a 1-hour retention interval between training and testing.

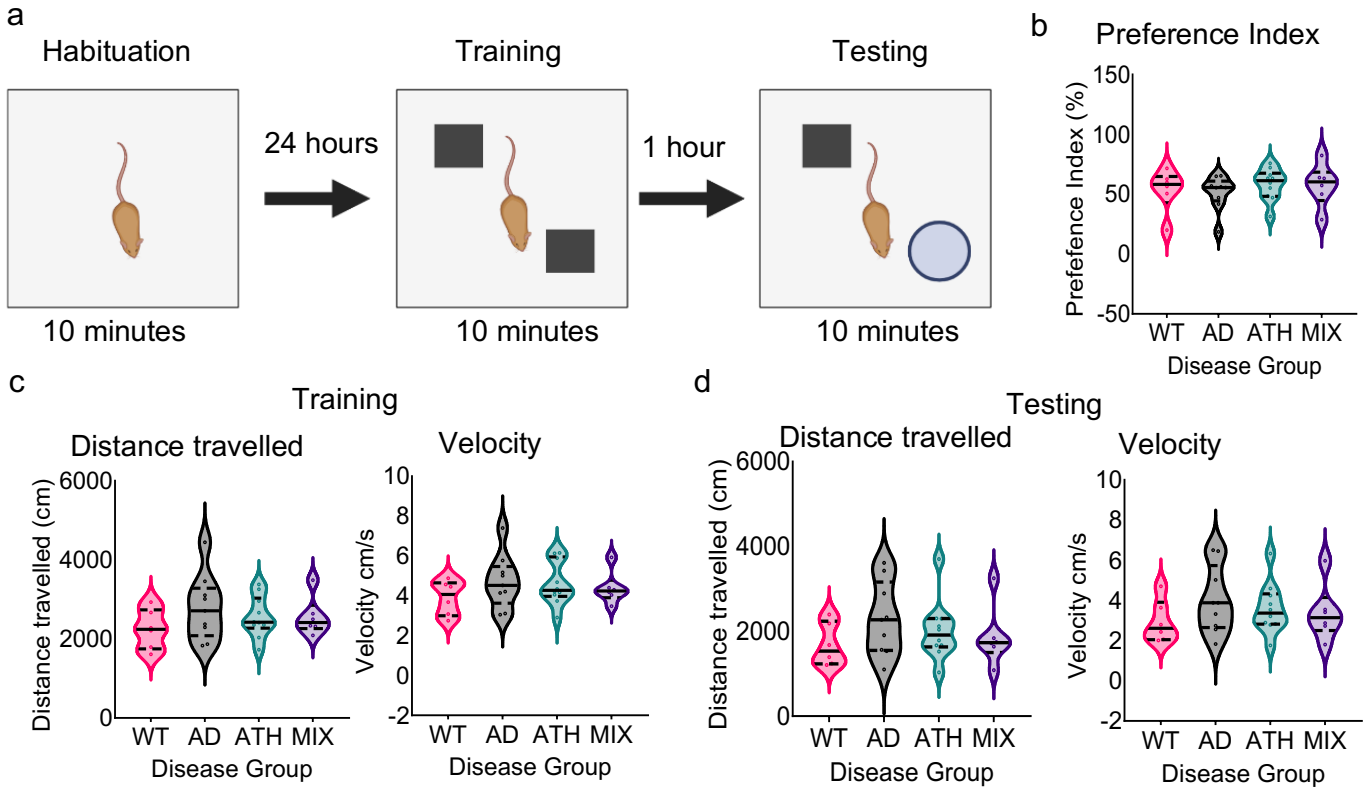

Figure 3.1: Recognition memory is preserved in AD, atherosclerosis and mixed disease mice as assessed by the NOR test

(a) *a schematic showing the NOR experimental procedure over a 2-day period. On day 2, the training and testing phases occur, with the testing phase occurring after a 1-hour retention interval.* ***(b)*** *a violin plot reveals the preference index (%) for the novel object (with individual preference indices shown for each animal). We found no difference in the preference index percentage scores across diseases groups suggesting recognition memory at a 1-hour retention period is intact in AD, atherosclerosis and mixed disease mice.* ***(c)*** *violin plots show the distance travelled (left) and velocity (right) across disease groups during the training phase. We found no differences in both distance travelled and velocity across disease groups during the training phase of the NOR test.* ***(d)*** *violin plots reveal the distance travelled (left) and velocity (right) across disease groups during the testing phase of the NOR. We also found no differences in the distance travelled or velocity across disease groups. Median (Black line) and interquartile range (dashed black line) shown. WT n= 6, AD n=9, ATH n=10 and Mix n=6.*

3.4.2 No effect of disease on locomotor behaviour during the training and testing phase of the NOR test

We also used the behavioural software to investigate locomotive behaviour during both training and testing phases of the NOR test. We found no significant differences across disease groups when assessing distance travelled and velocity of mice during both the training and testing sessions of the NOR test (Kruskal Wallis tests: distance travelled training; H (3 n=31) = 2.710, p=.439, velocity training; H(3 n=31)=1.452, p=.693, distance travelled testing; H(3 n=31)=2.090, p=.554, velocity testing; H(3 n=31)=2.197, p=.533) (Figures 3.1 c, d).

3.4.3 No effect of disease on evoked-haemodynamic responses when locomotion is ignored

Having assessed cognitive function, we next assessed haemodynamic responses to see whether there were differences in evoked haemodynamic responses, to a 2s whisker stimulation, to assess whether neurovascular function was affected by different diseases. To do this, we used 2D-OIS to measure haemoglobin changes (HbT, HbO and HbR) evoked by a 2s whisker stimulation in awake mice. Thirty 2s whisker stimulation trials were completed in head-fixed, awake mice whilst they were free to locomote on a spherical treadmill. Peak responses for HbT, HbO and HbR were taken by collecting maximal responses between 5 and 12s (with the whisker stimulation occurring between 5-7s). The peak responses per trial were averaged to generate a peak response per session, with each session contributing a single value to the overall group average.

When locomotion was ignored, we found that there was no effect of disease on evoked-haemodynamic responses. We found no differences in evoked median peak HbT, HbO and HbR responses to a 2s whisker stimulation when comparing WT mice with AD, atherosclerosis and mixed disease mice (Kruskal Wallis tests: HbT; H (3 n=132) = 4.351, p=.226, HbO; H (3 n=132) = 4.681, p=.197, HbR; H(3 n=132) = 5.550, p=.136) (Figure 3.2).

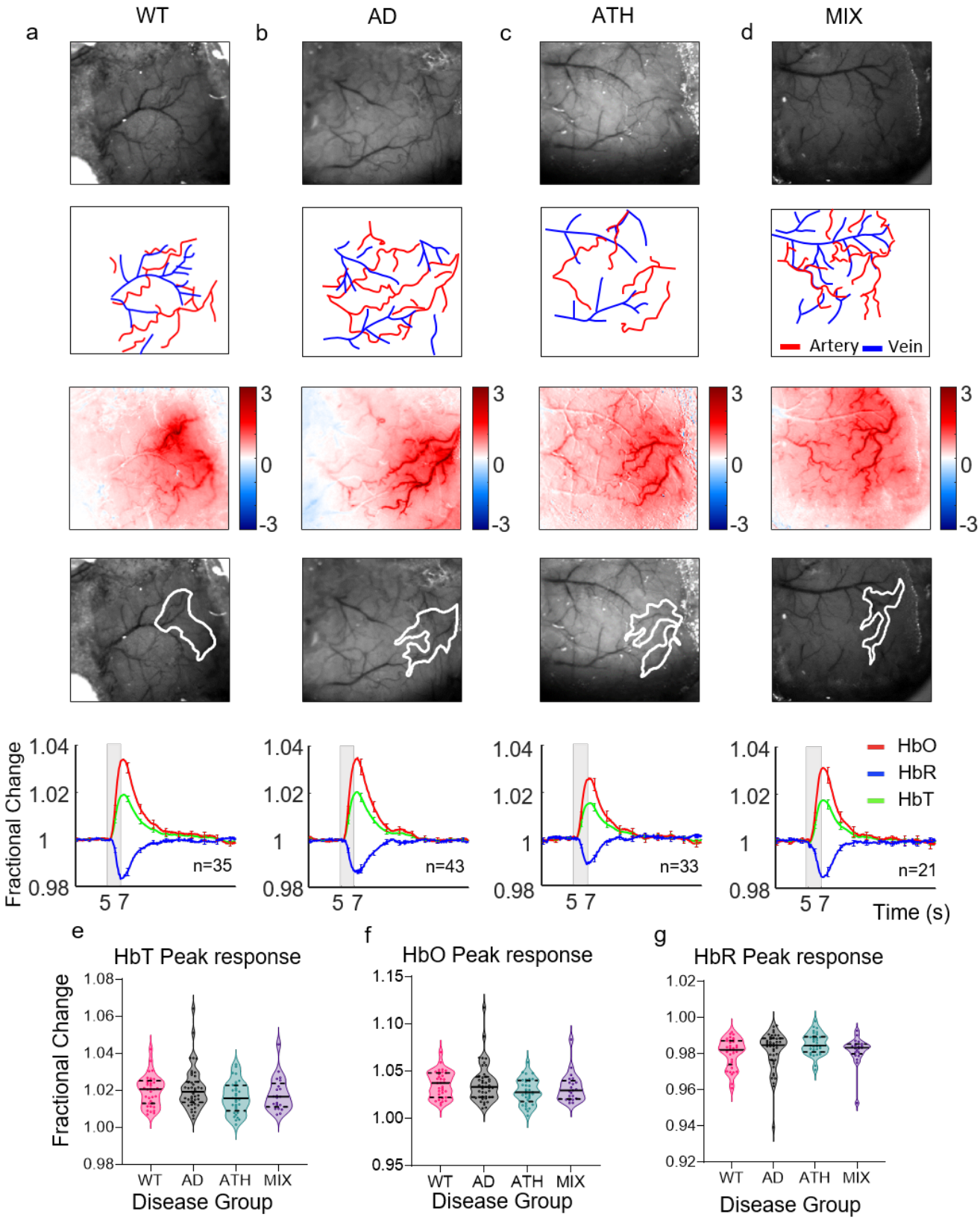

Figure 3.2: No effect of disease on evoked-haemodynamic peak responses when locomotion is ignored

Representative animal from each disease group ***(a)*** *WT* ***(b)*** *AD* ***(c)*** *ATH* ***(d)*** *Mix revealing the thinned window region (**row one**), vessel maps revealing arteries and veins (**row two**), a spatial map of hbt changes to a 2s whisker stimulation (**row three**) with red colours indicating an increase in HbT in response to a 2s whisker stimulation.* ***Row four*** *shows the group average for 2s whisker stimulation trials. From left to right: WT (n=35 (from 11 mice)), AD (n=43 (from 12 mice)), ATH (n=33 (from 10 mice)) and Mix (n=21 (from 6 mice)). Thirty, 2s whisker-stimulation trials were conducted per experimental session and included in the above time series analysis. Peak HbT, HbO and HbR values evoked by the 2s whisker stimulation (gray bar) were taken between 5-12s for all 30 trials per session. The peak value from each trial was then averaged together to produce an average peak value of HbT, HbO, HbR per session. Each average peak value per session was then included in the group average. Violin plots show* ***(e)*** *peak HbT,* ***(f)*** *HbO and* ***(g)*** *HbR responses to a 2s whisker stimulation. Median (Black line) and interquartile range (dashed black line) shown. Error bars show standard error of the mean (SEM). Individual mean peak values shown.*

3.4.4 No effect of disease when locomotion is ranked across the whole trial

Next, we assessed whether general walking activity throughout the whole trial had an effect on whisker-evoked responses. We previously reported that ranking locomotion across the entire trial did not affect the size of the haemodynamic response, but did affect the return to baseline, when comparing most locomotion vs least locomotion[46].

To assess the impact of general walking activity on whisker-evoked responses we ranked trials by locomotion. The top and bottom 20% (most locomotion n=6 and least locomotion n=6) were used within the study. In order to do this, we ranked the 30 trials, per individual session by locomotion during the entire trial (across the 25s trial). Trials were ranked in descending order, with the trials with the most locomotion being ranked from 1 all the way to trials with the least locomotion at 30. A top locomotion and bottom locomotion value (average of the top and bottom 6 trials) was taken for each session and then an average was taken for all sessions included in a group. Corresponding haemodynamic responses to the ranked locomotion trials were then plotted. (Figure 3.3).

We found that when locomotion was ranked across the entire 25s trial there were no significant differences in the amount of summed locomotion for the most locomotion trials during the 25s trial across disease groups (Kruskal Wallis tests: H (3 n=132) = 3.228, p=.358) (Figure 3.3 e). We also observed that the corresponding evoked haemodynamic responses (when locomotion was ranked across the entire 25s trial) were also not significantly different across disease groups. Kruskal Wallis tests were run to assess whether there were differences in peak HbT, HbO and HbR responses across disease groups to a 2s whisker stimulation when animals walked the most during the entire trial. Median peak HbT, HbO and HbR responses were not significantly different across disease groups (Kruskal Wallis tests: HbT; H (3 n=132) = 3.20, p=.362, HbO; H (3 n=132) = 4.959, p=.175, HbR; H (3 n=132) = 1.778, p=.620) (Figure 3.3 f, g, h).

We completed the same analysis for trials where the least locomotion occurred across the entire 25s trials. We observed that when locomotion was ranked across the entire 25s trial there were significant differences in the median amount of summed locomotion for the least locomotion trials across the disease groups (Kruskal Wallis

tests: H (3 n=132) = 15.654, p=.001) (median least locomotion across trial: WT=3, AD=17.67, ATH=17, MIX=18.83) (Figure 3.3 i).

Post hoc tests with a Bonferroni correction found that, summed least locomotion trials were greater in the AD group (median = 17.67) as compared with the WT group (median = 3) p=0.000 (Bonferroni corrected). However, even though there were statistically significant differences in the amounts of locomotion across disease groups we observed no differences in the corresponding evoked haemodynamic responses (when locomotion was ranked across the entire 25s trial). Kruskal Wallis tests were run to assess whether there were differences in peak HbT, HbO and HbR responses across disease groups to a 2s whisker stimulation when animals walked the least during the entire trial. Median peak HbT, HbO and HbR responses were not significantly different across disease groups (Kruskal Wallis tests: HbT; H (3 n=132) = 4.366, p=.225, HbO; H (3 n=132) = 3.271, p=.352, HbR; H(3 n=132) = 0.319, p=.956) (Figures 3.3 i, j, k, l).

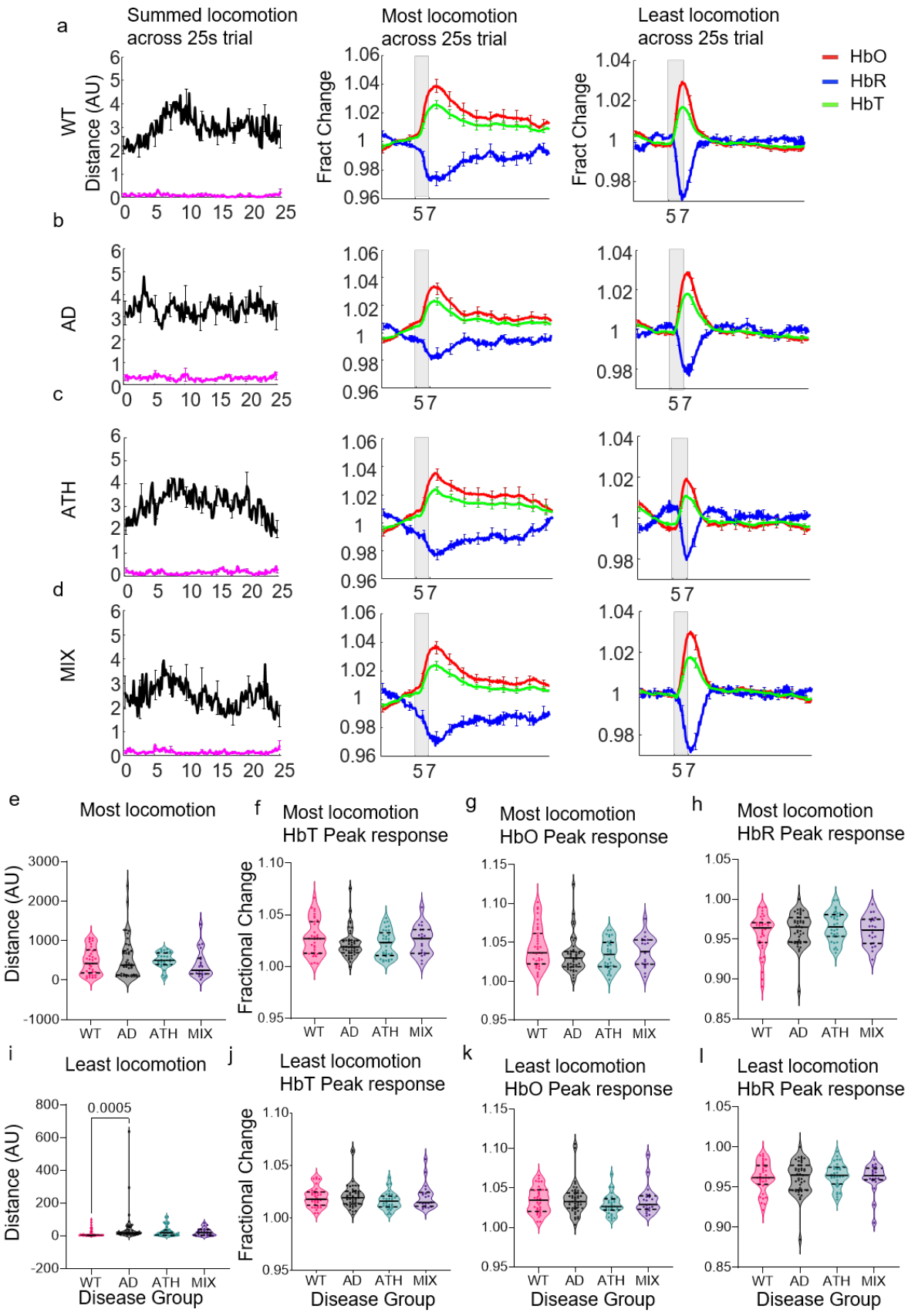
a
Summed locomotion across 25s trial
Most locomotion across 25s trial
Least locomotion across 25s trial
HbO
HbR
HbT
WT
Distance (AU)
Fract Change
b
AD
c
ATH
d
MIX
e
Most locomotion
f
Most locomotion HbT Peak response
g
Most locomotion HbO Peak response
h
Most locomotion HbR Peak response
i
Least locomotion
0.0005
j
Least locomotion HbT Peak response
k
Least locomotion HbO Peak response
l
Least locomotion HbR Peak response
Fractional Change
WT AD ATH MIX
Disease Group

Figure 3.3: No effect of disease on evoked-haemodynamic peak responses when locomotion is ranked across the whole trial

Locomotion was ranked across the whole 25s trial. The most locomotion trials (top 6) and least locomotion trials (bottom 6) were averaged per session, then included in the overall group average (left column) (pink line = most locomotion and black line = least locomotion). The corresponding whisker-evoked haemodynamic responses were plotted for most (middle column) and least (right column) locomotion. ***(a)*** *the summed locomotion across the trial, and corresponding haemodynamic responses to a 2s-whisker stimulation for the most and least locomotion for the WT group ((n=35 (from 11 mice))* ***(b)*** *the AD group (n=43 (from 12 mice))* ***(c)*** *the ATH group (n=33 (from 10 mice)).* ***(d)*** *the MIX group (n=21 (from 6 mice)). Violin plots show* ***(e)*** *distance travelled during most locomotion trials* ***(f)*** *peak HbT* ***(g)*** *HbO and* ***(h)*** *HbR responses to a 2s whisker stimulation and* ***(i)*** *distance travelled for the least locomotion trials and* ***(j),*** *peak HbT,* ***(k)*** *HbO and* ***(l)*** *HbR responses to a 2s whisker stimulation. Median (Black line) and interquartile range (dashed black line) shown. Error bars show standard error of the mean (SEM). Individual mean peak values shown.*

3.4.5 There is an effect of disease when locomotion is ranked during the whisker stimulation

We have previously shown that locomotion has the greatest effect on evoked haemodynamic responses when it occurs prior to or during the whisker stimulation[46]. Therefore, we assessed whether locomotion during the whisker stimulation impacted vascular function across disease groups.

Similar to the above analysis, we found that there were no significant differences in the amount of locomotion for the most locomotion trials, when locomotion was ranked during the stimulation (5-10s). Median summed most locomotion responses (distance travelled) during the whisker stimulation were not significantly different across disease groups (Kruskal Wallis tests: H (3 n=132) = 2.699, p=.440) (Figure 3.4 e). We also found that the corresponding evoked haemodynamic responses (when locomotion was ranked at 5-10s) were also not significantly different across disease groups. Median peak HbT, HbO and HbR responses were not significantly different across disease groups for the most locomotion trials when locomotion was ranked at 5-10s (Kruskal Wallis tests: HbT; H (3 n=132) = 1.649, p=.648, HbO; H (3 n=132) = 2.174, p=.537, HbR; H (3 n=132) = 3.872, p=.276) (Figure 3.4 f, g, h).

However, we did find that there were significant differences in least walking responses (distance travelled) during the stimulation (5-10s) across the different disease groups. Median, summed least locomotion responses when ranked at 5-10s were significantly different across disease groups (Kruskal Wallis tests: H (3 n=132) = 27.519, p=0.000) (median least locomotion during 5-10s: WT=0, AD=1.5, ATH=0.33, MIX=1). Post hoc tests with a Bonferroni correction found that median summed locomotion for the least locomotion trials (ranked between 5-10s) was greater for the AD group (median=1.5), compared to the WT group (median = 0) p=0.000. The mixed disease group (median=1) also locomoted more than the WT group (median=0) p=0.048. Median summed locomotion was also significantly different in the atherosclerosis group compared with the AD group, with the atherosclerosis group locomoting less (median = 0.33) than the AD group (median = 1.5) p=0.003) (Figure 3.4 i).

We also observed significant differences in the corresponding evoked haemodynamic responses for the least locomotion trials. Kruskal Wallis tests were run to assess

whether there were differences in peak HbT, HbO and HbR responses across disease groups to a 2s whisker stimulation when animals walked the least during the stimulation (5-10s). Median peak HbT, HbO and HbR responses were all significantly different across disease groups (Kruskal Wallis tests: HbT; H (3 n=132) = 10.550, p=0.014, HbO; H (3 n=132) = 8.901, p=0.031, HbR; H(3 n=132) = 8.133, p=.043). Post-hoc tests with a Bonferroni correction were conducted and found that median peak HbT responses during the least locomotion trials (when locomotion was ranked at 5-10s) were smaller in the atherosclerosis group (median = 1.00) compared with the AD group (median= 1.015) p=0.040 and compared with the WT group (median = 1.015) p=.018. Additionally, median peak HbO responses during the least locomotion trials (when ranked at 5-10s) were smaller in the atherosclerosis group (median= 1.015) compared with the WT group (median = 1.028) p=0.022. Median peak HbR responses during the least locomotion trials (when ranked at 5-10s) were larger in the atherosclerosis group (median= 0.979) compared with the WT group (median = 0.967) p=0.031) (Figure 3.4 j, k, l).

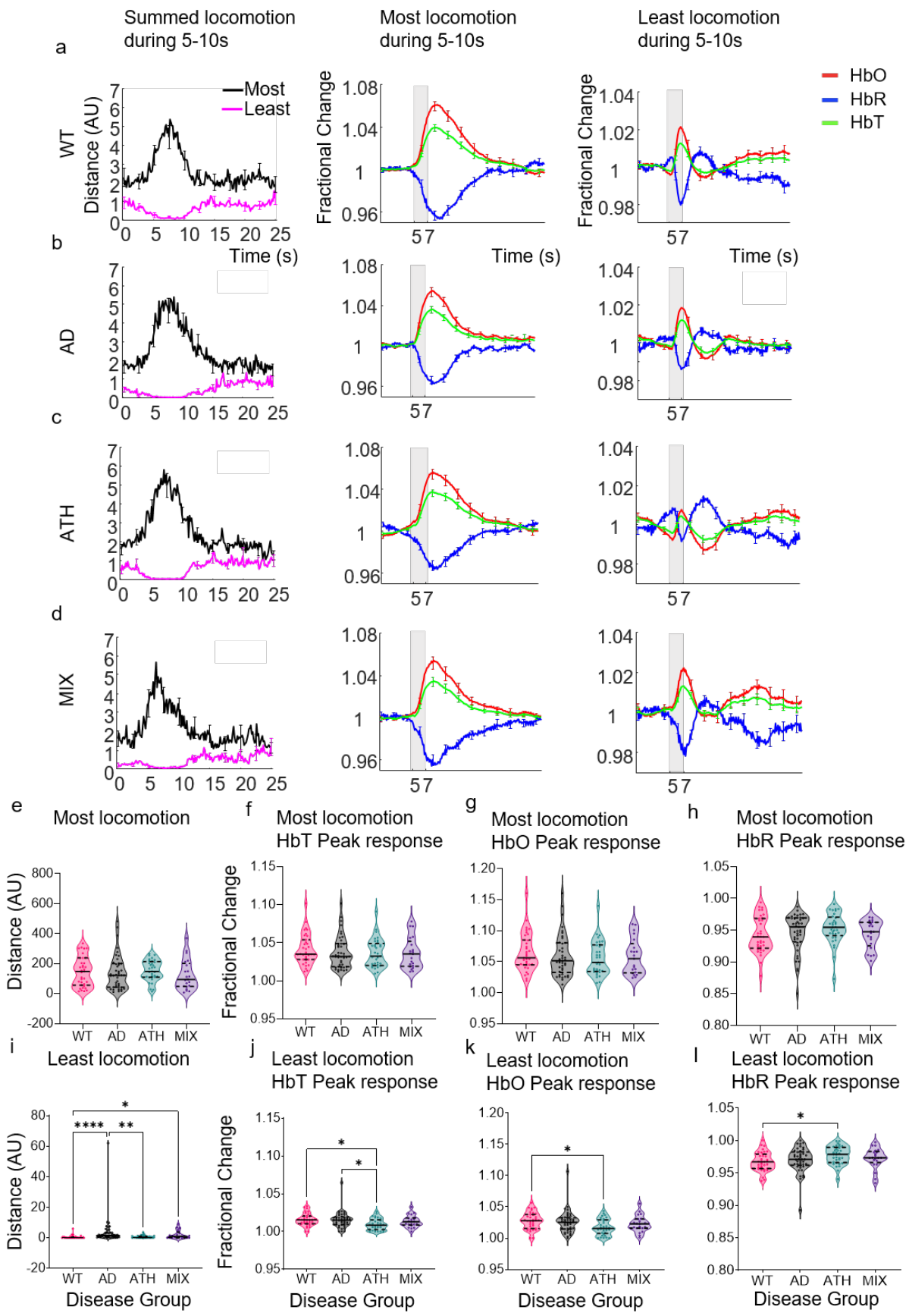

Figure 3.4: There is an effect of disease when locomotion is ranked during the whisker stimulation

Locomotion was ranked during 5-10s (with the whisker stimulation occurring between 5-7 seconds (gray bar)). The most locomotion trials (top 6) and least locomotion trials (bottom 6) were averaged per session, then included in the overall group average (left column) (pink = most locomotion and black = least locomotion). Corresponding whisker-evoked haemodynamic responses for most (middle column) and least (right column) locomotion are shown. ***(a)*** *summed locomotion across the trial, and corresponding haemodynamic responses to a 2s-whisker stimulation for the most and least locomotion when locomotion was ranked between 5 and 10s for the WT group ((n=35 (from 11 mice))* ***(b)*** *the AD group (n=43 (from 12 mice))* ***(c)*** *the ATH group (n=33 (from 10 mice))* ***(d)*** *the MIX group (n=21 (from 6 mice)). Violin plots show* ***(e)*** *distance travelled during most locomotion trials* ***(f)*** *peak HbT,* ***(g)*** *HbO and* ***(h)*** *HbR responses to a 2s whisker stimulation and (****i****) distance travelled for the least locomotion trials and* ***(j)*** *peak HbT (****k****) HbO and* ***(l)*** *HbR responses to a 2s whisker stimulation. Median (Black line) and interquartile range (dashed black line) shown. Error bars show standard error of the mean (SEM). Individual mean peak values shown.*

3.4.6 Mixed disease does not enhance atherosclerotic plaque burden

To induce atherosclerosis, we used a gain-of-function mutation of PCSK9 via a viral injection, paired with a western diet. The viral injection was given at 11 weeks and the western diet started at 12 weeks up until the end of the study (approximately 7-8 months of western diet). We found evidence of atherosclerotic plaques within the aortic arch in both atherosclerotic and mixed disease mice (Figure 3.5 a). We assessed whether the presence of amyloid beta within the brain may affect the systemic vasculature. However, we found that there were no significant differences in aortic arch plaque burden between the atherosclerotic and mixed disease mice (Mann Whitney U test: median aortic arch plaque burden scores for atherosclerosis (Median=18.76) and mixed disease (median=16.33) groups were not significantly different U = 19, z = -.943, p = 0.388) (Figure 3.5 b).

3.4.7 Amyloid plaque burden is not greater in the comorbid mixed models of heart disease and Alzheimer's disease

Amyloid plaque burden was assessed using immunohistochemistry (Figure 3.5 c). The presence of amyloid was identified using an anti-amyloid antibody with DAB. We assessed whether the presence of systemic atherosclerosis in addition to AD could impact amyloid plaque load within the hippocampus – as has previously been observed[33,34]. We found no significant differences in amyloid plaque burden (percentage) when comparing the AD (mean and SD = 0.50 ± .266) and the mixed (mean and SD = 0.31 ± .09) disease group $t(9) = 1.564$, p = .152 as assessed using an independent sample t test (Figure 3.5 d).

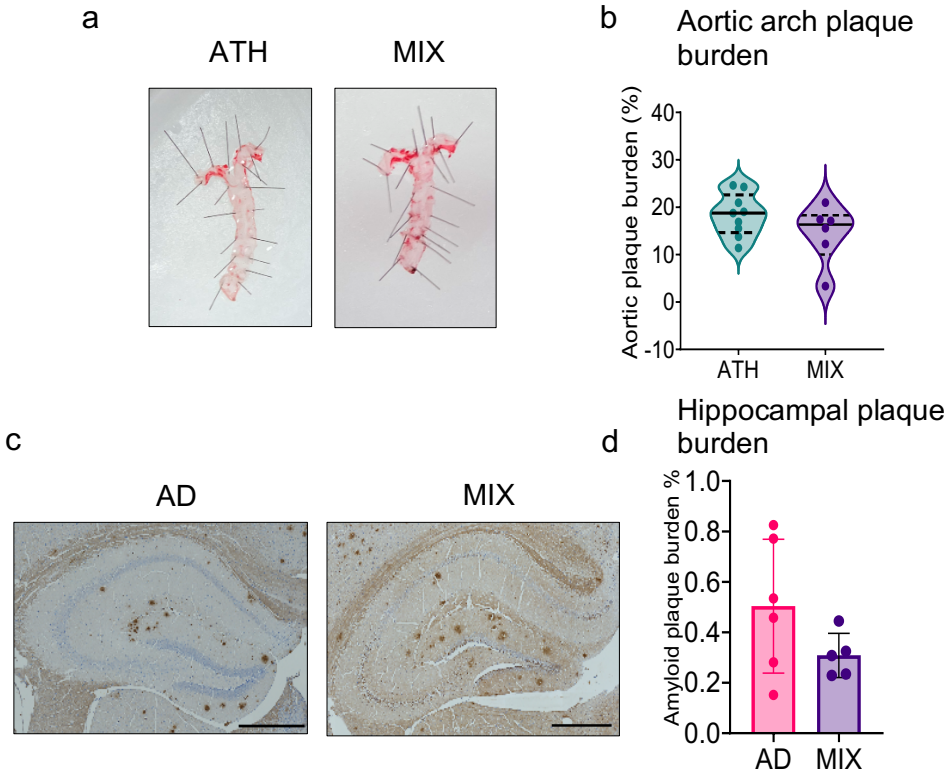

Figure 3.5: Atherosclerotic and amyloid pathology are not enhanced by the presence of comorbid disease

__(a)__ the aorta was dissected, fat removed and stained with Oil Red O to detect the presence of lipids within the aortic arch (left = atherosclerosis only n=9) (right = mixed disease n=6). Red regions indicate the presence of lipids __(b)__ a violin plot reveals aortic atherosclerotic plaque burden between both groups. Aortic plaque burden was calculated as the percentage of red stained regions inside the aortic arch. __(c)__ Immunohistochemistry was completed to assess amyloid plaque burden in the hippocampus between AD and Mixed disease groups. Darker brown regions indicate amyloid plaque pathology. __(d)__ A violin plot reveals hippocampal amyloid burden in AD (n=6) and Mixed (n=5) disease mice. Black line = 500um.

3.5 Discussion

In the current study we investigated cognitive and vascular function in Alzheimer's, atherosclerosis and mixed disease mouse models. We used the NOR as a test of non-spatial recognition memory, 2D-OIS to investigate changes in cortical haemoglobin concentrations to a 2s whisker stimulation, and immunohistochemistry to assess amyloid plaque load within the hippocampus. We found preserved recognition memory in all disease groups, as assessed using the NOR test, with a retention interval of 1 hour. We also observed that when we ignored locomotion there was no effect of disease on sensory-evoked haemodynamic responses in the AD group, atherosclerosis group and the mixed disease group. However, in support of our previous work, (showing the large effects locomotion can have on haemodynamic responses)[46] we did find an effect of disease when we controlled for the confound of locomotion. When locomotion was ranked during the whisker stimulation (5-10s), during the least locomotion trials, we observed that whisker-evoked peak haemodynamic responses in the atherosclerosis group were significantly smaller than the WT group. This supported previous work completed by our research group, and therefore extended the findings that peripheral vascular changes, such as atherosclerosis can impact neurovascular function[34]. However, even when locomotion was controlled for, we did not find any changes in whisker-evoked peak responses in the AD, or mixed groups. Finally, our immunohistochemistry experiments to assess amyloid plaque load found no difference in amyloid burden in the mixed disease group compared with the AD only group, as has previously been reported[33,34].

It was unexpected that we found no effect of disease on non-spatial recognition memory as assessed by the NOR test. However, cognitive measures in mice often produce contradictory results, with groups finding recognition memory deficits in the APP/PS1 mice[40,41] and other groups not[50,51]. The aforementioned studies which found no effect of disease on cognition were conducted at a younger age (than the mice included in this study), however, other groups have found no effects of disease on recognition memory in mice aged between 9 and 12 months[52], similar to the age groups used within this study. Due to the rigid exclusion criteria (2 sessions excluded), and in some sessions the camera did not record (1 session excluded) this resulted in some of the groups having a smaller sample. Larger samples are needed when

conducting measures of cognition in rodents. Additionally, the study only investigated a retention interval of 1 hour. Future work could use more short term (e.g., 3 minutes) and longer term (e.g., 24 hour) retention intervals to get a more extensive understanding of recognition memory in the above disease models.

This work was able to extend and replicate previous work from our research group, regarding vascular function in atherosclerosis. In our previous work we found that atherosclerosis had an effect on evoked-haemodynamic responses in lightly anaesthetised mice, whereby we observed smaller whisker-evoked-haemodynamic responses compared to the WT group[34]. In the current study we also found smaller whisker-evoked-haemodynamic responses in atherosclerotic mice (in a different background strain), when mice walked the least during the whisker stimulation. Importantly we found these similar findings regarding a potential impairment in whisker-evoked haemodynamic responses in an awake preparation. Being able to extend and replicate the previous work of Shabir et al.,[34] further highlights the importance of systemic vascular changes and the impact they can have on neurovascular function – emphasising the importance of the link between heart and brain health[53]. However, similar to the previous study, we also found no effects of mixed AD and atherosclerotic disease on evoked-haemodynamic peak responses. We hypothesised that the mixed disease group would have the most reduced haemodynamic peak responses, due to the presence of AD and atherosclerosis (both diseases which impact the vasculature), in addition to this being a more 'severe'[37] model of AD than used in the previous paper[34]. However, it could be that there are no deficits in the surface vessels of the brain in mixed disease mice, as our imaging method used only focuses on the large pial vessels. Previous work, conducted using the $LDLR^{-/-}$ model of atherosclerosis has reported microvascular changes and reduced tissue oxygenation within cortical capillaries in these mice at 12 months of age[30,31]. Therefore, it's imperative further work is completed using methods such as two-photon microscopy to assess whether there are any effects of mixed disease at different locations along the vascular tree. Furthermore, we only investigated mixed disease in 'mid-life', between the ages of 9-12 months. It could be that impacts on large cerebral vessels may not occur at this mid-life time point. If the same studies were completed

in older age mice e.g 15-17 months it would be interesting to see how the vasculature is impacted at these older ages.

Surprisingly, we did not find any effects of AD on evoked-haemodynamic responses. Previous research, using optical imaging spectroscopy in awake mice has found differences in whisker stimulation evoked-responses in the APP/PS1 (AD group) mice, at 6 months of age[43]. Studies using other sensory stimulations in awake mice have also found similar effects of disease on evoked-hemodynamic responses. Van veluw et al[42]., observed a reduced arterial dilation in response to a visual stimulation in the same strain of AD mice, at the same age as the mice used within our study. Our differential results could be explained by a number of things, including different surgical procedures. In our work we completed a less invasive thinned window procedure, whereas the above study completed a cranial window. We also used different imaging techniques to investigate haemodynamic responses. Our optical imaging spectroscopy method investigates concentration changes in haemoglobin, whereas the above study used two-photon microscopy to investigate arterial dilation. Finally, even though in both studies sensory stimuli were used, the stimuli were different, with whisker stimulation being used in the current work and a visual stimulation being used in the above study. These stimuli may have differential effects on haemodynamics within the cortex, as these stimuli activate different parts of the cortex. Therefore, different areas of the brain were imaged in both these studies, with our current study focusing on haemodynamic responses within the whisker region of the somatosensory cortex, and van Veluw's study focusing on the visual cortex.

Opposing findings have previously been reported regarding cerebrovascular responses in the APP/PS1 AD model. Between 7 and 9 months, some groups report impaired CBF[54,55], and reduced relative CBV (rCBV)[56], whereas other groups report increased haemodynamic responses at 7 months of age, yet find no differences in evoked-haemodynamic responses at earlier (3 months) or later ages (22 months)[57]. Other groups have corroborated the observation of preserved vascular responses at 18 months of age[58]. In addition to this, we have previously published two research papers[34,48] using the J20 Alzheimer's model where we have reported preserved neurovascular coupling in Alzheimer's mice. Additionally, Munting et al.,[59] also

observed persevered cerebrovascular responses in a different AD mouse model (Tg-SwDI). More recently, Zhukov et al.,[60] also observed preserved neurovascular coupling responses in the 5xFAD model. They found no significant differences in the diameter change of penetrating arterioles, and in 1st and 2nd order capillaries. In the current study we only focused on haemodynamic changes in the surface, pial vessels of the brain, therefore it could be plausible that there are effects of disease at other locations along the vascular tree. Other studies have used the APP/PS1 mouse model and using 2-photon microscopy they have found impairments in capillary function. Cruz-Hernandes et al., [55] observed a larger number of 'stalled' capillaries in the APP/PS1 mouse model, compared with WT mice. Additionally, when given a neutrophil antibody they found that the number of stalled capillaries was reduced and CBF increased, as well as short term memory also being improved. The study highlights the important role of capillaries in brain blood flow and further reinforces the importance of conducting more studies using two-photon microscopy in AD mouse models. However, it must be noted that even though this study used the APP/PS1 mouse model, they used the model on the B6-Cg background (whereas in the current study we used the B6-C3). The background strain is important, as it has been reported that some mice on the B6-Cg background exhibit seizure activity[61] therefore, it could be proposed that the neuronal hyperexcitability may impact capillary function, as it has been reported that in a number of mouse models of epileptic activity, a greater number of capillary constrictions occurred within the hippocampus[62]

In the current study we observed no effects of disease on evoked-haemodynamic responses when we ignored locomotion, and during trials in which the mice walked the most during whisker stimulation. However, we did find a significant effect of disease when the least locomotion occurred during the whisker stimulation. Previous research has evidenced that locomotion itself can have huge effects on haemodynamic responses within the brain[46,63–65]. However, our findings, may suggest that there are different neurovascular mechanisms controlling locomotion haemodynamic responses compared with whisker-evoked haemodynamic responses, with the whisker evoked responses being impaired in the atherosclerotic mouse model. Our results show the importance of monitoring locomotion in awake mice, as there may be subtle vascular deficits across diseases, and recording locomotion in

order to be able to dissect out the effects of this behaviour may allow for the field to fully assess subtle differences in vascular function across disease groups.

Our amyloid immunohistochemistry studies surprisingly did not reveal any significant differences in amyloid plaque load between the AD and the MIX groups, as has previously been reported[33,34]. The aforementioned studies both counted the number of plaques and in the current study plaque load was calculated using a threshold analysis in ImageJ. Therefore, it could be that there are actually a greater number of amyloid plaques in the MIX group mice – further studies should investigate if this is the case.

In summary, we found no effect of disease on non-spatial recognition memory; however, this may be due to the small sample used in the cognitive tests. We found no effect of disease on whisker-evoked peak haemodynamic responses, (when we ignored the presence of locomotion). However, in support of our previous work we found that the presence of locomotion can confound haemodynamic responses, as when we ranked locomotion during the whisker stimulation, we did observe an effect of disease. When locomotion was ranked during the whisker stimulation, during the least locomotion trials the atherosclerosis disease group had the most reduced peak haemodynamic response to sensory evoked haemodynamic responses in awake animals. This finding replicates and extends work previously completed regarding the impacts of heart disease on neurovascular function in lightly anaesthetised mice[34]. Finally, we did not observe a greater amyloid burden in the mixed disease model compared with the AD only model – however this could be explained by the method used to assess amyloid burden. In summary, this study shows the importance of monitoring locomotion when completing assessments of haemodynamic responses in awake mice. And we also further reinforce the observation that diseases of the systemic vasculature can have a substantial effect on brain cerebrovascular control.

3.6 References

1. Nichols, E. *et al.* Estimation of the global prevalence of dementia in 2019 and forecasted prevalence in 2050: an analysis for the Global Burden of Disease Study 2019. *Lancet Public Health* **7**, e105–e125 (2022).
2. Hardy, J. A. & Higgins, G. A. Alzheimer's Disease: The Amyloid Cascade Hypothesis. *Science* **256**, 184–185 (1992).
3. Grundke-Iqbal, I. *et al.* Abnormal phosphorylation of the microtubule-associated protein tau (tau) in Alzheimer cytoskeletal pathology. *Proc. Natl. Acad. Sci.* **83**, 4913–4917 (1986).
4. The Alzheimer's Disease Neuroimaging Initiative *et al.* Early role of vascular dysregulation on late-onset Alzheimer's disease based on multifactorial data-driven analysis. *Nat. Commun.* **7**, 11934 (2016).
5. Zlokovic, B. V. Neurovascular pathways to neurodegeneration in Alzheimer's disease and other disorders. *Nat. Rev. Neurosci.* **12**, 723–738 (2011).
6. Wisniewski, H. M., Vorbrodt, A. W. & Wegiel, J. Amyloid Angiopathy and Blood–Brain Barrier Changes in Alzheimer's Diseasea,b. *Ann. N. Y. Acad. Sci.* **826**, 161–172 (1997).
7. Kurz, C., Walker, L., Rauchmann, B.-S. & Perneczky, R. Dysfunction of the blood–brain barrier in Alzheimer's disease: Evidence from human studies. *Neuropathol. Appl. Neurobiol.* **48**, e12782 (2022).
8. Korte, N., Nortley, R. & Attwell, D. Cerebral blood flow decrease as an early pathological mechanism in Alzheimer's disease. *Acta Neuropathol. (Berl.)* **140**, 793–810 (2020).
9. Feng, T. *et al.* Chronic cerebral hypoperfusion accelerates Alzheimer's disease pathology with the change of mitochondrial fission and fusion proteins expression in a novel mouse model. *Brain Res.* **1696**, 63–70 (2018).
10. Park, J.-H. *et al.* The effect of chronic cerebral hypoperfusion on the pathology of Alzheimer's disease: A positron emission tomography study in rats. *Sci. Rep.* **9**, 14102 (2019).
11. Santiago, J. A. & Potashkin, J. A. The Impact of Disease Comorbidities in Alzheimer's Disease. *Front. Aging Neurosci.* **13**, 631770 (2021).
12. Browne, J., Edwards, D. A., Rhodes, K. M., Brimicombe, D. J. & Payne, R. A. Association of comorbidity and health service usage among patients with dementia in the UK: a population-based study. *BMJ Open* **7**, e012546 (2017).
13. Edwards III, G. A., Gamez, N., Escobedo Jr., G., Calderon, O. & Moreno-Gonzalez, I. Modifiable Risk Factors for Alzheimer's Disease. *Front. Aging Neurosci.* **11**, (2019).
14. Breteler, M. M. B. Vascular risk factors for Alzheimer's disease:: An epidemiologic perspective. *Neurobiol. Aging* **21**, 153–160 (2000).
15. Gottesman, R. F. *et al.* Associations Between Midlife Vascular Risk Factors and 25-Year Incident Dementia in the Atherosclerosis Risk in Communities (ARIC) Cohort. *JAMA Neurol.* **74**, 1246–1254 (2017).

16. Kivipelto, M. Midlife vascular risk factors and Alzheimer's disease in later life: longitudinal, population based study. *BMJ* **322**, 1447–1451 (2001).
17. Cummings, J. L., Morstorf, T. & Zhong, K. Alzheimer's disease drug-development pipeline: few candidates, frequent failures. *Alzheimers Res. Ther.* **6**, 37 (2014).
18. Vitek, M. P. *et al.* Translational animal models for Alzheimer's disease: An Alzheimer's Association Business Consortium Think Tank. *Alzheimers Dement. Transl. Res. Clin. Interv.* **6**, e12114 (2020).
19. Zlokovic, B. V. *et al.* Vascular contributions to cognitive impairment and dementia (VCID): A report from the 2018 National Heart, Lung, and Blood Institute and National Institute of Neurological Disorders and Stroke Workshop. *Alzheimers Dement.* **16**, 1714–1733 (2020).
20. Deaths registered summary statistics, England and Wales - Office for National Statistics. https://www.ons.gov.uk/peoplepopulationandcommunity/birthsdeathsandmarriages/deaths/datasets/deathsregisteredsummarystatisticsenglandandwales.
21. Lusis, A. J. Atherosclerosis. *Nature* **407**, 233–241 (2000).
22. Björkegren, J. L. M. & Lusis, A. J. Atherosclerosis: Recent developments. *Cell* **185**, 1630–1645 (2022).
23. Song, P. *et al.* Global and regional prevalence, burden, and risk factors for carotid atherosclerosis: a systematic review, meta-analysis, and modelling study. *Lancet Glob. Health* **8**, e721–e729 (2020).
24. Roher, A. E., Esh, C., Rahman, A., Kokjohn, T. A. & Beach, T. G. Atherosclerosis of Cerebral Arteries in Alzheimer Disease. *Stroke* **35**, 2623–2627 (2004).
25. Wingo, A. P. *et al.* Shared proteomic effects of cerebral atherosclerosis and Alzheimer's disease on the human brain. *Nat. Neurosci.* **23**, 696–700 (2020).
26. Xie, B., Shi, X., Xing, Y. & Tang, Y. Association between atherosclerosis and Alzheimer's disease: A systematic review and meta-analysis. *Brain Behav.* **10**, e01601 (2020).
27. Ilyas, I. *et al.* Mouse models of atherosclerosis in translational research. *Trends Pharmacol. Sci.* **43**, 920–939 (2022).
28. Ishibashi, S., Goldstein, J. L., Brown, M. S., Herz, J. & Burns, D. K. Massive xanthomatosis and atherosclerosis in cholesterol-fed low density lipoprotein receptor-negative mice. *J. Clin. Invest.* **93**, 1885–1893 (1994).
29. Nakashima, Y., Plump, A. S., Raines, E. W., Breslow, J. L. & Ross, R. ApoE-deficient mice develop lesions of all phases of atherosclerosis throughout the arterial tree. *Arterioscler. Thromb. J. Vasc. Biol.* **14**, 133–140 (1994).
30. Lu, Y. *et al.* Impact of atherosclerotic disease on cerebral microvasculature and tissue oxygenation in awake LDLR−/−hApoB+/+ transgenic mice. *Neurophotonics* **6**, 045003 (2019).
31. Li, B. *et al.* Atherosclerosis is associated with a decrease in cerebral microvascular blood flow and tissue oxygenation. *PLOS ONE* **14**, e0221547 (2019).

32. Bjørklund, M. M. *et al.* Induction of Atherosclerosis in Mice and Hamsters Without Germline Genetic Engineering. *Circ. Res.* **114**, 1684–1689 (2014).
33. Grames, M. S. *et al.* Gene Transfer Induced Hypercholesterolemia in Amyloid Mice. *J. Alzheimers Dis.* **65**, 1079–1086 (2018).
34. Shabir, O. *et al.* Assessment of neurovascular coupling and cortical spreading depression in mixed mouse models of atherosclerosis and Alzheimer's disease. *eLife* **11**, e68242 (2022).
35. Park, S. W., Moon, Y.-A. & Horton, J. D. Post-transcriptional Regulation of Low Density Lipoprotein Receptor Protein by Proprotein Convertase Subtilisin/Kexin Type 9a in Mouse Liver *. *J. Biol. Chem.* **279**, 50630–50638 (2004).
36. Abifadel, M. *et al.* Mutations in PCSK9 cause autosomal dominant hypercholesterolemia. *Nat. Genet.* **34**, 154–156 (2003).
37. Whitesell, J. D. *et al.* Whole brain imaging reveals distinct spatial patterns of amyloid beta deposition in three mouse models of Alzheimer's disease. *J. Comp. Neurol.* **527**, 2122–2145 (2019).
38. Yokoyama, M., Kobayashi, H., Tatsumi, L. & Tomita, T. Mouse Models of Alzheimer's Disease. *Front. Mol. Neurosci.* **15**, (2022).
39. Gao, Y.-R. *et al.* Time to wake up: Studying neurovascular coupling and brain-wide circuit function in the un-anesthetized animal. *NeuroImage* **153**, 382–398 (2017).
40. Zhang, R. *et al.* Novel Object Recognition as a Facile Behavior Test for Evaluating Drug Effects in AβPP/PS1 Alzheimer's Disease Mouse Model. *J. Alzheimers Dis.* **31**, 801–812 (2012).
41. Shen, L. *et al.* Amelioration of cognitive impairments in APPswe/PS1dE9 mice is associated with metabolites alteration induced by total salvianolic acid. *PLoS ONE* **12**, e0174763 (2017).
42. van Veluw, S. J. *et al.* Vasomotion as a Driving Force for Paravascular Clearance in the Awake Mouse Brain. *Neuron* **105**, 549-561.e5 (2020).
43. Lu, X. *et al.* A Pilot Study Investigating Changes in Capillary Hemodynamics and Its Modulation by Exercise in the APP-PS1 Alzheimer Mouse Model. *Front. Neurosci.* **13**, (2019).
44. Jankowsky, J. L. *et al.* Mutant presenilins specifically elevate the levels of the 42 residue β-amyloid peptide in vivo: evidence for augmentation of a 42-specific γ secretase. *Hum. Mol. Genet.* **13**, 159–170 (2004).
45. Lm, L. Novel Object Recognition Test for the Investigation of Learning and Memory in Mice. *J. Vis. Exp. JoVE* (2017) doi:10.3791/55718.
46. Eyre, B. *et al.* The effects of locomotion on sensory-evoked haemodynamic responses in the cortex of awake mice. *Sci. Rep.* **12**, 6236 (2022).
47. Sharp, P. S. *et al.* Comparison of stimulus-evoked cerebral hemodynamics in the awake mouse and under a novel anesthetic regime. *Sci. Rep.* **5**, 12621 (2015).
48. Sharp, P. S. *et al.* Neurovascular coupling preserved in a chronic mouse model of Alzheimer's disease: Methodology is critical. *J. Cereb. Blood Flow Metab.* **40**, 2289–2303 (2020).

49. Christensen, A. & Pike, C. J. Staining and Quantification of β-Amyloid Pathology in Transgenic Mouse Models of Alzheimer's Disease. *Methods Mol. Biol. Clifton NJ* **2144**, 211–221 (2020).
50. Campos, H. C. *et al.* Neuroprotective effects of resistance physical exercise on the APP/PS1 mouse model of Alzheimer's disease. *Front. Neurosci.* **17**, 1132825 (2023).
51. Cheng, D., Low, J. K., Logge, W., Garner, B. & Karl, T. Novel behavioural characteristics of female APPSwe/PS1ΔE9 double transgenic mice. *Behav. Brain Res.* **260**, 111–118 (2014).
52. Georgevsky, D., Retsas, S., Raoufi, N., Shimoni, O. & Golzan, S. M. A longitudinal assessment of retinal function and structure in the APP/PS1 transgenic mouse model of Alzheimer's disease. *Transl. Neurodegener.* **8**, 30 (2019).
53. Scheffer, S., Hermkens, D. M. A., van der Weerd, L., de Vries, H. E. & Daemen, M. J. A. P. Vascular Hypothesis of Alzheimer Disease. *Arterioscler. Thromb. Vasc. Biol.* **41**, 1265–1283 (2021).
54. Shen, Z. *et al.* Multifaceted assessment of the APP/PS1 mouse model for Alzheimer's disease: Applying MRS, DTI, and ASL. *Brain Res.* **1698**, 114–120 (2018).
55. Cruz Hernández, J. C. *et al.* Neutrophil adhesion in brain capillaries reduces cortical blood flow and impairs memory function in Alzheimer's disease mouse models. *Nat. Neurosci.* **22**, 413–420 (2019).
56. Zerbi, V. *et al.* Microvascular cerebral blood volume changes in aging APPswe/PS1dE9 AD mouse model: a voxel-wise approach. *Brain Struct. Funct.* **218**, 1085–1098 (2013).
57. Kim, J. & Jeong, Y. Augmentation of Sensory-Evoked Hemodynamic Response in an Early Alzheimer's Disease Mouse Model. *J. Alzheimers Dis. JAD* **37**, (2013).
58. Hooijmans, C. R. *et al.* Changes in cerebral blood volume and amyloid pathology in aged Alzheimer APP/PS1 mice on a docosahexaenoic acid (DHA) diet or cholesterol enriched Typical Western Diet (TWD). *Neurobiol. Dis.* **28**, 16–29 (2007).
59. Munting, L. P. *et al.* Cerebral blood flow and cerebrovascular reactivity are preserved in a mouse model of cerebral microvascular amyloidosis. *eLife* **10**, e61279 (2021).
60. Zhukov, O. *et al.* Preserved blood-brain barrier and neurovascular coupling in female 5xFAD model of Alzheimer's disease. *Front. Aging Neurosci.* **15**, (2023).
61. Minkeviciene, R. *et al.* Amyloid β-Induced Neuronal Hyperexcitability Triggers Progressive Epilepsy. *J. Neurosci.* **29**, 3453–3462 (2009).
62. Leal-Campanario, R. *et al.* Abnormal Capillary Vasodynamics Contribute to Ictal Neurodegeneration in Epilepsy. *Sci. Rep.* **7**, 43276 (2017).
63. Gao, Y.-R. & Drew, P. J. Effects of Voluntary Locomotion and Calcitonin Gene-Related Peptide on the Dynamics of Single Dural Vessels in Awake Mice. *J. Neurosci.* **36**, 2503–2516 (2016).

64. Huo, B.-X., Smith, J. B. & Drew, P. J. Neurovascular Coupling and Decoupling in the Cortex during Voluntary Locomotion. *J. Neurosci.* **34**, 10975–10981 (2014).
65. Huo, B.-X., Greene, S. E. & Drew, P. J. Venous cerebral blood volume increase during voluntary locomotion reflects cardiovascular changes. *NeuroImage* **118**, 301–312 (2015).

3.7 Supplementary Tables

NOR statistics outputs

Supplementary table 1: Shapiro Wilks test of normality for distance travelled in the training phase of the NOR test across disease groups

	Distance travelled		
Disease group	**Statistic**	**df**	**p**
WT	.962	6	.837
AD	.937	9	.549
ATH	.953	10	.706
MIX	.837	6	.124

Supplementary table 2: Kruskal Wallis test results for distance travelled in the training phase of the NOR test across disease groups

Distance travelled	**N**	**Statistic**	**df**	**p**	**E^2_R**
Distance travelled across groups	31	2.719	3	.439	0.090

The epsilon[2] estimate of effect size was calculated using the following formula:

$$E_R^2 \frac{H}{(n^2 - 1)/\,(n + 1)}$$

H = Kruskall wallis test statistic, n = number of observations. Small effect (0.01 - <0.06), moderate effect (0.06 - <0.14), large effect (>0.14). The sample size used in the study indicates a moderate effect size.

Supplementary table 3: Descriptive statistics for distance travelled in the training phase of the NOR test across disease

Distance travelled in training phase	**N**	**Mean**	**Median**	**STD**
WT	6	2247.54	2242.97	501.81
AD	9	2787.06	2710.41	831.43
ATH	10	2555.85	2421.14	517.87
MIX	6	2559.75	2414.41	490.12

Supplementary table 4: Shapiro Wilks test of normality for velocity in the training phase of the NOR test across disease groups

	Velocity		
Disease group	**Statistic**	**df**	**p**
WT	.919	6	.496
AD	.940	9	.585
ATH	.901	10	.227
MIX	.844	6	.140

Supplementary table 5: Kruskal Wallis test results and for velocity in the training phase of the NOR test across disease groups

Velocity	N	Statistic	df	p	E^2_R
Velocity across groups	31	1.452	3	.693	0.048

The sample size used in the study indicates a small effect size.

Supplementary table 6: Descriptive statistics for velocity in the training phase of the NOR test across disease

Velocity in training phase	N	Mean	Median	STD
WT	6	3.90	4.06	.864
AD	9	4.71	3.05	1.34
ATH	10	4.63	4.27	1.09
MIX	6	4.39	4.24	.819

Supplementary table 7: Shapiro Wilks test of normality for distance travelled in the testing phase of the NOR test across disease groups

	Distance travelled		
Disease group	**Statistic**	**df**	**p**
WT	.878	6	.260
AD	.946	9	.646
ATH	.875	10	.114
MIX	.806	6	.066

Supplementary table 8: Kruskal Wallis test results for distance travelled in the testing phase of the NOR test across disease groups

Distance travelled	N	Statistic	df	p	E^2_R
Distance travelled across groups	31	2.090	3	.554	0.069

The sample size used in the study indicates a moderate effect size.

Supplementary table 9: Descriptive statistics for distance travelled in the testing phase of the NOR test across disease groups

Distance travelled in testing phase	N	Mean	Median	STD
WT	6	1681.38	1532.61	503.81
AD	9	2292.51	2271.45	870.91
ATH	10	2013.14	1910.95	709.28
MIX	6	1878.86	1731.94	723.57

Supplementary table 10: Shapiro Wilks test of normality for velocity in the testing phase of the NOR test across disease groups

	Velocity		
Disease group	**Statistic**	**df**	**p**
WT	.883	6	.285
AD	.921	9	.398
ATH	.936	10	.508
MIX	.881	6	.272

Supplementary table 11: Kruskal Wallis test results for velocity in the testing phase of the NOR test across disease groups

Velocity	**N**	**Statistic**	**df**	**p**	**E^2_R**
Velocity across groups	31	2.197	3	.533	0.073

The sample size used in the study indicates a moderate effect size.

Supplementary table 12: Descriptive statistics for velocity in the testing phase of the NOR test across disease groups

Velocity in testing phase	**N**	**Mean**	**Median**	**STD**
WT	6	2.94	2.61	1.05
AD	9	4.02	3.88	1.66
ATH	10	3.60	3.37	1.05
MIX	6	3.39	3.14	1.41

Supplementary table 13: Shapiro Wilks test of normality for the preference index across disease groups

	Preference index		
Disease group	**Statistic**	**df**	**p**
WT	.854	6	.170
AD	.830	9	.045
ATH	.955	10	.724
MIX	.960	6	.819

Supplementary table 14: Kruskal Wallis test results for preference index across disease groups

Preference Index	**N**	**Statistic**	**df**	**p**	**E^2_R**
Preference index across groups	31	1.399	3	.706	0.046

The sample size used in the study indicates a small effect size.

Supplementary table 15: Descriptive statistics for preference index across disease groups

Preference Index	N	Mean	Median	STD
WT	6	53.25	58.15	17.85
AD	9	51.25	55.50	14.38
ATH	10	58.18	61.28	13.18
MIX	6	57.54	60.24	17.73

Peak responses to 2s whisker stimulation across disease, ignoring locomotion

Supplementary table 16: Shapiro Wilks test of normality for peak haemodynamic responses to a 2s whisker stimulation, when locomotion is ignored across disease groups

Locomotion ignored									
		HbT			**HbO**			**HbR**	
Group	Statistic	df	p	Statistic	df	p	Statistic	df	p
WT	.961	35	.249	.961	35	.241	.929	35	.026
AD	.874	43	.000	.859	43	.000	.858	43	.000
ATH	.976	33	.654	.983	33	.879	.986	33	.929
MIX	.897	21	.030	.842	21	.003	.745	21	.000

Supplementary table 17: Kruskal Wallis test results for peak haemodynamic responses to a 2s whisker stimulation, when locomotion is ignored across disease groups

Peak Hemodynamic response	**N**	**Statistic**	**df**	**p**	**E^2_R**
HbT across groups	132	4.351	3	.226	0.033
HbR across groups	132	5.550	3	.136	0.042
HbO across groups	132	4.681	3	.197	0.035

The sample size used in the study indicates a small effect size

Supplementary table 18: Descriptive statistics for peak haemodynamic responses to a 2s whisker stimulation, when locomotion is ignored across disease groups

HbT	**N**	**Mean**	**Median**	**STD**
WT	35	1.02	1.02	.008
AD	43	1.02	1.02	.012
ATH	33	1.02	1.02	.009
MIX	21	1.02	1.02	.009
HbO				
WT	35	1.04	1.04	.014
AD	43	1.04	1.04	.021
ATH	33	1.03	1.03	.014
MIX	21	1.03	1.03	.016
HbR				
WT	35	.980	.982	.008
AD	43	.981	.985	.011
ATH	33	.985	.984	.006
MIX	21	.982	.983	.008

Peak responses to 2s whisker stimulation across disease when locomotion is ranked across the whole trial

Supplementary table 19: Shapiro Wilks test of normality for ranked locomotion across the whole trial and across disease groups

	Most locomotion summed		
Disease group	**Statistic**	**df**	**p**
WT	.921	35	.015
AD	.809	43	.000
ATH	.942	33	.080
MIX	.844	21	.003
Least locomotion summed			
WT	.635	35	.000
AD	.399	43	.000
ATH	.775	33	.000
MIX	.994	21	.017

Supplementary table 20: Kruskal Wallis test results for most and least summed locomotion when locomotion was ranked across the whole trial, across disease groups

Amount of locomotion across disease	**N**	**Statistic**	**df**	**p**	**E^2_R**
Most summed locomotion	132	3.228	3	.358	0.024
Least summed locomotion	132	15.654	3	.001	0.119

The sample size used in the study indicates a small effect size for most summed locomotion and a moderate effect size for least summed locomotion.

Supplementary table 21: Descriptive statistics for most and least summed locomotion when locomotion was ranked across the whole trial, across disease groups

Most summed locomotion	**N**	**Mean**	**Median**	**STD**
WT	35	479.56	420.17	333.90
AD	43	539.08	376.50	521.45
ATH	33	502.47	499.83	191.30
MIX	21	396.56	248.00	354.25
Least summed locomotion				
WT	35	14.92	3.00	24.69
AD	43	48.22	17.67	103.62
ATH	33	27.29	17.00	33.09
MIX	21	23.18	18.83	22.92

Supplementary table 22: Pairwise comparisons for least summed locomotion when locomotion was ranked across the whole trial, across disease groups

Pairwise comparisons least locomotion	Statistic	Standard error	Standard test statistic	p	Adjusted p
WT vs MIX	-20.39	10.56	-1.931	.053	.321
WT vs ATH	-21.05	9.28	-2.268	.023	.140
WT vs AD	34.36	8.71	3.947	.000	.000
MIX vs ATH	.658	10.68	.062	.951	1.00
MIX vs AD	13.97	10.18	1.372	.170	1.00
ATH vs AD	13.31	8.85	1.504	.133	.795

Supplementary table 23: Shapiro Wilks test of normality for peak haemodynamic responses for most locomotion trials when locomotion was ranked across the whole trial and across disease groups

Most locomotion ranked across whole trial									
		HbT			HbO			HbR	
Group	Statistic	df	p	Statistic	df	p	Statistic	df	p
WT	.943	35	.070	.941	35	.058	.915	35	.011
AD	.872	43	.000	.842	43	.000	.919	43	.005
ATH	.927	33	.029	.946	33	.103	.969	33	.445
MIX	.966	21	.640	.955	21	.419	.985	21	.980

Supplementary table 24: Kruskal Wallis test results for peak haemodynamic responses for most locomotion trials when locomotion was ranked across the whole trial and across disease groups

Haemodynamic responses for most locomotion trials	N	Statistic	df	p	E^2_R
Peak HbT	132	3.200	3	.362	0.024
Peak HbO	132	4.959	3	.175	0.037
Peak HbR	132	1.778	3	.620	0.013

The sample size used in the study indicates a small effect.

Supplementary table 25: Descriptive statistics for peak haemodynamic responses for most locomotion trials when locomotion was ranked across the whole trial and across disease groups

HbT	**N**	**Mean**	**Median**	**STD**
WT	35	1.03	1.03	.017
AD	43	1.02	1.02	.014
ATH	33	1.02	1.03	.013
MIX	21	1.03	1.03	.014
HbO				
WT	35	1.04	1.04	.026
AD	43	1.03	1.03	.023
ATH	33	1.03	1.03	.019
MIX	21	1.04	1.03	.020
HbR				
WT	35	.957	.964	.025
AD	43	.962	.965	.021
ATH	33	.966	.965	.018
MIX	21	.960	.961	.018

Supplementary table 26: Shapiro Wilks test of normality for peak haemodynamic responses for least locomotion trials when locomotion was ranked across the whole trial and across disease groups

Least locomotion when ranked across whole trial									
		HbT			**HbO**			**HbR**	
Group	Statistic	df	p	Statistic	df	p	Statistic	df	p
WT	.952	35	.128	.968	35	.401	.958	35	.193
AD	.830	43	.000	.855	43	.000	.919	43	.005
ATH	.952	33	.149	.949	33	.124	.978	33	.713
MIX	.817	21	.001	.816	21	.001	.810	21	.001

Supplementary table 27: Kruskal Wallis test results for peak haemodynamic responses for least locomotion trials when locomotion was ranked across the whole trial and across disease groups

Haemodynamic responses for least locomotion trials	N	Statistic	df	p	E^2_R
Peak HbT	132	4.366	3	.225	0.033
Peak HbO	132	3.271	3	.352	0.024
Peak HbR	132	.319	3	.956	0.002

The sample size used in the study indicates a small effect for peak HbT and HbO

Supplementary table 27: Descriptive statistics for peak haemodynamic responses for least locomotion trials when locomotion was ranked across the whole trial and across disease groups

HbT	N	Mean	Median	STD
WT	35	1.02	1.02	.009
AD	43	1.02	1.02	.012
ATH	33	1.02	1.02	.008
MIX	21	1.02	1.01	.012
HbO				
WT	35	1.03	1.03	.016
AD	43	1.04	1.03	.020
ATH	33	1.03	1.03	.013
MIX	21	1.03	1.03	.018
HbR				
WT	35	.962	.962	.018
AD	43	.962	.965	.021
ATH	33	.965	.964	.015
MIX	21	.962	.964	.018

Peak responses to 2s whisker stimulation across disease when locomotion is ranked during the whisker stimulation

Supplementary table 28: Shapiro Wilks test of normality for ranked locomotion responses across the whole trial and across disease groups

	Most locomotion summed		
Disease group	**Statistic**	**df**	**p**
WT	.932	35	.032
AD	.884	43	.000
ATH	.965	33	.359
MIX	.912	21	.061
Least locomotion summed			
WT	.505	35	.000
AD	.344	43	.000
ATH	.818	33	.000
MIX	.784	21	.017

Supplementary table 29: Kruskal Wallis test for most and least summed locomotion when locomotion was ranked across the whole trial, across disease groups

Amount of locomotion across disease	**N**	**Statistic**	**df**	**p**	**E^2_R**
Most summed locomotion	132	2.699	3	.440	0.020
Least summed locomotion	132	27.519	3	.000	0.210

The sample size used in the study indicates a small effect for most summed locomotion and a large effect for least summed locomotion.

Supplementary table 30: Descriptive statistics for most and least summed locomotion when locomotion was ranked across the whole trial, across disease groups

Most summed locomotion	**N**	**Mean**	**Median**	**STD**
WT	35	147.23	147.33	98.96
AD	43	141.00	122.67	114.36
ATH	33	153.86	148.33	69.17
MIX	21	124.92	94.83	100.15
Least summed locomotion				
WT	35	.514	.000	1.114
AD	43	3.84	1.50	9.46
ATH	33	.697	.333	.823
MIX	21	2.70	1.00	1.00

Supplementary table 30: Pairwise comparisons for least summed locomotion when locomotion was ranked across the whole trial, across disease groups

Pairwise comparisons least locomotion	Statistic	Standard error	Standard test statistic	p	Adjusted p
WT vs ATH	-12.08	9.12	-1.324	.186	1.00
WT vs MIX	-27.54	10.38	-2.654	.008	.048
WT vs AD	42.54	8.56	4.970	.000	.000
ATH vs MIX	-15.47	10.50	-1.474	.141	.843
ATH vs AD	30.46	8.70	3.501	.000	.003
MIX vs AD	14.99	10.01	1.498	.134	.805

Supplementary table 31: Shapiro Wilks test of normality for peak haemodynamic responses for most locomotion trials when locomotion was ranked during the whisker stim and across disease groups

Most locomotion when ranked during whisker stim									
		HbT			HbO			HbR	
Group	Statistic	df	p	Statistic	df	p	Statistic	df	p
WT	.939	35	.052	.936	35	.043	.960	35	.232
AD	.902	43	.001	.906	43	.002	.894	43	.001
ATH	.936	33	.052	.929	33	.134	.933	33	.042
MIX	.908	21	.050	.903	21	.040	.913	21	.064

Supplementary table 32: Kruskal Wallis test results for for peak haemodynamic responses for most locomotion trials when locomotion was ranked during the whisker stim and across disease groups

Haemodynamic responses for most locomotion trials	N	Statistic	df	p	E^2_R
Peak HbT	132	1.649	3	.648	0.012
Peak HbO	132	2.174	3	.537	0.016
Peak HbR	132	3.872	3	.276	0.029

The sample size used in the study indicates a small effect.

Supplementary table 33: Descriptive statistics for peak haemodynamic responses for most locomotion trials when locomotion was ranked during the whisker stim and across disease groups

HbT	**N**	**Mean**	**Median**	**STD**
WT	35	1.04	1.04	.020
AD	43	1.04	1.03	.021
ATH	33	1.04	1.03	.019
MIX	21	1.04	1.04	.020
HbO				
WT	35	1.06	1.06	.031
AD	43	1.06	1.05	.033
ATH	33	1.06	1.05	.028
MIX	21	1.06	1.05	.029
HbR				
WT	35	.942	.939	.028
AD	43	.946	.955	.030
ATH	33	.953	.954	.024
MIX	21	.943	.947	.022

Supplementary table 24: Shapiro Wilks test of normality for peak haemodynamic responses for least locomotion trials when locomotion was ranked during the whisker stim and across disease groups

Least locomotion when ranked during whisker stim									
		HbT			**HbO**			**HbR**	
Group	Statistic	df	p	Statistic	df	p	Statistic	df	p
WT	.971	35	.459	.983	35	.859	.983	35	.862
AD	.812	43	.000	.826	43	.000	.895	43	.001
ATH	.944	33	.086	.948	33	.116	.969	33	.704
MIX	.967	21	.674	.969	21	.704	.929	21	.129

Supplementary table 35: Kruskal Wallis test results for peak haemodynamic responses for least locomotion trials when locomotion was ranked during the whisker stim and across disease groups

Haemodynamic responses for least locomotion trials	**N**	**Statistic**	**df**	**p**	**E^2_R**
Peak HbT	132	10.55	3	.014	0.080
Peak HbO	132	9.901	3	.031	0.075
Peak HbR	132	8.133	3	.043	0.062

The sample size used in the study indicates a moderate effect size.

Supplementary table 36: Descriptive statistics for peak haemodynamic responses for least locomotion trials when locomotion was ranked during the whisker stim and across disease groups

HbT	N	Mean	Median	STD
WT	35	1.02	1.03	.008
AD	43	1.02	1.02	.011
ATH	33	1.01	1.01	.008
MIX	21	1.01	1.01	.008
HbO				
WT	35	1.03	1.03	.014
AD	43	1.03	1.03	.018
ATH	33	1.02	1.02	.013
MIX	21	1.02	1.02	.013
HbR				
WT	35	.967	.967	.015
AD	43	.970	.971	.019
ATH	33	.977	.979	.014
MIX	21	.973	.973	.016

Supplementary table 37: Pairwise comparisons for peak HbT haemodynamic responses for least locomotion trials when locomotion was ranked during the whisker stim and across disease groups

Pairwise comparisons least locomotion HbT	Statistic	Standard error	Standard test statistic	p	Adjusted p
ATH vs MIX	-16.70	10.68	-1.564	.118	.706
ATH vs AD	24.04	8.85	2.716	.007	.040
ATH vs WT	27.47	9.28	2.961	.003	.018
MIX vs AD	7.34	10.18	.721	.471	1.00
MIX vs WT	10.77	10.56	1.020	.308	1.00
AD vs WT	-3.43	8.71	-.394	.693	1.00

Supplementary table 38: Pairwise comparisons for peak HbO haemodynamic responses for least locomotion trials when locomotion was ranked during the whisker stim and across disease groups

Pairwise comparisons least locomotion HbO	Statistic	Standard error	Standard test statistic	p	Adjusted p
ATH vs MIX	-14.05	10.68	-1.316	.188	1.00
ATH vs AD	19.79	8.85	2.123	.034	.203
ATH vs WT	26.94	9.28	2.903	.004	.022
MIX vs AD	4.74	10.18	.466	.641	1.00
MIX vs WT	12.90	10.56	1.221	.222	1.00
AD vs WT	-8.15	8.71	-.936	.349	1.00

Supplementary table 39: Pairwise comparisons for peak HbR haemodynamic responses for least locomotion trials when locomotion was ranked during the whisker stim and across disease groups

Pairwise comparisons least locomotion HbR	Statistic	Standard error	Standard test statistic	p	Adjusted p
WT vs AD	10.46	8.71	1.201	.230	1.00
WT vs MIX	-16.21	10.56	-1.535	.125	.748
WT vs ATH	-25.94	9.28	-2.795	.005	.031
AD vs MIX	-5.75	10.18	-.565	.572	1.00
AD vs ATH	-15.48	8.85	-1.749	.080	4.82
MIX vs ATH	9.73	10.68	.911	.362	1.00

Aortic arch atherosclerotic plaque burden statistical outputs

Supplementary table 40: Shapiro Wilks test of normality for the aortic arch atherosclerotic plaque burden

Aortic plaque burden			
Disease group	**Statistic**	**df**	**p**
ATH	.964	9	.838
MIX	.889	6	.312

Supplementary table 41: Mann Whitney U test results for aortic arch atherosclerotic plaque burden

Plaque burden	N	U	W	Standard error	Standardised test statistic	Asym p	Exact p	Effect size
Plaque burden	15	19	40	8.49	-.943	.346	.388	0.728

Using Cohen's d estimates of effect size (0.2 = small, 0.5 = moderate, 0.8 = large) the sample size used in the above test indicate a large effect size.

Supplementary table 42: Descriptive statistics for aortic arch atherosclerotic plaque burden

Preference Index	N	Mean	Median	STD
ATH	9	18.35	18.76	4.49
MIX	6	14.43	16.33	6.12

Hippocampal amyloid plaque burden statistical outputs

Supplementary table 43: Shapiro Wilks test of normality for the hippocampal amyloid plaque burden

	Hippocampal amyloid plaque burden		
Disease group	**Statistic**	**df**	**p**
AD	.948	6	.727
MIX	.891	5	.363

Supplementary table 44: Independent samples t test results for hippocampal amyloid plaque burden

	Mean diff	**SE diff**	**t**	**df**	**p**	**Lower**	**Upper**	**Effect size**
Plaque burden in AD vs MIX	-.195	.125	1.564	9	.152	-.087	.478	0.989

Using Cohen's d estimates of effect size (0.2 = small, 0.5 = moderate, 0.8 = large) the sample size used in the above test indicate a large effect size.

Supplementary table 45: Descriptive statistics for hippocampal amyloid plaque burden

Amyloid plaque burden	**N**	**Mean**	**Median**	**STD**
AD	6	.504	.496	.265
MIX	5	.308	.308	.039

Chapter 4: The B of the neurovascular bang: early, remote changes in large cerebral veins in response to spontaneous locomotion

This manuscript has been prepared for submission to a journal

The B of the neurovascular bang: early, remote changes in large cerebral veins in response to spontaneous locomotion

Beth Eyre[1,2,3]*, Sheila Francis[2,3,4], Clare Howarth[1,2,3+], Jason Berwick[1,2,3+]

[1]Sheffield Neurovascular Lab, Department of Psychology, University of Sheffield, Alfred Denny Building, Western Bank, Sheffield, S10 2TN (United Kingdom)
[2]Neuroscience Institute, University of Sheffield, Sheffield, S10 2TN (United Kingdom)
[3]Healthy lifespan Institute, University of Sheffield, Sheffield, S10 2TN (United Kingdom)
[4]Department of Infection, Immunity & Cardiovascular Disease (IICD), University of Sheffield Medical School, Royal Hallamshire Hospital, Beech Hill Road, Sheffield, S10 2RX (United Kingdom)
[+]These authors contributed equally. * Corresponding author.

I Beth Eyre am sole first author on this manuscript. I completed surgeries, and haemodynamic imaging data collection. I completed data analysis, statistical tests and wrote up the manuscript.

Myself, Clare Howarth and Jason Berwick analysed the data. Myself, Clare Howarth and Jason Berwick wrote code for the analysis. Sheila Francis provided the expertise on the atherosclerosis side of the project. Myself, Clare Howarth and Jason Berwick edited and proofread the manuscript.

4.1 Abstract

Neurovascular coupling (NVC) is a mechanism that increases cerebral blood flow (CBF) and volume (CBV) to areas of increased neural activity. The brain is essentially a fluid filled volume which is enclosed in an inflexible space (the skull). Therefore, if areas of the brain have an increase in CBF and CBV due to NVC, where does the necessary space come from? This study explores the possibility that space is created in the large cerebral veins prior to subsequent large increases in CBF and CBV arising from voluntary locomotion in awake mice. Male and female mice aged 9-12m were used: (AD (APP/PS1 (B6;C3Tg(APPswe,PSEN1dE9)85Dbo/Mmjax)), WT (APP/PS1-WT littermates), atherosclerosis (WT + rAAV8-mPCSK9-D377Y + Western Diet (male only)) and comorbid AD and atherosclerosis (APP/PS1 + rAAV8-mPCSK9-D377Y + Western Diet (male only)). Mice were head-fixed upon a spherical treadmill while 2D-optical imaging spectroscopy was used to measure changes in cortical CBV. Haemodynamic measures evoked by spontaneous locomotion and 2s whisker stimulations were collected. In response to spontaneous locomotion, an initial decrease in CBV was observed in draining veins, occurring prior to CBV increases in arteries and veins within the whisker barrel cortex. The onset of CBV change in the draining vein was quickest compared to CBV change in whisker barrel cortical arteries and veins. We also assessed whether this early response in the draining vein was impacted by disease, and observed that there was no effect of disease on the response. Large cerebral draining veins display an initial, fast early decrease in CBV at the onset of locomotion (which is not impacted by disease). This decrease occurs prior to increases in arterial and venous CBV within the whisker region of the cortex. We suggest this initial reduction in CBV within the draining vein serves as a 'space saving' mechanism, to allow for the subsequent large increases in CBV that are associated with locomotion.

4.2 Introduction

In order for the brain's high energy demands to be met[1,2], constant blood flow is needed. A continuous supply of blood is controlled by neurons communicating with cells of the neurovascular unit, ultimately resulting in the dilation of blood vessels in active regions of the brain. This relationship between neural activity and a subsequent increase in blood flow is known as neurovascular coupling (NVC)[3,4]. Over recent years

our knowledge about this important mechanism has increased exponentially[5–10]. However, there are still many unanswered questions regarding how active regions of the brain make 'space' for the large influx of blood that follows neural activity. The brain itself is essentially a fluid filled volume, enclosed within a hard case (the skull)[11,12]. Large intracranial pressure (ICP) changes can be ultimately devistating[13]. However, it is largely unknown how space is created within the brain to allow blood flow increases to meet metabolic demands.

Over the past decade NVC research has transitioned from using acutely anaesthetised preparations[5,14,15] to performing studies in awake, behaving animals[10,16–18]. While awake imaging studies avoid the potential confounds caused by anaesthetics, these studies have their own confounds of behaviour, including the impacts of locomotion[18,19]. However, an array of behaviours can be monitored[20] allowing the field to gain a more in-depth understanding of how certain behaviours may impact NVC. For example, locomotion has been shown to have a large and robust effect on NVC, where large increases in blood flow in pial arteries and veins occur at the onset of locomotion[16,21]. In addition, Gao et al.,[22] examined the effects of locomotion on dural vessels of the brain (which lie superficial to the brain surface) and found that these vessels constrict at the onset of locomotion, which could potentially serve as a space-saving mechanism for the subsequent large locomotion-evoked increases in blood flow. Despite this finding, many NVC studies have focussed on the smaller diameter cerebral blood vessels and capillaries[23,24] and there has not been a systematic investigation into the effects on the large midline pial veins that drain into the sagittal sinus[25] (referred to as draining veins). Interestingly, prior work has explored an alternative explanation of how 'space' is created in the brain when there are large increases of CBV. Krieger et al.,[26] suggested that changes in CBV may be aided via the exchange of water from capillaries into neighbouring tissue. However, this idea is based upon modelled data and experimental support for this idea is lacking.

Although generally assumed to be passive, remote bystanders of the vasculature, the large surface cerebral veins potentially play an important role in NVC. Early work which investigated the role of veins within NVC suggested that veins played a passive role, acting as 'balloons', and responded to pressure changes[27], more recent work suggests

that they could play a more 'active' role. For example, Driver et al.,[28] reported the observation of pulsatility within small cerebral veins[28]. Additionally, veins are also thought to play a role in clearance pathways of the brain, with solutes emptying along the venous circulation[29,30].

Widefield optical imaging techniques such as 2-dimensional optical imaging spectroscopy (2D-OIS) offer the opportunity to investigate the responses of the large surface pial vessels in awake head-fixed animals[18]. In our previous study, we focussed on how spontaneous locomotion occurring at or around the time of sensory stimulation can affect the magnitude of NVC responses[16,18]. In the current study we will focus on spontaneous locomotion in isolation and how the initial vascular response develops within the surface vessels of the cortex.

These experiments were performed on four groups of animals, a wildtype control group and three disease groups (Alzheimer's Disease (AD), Atherosclerosis (ATH) and a mixed AD and ATH group) which formed part of a larger study to investigate cerebrovascular function in health and disease (Chapter 3, Eyre 2023, in preparation). We found an initial fast decrease in CBV in the large branches of the surface draining veins that preceded the large increase in CBV across all vascular compartments driven by the pial arteries. The effect was consistent across all animal groups with no effect of disease and was also significantly smaller for a whisker stimulation. Therefore, the initial draining vein response represents a previously unreported, fast, remote neurovascular signal that may be important in the overall regulation of NVC, especially to large bilateral increases in brain metabolism.

4.3 Methods

4.3.1 Animals

Male and female mice aged between 9-12m were included in the study. Four groups of mice were used: the APP/PS1 (B6.C3-Tg(APPswe,PSEN1dE9)85Dbo/Mmjax #34829)[31] Alzheimer's model, WT littermates, an atherosclerosis model (male only): WT-littermates injected with rAAV8-mPCSK9-D377Y (6×10^{12} virus molecules/ml) (Vector Core, Chapel Hill, NC) at 11 weeks of age (i/v or i/p + a western diet at 12 weeks (21% fat, 0.15% cholesterol, 0.03% cholate, 0.296% sodium; #829100, Special

Diet Services UK) and a mixed disease group (male only): APP/PS1 mice injected with rAAV8-mPCSK9-D377Y (6×10^{12} virus molecules/ml) (Vector Core, Chapel Hill, NC) at 11 weeks of age (i/v or i/p + a western diet at 12 weeks). Mice were housed in groups where possible, and were singly housed if there was no available littermate. After surgery all mice were individually housed. Food and water were available ad-libitum (western diet was restricted to 5g per day) and mice were housed on a 12hr dark/light cycle (lights on 06:00-18:00). All experiments were carried out during the lights on hours. All procedures were approved by the UK Home Office and in agreement with the guidelines and scientific regulations of the Animals (Scientific Procedures) Act 1986, with additional approval received from the University of Sheffield licensing committee and ethical review board. The following study is reported in accordance with the ARRIVE guidelines. Mice selection from the colony was randomised. The experimenter was blinded to genotype (where possible) during experiments and blinded during analysis.

4.3.2 Surgery

Animals were anesthetised with ketamine (50mg/kg) and medetomidine (0.65mg/kg) (subcutaneously, s/c) with isoflurane used to maintain surgical plane of anaesthesia (0.5-0.8% in 100% oxygen). Carprofen (10mg/kg) was administered prior to a scalpel being used to remove hair from the head. Animals were positioned in a stereotaxic frame (Kopf Instruments) and eyes protected with viscotears (Novartis). Body temperature was monitored and maintained with the use of a rectal thermometer and a homeothermic blanket (Harvard Apparatus). Iodine and bupivacaine (50-100mcL at 0.025%) was applied prior to revealing the skull. Suture lines were covered with cyanoacrylate glue and a dental scraper was used to score the contralateral side of the skull, to increase headplate stability. A dental drill was used to thin the bone over the right somatosensory cortex (~4mm^2). The skull was thinned until the pial vasculature was observed. Cyanoacrylate glue was spread across the thinned region. A metal headplate was attached using dental cement (Superbond C & B; Sun Medical). Atipamezole (2mg/kg in 0.3ml warm sterile saline s/c) was given at the end of the procedure to reverse the effects of medetomidine. Following surgery, mice were placed in an incubator (29 degrees) and monitored. Post-surgery, mice were singly housed and given at least one week to recover before habituation to the awake

imaging apparatus and imaging. Mice were closely monitored for weight loss and signs of pain for 3-days post-surgery and given carprofen jelly (10mg/kg) for at least 1-day after surgery.

4.3.3 Awake Imaging

The same awake imaging set up and similar habituation procedure were used as described previously[18] and in chapter 3. Briefly, one-week post-surgery mice were habituated to the awake imaging set up. Over a 5-day period, mice were habituated to the room, experimenter and the apparatus. On day one, mice were placed on the spherical treadmill, with the room light on, without head fixation for approximately 10 minutes. On day 2, mice were head fixed to the ball, room lights were turned off and 2s whisker stimulations were conducted. This lasted approximately 20 minutes. Day 3 was similar to day 2, with an additional 'spontaneous' trial collected, whereby no whisker stimulations were conducted but haemodynamic measurements were collected. Mice were on the ball for approximately 30 minutes. Day 4 followed the same regime as the prior two days; however, a 16s whisker stimulation experiment was added (and analysed in a different study). Mice were on the ball for approximately 45 minutes to 1 hour. Day 5 was the same as day 4. Mice were briefly anaesthetised with isoflurane (3-4%) to get them onto the awake imaging apparatus.

4.3.4 Locomotion data collection and analysis

Locomotion tracking was completed in the same way as mentioned previously in Eyre et al., 2022[18]. Briefly, locomotion was collected using a spherical treadmill with an attached optical motion sensor. Once locomotion data was collected, in house Matlab scripts (MathWorks, R2019b) were used to analyse the data. As previously described[18] the optical motion sensor recorded the spherical treadmill movement during experiments. Each file comprised of the locomotion data; (this was a vector which corresponded to the rotation of the treadmill, at times when the mouse was stationery this was represented as 0, the faster the treadmill the larger the integer, this was plotted as distance (arbitrary unit, AU). The file was also comprised of the time vector; this allowed locomotion data to be measured across time (in seconds) and the trigger points were also included in the file; these provided the timing of whisker stimulations during the different trials, and allowed us to match locomotion to the exact

timing of the analogous haemodynamic responses (when we investigated whisker stimulations).

4.3.5 2D-Optical imaging spectroscopy

Widefield imaging was used to investigate blood volume changes across the surface vasculature. Two-dimensional optical imaging (2D-OIS) uses light to assess changes in oxygenated (HbO), deoxygenated (HbR) and total levels of haemoglobin (HbT) in the surface vessels of the cortex. To measure cortical haemodynamics 4 different wavelengths of light (494 ± 20 nm, 560 ± 5 nm, 575 ± 14 nm and 595 ± 5 nm) were shone on to the thinned window, using a Lambda DG-4 high-speed galvanometer (Sutter Instrument Company, USA). A Dalsa 1M60 CCD camera was used to capture remitted light at 184×184 pixels, at a 32 Hz frame rate, this provided a resolution of ~ 75 µm.

2D-OIS can also be used to create 2D spatial maps of micromolar changes in HbO, HbR and HbT, revealing the vasculature of the cortex. This is achieved by using the path length scale algorithm (PLSA) to complete a spectral analysis[14,32]. The PLSA works by using the modified Beer Lambert Law, with a path-length correction factor, as well as predicted absorption value of HbT, HbO and HbR. The relative concentration estimates were acquired from baseline values, where the concentration of haemoglobin within tissue was estimated as 100 µM, and tissue saturation of oxygen estimated at 70% in the whisker region, 80% in the whisker barrel artery, 60% in the whisker barrel vein, 70% in the parenchyma and 60% in the draining vein.

4.3.6 Regions of Interest (ROI) from 2D spatial maps

Custom, in-house MATLAB (MathWorks, 2019b) scripts were used to create ROIs from 2D spatial maps generated using 2D-OIS. A whisker region was generated using code that selected the region of the cortex with the largest change in HbT to a 2s whisker stimulation. The code assessed pixels as being ‘active’ if their value was >1.5 STD across the whole of the spatial map. Therefore, the whisker ROI represented the area of the cortex with the largest HbT response to a 2s whisker stimulation. A ‘whisker barrel artery’ (an artery inside the already defined whisker region, that responded to the 2s whisker stimulation) and ‘whisker barrel vein’ (a vein inside the already defined

whisker region, that responded to the 2s whisker stimulation) were then manually selected from inside the whisker region ROI. The above was completed for each imaging session, with care taken to select the same whisker artery and veins across days. In order to generate the draining vein ROI, a locomotion trial was generated (see below). This locomotion spectroscopy file was loaded into our in-house software and the draining vein ROI was manually selected using principal component analysis (PCA). The draining vein was a large cerebral vein, protruding from the midline outside of the 'whisker region' The time series analyses shown within the study were completed for the whisker barrel artery, whisker barrel vein and draining vein.

4.3.7 Haemodynamic data analysis

Data analysis was conducted in Matlab (MathWorks, R2019b) using custom-made scripts. Imaging sessions were excluded from data analysis where there was visible, excessive motion, indicated by shadows on the 2D spatial maps. Thirty 2s whisker stimulation trials were conducted at 5Hz. Each trial was 25s in length (750 seconds of continuous data collection). A mechanical whisker stimulation occurred between 5-7 seconds and corresponding haemodynamic and locomotion data were concurrently recorded for each imaging session. An average of the all 30 trials was taken from each imaging session and included in the group average.

Spontaneous trials were also collected, whereby continuous haemodynamic activity (changes in haemoglobin levels) and simultaneous locomotion were collected for 750 seconds (with no whisker stimulations). This continuous recording of haemodynamics and concurrent locomotion was loaded into Matlab and 25s locomotion trials were generated. To create the 25s spontaneous locomotion trial, walking events, which resulted in an obvious increase in HbT were manually selected. Walking events were not chosen if a previous walking event occurred within 2-3s prior. Long, continuous walking events that increased HbT for longer durations were also not selected, as this would not have matched the timing of the 2s whisker stimulation. The selected individual walking events, and the corresponding haemodynamics were averaged into a 25s trial that had the same timing parameters as the 2s whisker stimulation trials for each imaging session. Numerous walking events and the corresponding haemodynamic responses were averaged together to create a locomotion trial for

each imaging session. An average of 7.6 (Range = 1-24) walking events were selected per imaging session and used to create a locomotion trial for each imaging session. This allowed us to compare haemodynamic responses evoked by 2s whisker stimulations and locomotion.

In order to accurately characterise initial HbT decreases, only imaging sessions in which an initial decrease in HbT (in response to the onset of locomotion) within the draining vein was observed were included in further data analysis. HbT responses within the draining vein were classified as an initial decrease if the peak HbT response between 5-7s (with the onset of locomotion occurring at 5s) was 2 standard deviations greater than the standard deviation of the baseline (taken from the first 5s). This analysis showed that for a large proportion of the imaging sessions there was an initial decrease in HbT within the draining vein, in response to locomotion (WT = 25/28 sessions, AD= 23/31, Athero=22/28 sessions and mixed =12/15 sessions). Peak HbT responses were used when comparing responses across vascular compartments. Peak HbT responses were calculated by looking for the greatest change in the concentration of HbT from baseline between 5 and 7s (with locomotion onset occurring at 5s) for the initial decrease in HbT within the draining vein and between 5-12s when assessing the increase in HbT in response to locomotion for the draining vein, whisker barrel artery and whisker barrel vein. Onset time was measured by calculating the 10% and 90% values of either peak decrease (for the initial response) or increase (for the late response) and extrapolating the point where the intercept crossed the baseline.

4.3.8 Statistical tests

Statistical tests were run in SPSS (Version 26) and figures created in Matlab (MathWorks, R2019b) and GraphPad Prism (Version 9). Assumptions of statistical tests were checked, if violated, appropriate non-parametric tests were implemented. Normality was assessed using the Shapiro Wilks test and the presence of outliers was assessed using box plots (outliers identified by being 1.5 standard deviations away from the box plot). If data were not normal, or outliers were present appropriate, non-parametric tests were conducted, such as the Friedman test and Kruskal Wallis tests. All outliers were kept within the data set. $P<.05$ was denoted as significant. If initial

tests found significant differences, post hoc tests with a Bonferroni correction were completed. Friedmans tests were used to assess whether there were significant differences in the onset time of a change in HbT within the draining vein, whisker artery and whisker vein. As well as being used to assess if there were significant differences in the onset time of the increase in HbT (in response to locomotion) within the draining vein, whisker artery and whisker vein. A Wilcoxon Signed Ranks test was completed to assess if there were significant differences between the amplitude of the early decrease in HbT within the draining vein in response to locomotion as compared to in response to a 2s whisker stimulation. Kruskal Wallis tests were conducted to establish if there were significant differences across disease groups in the spontaneous locomotion response (as assessed by AUC), in addition to being used to assess if there were significant differences in the onset, rise times and size of the initial decrease in HbT and increase in HbT in the draining vein in response to spontaneous locomotion across disease groups. Kruskall Wallis tests were also conducted to establish if there were significant differences across disease groups in the onset, rise time and size of the increase in HbT in the whisker barrel artery and whisker barrel vein in response to spontaneous locomotion. Descriptive statistics and detailed statistical outputs can be found in the supplementary tables. Apriori power calculations were not conducted for this study, as the dataset had already been collected as part of a previous study (chapter 3). However, effect sizes for statistical tests conducted can be found in the supplementary tables.

4.4 Results

4.4.1 Large cerebral draining veins display an initial, fast, early decrease in HbT at the onset of locomotion

A thinned window surgery was completed prior to imaging to aid with the visualisation of cerebral vessels, in order for 2D-OIS to be used to measure changes in HbO, HbR and HbT (CBV) in response to spontaneous locomotion and whisker stimulation in different vascular compartments. For each imaging session locomotion was collected concurrently to haemodynamics during ‘spontaneous’ trials, in which no whisker stimulation occurred, as well as during 2s whisker stimulation trials. Briefly, to generate spontaneous locomotion trials walking events were selected which corresponded with an increase in HbT. These were averaged together to produce a locomotion trial with the same timing parameters (25s) as the whisker stimulation trial (Figure 4.1 a).

Changes in HbT – (closely corresponding to CBV) in response to the 25s spontaneous locomotion trial were plotted for the draining vein, whisker barrel artery and whisker barrel vein (Figure 4.1 b).

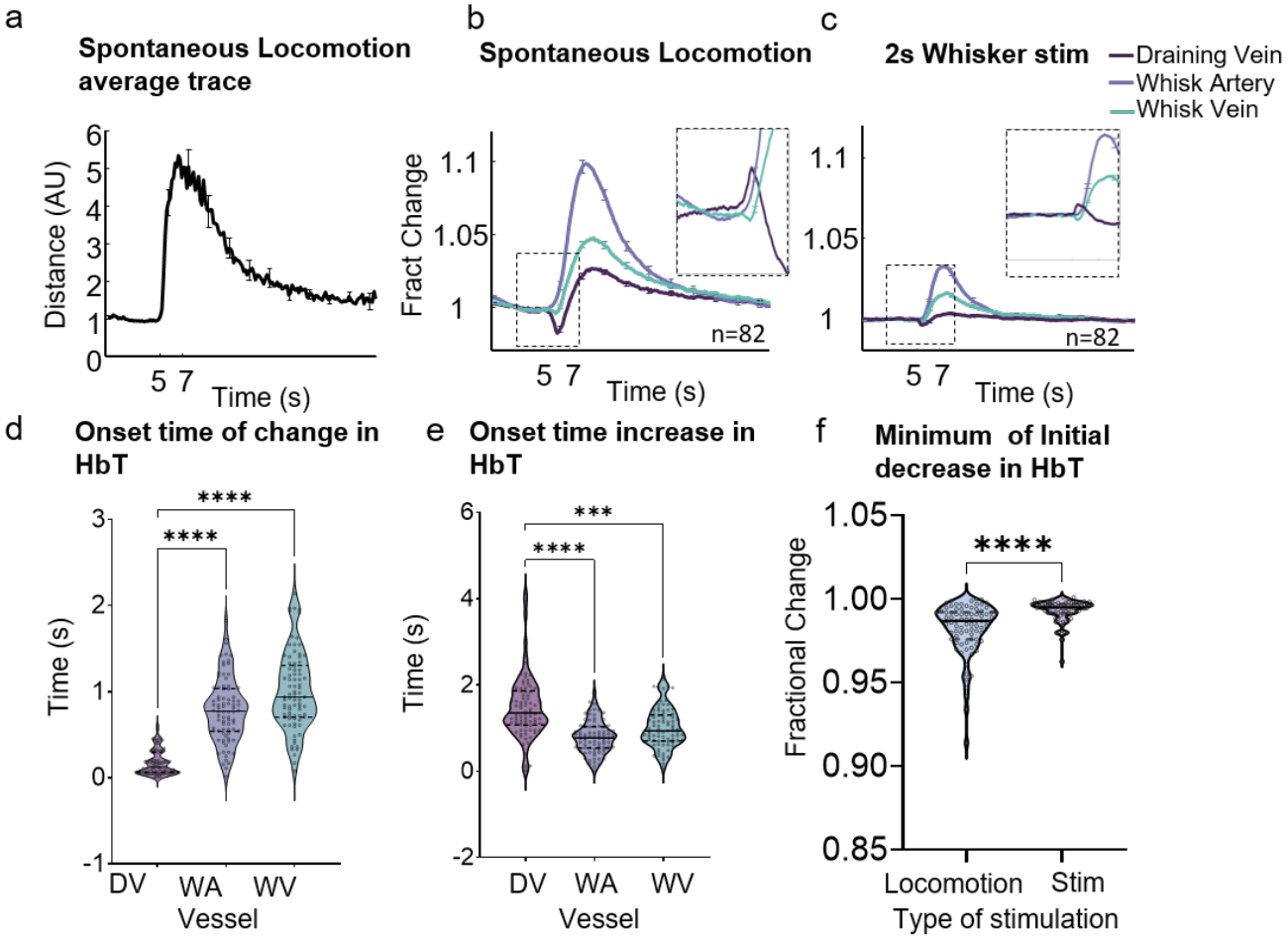

Figure 4.1: Large cerebral draining veins display an initial, fast, early decrease in HbT at the onset of locomotion

(a) *Spontaneous locomotion and corresponding haemodynamics were collected using 2D-OIS. A mean 25s locomotion trial was created for each imaging session (n=82 from 35 mice) and averaged to show the average 25s locomotion trial.* ***(b)*** *a time series graph showing locomotion-evoked fractional change in HbT in the draining vein (dark purple), whisker barrel artery (lilac) and the whisker barrel vein (light blue). Inset shows the draining vein trace 'flipped' revealing that this change in HbT within the draining vein occurs prior to changes in HbT within arteries and veins within the whisker cortex.* ***(c)*** *a time series graph showing fractional change in HbT to a 2s whisker stimulation in the draining vein (dark purple), whisker barrel artery (lilac) and whisker barrel vein*

(light blue). A zoomed in view shows the draining vein trace 'flipped'. ***(d)*** *A violin plot with individual onset times to a decrease in HbT within the draining vein and an increase in HbT within the whisker barrel artery and vein. The onset of CBV change in the draining vein was quickest compared to CBV change in whisker barrel cortical arteries and veins* ***(e)*** *A violin plot with individual onset times for the onset of dilation in the draining vein (DV), whisker barrel artery (WA) and whisker barrel vein (WV). The onset of dilation in the draining vein was slowest compared to the onset of dilation in the whisker barrel cortical arteries) and veins* ***(f)*** *A violin plot with individual HbT minimum values taken between the onset of stimulation and 2.5s after for spontaneous locomotion and 2s whisker stimulation. The initial, early decrease in HbT in the draining vein to spontaneous locomotion had a significantly lower median fractional change value compared to the slight decrease in HbT in the draining vein to a 2s whisker. (Error bars = sem, black line = median, dashed black line = interquartile range).*

Surprisingly, we observed a fast, initial decrease in HbT at the onset of locomotion within the draining vein (Figure 4.1 b and d, Figure 4.2). This initial decrease in HbT within the draining vein occurred before any subsequent increases of HbT within the whisker barrel artery or whisker barrel vein (Friedman test; ($x^2(2) = 105.585$, $p < 0.0005$, (n=82 sessions, from 35 mice)). The onset of CBV change in the draining vein was quickest (median=0.125s, $p < 0.0005$) compared to CBV change in whisker barrel region cortical arteries (median=0.773s, $p<0.0005$) and whisker barrel region veins (median=0.937s, $p<0.0005$). The increase in HbT, (revealing an increase in CBV) in response to spontaneous locomotion was slowest in the draining vein (Friedman test; ($x^2(2) = 40.195$, $p < 0.0005$, (n=82 sessions, from 35 mice)).The onset of the increase in HbT in the draining vein following locomotion was slowest (median= 1.35s, $p <0.0005$) compared to the onset of the increase in HbT in the whisker region cortical arteries (median= 0.773s, $p<0.0005$) and veins (median=0.937s, $p<0.0005$).

4.4.2 The Initial fast, early decrease in HbT in the draining vein is substantially reduced in response to whisker stimulation

To our knowledge, this early decrease in HbT in large draining veins of the brain has not been reported previously. Therefore, we wanted to establish whether it was a finding specific to spontaneous locomotion. To do this, we also conducted 2s whisker

stimulation experiments. 2s whisker stimulation experiments consisted of thirty 2s whisker stimulation trials, averaged together across each imaging session and then all imaging sessions were also averaged together (Figure 4.1 b). Each individual trial was 25s in length, with whisker stimulation occurring 5s into the trial. As this was the same timings as the spontaneous locomotion trials, we were able to compare evoked HbT to both spontaneous locomotion and to 2s whisker stimulation trials (Figures 4.1 b, 1c). To assess whether the early decrease in HbT at the onset of locomotion within the draining vein was an effect specific to spontaneous locomotion we compared the amplitude of the decrease in HbT within the draining vein across the spontaneous locomotion trials with the 2s whisker stimulation trials from the same imaging sessions (Figure 4.1 f). The initial, early decrease in HbT in the draining vein evoked by spontaneous locomotion had a significantly lower median fractional change value (median =.98) compared to the slight decrease in HbT in the draining vein in response to a 2s whisker stimulation (median =.99) (Wilcoxon Signed ranks test; z=5.351, p <.0005 (n=82 sessions, from 35 mice)).

4.4.3 Disease does not affect the onset time or size of the early decrease in HbT in large draining veins

As NVC has been suggested to be altered with disease[33,34], we assessed whether the above observation is impacted by disease. Figure 4.2 shows representative examples of changes in HbT across the cortex 1s prior to and 5s after spontaneous locomotion onset. 1s after spontaneous locomotion, a decrease in the large draining vein can be observed (blue within the large draining vein). This decrease in HbT is quickly followed by an increase in HbT within the whisker cortex (shown in red, increasing in intensity from 2s post spontaneous locomotion).

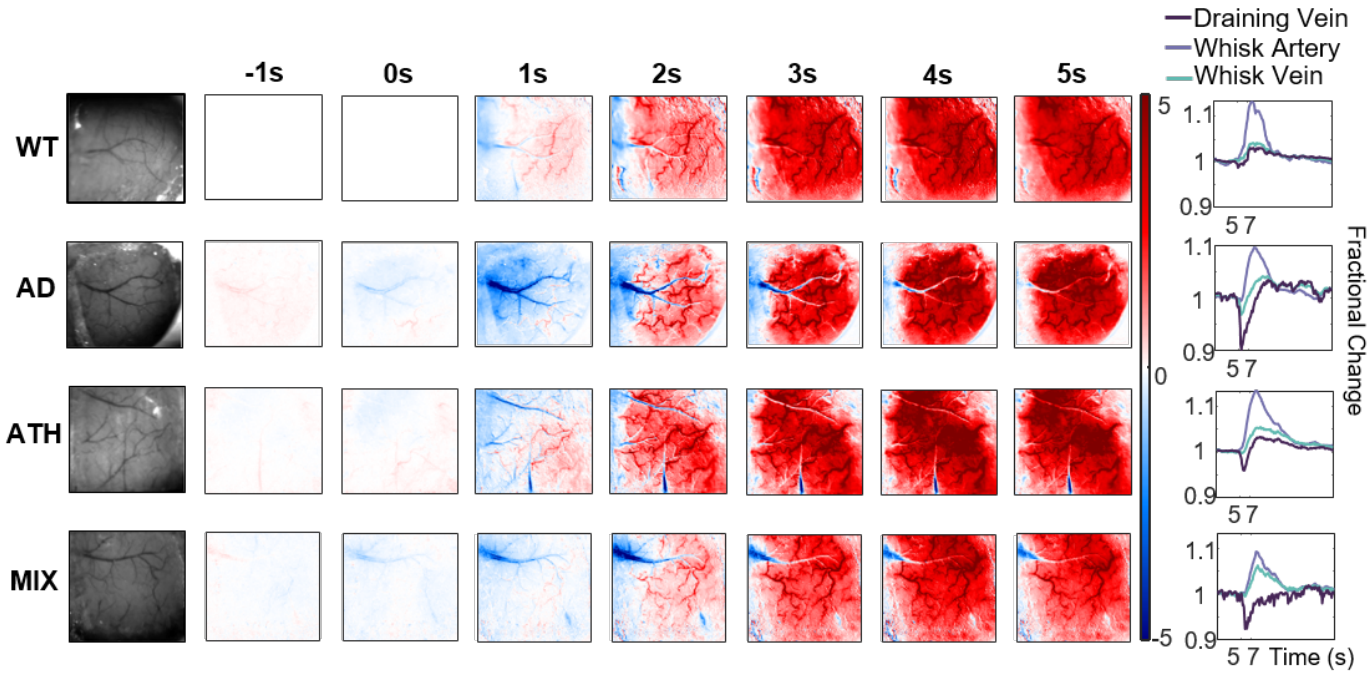

Figure 4.2: HbT spatial responses to spontaneous locomotion reveal an early decrease in HbT within the large draining vein of the brain

Representative examples of the changes in HbT across the cortex 1s before and 5s after onset of spontaneous locomotion (0s) for each disease group, accompanied by representative time series data for the spatial response. Red=increase in HbT, Blue=decrease in HbT. Spatial responses show that within 1s of the onset of spontaneous locomotion, a decrease in HbT occurs within the large draining vein, slowly followed by an increase in HbT within the whisker region of the cortex.

To assess whether the above observation may be impacted by disease we split the above 82 sessions into their respective disease groups. Disease groups included AD, Atherosclerosis, mixed disease and the WT-littermate control group. We found no significant differences in spontaneous walking, assessed by comparing the area under the curve of the spontaneous walking trial (Figure 4.3 a) across groups. Median, area under the curve to spontaneous walking were similar across groups, (Kruskal Wallis: H (3 n=82) = 7.181, p=.068) (WT; median=180.36, AD; median=105.55, Athero; median=154.35, Mixed; median=287) (Figure 4.3 a, b). We also found no significant differences in the amplitude of the early reduction in HbT, which corresponds to the size of the reduction in HbT within the draining vein. Median amplitude of HbT was not significantly different across disease groups (Kruskall Wallis: H (3 n=82) = 6.848, p = .077). Having assessed that disease did not affect the initial decrease in HbT to locomotion, we next investigated whether there were differences across groups for the onset and rise time of the haemodynamic response (Figures 4.3 c, d, e, f). We found no significant differences in the onset or rise times of the initial decrease in HbT within the large draining vein. Median onset and rise times were not significantly different across disease groups (onset time: Kruskall Wallis: H (3 n=82) =6.883, p=.076, (rise time: Kruskall Wallis: H(3 n=82) =5.758, p=.124) in response to spontaneous locomotion.

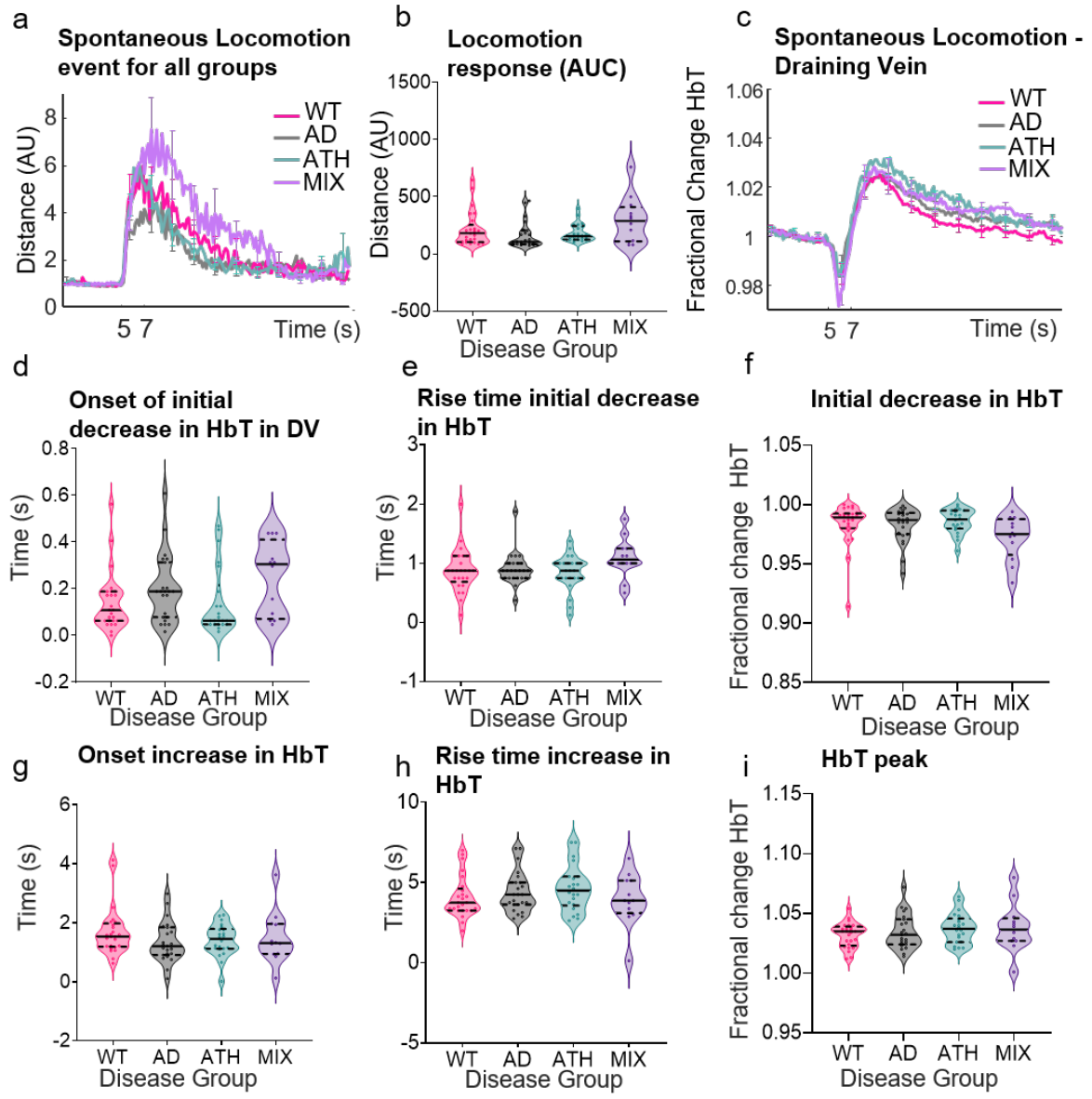

Figure 4.3: There is no effect of disease on the draining vein responses

(a) *Average spontaneous locomotion response for each disease group.* ***(b)*** *a violin plot showing AUC of the locomotion response (distance AU for each group revealing no significant differences in the amount of spontaneous locomotion across diseases* ***(c)*** *a time series graph showing fractional change in HbT in the draining vein to a 25s locomotion trial for the different disease groups.* ***(d)*** *A violin plot with each individual onset times to the initial decrease in HbT within the draining vein across disease* ***(e)*** *A violin plot with individual rise times for the initial decrease in HbT within the draining vein across disease groups* ***(f)*** *A violin plot with individual HbT minimum values taken between the onset of stimulation and 2.5s after the onset of spontaneous locomotion. (Error bars = sem, black line = median, dashed black line = interquartile range).*

4.4.4 Disease does not affect the onset, rise time or size of the increase in HbT in large cerebral draining veins in response to spontaneous locomotion

Although we found no effect of disease on the early vascular response observed within the draining vein in response to locomotion onset, we wanted to investigate how disease may impact the increase in HbT (that follows the onset of locomotion). To do this we investigated whether there were differences across groups for the onset, rise time and peak response of the increase in HbT within the draining vein in response to spontaneous locomotion (Figure 4.3 c, g, h, i). We found no significant differences across disease group for the onset, rise time or the peak response to spontaneous locomotion within the draining vein. We observed that median onset times of the increase in HbT were not significantly different across disease groups (Kruskall Wallis: H (3 n=82) = 2.628, p=.453. We also found that median rise times were not significantly different across disease groups (Kruskall Wallis: H (3 n=82) = 2.477, p=.480). Furthermore, median peak responses of HbT were not significantly different across disease groups (Kruskall Wallis: H (3 n=82) = 2.256, p=.521). The above results indicate that locomotion-evoked increase in HbT in the draining vein is not affected by disease.

4.4.5 Disease affects peak responses to spontaneous locomotion within the whisker barrel artery and vein

As 2D-OIS has the capability to investigate haemodynamic responses within different vascular compartments, we assessed how spontaneous locomotion affects the haemodynamic response within arteries and veins within the whisker barrel cortex (Figures 4.4 a, d). We observed that both within the whisker barrel artery and whisker barrel vein there were some significant differences between disease groups in the size of the peak response to locomotion.

For the whisker barrel artery there were significant differences between the size of the arterial peak response to spontaneous locomotion when comparing the Alzheimer's group with the mixed disease group. Median HbT peak responses were significantly different across disease groups (Kruskall Wallis: H (3 n=82) = 12.593, p=.006), with the mixed disease group (median=1.13) having a larger arterial response compared with the Alzheimer's group (median=1.09, p=.010) The atherosclerosis group also had a larger arterial HbT response (median=1.12) compared to the Alzheimer group

(median = 1.09, p=.033). There were no significant differences comparing WT mice and the other disease groups (WT compared with AD; p=.598, WT compared with atherosclerosis; p=1.00, WT compared with mixed; p=.413 (Bonferroni corrected)). Additionally, we observed no effect of disease on the onset or rise time of the peak response to spontaneous locomotion (onset time; Kruskall Wallis: H (3 n=82) = 4.216, p=.239, rise time; Kruskall Wallis: H (3 n=82) = 2.299, p=.513).

We also observed a significant difference in the size of the peak HbT response within the whisker barrel vein when comparing the Alzheimer's and mixed disease group (Kruskall Wallis: H (3 n=82) = 8.304, p=.040), with the mixed disease group having a larger response to spontaneous locomotion within the whisker barrel vein (median=1.06) compared with the Alzheimer's group (median=1.04, p=.034). There were no significant differences between the other groups. We also found no effect of disease on the onset or rise time of the increase in HbT within the whisker barrel vein in response to spontaneous locomotion (onset time; Kruskall Wallis: H (3 n=82) = 0.790, p=.852), rise time; Kruskall Wallis: H (3 n=82) = 4.264, p=.234)).

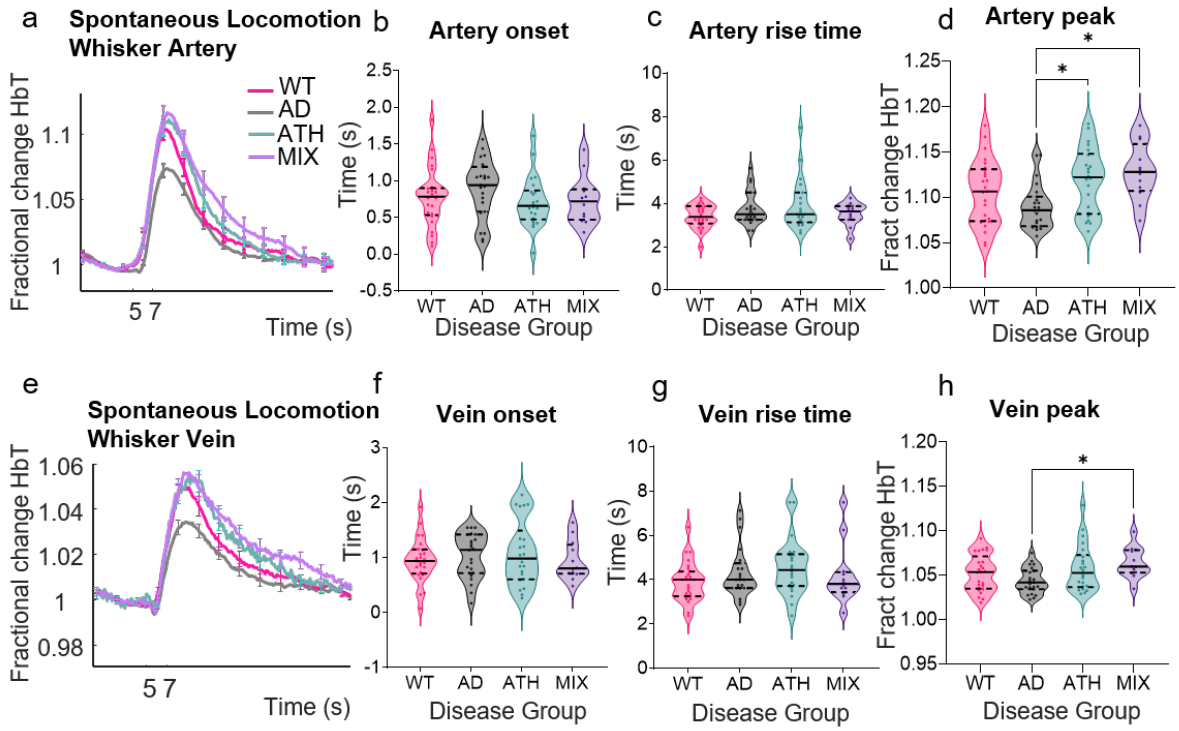

Figure 4.4: There is a difference across disease groups for peak HbT response to spontaneous locomotion events within the whisker barrel artery and whisker barrel vein

(a) *a time series graph showing fractional change in HbT in the whisker barrel artery to a 25s mean locomotion trial for the different disease groups.****(b)*** *A violin plot with each individual onset time to the increase in HbT observed within the whisker barrel artery in response to spontaneous locomotion across disease groups* ***(c)*** *A violin plot with individual rise times to the increase in HbT observed within the whisker barrel artery in response to spontaneous locomotion across disease* ***(d)*** *A violin plot with individual HbT peak values taken between the onset of stimulation (5s) and 7.5s after the onset of spontaneous locomotion in the whisker barrel artery across disease.* ***(e)*** *a time series graph showing fractional change in HbT in the whisker vein to a 25s mean locomotion trial for the different disease groups.****(f)*** *A violin plot with each individual onset time to the increase in HbT observed within the whisker barrel vein in response to spontaneous locomotion across disease* ***(g)*** *A violin plot with individual rise times to the increase in HbT observed within the whisker barrel vein in response to spontaneous locomotion across disease* ***(h)*** *A violin plot with individual HbT peak values taken between the onset of stimulation (5s) and 7.5s after the onset of spontaneous locomotion in the whisker barrel vein across disease. (Error bars = sem, black line = median, dashed black line = interquartile range).*

4.5 Discussion

In this study we collected haemodynamic responses to spontaneous locomotion in awake, head-fixed mice whilst they locomoted on a spherical treadmill. Surprisingly, we observed that large cerebral draining veins had a rapid and early decrease in HbT at the onset of locomotion. This observation occurred prior to increases in HbT within the whisker barrel artery and whisker barrel vein. We assessed whether this initial decrease in HbT within the draining vein was affected by pathological conditions. We found that there was no effect of disease, and that this early response in the draining vein was observed in WT, AD, ATH and MIX disease mice. The draining vein HbT decrease was also significantly smaller when evoked by a unilateral whisker stimulation. This suggests that this early neurovascular response could play an important role in the regulation of CBV within the brain and may play an important 'space-saving' role within the brain in response to events that result in large increases of CBV.

Our findings of a decrease in HbT in large pial draining veins was present in the majority of imaging sessions (82/102) and in all four disease groups. This raises the question – why has this observation not been reported previously? Other groups have investigated the effects of locomotion on both pial vessels and dural vessels[22]. Gao et al.,[22] found that there was a pronounced constriction of dural vessels in response to locomotion (this response was of a similar shape as the draining pial vein response we report in this paper). They showed that the response in these vessels was not related to changes in intra-cranial pressure and was distinct from pial vessel responses. Although Gao et al.,[22] suggested that the dural constriction must be a separate mechanism compared to pial brain vessels our results from this study suggest the dural vessels and large pial veins may be showing the same conserved response at the onset of locomotion.

The same group published a follow up paper assessing the effects of locomotion of cerebral oxygenation and how it was modulated by respiration[35]. In this study widefield imaging was used similar to our 2D-OIS technology but the focus of the paper was on the longitudinal effect of locomotion and not on the initial onset. Although they do not report an initial decrease in blood volume response in the draining veins, single

wavelength responses in Figure 2f after one and two seconds indicate the draining vein at the bottom of the image having a response very similar to those observed in our study. Additionally, Zhang et al[35] developed a new method of fast kilohertz two-photon imaging in awake mice. As part of their methodological approach, they investigated the diameter of the large pial veins close to the sagittal sinus (draining veins). They reported sharp constrictions in vein diameter in the awake animal at multiple time points but did not correlate this with behaviour such as locomotion.

All these results suggest that prior to a large increase in bilateral perfusion, large pial draining veins reduce their size. Further research using bi-lateral cranial windows and simultaneous measurements of neuronal activity, potentially using GCAMP imaging technologies will help understand this response further with respect to brain metabolism. Although in this study we show no effect of disease on this response it would also be important to assess whether this response is affected by age related vascular decline.

Unlike the aforementioned study[22], we did not measure intracranial pressure. As mentioned, we hypothesised that this early decrease in HbT within the large draining veins of the brain may potentially occur due to making more ‘space’ within the brain for the subsequent large increases in CBV induced by spontaneous locomotion. As we did not measure ICP during these experiments we cannot make any causal inferences about pressure changes within the brain when these early responses occur. However, Gao & Drew have conducted extensive experiments assessing ICP changes in awake, behaving mice[22]. They reported that ICP increases were observed during locomotion, these occurred rapidly and returned to baseline values once locomotion ceased. They further reported that when fitting the data to a linear convolution model they observed that ICP increases occurred just prior to locomotion. Therefore, it could be suggested that the decrease in HbT within the large draining veins could be explained by increases in ICP compressing these large veins to make space for the subsequent large increase in CBV that follows locomotion. However, due to the methods, we used (2D-Optical imaging spectroscopy), we are unable to explicitly state that a constriction occurred within these large cerebral veins (hence why we use the word compression). It would therefore be informative to investigate

the above findings using 2-photon microscopy[21,35,36,17] whereby vessel dynamics could be explicitly measured, in addition to being able to investigate absolute blood flow changes within the vessels.

We also had no measure of neural activity within the study. It would be beneficial to establish how neural activity is affected by spontaneous locomotion and the relationship this may have with the draining vein. Other studies have investigated how neural activity is impacted by spontaneous locomotion[21,16]. However, it would be especially interesting to focus on neuronal responses near the draining vein, as this has not previously been explored. In future work, similar experiments could be conducted using GCaMP mice[37], in order to investigate neural activity and haemodynamics concurrently in awake mice. These experiments would provide us with a more detailed understanding of the dynamics of the neurovascular responses that occur around the draining veins of the brain.

The differences observed in haemodynamic responses to locomotion events across disease could potentially be explained by the fact that there was a trend towards differences between averaged locomotion events across disease groups (Locomotion events AUC: WT; median=180.35, AD; median=105.55, Athero; median=154.34, Mixed; median=287) (Figure 3b). Even though there were no significant differences between averaged locomotion events across diseases, peak haemodynamic HbT responses to this locomotion were different across diseases. The AD group locomoted the least and the mixed group locomoted the most. Therefore, it is logical that the arterial and whisker vein HbT peak responses to locomotion were smaller within the AD group compared to the atherosclerosis and mixed disease groups, due to differences in the amount of locomotion. A trend towards greater amounts of locomotion may have resulted in greater peak HbT responses – as locomotion induced vascular responses were preserved across disease groups.

It has been suggested that very early vascular responses may just represent artifacts, potentially as a result of the startle response of the animals. To address this issue, we included whisker stimulation trials. In response to whisker stimulation, we show that the rapid change in CBV within the draining vein is negligible in comparison to the

reduction of CBV within the draining vein in response to spontaneous locomotion, thus suggesting that the draining vein response is not due to startle. Additionally, the spontaneous locomotion trials were created from individual walking events during a trial in which there were no whisker stimulations. It would be odd to suggest that the animal walking would cause itself to startle. Locomotion is not a reflex response and in order for the mouse to move, the animal has to initiate this response[38], therefore making it very unlikely that these findings are the effects of the startle response.

In summary, we report a fast distal vascular response related to the onset of locomotion in mice. It was visible in most imaging sessions and stable across wild-type and three models of disease. We suggest that this may be an important 'space-saving' mechanism involved in NVC and may allow for the large increase in CBV that follows locomotion. Further studies are warranted using 2-photon microscopy to assess whether the early reduction in HbT within the draining vein is the result of a constriction of large draining veins at the onset of locomotion. This research shows that large cerebral veins may be important components of the neurovascular response and not just passive bystanders or balloons waiting to be inflated.

4.6 References

1. Attwell, D. *et al.* Glial and neuronal control of brain blood flow. *Nature* **468**, 232–243 (2010).
2. Howarth, C., Gleeson, P. & Attwell, D. Updated Energy Budgets for Neural Computation in the Neocortex and Cerebellum. *J. Cereb. Blood Flow Metab.* **32**, 1222–1232 (2012).
3. Iadecola, C. The Neurovascular Unit Coming of Age: A Journey through Neurovascular Coupling in Health and Disease. *Neuron* **96**, 17–42 (2017).
4. Schaeffer, S. & Iadecola, C. Revisiting the neurovascular unit. *Nat. Neurosci.* **24**, 1198–1209 (2021).
5. Lee, L. *et al.* Key Aspects of Neurovascular Control Mediated by Specific Populations of Inhibitory Cortical Interneurons. *Cereb. Cortex* **30**, 2452–2464 (2020).
6. Lind, B. L. *et al.* Fast Ca2+ responses in astrocyte end-feet and neurovascular coupling in mice. *Glia* **66**, 348–358 (2018).
7. Longden, T. A. *et al.* Capillary K+-sensing initiates retrograde hyperpolarization to increase local cerebral blood flow. *Nat. Neurosci.* **20**, 717–726 (2017).
8. Mishra, A. *et al.* Astrocytes mediate neurovascular signaling to capillary pericytes but not to arterioles. *Nat. Neurosci.* **19**, 1619–1627 (2016).
9. Kisler, K. *et al.* Acute Ablation of Cortical Pericytes Leads to Rapid Neurovascular Uncoupling. *Front. Cell. Neurosci.* **14**, (2020).
10. Institoris, A. *et al.* Astrocytes amplify neurovascular coupling to sustained activation of neocortex in awake mice. *Nat. Commun.* **13**, 7872 (2022).
11. Kellie, G. An Account of the Appearances Observed in the Dissection of Two of Three Individuals Presumed to Have Perished in the Storm of the 3d, and Whose Bodies Were Discovered in the Vicinity of Leith on the Morning of the 4th, November 1821; with Some Reflections on the Pathology of the Brain: Part I. *Trans. Medico-Chir. Soc. Edinb.* **1**, 84–122 (1824).
12. Monro, A. Observations on the structure and functions of the nervous system. (1783).
13. Shen, L. *et al.* Effects of Intracranial Pressure Monitoring on Mortality in Patients with Severe Traumatic Brain Injury: A Meta-Analysis. *PLoS ONE* **11**, e0168901 (2016).
14. Berwick, J. *et al.* Neurovascular coupling investigated with two-dimensional optical imaging spectroscopy in rat whisker barrel cortex. *Eur. J. Neurosci.* **22**, 1655–1666 (2005).
15. Sharp, P. S. *et al.* Neurovascular coupling preserved in a chronic mouse model of Alzheimer's disease: Methodology is critical. *J. Cereb. Blood Flow Metab.* **40**, 2289–2303 (2020).
16. Huo, B.-X., Smith, J. B. & Drew, P. J. Neurovascular Coupling and Decoupling in the Cortex during Voluntary Locomotion. *J. Neurosci.* **34**, 10975–10981 (2014).

17. Tran, C. H. T., Peringod, G. & Gordon, G. R. Astrocytes Integrate Behavioral State and Vascular Signals during Functional Hyperemia. *Neuron* **100**, 1133-1148.e3 (2018).
18. Eyre, B. *et al.* The effects of locomotion on sensory-evoked haemodynamic responses in the cortex of awake mice. *Sci. Rep.* **12**, 6236 (2022).
19. Gao, Y.-R. *et al.* Time to wake up: Studying neurovascular coupling and brain-wide circuit function in the un-anesthetized animal. *NeuroImage* **153**, 382–398 (2017).
20. Zhang, Q., Turner, K. L., Gheres, K. W., Hossain, M. S. & Drew, P. J. Behavioral and physiological monitoring for awake neurovascular coupling experiments: a how-to guide. *Neurophotonics* **9**, 021905 (2022).
21. Huo, B.-X., Greene, S. E. & Drew, P. J. Venous cerebral blood volume increase during voluntary locomotion reflects cardiovascular changes. *NeuroImage* **118**, 301–312 (2015).
22. Gao, Y.-R. & Drew, P. J. Effects of Voluntary Locomotion and Calcitonin Gene-Related Peptide on the Dynamics of Single Dural Vessels in Awake Mice. *J. Neurosci.* **36**, 2503–2516 (2016).
23. Zhukov, O. *et al.* Preserved blood-brain barrier and neurovascular coupling in female 5xFAD model of Alzheimer's disease. *Front. Aging Neurosci.* **15**, (2023).
24. Cai, C. *et al.* Impaired dynamics of precapillary sphincters and pericytes at first-order capillaries predict reduced neurovascular function in the aging mouse brain. *Nat. Aging* **3**, 173–184 (2023).
25. Weis, S. *et al.* Venous Drainage of the Brain. in *Imaging Brain Diseases: A Neuroradiology, Nuclear Medicine, Neurosurgery, Neuropathology and Molecular Biology-based Approach* (eds. Weis, S. et al.) 211–224 (Springer, 2019). doi:10.1007/978-3-7091-1544-2_9.
26. Krieger, S. N., Streicher, M. N., Trampel, R. & Turner, R. Cerebral blood volume changes during brain activation. *J. Cereb. Blood Flow Metab.* **32**, 1618–1631 (2012).
27. Buxton, R. B., Wong, E. C. & Frank, L. R. Dynamics of blood flow and oxygenation changes during brain activation: The balloon model. *Magn. Reson. Med.* **39**, 855–864 (1998).
28. Driver, I. D., Traat, M., Fasano, F. & Wise, R. G. Most Small Cerebral Cortical Veins Demonstrate Significant Flow Pulsatility: A Human Phase Contrast MRI Study at 7T. *Front. Neurosci.* **14**, (2020).
29. Iliff, J. J. *et al.* Impairment of Glymphatic Pathway Function Promotes Tau Pathology after Traumatic Brain Injury. *J. Neurosci.* **34**, 16180–16193 (2014).
30. Jessen, N. A., Munk, A. S. F., Lundgaard, I. & Nedergaard, M. The Glymphatic System – A Beginner's Guide. *Neurochem. Res.* **40**, 2583–2599 (2015).
31. Jankowsky, J. L. *et al.* Mutant presenilins specifically elevate the levels of the 42 residue β-amyloid peptide in vivo: evidence for augmentation of a 42-specific γ secretase. *Hum. Mol. Genet.* **13**, 159–170 (2004).

32. Mayhew, J. *et al.* Spectroscopic Analysis of Changes in Remitted Illumination: The Response to Increased Neural Activity in Brain. *NeuroImage* **10**, 304–326 (1999).
33. Tarantini, S., Tran, C. H. T., Gordon, G. R., Ungvari, Z. & Csiszar, A. Impaired neurovascular coupling in aging and Alzheimer's disease: Contribution of astrocyte dysfunction and endothelial impairment to cognitive decline. *Exp. Gerontol.* **94**, 52–58 (2017).
34. Park, L. *et al.* Tau induces PSD95–neuronal NOS uncoupling and neurovascular dysfunction independent of neurodegeneration. *Nat. Neurosci.* **23**, 1079–1089 (2020).
35. Zhang, Q. *et al.* Cerebral oxygenation during locomotion is modulated by respiration. *Nat. Commun.* **10**, 5515 (2019).
36. Echagarruga, C. T., Gheres, K. W., Norwood, J. N. & Drew, P. J. nNOS-expressing interneurons control basal and behaviorally evoked arterial dilation in somatosensory cortex of mice. *eLife* **9**, e60533 (2020).
37. Ma, Y. *et al.* Resting-state hemodynamics are spatiotemporally coupled to synchronized and symmetric neural activity in excitatory neurons. *Proc. Natl. Acad. Sci.* **113**, E8463–E8471 (2016).
38. Chalif, J. I., Martínez-Silva, M. de L., Pagiazitis, J. G., Murray, A. J. & Mentis, G. Z. Control of mammalian locomotion by ventral spinocerebellar tract neurons. *Cell* **185**, 328-344.e26 (2022).

4.7 Supplementary tables

Supplementary table 1: Shapiro Wilks test of normality for HbT decrease in the draining vein during spontaneous locomotion and whisker stimulation trials

Haem Measure	Statistic	df	p
Spontaneous locomotion vs Whisker stim	.149	82	.000

Supplementary table 2: Wilcoxon Signed Ranks test results for HbT decrease during spontaneous locomotion trials and whisker stimulation trials

Wilcoxon Signed Rank	N	Statistic	Standard error	z	p
Locomotion vs Whisker stim	82	2859	216.31	5.351	.000

Supplementary table 3: Descriptive statistics for HbT decrease during spontaneous locomotion trials and whisker stimulation trials

Type of trial	N	Mean	Median	SEM
Spontaneous locomotion	82	.982	.987	.016
2s whisker stim	82	.993	.995	.006

Supplementary table 4: Shapiro Wilks test of normality for onset time of initial change in HbT in response to locomotion

	Onset Time		
Vessel	**Statistic**	**df**	**p**
Draining Vein	.864	82	.000
Whisker barrel artery	.986	82	.541
Whisker barrel vein	.978	82	.170

Supplementary table 5: Friedmans test results for onset time of initial change in HbT within the draining vein, whisker barrel artery and whisker barrel vein

Onset time	N	Statistic	df	p	Kendall's w
Draining vein vs whisker barrel artery vs whisker barrel vein	82	105.585	2	.000	.644

Kendall's w used to assess effect size for Friedman test. As the Kendall's W test uses the same parameters as Cohens d (0.2 = small, 0.5 = moderate, 0.8 = large) the sample size used in the study indicates a moderate effect size.

Supplementary table 6: Pairwise comparisons for onset time of initial change in HbT within the draining vein, whisker barrel artery and whisker barrel vein

Pairwise comparisons onset time	Statistic	Standard error	Standard test statistic	p	Adjusted p
Draining vein vs whisker barrel artery	-1.244	.156	-7.965	.000	.000
Draining vein vs whisker barrel vein	-1.500	.156	-9.605	.000	.000
Whisker barrel artery vs whisker barrel vein	-.256	.156	-1.640	.101	.303

Supplementary table 7: Descriptive statistics for onset time of initial change in HbT within the draining vein, whisker barrel artery and whisker barrel vein

Vessel HbT initial change onset time	N	Mean	Median	SEM	STD
Draining Vein	82	0.173	0.125	.016	.144
Whisker barrel artery	82	0.787	0.773	.004	.375
Whisker barrel vein	82	1.006	0.938	.050	.451

Supplementary table 8: Shapiro Wilks test of normality for onset time of increase in HbT in response to locomotion

Onset Time increase in HbT			
Vessel	**Statistic**	**df**	**p**
Draining Vein	.914	82	.000
Whisker barrel artery	.986	82	.541
Whisker barrel vein	.978	82	.170

Supplementary table 9: Friedmans test results for onset time of increase in HbT in response to locomotion within the draining vein, whisker barrel artery and whisker barrel vein

Onset time increase in HbT	N	Statistic	df	p	Kendall's w
Draining vein vs whisker barrel artery vs whisker barrel vein	82	40.195	2	.000	0.245

Kendall's w used to assess effect size for Friedmans test. As the Kendall's W test uses the same parameters as Cohens d (0.2 = small, 0.5 = moderate, 0.8 = large) the sample size used in the study indicates a small effect size.

Supplementary table 10: Pairwise comparisons for onset time of increase in HbT in response to locomotion within the draining vein, whisker barrel artery and whisker barrel vein

Pairwise comparisons increase in HbT onset time	Statistic	Standard error	Standard test statistic	p	Adjusted p
Whisker barrel artery vs whisker barrel vein	-.341	.156	-2.186	.029	.086
Whisker barrel artery vs Draining vein	.976	.156	6.247	.000	.000
Whisker barrel vein vs Draining vein	.634	.156	4.061	.000	.000

Supplementary table 11: Descriptive statistics for onset time of increase in HbT in response to locomotion within the draining vein, whisker barrel artery and whisker barrel vein

Increase in HbT onset time	N	Mean	Median	STD
Draining Vein	82	1.492	1.352	.728
Whisker barrel artery	82	0.787	0.773	.375
Whisker barrel vein	82	1.006	0.938	.451

Supplementary table 12: Shapiro Wilks test of normality for summed locomotion across disease groups

Summed locomotion (AUC)			
Disease group	**Statistic**	**df**	**p**
WT	.793	25	.000
AD	.756	23	.000
ATH	.850	22	.003
MIX	.906	12	.188

Supplementary table 13: Kruskal Wallis test results for summed locomotion responses across disease groups

Summed locomotion (AUC)	N	Statistic	df	p	E^2_R
Locomotion across groups	82	7.118	3	.068	0.087

The epsilon^2 estimate of effect size was calculated using the following formula:

$$E_R^2 \frac{H}{(n^2 - 1)/\,(n + 1)}$$

H = Kruskall wallis test statistic, n = number of observations. Small effect (0.01 - <0.06), moderate effect (0.06 - <0.14), large effect (>0.14)
The sample size used in the study indicates a moderate effect size.

Supplementary table 14: Descriptive statistics for summed locomotion responses across disease groups

Summed locomotion	N	Mean	Median	STD
WT	25	215.36	180.36	150.12
AD	23	163.15	105.55	114.70
ATH	22	184.51	154.35	78.31
MIX	12	294.45	287.00	201.95

Supplementary table 15: Shapiro Wilks test of normality for onset time for the decrease in HbT in the draining vein across disease groups

Onset time of decrease in HbT			
Disease group	**Statistic**	**df**	**p**
WT	.805	25	.000
AD	.888	23	.015
ATH	.741	22	.000
MIX	.860	12	.049

Supplementary table 16: Kruskal Wallis test results for onset time of decrease in HbT in the draining vein across disease groups

Onset time decrease in HbT draining vein	N	Statistic	df	p	E^2_R
HbT decrease onset time across groups	82	6.883	3	.076	0.084

The sample size used in the study indicates a moderate effect size.

Supplementary table 17: Descriptive statistics for onset time of decrease in HbT in the draining vein across disease groups

Onset time decrease in HbT in draining vein	N	Mean	Median	STD
WT	25	.141	.109	.127
AD	23	.197	.188	.145
ATH	22	.143	.063	.145
MIX	12	.249	.305	.156

Supplementary table 18: Shapiro Wilks test of normality for the rise time of the decrease in HbT in the draining vein across disease groups

	Rise time of decrease in HbT		
Disease group	**Statistic**	**df**	**p**
WT	.929	25	.084
AD	.808	23	.001
ATH	.928	22	.112
MIX	.946	12	.576

Supplementary table 19: Kruskal Wallis test results for rise time of decrease in HbT in the draining vein across disease groups

Rise time decrease in HbT draining vein	N	Statistic	df	p	E^2_R
HbT decrease rise time across groups	82	5.758	3	.124	0.068

The sample size used in the study indicates a small effect size.

Supplementary table 20: Descriptive statistics for rise time of decrease in HbT in the draining vein across disease groups

Rise time decrease in HbT in draining vein	N	Mean	Median	STD
WT	25	.880	.875	.365
AD	23	.907	.875	.272
ATH	22	.846	.875	.303
MIX	12	1.09	1.06	.338

Supplementary table 21: Shapiro Wilks test of normality for minimum peak of the decrease in HbT in the draining vein across disease groups

	Minimum of HbT		
Disease group	**Statistic**	**df**	**p**
WT	.713	25	.000
AD	.866	23	.005
ATH	.945	22	.254
MIX	.916	12	.254

Supplementary table 22: Kruskal Wallis test results for minimum peak of HbT in the draining vein across disease groups

Minimum HbT draining vein	N	Statistic	df	p	E^2_R
HbT decrease across groups	82	6.848	3	.077	0.084

The sample size used in the study indicates a moderate effect size.

Supplementary table 23: Descriptive statistics for minimum peak of HbT in the draining vein across disease groups

Minimum HbT in draining vein	N	Mean	Median	STD
WT	25	.984	.989	.018
AD	23	.983	.987	.015
ATH	22	.986	.987	.010
MIX	12	.972	.975	.018

Supplementary table 24: Shapiro Wilks test of normality for increase in HbT onset time in the draining vein across disease groups

Onset time of increase in HbT			
Disease group	**Statistic**	**df**	**p**
WT	.808	25	.000
AD	.955	23	.377
ATH	.965	22	.585
MIX	.905	12	.185

Supplementary table 25: Kruskal Wallis test results for increase in HbT onset time in the draining vein across disease groups

Increase in HbT onset time draining vein	**N**	**Statistic**	**df**	**p**	**E^2_R**
HbT increase onset time across groups	82	2.628	3	.453	0.032

The sample size used in the study indicates a small effect size.

Supplementary table 26: Descriptive statistics for increase in HbT onset time in the draining vein across disease groups

Increase in HbT onset time draining vein	**N**	**Mean**	**Median**	**STD**
WT	25	1.69	1.53	.826
AD	23	1.35	1.20	.684
ATH	22	1.41	1.45	.539
MIX	12	1.49	1.31	.876

Supplementary table 27: Shapiro Wilks test of normality for increase in HbT rise time in the draining vein across disease groups

Rise time of increase in HbT			
Disease group	**Statistic**	**df**	**p**
WT	.899	25	.018
AD	.913	23	.048
ATH	.943	22	.233
MIX	.933	12	.411

Supplementary table 28: Kruskal Wallis test results for increase in HbT rise time in the draining vein across disease groups

Increase in HbT rise time draining vein	N	Statistic	df	p	E^2_R
HbT increase rise time across groups	82	2.477	3	.480	0.030

The sample size used in the study indicates a small effect size.

Supplementary table 29: Descriptive statistics for increase in HbT rise time in the draining vein across disease groups

Increase in HbT rise time draining vein	N	Mean	Median	STD
WT	25	4.09	3.75	1.29
AD	23	4.40	4.25	1.27
ATH	22	4.64	4.50	1.42
MIX	12	3.95	3.88	1.62

Supplementary table 30: Shapiro Wilks test of normality for increase in HbT peak in the draining vein across disease groups

	Peak of increase in HbT		
Disease group	**Statistic**	**df**	**p**
WT	.975	25	.776
AD	.944	23	.217
ATH	.958	22	.447
MIX	.951	12	.645

Supplementary table 31: Kruskal Wallis test results for increase in HbT peak in the draining vein across disease groups

Increase in HbT peak draining vein	N	Statistic	df	p	E^2_R
HbT increase peak across groups	82	2.256	3	.521	0.027

The sample size used in the study indicates a small effect size.

Supplementary table 32: Descriptive statistics for increase in HbT peak in the draining vein across disease groups

Increase in HbT peak draining vein	N	Mean	Median	STD
WT	25	1.03	1.03	.010
AD	23	1.03	1.03	.014
ATH	22	1.04	1.04	.013
MIX	12	1.04	1.04	.020

Supplementary table 33: Shapiro Wilks test of normality for increase in HbT onset in the whisker barrel artery across disease groups

	Increase in HbT onset whisker barrel artery		
Disease group	**Statistic**	**df**	**p**
WT	.959	25	.403
AD	.952	23	.322
ATH	.948	22	.293
MIX	.937	12	.465

Supplementary table 34: Kruskal Wallis test results increase in HbT onset in the whisker barrel artery across disease groups

Increase in HbT onset whisker barrel artery	N	Statistic	df	p	E^2_R
HbT increase onset across groups	82	4.216	3	.239	0.052

The sample size used in the study indicates a small effect size.

Supplementary table 35: Descriptive statistics for the increase in HbT onset in the whisker barrel artery across disease groups

Increase in HbT onset whisker barrel artery	N	Mean	Median	STD
WT	25	.780	.781	.400
AD	23	.890	.938	.397
ATH	22	.714	.656	.346
MIX	12	.737	.719	.328

Supplementary table 36: Shapiro Wilks test of normality for increase in HbT rise time in the whisker barrel artery across disease groups

	Increase in HbT rise time whisker barrel artery		
Disease group	**Statistic**	**df**	**p**
WT	.962	25	.466
AD	.896	23	.021
ATH	.840	22	.002
MIX	.946	12	.580

Supplementary table 37: Kruskal Wallis test results for the increase in HbT rise time in the whisker barrel artery across disease groups

Increase in HbT rise time whisker barrel artery	**N**	**Statistic**	**df**	**p**	**E^2_R**
HbT increase rise time across groups	82	2.299	3	.513	0.028

The sample size used in the study indicates a small effect size.

Supplementary table 38: Descriptive statistics for the increase in HbT rise time in the whisker barrel artery across disease groups

Increase in HbT rise time whisker barrel artery	**N**	**Mean**	**Median**	**STD**
WT	25	3.40	3.38	.538
AD	23	3.77	3.50	.757
ATH	22	3.92	3.50	1.15
MIX	12	3.51	3.63	.523

Supplementary table 39: Shapiro Wilks test of normality for increase in HbT peak in the whisker barrel artery across disease groups

	Increase in HbT peak whisker barrel artery		
Disease group	**Statistic**	**df**	**p**
WT	.972	25	.701
AD	.902	23	.028
ATH	.953	22	.364
MIX	.977	12	.966

Supplementary table 40: Kruskal Wallis test results for increase in HbT peak in the whisker barrel artery across disease groups

Increase in HbT peak whisker barrel artery	N	Statistic	df	p	E^2_R
HbT increase rise time across groups	82	12.593	3	.006	0.155

The sample size used in the study indicates a large effect size.

Supplementary table 41: Pairwise comparisons for increase in HbT peak in the whisker barrel artery across disease groups

Pairwise comparisons increase in HbT peak	Statistic	Standard error	Standard test statistic	p	Adjusted p
AD vs WT	-11.33	6.88	-1.647	.100	.598
AD vs ATH	-19.72	7.10	-2.777	.005	.033
AD vs MIX	-26.55	8.48	-3.130	.002	.010
WT vs ATH	-8.39	6.96	-1.205	.228	1.00
WT vs MIX	-15.22	8.36	-1.819	.069	.413
ATH vs MIX	-6.83	8.55	-.799	.424	1.00

Supplementary table 42: Descriptive statistics for increase in HbT peak in the whisker barrel artery across disease groups

Increase in HbT peak whisker barrel artery	N	Mean	Median	STD
WT	25	1.11	1.11	.035
AD	23	1.09	1.09	.025
ATH	22	1.12	1.12	.036
MIX	12	1.13	1.13	.031

Supplementary table 43: Shapiro Wilks test of normality for increase in HbT onset in the whisker barrel vein across disease groups

	Increase in HbT onset whisker barrel vein		
Disease group	Statistic	df	p
WT	.976	25	.805
AD	.942	23	.197
ATH	.917	22	.065
MIX	.912	12	.225

Supplementary table 44: Kruskal Wallis test results for the increase in HbT onset in the whisker barrel vein across disease groups

Increase in HbT onset whisker barrel vein	N	Statistic	df	p	E^2_R
HbT increase onset across groups	82	.790	3	.852	0.009

The sample size used in the study indicates less than a small effect size.

Supplementary table 45: Descriptive statistics for the increase in HbT onset in the whisker barrel vein across disease groups

Increase in HbT onset whisker barrel vein	N	Mean	Median	STD
WT	25	.951	.938	.400
AD	23	1.02	1.14	.406
ATH	22	1.08	.984	.590
MIX	12	.943	.805	.359

Supplementary table 46: Shapiro Wilks test of normality for increase in HbT rise time in the whisker barrel vein across disease groups

	Increase in HbT rise time whisker barrel vein		
Disease group	**Statistic**	**df**	**p**
WT	.958	25	.373
AD	.861	23	.004
ATH	.936	22	.167
MIX	.819	12	.015

Supplementary table 47: Kruskal Wallis test results for the increase in HbT rise time in the whisker barrel vein across disease groups

Increase in HbT rise time whisker barrel vein	N	Statistic	df	p	E^2_R
HbT increase rise time across groups	82	4.264	3	.234	0.052

The sample size used in the study indicates a small effect size.

Supplementary table 48: Descriptive statistics for the increase in HbT rise time in the whisker barrel vein across disease groups

Increase in HbT rise time whisker barrel vein	N	Mean	Median	STD
WT	25	3.91	4.00	.909
AD	23	4.32	4.00	1.13
ATH	22	4.57	4.44	1.29
MIX	12	4.20	3.81	1.37

Supplementary table 49: Shapiro Wilks test of normality for increase in HbT peak in the whisker barrel vein across disease groups

	Increase in HbT peak whisker barrel vein		
Disease group	**Statistic**	**df**	**p**
WT	.955	25	.327
AD	.960	23	.457
ATH	.898	22	.027
MIX	.961	12	.804

Supplementary table 50: Kruskal Wallis test results for the increase in HbT peak in the whisker barrel vein across disease groups

Increase in HbT peak whisker barrel vein	N	Statistic	df	p	E^2_R
HbT increase peak across groups	82	8.304	3	.040	0.102

The sample size used in the study indicates a moderate effect size.

Supplementary table 51: Pairwise comparisons for the increase in HbT peak in the whisker barrel vein across disease groups

Pairwise comparisons increase in HbT peak	Statistic	Standard error	Standard test statistic	p	Adjusted p
AD vs WT	-9.55	6.88	-1.388	.165	.991
AD vs ATH	-13.21	7.10	-1.860	.063	.377
AD vs MIX	-23.48	8.48	-2.768	.006	.034
WT vs ATH	-3.66	6.96	-.525	.599	1.00
WT vs MIX	-13.92	8.36	-1.665	.096	.576
ATH vs MIX	-10.27	8.55	-1.201	.230	1.00

Supplementary table 52: Descriptive statistics for the increase in HbT peak in the whisker barrel vein across disease groups

Increase in HbT peak whisker barrel vein	N	Mean	Median	STD
WT	25	1.05	1.05	.021
AD	23	1.04	1.04	.015
ATH	22	1.06	1.05	.026
MIX	12	1.06	1.06	.017

Chapter 5: Overall discussion, conclusions and future directions

Overall discussion, conclusions and future directions

5.1 Overview

This PhD focused on the investigation of the effects of locomotion on sensory-evoked haemodynamic responses. I also investigated cognitive and cerebrovascular function in three different disease mouse models: APP/PS1-AD model, PCSK9-Atherosclerosis model and in a mixed disease APP/PS1-PCSK9 model, in awake mice. Below I discuss and bring together the principal findings of the previous chapters – relating the work completed in each chapter as well as considering potential future research directions. My findings reveal the importance of monitoring locomotion in awake imaging experiments, in addition to replicating and extending findings regarding impaired haemodynamic responses (under certain conditions) in PCSK9-atherosclerotic mice. Another main finding is the extension and replication of preserved NVC in AD and mixed models (extended both to awake and a more severe AD model). Furthermore, I propose a novel observation suggesting the potential role of large draining veins in neurovascular responses to locomotion.

5.2 Locomotion can have significant impacts on the size and shape of sensory-evoked haemodynamic responses

The first part of my PhD (chapter 2) required me to analyse a pre-existing data set collected in our research group. The data set comprised of whisker stimulation and spontaneous (no whisker stimulation) experiments conducted in awake, behaving mice which were head-fixed to a spherical treadmill. Haemodynamic responses were collected from surface vessels of the brain using 2D-optical imaging spectroscopy (2D-OIS). My aim was to investigate how locomotion may affect sensory-evoked haemodynamic responses. It is integral to be aware of the impact of locomotion, especially when completing studies in different disease models, because if mice locomote differential amounts, this may impact overall findings regarding neurovascular function. In order to investigate how the amount and timing of locomotion impacted evoked haemodynamic responses, I ranked locomotion (most vs least) at different time points (0-5s, 5-10s, 10-15s, 15-20s, 20-25s) during whisker stimulation trials and assessed the corresponding evoked haemodynamic responses.

In this study, I found that locomotion can have significant effects on evoked-haemodynamic responses when it occurs prior (0-5s) to or during (5-10s) whisker stimulation. Prior work has shown that locomotion itself can have large impacts on haemodynamics within the cortex[1–4] however, few studies have looked at the effect of locomotion on whisker-evoked haemodynamic responses[5]. The studies that had previously investigated the effects of locomotion on evoked-haemodynamic responses found locomotion to have no effect on arterial dilation[5]. Thus, the current study was the first to explicitly show that the amount and timing of locomotion (relative to whisker stimulation) can have significant effects on corresponding haemodynamic responses.

This work set an important foundation for my main experimental chapter (chapter 3), whereby I used an awake imaging set up to investigate the impact of different diseases (Alzheimer's disease, atherosclerosis and mixed Alzheimer's and atherosclerosis) on cognitive and vascular responses. Due to the findings from my initial PhD work (chapter 2), I knew it was essential to monitor locomotion when investigating the impacts of disease on evoked-haemodynamic responses. By monitoring locomotion, it would allow me to understand how evoked-haemodynamic responses are affected by disease, and importantly if locomotion may confound these results.

5.2.1 Limitations, links to previous work and future directions

One of the major issues within chapter 2 is that the dataset I was working with had not previously collected any neural data in the awake experiments. Therefore, I was unable to investigate any changes in neural activity in response to locomotion. However, other groups have investigated this. Using electrodes to record neural activity in awake mice Huo et al.,[1] observed that neuronal activity was increased in both sensory and frontal brain regions during locomotion. Interestingly, they did report a decoupling of neural activity and haemodynamics within the frontal cortex, in response to locomotion, with CBV remaining unchanged in the frontal cortex in response to locomotion, whereas firing rate and gamma band power were increased. The study shows the importance of recording both neural activity and haemodynamic changes concurrently, as uncoupling between the two can occur within different brain regions. More recent work has been conducted using GCaMP mice, as a less invasive way of measuring neural activity, by assessing Ca^{2+} changes within neurons[6].

Moreover, even though locomotion was measured within this study, there are still numerous other confounds of awake imaging experiments. Many other variables can impact awake imaging studies, including whisking and arousal state[7]. Even fidgeting behaviours (such as postural adjustments, blinking and whisking) have been shown to have large effects on haemodynamic responses[8,9]. Additionally, cortical state can also impact haemodynamic signals within the brain[8]. Pupil dilation can be monitored using a camera, and this measure can give an insight into arousal level of the mouse[10] – which is important as when the mouse is awake, pupil diameter has been shown to correlate with body movements, whisking and a subsequent increase in CBV. However, when in REM sleep, pupil diameter is reportedly constricted and in NREM sleep pupil diameter fluctuates between dilated and constricted states[11]. It is helpful that research groups have provided guidelines on what to monitor as well as how to monitor behaviours that can impact haemodynamic responses in awake mice[7]. However, it is difficult for all research groups to be able to monitor all aspects of behaviour due to financial constraints and project time scales. Nevertheless, it would be helpful if as a group we start to monitor more than just locomotion in order to give a more in-depth understanding of how our studies may be impacted by behaviour. For example, we could continue to monitor locomotion but additionally monitor pupil diameter as a measure of arousal[12].

5.3 Impaired evoked haemodynamic peak responses (during least locomotion trials) in an atherosclerosis mouse model in awake mice, when locomotion is ranked during the whisker stimulation but preserved responses in the AD and mixed models

As previously mentioned, chapter 2 was integral to the findings uncovered regarding cerebrovascular function in three disease mouse models: Alzheimer's, atherosclerosis and mixed Alzheimer's and atherosclerosis. One aim of my PhD was to try to replicate and extend previous findings within our research group, where we had previously investigated neurovascular function in Alzheimer's, atherosclerosis and mixed disease mice. In this prior work, completed in lightly anesthetised mice, we found that evoked-haemodynamic responses were impaired in the PCSK9-atherosclerosis mouse model in addition to haemodynamic responses being preserved in the J20-Alzheimers model and the mixed-J20-PCSK9 disease model[13].

Due to my findings in chapter 2, I decided to investigate the impact of disease on evoked-haemodynamic responses when locomotion was ignored, when locomotion was ranked across the entire trial and when locomotion was ranked during the whisker stimulation. When the presence of locomotion was completely ignored, I observed no effect of disease on evoked-haemodynamic responses. Additionally, when I ranked locomotion during the entire 25s trial, and investigated the corresponding evoked-haemodynamic responses for the most and least locomotion trials, again, I found no effect of disease on evoked-haemodynamic responses. However, when locomotion was ranked during the whisker stimulation, there were significant differences in the corresponding evoked haemodynamic responses. During the least locomotion trials, I observed that the PCSK9-atherosclerosis group had the smallest evoked haemodynamic response, compared with the WT group. Interestingly, when the most locomotion occurred there were no significant differences when comparing corresponding evoked haemodynamic responses. This preservation of locomotion-induced haemodynamic responses in the PCSK9-atherosclerosis group, compared with the reduction in the size of the whisker-evoked haemodynamic response in the same group could suggest differential mechanisms for locomotion and whisker-evoked haemodynamic responses. It has been reported that locomotion is driven by nNOS interneurons[14]. However, other studies have reported that LNAME (a NOS inhibitor), does not block whisker-evoked responses[15], suggesting that sensory-evoked haemodynamic responses may not be nitric oxide (NO) dependent. This implies that locomotion and whisker-evoked haemodynamic responses may indeed have differing mechanisms, which may be impacted differently in disease. This is an interesting hypothesis to test in future work.

In addition to investigating cerebrovascular responses in AD, atherosclerosis and mixed disease mice, I also assessed non-spatial cognition in these mice, using the novel object recognition test (NOR). However, I observed preserved recognition memory in all disease groups at 9 months of age.

5.3.1 Limitations, links to previous work and future directions

5.3.1.1 Monitoring behaviour in awake mice

The findings from this chapter highlight that it is especially important to monitor, and be aware of when and how much animals locomote during trials, as locomotion can clearly confound haemodynamic responses, when comparing across groups. To my knowledge, I am also the first to report that there are no deficits in haemodynamic responses in the APP/PS1-AD model in awake mice. Other studies have been conducted in awake mice comparing evoked-haemodynamic responses in APP/PS1 mice vs WT mice[16]. This study found differences in evoked-haemodynamic responses, with the APP/PS1-AD group having reduced responses compared with the WT group. Even though the same mouse model, at the same age were used in both studies differences in results were still observed. It could be suggested that the reduction in the size of the evoked-haemodynamic response that was observed in the AD group may have been the result of differences in the amounts of locomotion that occurred between groups. However, locomotion was not monitored within the study, so it cannot be known if the difference may or may not be attributable to locomotion or not.

5.3.1.2 Effects of anaesthesia on haemodynamic responses

Many studies have found that NVC is impaired in AD[16–23]. However, many of these studies were conducted in an anesthetised preparation[17–23]. We know the large effects that anaesthesia can have upon NVC[24] – which is why I decided to complete my studies using an awake imaging setup. However, some anaesthetic regimes used can produce responses similar to those observed in an awake preparation[13,25–27]. Studies using light anaesthesia are certainly still needed, as studies in awake mice bring new confounds[8,24] – however, what is important is that researchers are aware of how the anaesthetic itself impacts NVC responses[28–30]. Importantly, different anaesthetic regimes can also be impacted by mouse background strain[28,31] The original plan within my PhD was to conduct studies in awake mice, then in an anaesthetised preparation and then a final acute anaesthetised experiment, where evoked-haemodynamic responses would be collected concurrent to neural activity – a similar experimental plan as conducted in Shabir et al.,[13]. However, at the beginning of my PhD the manufacturers of the anaesthetic the research group had spent numerous years perfecting stopped making part of the anaesthetic we had previously been using. This

resulted in having to trial and generate a new anaesthetic to be used within the research group. I had to recreate our original anaesthetic, but instead of using a solution of fentanyl-fluanisone I had to dilute the fluanisone myself. Previous work has indicated that the background strain of the mice used within my PhD (B6C3) have known irregularities in respiratory responses to hypoxia and hypercapnia compared with other strains[32]. Unfortunately, the background mouse strain of all of my mice had variable responses to the anaesthetic – whereas other mouse strains seemed to respond to it well. Due to the profound and variable effects that this anaesthesia had on my mice I chose not to include this data within my overall thesis. However, in the future I am hoping to use this data to show how as research groups we can establish when, under anaesthetised conditions we have 'good' and 'bad' responses, an important addition to the neurovascular field regarding our understanding of anaesthetic impacts on vascular responses.

5.3.1.3 Differential findings in the APP/PS1 model across research groups

There are mixed findings regarding the impairment of vascular function in the APP/PS1 model of AD. Between 7 and 9 months groups have reported impaired CBF[33,34], impaired vascular responses to visual stimulations[16] and reduced relative CBV (rCBV) changes[35]. Conversely, some groups have reported enhanced haemodynamic responses to whisker stimulation at 7 months, whilst observing no change in vascular responses at 3 or 22 months[36]. With other groups reporting no changes in rCBV or CBF in APP/PS1 mice at 18 months[37]. Chapter 3 adds to the literature reporting no changes in CBV in APP/PS1 mice within surface vessels of the brain. Therefore, the question remains as to why are there such contradictory results across research groups in the same AD mouse models? As mentioned, anaesthesia can have significant impacts on vascular responses[38,39], and some of the above studies, which found impairments in vascular responses were conducted in anaesthetised mice[33–35]. However, one study which did find impairments in vascular responses to visual stimulations was conducted in awake mice[16]. Therefore, anaesthesia may only be able to explain some of the discrepancies we observe in vascular responses in AD mice.

5.3.1.4 Impact of surgical procedures on NVC responses

Just as anaesthesia can impact NVC responses, surgical procedures used in these studies could also potentially explain some of the differing observations. The most common procedures that are used in NVC studies are thinned window[25,40] and cranial window surgeries[41,42]. With thinned window surgeries being less invasive than cranial window procedures, due to the skull being kept intact. Many experiments which have observed impairments in NVC responses in AD mice were conducted in an acute manner. For example, where haemodynamic imaging was completed on the same day as the surgical procedure[17,18,20,23]. Some surgical procedures, can result in inflammation especially within the first 14 days post-surgery[43]. Moreover, studies have shown that some surgical procedures[44] and penetrating the dura[13] can result in cortical spreading depression (CSD). CSD is a wave of depolarisation across the cortex, whereby neuronal activity is silenced, followed by a subsequent reduction in blood flow across the cortex. Importantly, it takes time to recover from CSD and it has been observed that diseased mice have more severe CSDs and prolonged periods of hypoxia[13]. This is important to be aware of, because if acute imaging sessions are being completed and studies find impairments in NVC responses in disease, by doing the imaging in an acute manner we cannot dissect whether the findings are a result of disease, or are the result of the brain's response to the surgical procedures. However, there have been studies, that have been conducted in an acute manner, as well as using anaesthesia, and they have reported no deficits in NVC. Zhukov et al.,[45] completed a cranial window surgery and on the same day imaged vessels withing the somatosensory cortex using 2-photon microscopy, in addition to measuring neural activity using a microelectrode. They observed no differences in LFP amplitudes in response to an electrical whisker stimulation, when comparing WT and AD mice. Additionally, they reported no differences in the dilation of the pial and penetrating vessels, sphincters or capillaries in response to the stimulation, when comparing WT and AD mice.

5.3.1.5 Standardisation of practises across research groups

It would be helpful for the field to come together and develop standardisation of surgical procedures across research groups - as there are reports that differences in surgical procedure used may even impact amyloid plaque growth[46], which inevitably

is problematic when investigating the impacts of disease on NVC. Some groups have published their surgical protocols online[40,47,48], however, most groups still complete their surgeries in different ways, and there is no real consensus on what is best. Additionally, there is no consensus on how long to wait between completing surgical procedures and then completing imaging procedures. Although it has been suggested that you can image straight away after completing a thinned window surgery there is at least a 1-2 week period where visualisation of the window may be impaired following the cranial window procedure[47]. Standardised surgical procedures may help with the replication and reproducibility issues the neuroscience field is experiencing[49,50]. It is important that we are able to reproduce findings, especially in the AD field as this research aims to better understand the pathogenesis of AD, in addition to potentially aiding with the detection of biomarkers and potential new treatments. If we cannot reproduce results in these models then this could be damaging for the AD field. The standardisation of both anaesthetic regimes and surgical procedures could potentially help with increasing reproducibility across findings relating to disease models.

5.3.1.6 Missing measures of neural activity

One of the major issues with this chapter (and the rest of the chapters) is that I did not record any neural data in my awake experiments. Therefore, future studies should be conducted using GCaMP to allow for the investigating of neural activity and corresponding haemodynamic responses. Studies have revealed hyperactive neurons in the APP/PS1 AD model[51], although recently, some groups have observed hypoactivity[52]. However, the above studies did not look at evoked-haemodynamic responses concurrently, so this is still an area that needs further exploration.

5.3.1.7 Missing assessment of the BBB

The studies conducted in my PhD only focused on the large surface vessels of the brain. Even though I observed no vascular impairments in these vessels (in AD and Mixed disease mice) there could be vascular deficits in the capillary bed and impairments in cells of the NVU in these models. Importantly, as the study included no additional immunohistochemistry investigating the health of the BBB[53] or any immunohistochemistry assessing neuronal loss, vascular health, microglia activation or astrocyte reactivity then I cannot make any claims as to why haemodynamic

responses are impaired (under certain conditions) in the atherosclerosis group, yet preserved in the AD and mixed groups. Are responses impaired due to damage to the vasculature? In our prior study, we did assess vascular reactivity using hypercapnia, however we found that vascular reactivity in the atherosclerosis model was preserved[13] and vessels still had the ability to dilate – which could suggest that this may be the case for my findings. This then raises the question: why are there impaired haemodynamic responses during the least locomotion trials when locomotion is ranked during the stimulation in the atherosclerosis group yet preserved haemodynamic responses in the mixed disease mice? This could be due to the interaction of atherosclerosis with the presence of amyloid which could lead to an enhanced vascular response. Future genomic and transcriptomic studies should be conducted on the cerebral vasculature to assess whether there are indeed differences in specific genes and the activity of these genes in specific vascular cells[54–56] which are important for vascular health. If there were differences, this may explain the greater evoked-haemodynamic responses observed in the mixed group. Importantly, finding the presence of a target on the vasculature may then result in targeted treatments[57] that could enhance CBF[33], which theoretically could reduce disease pathology.

5.3.1.8 Implementing a battery of cognitive tests

As mentioned in chapter 3, I observed preserved recognition memory in all disease groups. This was unexpected as other groups have found deficits in recognition memory in AD mice[58,59], although observations of recognition memory impairment in AD are not always reported[60,61]. To my knowledge, this is the first study to assess recognition memory using the NOR in atherosclerosis mice (induced with a PCSK9 gain-of-function mutation) and mixed AD and atherosclerosis mice. Some studies have assessed cognition in other mouse models of atherosclerosis and found no effect of atherosclerosis on recognition memory[62]. Although, other aspects of cognition such as spatial cognition (assessed using the Morris water maze) have been reported to be impaired in atherosclerosis mice[63]. One important aspect to note is that in the NOR test, I only used a retention interval of 1-hour, therefore it would be beneficial for future studies to use both short term (e.g 3 minutes) and long-term (e.g 24 hour) retention intervals to probe recognition memory further. As it is possible that there are recognition memory deficits in these groups of mice, yet due to the experimental

parameters I chose these may not have been observed. Moreover, I only assessed one aspect of cognition (recognition memory). Cognition is complex, and not all aspects of cognition are impacted to the same extent by disease[61]. Further to this, due to the exclusion criteria I used within the recognition memory test this resulted in some sessions not being included in the final analysis. This meant that for the WT group the sample size was low. Therefore, future studies should use larger sample sizes and include a battery of cognitive tests[64], such as the NOR test (recognition memory), the Barnes maze[65] (spatial memory) and the spontaneous Y maze[66] (spatial working and reference memory). Using an array of tests, with large sample sizes would allow for a more in-depth analysis of different types of memory that may be impacted by disease, as has been previously completed in other studies assessing neurovascular function in models of Alzheimer's disease[19,33].

5.3.1.9 Effect of sex on cognitive and cerebrovascular responses

In chapters 3 and 4, I used both male and female mice in the AD and WT groups – however, in my analysis I did not include sex as a factor. Some research indicates that there may be potential sex effects in the APP/PS1 AD model, regarding soluble and insoluble levels of amyloid beta, with levels being higher in female mice. Additionally, female mice reportedly also performed worse than male mice at 9 months of age on the Morris water maze[67]. Yet, other groups have shown that at 9 months of age (the age used in this thesis), there are no effects of sex on cognition[64]. Although, studies have shown that from 12 months of age, female mice have a greater amyloid burden and plaque number[68]. Therefore, it is warranted that future studies assess the effect of sex on cognition, vascular function and amyloid pathology. Even though I used both male and female mice in the AD and WT groups, I only used male mice in the atherosclerosis and mixed group. Prior studies have shown that using PCSK9-gain-of-function mutation with a western diet induces lower levels of hypercholesterinaemia in female mice[69,70]. Due to time constraints of the project, I opted to only use male mice. However, in the future, it is vital that studies are conducted on both male and female mice when investigating atherosclerosis and mixed Alzheimer's and atherosclerosis. Heart disease is one of the leading causes of death of women in the UK[71]; women also have a heightened risk of cardiovascular disease and atherosclerosis postmenopause[72–74]. Therefore, it is fundamental that research

investigating the impacts of atherosclerosis and mixed disease is also conducted in female mice – as females are significantly affected by cardiovascular disease.

5.3.1.10 Implications of the vascular machinery being intact

Finally, the data within this chapter reveals that the vascular machinery in AD and mixed disease models are intact in the surface vessels of the brain. This is important, as it means that these models would be good to use in studies that wish to assess how treatments may impact vessels. As the vascular machinery is not damaged, it gives treatments an opportunity to show if they are effective or not. For example, treatments aimed to increase blood flow via the relaxation of VSMCs[75] (e.g sildenafil). Additionally, it is important to conduct future experiments within these models, using 2-photon microscopy, because even though I observed preserved vascular responses to whisker stimulation in the AD and Mixed groups, it could be that there are impairments, yet these may be at a different location along the vascular tree. For example, groups have observed alterations in capillaries within APP/PS1 mouse models[33] and reported that the presence of amyloid oligomers can constrict brain capillaries[76]. Further to this, it has also been reported that atherosclerosis mice also have alterations in capillaries[77].

5.4 Large cerebral draining veins display an initial, fast, early decrease in HbT at the onset of locomotion – and this is not impacted by disease

My final chapter proposes a novel observation, which is the result of investigating locomotion responses in awake mice. Initial observations in my disease study revealed that when mice locomoted, there appeared to be an initial change in HbT within large veins of the brain. In my final chapter (chapter 4), I investigated this by using the spontaneous trials I had collected during my initial experiments. By using 'spontaneous' trials (with no whisker stimulation), I was able to investigate locomotion alone and the corresponding haemodynamics evoked by locomotion. In addition to this, as 2D-OIS can be used to investigate changes in haemodynamics within different vascular compartments of the brain[25,26], I was also able to investigate how locomotion impacted haemodynamic responses in arteries, veins and large draining veins. The finding that when locomotion occurs, there is an initial, early decrease in HbT within

large draining veins is a novel finding not previously reported. Prior work has observed constrictions in dural vessels during locomotion[3], however the group did not observe initial changes in HbT within large draining veins. As the focus of chapter 3 was on how disease may impact cerebrovascular responses, I decided to assess how disease may or may not affect this novel neurovascular response. However, I found no effect of disease on the size or onset of this initial early change in HbT within the large draining veins of the brain. The observation of an early decrease in CBV within large draining veins of the brain was observed in the majority of mice, and in the majority of imaging sessions. This led me to conclude that this may be an important early neurovascular response that may occur due to the brain making 'space' for the subsequent large increases in CBV that follow locomotion. Making 'space' within the brain is integral in order to avoid large increases in intracranial pressure, which can be devastating[78].

5.4.1 Limitations, links to previous work and future directions

These findings, and the data shown within chapter 4 provide information on these initial observations. However, the chapter does not provide any information on any mechanisms of this early neurovascular response. It would be beneficial for future studies to monitor neural activity concurrently to assess how neural activity may change prior to the initial decrease in HbT within the draining veins.

Additionally, these studies should also be conducted using 2-photon microscopy in order to get an absolute measure of changes in blood flow and vessel dilation. By using 2-photon microscopy, it can be ascertained if the observation of the decrease in CBV that I have observed in my PhD work is due to a constriction in the draining vein, in response to the onset of locomotion. Additionally, using two-photon microscopy and GCaMP mice I would be able to assess changes in neural activity and the consequent changes in vessel diameter at numerous parts of the vascular tree, concurrently.

Surprisingly, this observation has not been reported before. Gao et al.,[3] did complete a study using 2-photon microscopy to assess the effects of locomotion on dural vessels in the brain. Interestingly, they reported that dural vessels constricted during locomotion but they did not mention the observation of this constriction in large

draining veins. However, it could be suggested that they did not report this due to differences in window positioning. They report that their window placement was more lateral, so they could decipher between dural and superficial pial vessels. However, in the experiments in this thesis windows were placed more medially, so that I could include the large draining veins that drain into the sagittal sinus. Additionally, in another study completed by the same group, it does appear that they may observe a decrease in HbT within a large pial vein, 1s after locomotion onset, which occurs prior to other changes in HbT in the cortex, however they do not mention this within the study (figure 2f)[4].

5.5 Contribution to the neurovascular and wider neuroscience field

The work completed in this thesis has provided original contributions to the neurovascular field, in addition to highlighting new avenues of research based upon the findings. The following section will highlight these original contributions, as well as how these findings are important to the wider neurovascular field.

5.5.1 Monitoring of behaviour in neurovascular studies

Chapter 2 of my PhD has added to the literature regarding the importance of monitoring certain behaviours in awake imaging experiments, where haemodynamic responses are measured. Additionally, if locomotion had not been monitored, I would not have observed the novel finding within the draining vein in response to locomotion (chapter 4). Further highlighting that the monitoring of certain behaviours can enhance our understanding of CBV responses within the brain. Furthermore, this work has highlighted the importance of monitoring behaviour in awake imaging studies in which sensory-stimulation is used to assess evoked-haemodynamic responses across disease groups. Studies using awake mice should therefore try to have some form of behavioural monitoring within their studies.

5.5.2 Better understanding of the models that may be more relatable to human disease

Many individuals with AD also have other health conditions[79]. The presence of comorbidities and AD is therefore especially important to investigate. Chapter 3 gives

a good overview of how disease can impact sensory-evoked haemodynamic responses in atherosclerosis mice. However, there are numerous questions that still remain unanswered. From the work conducted within this thesis we still do not fully understand how AD, atherosclerosis and mixed disease impact cognition. Therefore, future studies should use a battery of cognitive tests to assess multiple aspects of cognition, in both short- and long-term scenarios to gain a much deeper understanding of how these diseases can affect numerous aspects of cognition. Additionally, a multimodal set of neural and haemodynamic imaging procedures should be utilised in order to gain a complete understanding of NVC in these different disease models. 2D-OIS should still be used, however 2-photon microscopy should also be implemented (in awake mice) to get an absolute measure of CBF within surfaces vessels, penetrating vessels and capillaries in order to assess how these different diseases may impact NVC at differing levels of the vascular tree[80]. It would also be beneficial for these mice to have GCAMP in order for the full NVC relationship to be assessed. This could either be completed by crossing disease mice with GCaMP lines (although this would be a costly and time consuming project) or viral injections of GCaMP[52,81] could be used instead. Finally, it would be helpful to complete ASL imaging in these mice to gain an idea of baseline CBF flow in order to fully understand if atherosclerosis and mixed disease can result in hypoperfusion. The above in vivo experiments would give an in-depth understanding of the function of the cerebral vasculature and the impacts that disease can have. As mentioned, immunohistochemistry was only used to assess amyloid burden within my thesis. It would therefore be interesting to use an array of antibodies to investigate the health of the BBB[53,82,83]. Assessing the BBB in these diseases, especially atherosclerosis[84] and mixed disease would allow us to make inferences about why there were impairments in evoked-haemodynamic responses when the least locomotion occurred during the whisker stimulation in the atherosclerosis group. Moreover, if it were established that the different diseases impacted different aspects of the BBB in different ways, it may help future studies when considering therapeutic interventions.

One of the main questions that arose from this work was why did the mixed disease group not have some impairment in haemodynamic responses when the atherosclerosis alone group did? This needs further investigation using genomic and

transcriptomic methods to assess if the addition of AD to atherosclerosis impacts specific genes of the vasculature and the activity of these specific genes – if this were to be observed then this may be an important avenue for therapeutic interventions.

5.5.3 Models of AD and mixed disease for treatment/intervention studies

Importantly, the findings from chapter 3 and 4 reveal that the surface vasculature of the brain in AD and mixed disease mice is still functionally intact. This is important when considering models to use to assess AD treatments/interventions. For example, treatments in which the aim is to increase blood flow in the brain need vessels to have the ability to dilate in order to increase blood flow. My findings suggest that the APP/PS1 mouse model is a suitable model in which to assess if blood flow increases can impact AD pathology.

5.6 Translational implications of the thesis

Using mouse models of disease allows us to make measures with higher temporal and spatial resolution than is possible in humans. By using a mixed model of disease, I aimed to increase the translational potential of my research, as in humans it is common for AD to be co-morbid with cardiovascular disease. However, when considering translational implications of the project it must be noted that an amyloid only model of AD was used in the above studies. Therefore, the work assessed how cerebrovascular function and non-spatial recognition memory was impacted by amyloid alone. It could be that other hallmark pathological features of Alzheimer's disease, such as the presence of hyperphosphorylated tau and neurofibrillary tangles, in addition to the interaction between amyloid and tau may impact cerebrovascular function and non-spatial recognition memory differently. Therefore, care should be taken when suggesting that AD may not affect vascular function or recognition memory (which the results of this thesis suggest). Furthermore, while my studies used an age point comparable to mid-life in humans, most individuals who develop AD develop it much later on in life. Therefore, the translation of the findings of this project may be limited to mid-life. However, as research indicates that the presence of vascular risk factors in mid-life may lead to an increased risk of developing dementia in the future, it is therefore important to look at mid-life. But future studies using older time points, more comparable to the age at which people develop AD are still warranted to see

how both amyloid and mixed amyloid and atherosclerosis impact cognitive and cerebrovascular function. Finally, an important aspect of translatability in preclinic AD research is the measure of cognition and memory, as this is what is impacted in humans, and is measured in clinical studies. In the thesis, I only used one measure of cognition, the NOR test, which is a measure of non-spatial recognition memory and I only completed one measure with a 1-hour retention interval. As other aspects of memory are impacted in humans, such as spatial memory it would aid the translatability of my findings for future studies to include other measures of memory, such as spatial memory, which can be assessed using the Barnes maze.

5.7 Conclusions

In summary the work that I completed during my PhD has allowed for a number of original contributions to the neurovascular field. Firstly, using an already collected data set I established that **locomotion can have significant effects on sensory-evoked haemodynamic responses** in awake behaving mice (published in Scientific Reports April 2022). I also assessed cognitive and vascular function in awake mice using three different disease models: AD, atherosclerosis and mixed disease. The second part of my PhD replicated and extended previous work from the research group[13] whereby I also observed that **evoked-haemodynamic responses are impaired in an atherosclerosis model (during the least locomotion trials, when locomotion was ranked during the whisker stimulation) but preserved in the APP/PS1-AD and mixed disease models**. Finally, in the last part of my PhD I report a novel, early neurovascular response within large draining veins of the brain, where I observed a **fast, initial decrease in CBV in response to locomotion, within draining veins of the brain.**

5.8 References

1. Huo, B.-X., Smith, J. B. & Drew, P. J. Neurovascular Coupling and Decoupling in the Cortex during Voluntary Locomotion. *J. Neurosci.* **34**, 10975–10981 (2014).
2. Huo, B.-X., Greene, S. E. & Drew, P. J. Venous cerebral blood volume increase during voluntary locomotion reflects cardiovascular changes. *NeuroImage* **118**, 301–312 (2015).
3. Gao, Y.-R. & Drew, P. J. Effects of Voluntary Locomotion and Calcitonin Gene-Related Peptide on the Dynamics of Single Dural Vessels in Awake Mice. *J. Neurosci.* **36**, 2503–2516 (2016).
4. Zhang, Q. *et al.* Cerebral oxygenation during locomotion is modulated by respiration. *Nat. Commun.* **10**, 5515 (2019).
5. Tran, C. H. T., Peringod, G. & Gordon, G. R. Astrocytes Integrate Behavioral State and Vascular Signals during Functional Hyperemia. *Neuron* **100**, 1133-1148.e3 (2018).
6. West, S. L. *et al.* Wide-Field Calcium Imaging of Dynamic Cortical Networks during Locomotion. *Cereb. Cortex* **32**, 2668–2687 (2022).
7. Zhang, Q., Turner, K. L., Gheres, K. W., Hossain, M. S. & Drew, P. J. Behavioral and physiological monitoring for awake neurovascular coupling experiments: a how-to guide. *Neurophotonics* **9**, 021905 (2022).
8. Twitches, Blinks, and Fidgets: Important Generators of Ongoing Neural Activity - Patrick J. Drew, Aaron T. Winder, Qingguang Zhang, 2019. https://journals.sagepub.com/doi/10.1177/1073858418805427.
9. Winder, A. T., Echagarruga, C., Zhang, Q. & Drew, P. J. Weak correlations between hemodynamic signals and ongoing neural activity during the resting state. *Nat. Neurosci.* **20**, 1761–1769 (2017).
10. Kristjansson, S. D., Stern, J. A., Brown, T. B. & Rohrbaugh, J. W. Detecting phasic lapses in alertness using pupillometric measures. *Appl. Ergon.* **40**, 978–986 (2009).
11. Yüzgeç, Ö., Prsa, M., Zimmermann, R. & Huber, D. Pupil Size Coupling to Cortical States Protects the Stability of Deep Sleep via Parasympathetic Modulation. *Curr. Biol.* **28**, 392-400.e3 (2018).
12. Institoris, A. *et al.* Astrocytes amplify neurovascular coupling to sustained activation of neocortex in awake mice. *Nat. Commun.* **13**, 7872 (2022).
13. Shabir, O. *et al.* Assessment of neurovascular coupling and cortical spreading depression in mixed mouse models of atherosclerosis and Alzheimer's disease. *eLife* **11**, e68242 (2022).
14. Echagarruga, C. T., Gheres, K. W., Norwood, J. N. & Drew, P. J. nNOS-expressing interneurons control basal and behaviorally evoked arterial dilation in somatosensory cortex of mice. *eLife* **9**, e60533 (2020).
15. Lee, L. *et al.* Nitric oxide is not responsible for the initial sensory-induced neurovascular coupling response in mouse cortex. 2022.05.24.493260 Preprint at https://doi.org/10.1101/2022.05.24.493260 (2022).

16. van Veluw, S. J. *et al.* Vasomotion as a Driving Force for Paravascular Clearance in the Awake Mouse Brain. *Neuron* **105**, 549-561.e5 (2020).
17. Tarantini, S. *et al.* Demonstration of impaired neurovascular coupling responses in TG2576 mouse model of Alzheimer's disease using functional laser speckle contrast imaging. *GeroScience* **39**, 465–473 (2017).
18. Li, L. *et al.* Impaired Hippocampal Neurovascular Coupling in a Mouse Model of Alzheimer's Disease. *Front. Physiol.* **12**, 715446 (2021).
19. Park, L. *et al.* Tau induces PSD95–neuronal NOS uncoupling and neurovascular dysfunction independent of neurodegeneration. *Nat. Neurosci.* **23**, 1079–1089 (2020).
20. Lourenço, C. F., Ledo, A., Barbosa, R. M. & Laranjinha, J. Neurovascular uncoupling in the triple transgenic model of Alzheimer's disease: Impaired cerebral blood flow response to neuronal-derived nitric oxide signaling. *Exp. Neurol.* **291**, 36–43 (2017).
21. Tong, X.-K., Lecrux, C. & Hamel, E. Age-Dependent Rescue by Simvastatin of Alzheimer's Disease Cerebrovascular and Memory Deficits. *J. Neurosci.* **32**, 4705–4715 (2012).
22. Duncombe, J. *et al.* Ageing causes prominent neurovascular dysfunction associated with loss of astrocytic contacts and gliosis. *Neuropathol. Appl. Neurobiol.* **43**, 477–491 (2017).
23. Mughal, A., Harraz, O. F., Gonzales, A. L., Hill-Eubanks, D. & Nelson, M. T. PIP2 Improves Cerebral Blood Flow in a Mouse Model of Alzheimer's Disease. *Function* **2**, zqab010 (2021).
24. Gao, Y.-R. *et al.* Time to wake up: Studying neurovascular coupling and brain-wide circuit function in the un-anesthetized animal. *NeuroImage* **153**, 382–398 (2017).
25. Sharp, P. S. *et al.* Comparison of stimulus-evoked cerebral hemodynamics in the awake mouse and under a novel anesthetic regime. *Sci. Rep.* **5**, 12621 (2015).
26. Sharp, P. S. *et al.* Neurovascular coupling preserved in a chronic mouse model of Alzheimer's disease: Methodology is critical. *J. Cereb. Blood Flow Metab.* **40**, 2289–2303 (2020).
27. Lee, L. *et al.* Key Aspects of Neurovascular Control Mediated by Specific Populations of Inhibitory Cortical Interneurons. *Cereb. Cortex* **30**, 2452–2464 (2020).
28. Munting, L. P. *et al.* Influence of different isoflurane anesthesia protocols on murine cerebral hemodynamics measured with pseudo-continuous arterial spin labeling. *Nmr Biomed.* **32**, e4105 (2019).
29. Schlegel, F., Schroeter, A. & Rudin, M. The hemodynamic response to somatosensory stimulation in mice depends on the anesthetic used: Implications on analysis of mouse fMRI data. *NeuroImage* **116**, 40–49 (2015).
30. Franceschini, M. A. *et al.* The effect of different anesthetics on neurovascular coupling. *NeuroImage* **51**, 1367–1377 (2010).

31. Zuurbier, C., Emons, V. & Ince, C. Hemodynamics of anesthetized ventilated mouse models: Aspects of anesthetics, fluid support, and strain. *Am. J. Physiol. Heart Circ. Physiol.* **282**, H2099-105 (2002).
32. Tankersley, C. G., Fitzgerald, R. S. & Kleeberger, S. R. Differential control of ventilation among inbred strains of mice. *Am. J. Physiol.-Regul. Integr. Comp. Physiol.* **267**, R1371–R1377 (1994).
33. Cruz Hernández, J. C. *et al.* Neutrophil adhesion in brain capillaries reduces cortical blood flow and impairs memory function in Alzheimer's disease mouse models. *Nat. Neurosci.* **22**, 413–420 (2019).
34. Shen, Z. *et al.* Multifaceted assessment of the APP/PS1 mouse model for Alzheimer's disease: Applying MRS, DTI, and ASL. *Brain Res.* **1698**, 114–120 (2018).
35. Zerbi, V. *et al.* Microvascular cerebral blood volume changes in aging APPswe/PS1dE9 AD mouse model: a voxel-wise approach. *Brain Struct. Funct.* **218**, 1085–1098 (2013).
36. Kim, J. & Jeong, Y. Augmentation of Sensory-Evoked Hemodynamic Response in an Early Alzheimer's Disease Mouse Model. *J. Alzheimers Dis. JAD* **37**, (2013).
37. Hooijmans, C. R. *et al.* Changes in cerebral blood volume and amyloid pathology in aged Alzheimer APP/PS1 mice on a docosahexaenoic acid (DHA) diet or cholesterol enriched Typical Western Diet (TWD). *Neurobiol. Dis.* **28**, 16–29 (2007).
38. Aksenov, D. P., Li, L., Miller, M. J., Iordanescu, G. & Wyrwicz, A. M. Effects of anesthesia on BOLD signal and neuronal activity in the somatosensory cortex. *J. Cereb. Blood Flow Metab.* **35**, 1819–1826 (2015).
39. Pisauro, M. A., Dhruv, N. T., Carandini, M. & Benucci, A. Fast Hemodynamic Responses in the Visual Cortex of the Awake Mouse. *J. Neurosci.* **33**, 18343–18351 (2013).
40. Shih, A. Y., Mateo, C., Drew, P. J., Tsai, P. S. & Kleinfeld, D. A Polished and Reinforced Thinned-skull Window for Long-term Imaging of the Mouse Brain. *J. Vis. Exp. JoVE* 3742 (2012) doi:10.3791/3742.
41. Kılıç, K. *et al.* Chronic Cranial Windows for Long Term Multimodal Neurovascular Imaging in Mice. *Front. Physiol.* **11**, (2021).
42. Dorand, R. D., Barkauskas, D. S., Evans, T. A., Petrosiute, A. & Huang, A. Y. Comparison of intravital thinned skull and cranial window approaches to study CNS immunobiology in the mouse cortex. *IntraVital* **3**, e29728 (2014).
43. Holtmaat, A. *et al.* Long-term, high-resolution imaging in the mouse neocortex through a chronic cranial window. *Nat. Protoc.* **4**, 1128–1144 (2009).
44. Srienc, A. I., Chiang, P.-P., Schmitt, A. J. & Newman, E. A. Cortical spreading depolarizations induced by surgical field blood in a mouse model of neurosurgery. *J. Neurosurg.* **132**, 1820–1828 (2020).
45. Zhukov, O. *et al.* Preserved blood-brain barrier and neurovascular coupling in female 5xFAD model of Alzheimer's disease. *Front. Aging Neurosci.* **15**, (2023).

46. Yan, P. *et al.* Characterizing the Appearance and Growth of Amyloid Plaques in APP/PS1 Mice. *J. Neurosci.* **29**, 10706–10714 (2009).
47. Yang, G., Pan, F., Parkhurst, C. N., Grutzendler, J. & Gan, W.-B. Thinned-skull cranial window technique for long-term imaging of the cortex in live mice. *Nat. Protoc.* **5**, 201–208 (2010).
48. Augustinaite, S. & Kuhn, B. Chronic Cranial Window for Imaging Cortical Activity in Head-Fixed Mice. *STAR Protoc.* **1**, 100194 (2020).
49. Hensel, W. M. Double trouble? The communication dimension of the reproducibility crisis in experimental psychology and neuroscience. *Eur. J. Philos. Sci.* **10**, 44 (2020).
50. Freedman, L. P., Venugopalan, G. & Wisman, R. Reproducibility2020: Progress and priorities. Preprint at https://doi.org/10.12688/f1000research.11334.1 (2017).
51. Busche, M. A. *et al.* Tau impairs neural circuits, dominating amyloid-β effects, in Alzheimer models in vivo. *Nat. Neurosci.* **22**, 57–64 (2019).
52. Algamal, M. *et al.* Reduced excitatory neuron activity and interneuron-type-specific deficits in a mouse model of Alzheimer's disease. *Commun. Biol.* **5**, 1–9 (2022).
53. Montagne, A. *et al.* APOE4 accelerates advanced-stage vascular and neurodegenerative disorder in old Alzheimer's mice via cyclophilin A independently of amyloid-β. *Nat. Aging* **1**, 506–520 (2021).
54. Skol, A. D. *et al.* Integration of genomics and transcriptomics predicts diabetic retinopathy susceptibility genes. *eLife* **9**, e59980 (2020).
55. Meneri, M., Bonato, S., Gagliardi, D., Comi, G. P. & Corti, S. New Insights into Cerebral Vessel Disease Landscapes at Single-Cell Resolution: Pathogenetic and Therapeutic Perspectives. *Biomedicines* **10**, 1693 (2022).
56. Yang, A. C. *et al.* A human brain vascular atlas reveals diverse mediators of Alzheimer's risk. *Nature* **603**, 885–892 (2022).
57. Grammas, P. *et al.* A New Paradigm for the Treatment of Alzheimer's Disease: Targeting Vascular Activation. *J. Alzheimers Dis.* **40**, 619–630 (2014).
58. Zhang, R. *et al.* Novel Object Recognition as a Facile Behavior Test for Evaluating Drug Effects in AβPP/PS1 Alzheimer's Disease Mouse Model. *J. Alzheimers Dis.* **31**, 801–812 (2012).
59. Shen, L. *et al.* Amelioration of cognitive impairments in APPswe/PS1dE9 mice is associated with metabolites alteration induced by total salvianolic acid. *PLoS ONE* **12**, e0174763 (2017).
60. Campos, H. C. *et al.* Neuroprotective effects of resistance physical exercise on the APP/PS1 mouse model of Alzheimer's disease. *Front. Neurosci.* **17**, 1132825 (2023).
61. Cheng, D., Low, J. K., Logge, W., Garner, B. & Karl, T. Novel behavioural characteristics of female APPSwe/PS1ΔE9 double transgenic mice. *Behav. Brain Res.* **260**, 111–118 (2014).
62. Fuentes, D. *et al.* Age-Related Changes in the Behavior of Apolipoprotein E Knockout Mice. *Behav. Sci.* **8**, 33 (2018).

63. Gao, H. *et al.* Effects of Oat Fiber Intervention on Cognitive Behavior in LDLR $^{-/-}$ Mice Modeling Atherosclerosis by Targeting the Microbiome–Gut–Brain Axis. *J. Agric. Food Chem.* **68**, 14480–14491 (2020).
64. Hulshof, L. A. *et al.* Both male and female APPswe/PSEN1dE9 mice are impaired in spatial memory and cognitive flexibility at 9 months of age. *Neurobiol. Aging* **113**, 28–38 (2022).
65. Attar, A. *et al.* A Shortened Barnes Maze Protocol Reveals Memory Deficits at 4-Months of Age in the Triple-Transgenic Mouse Model of Alzheimer's Disease. *PLoS ONE* **8**, e80355 (2013).
66. Kraeuter, A.-K., Guest, P. C. & Sarnyai, Z. The Y-Maze for Assessment of Spatial Working and Reference Memory in Mice. in *Pre-Clinical Models: Techniques and Protocols* (ed. Guest, P. C.) 105–111 (Springer, 2019). doi:10.1007/978-1-4939-8994-2_10.
67. Li, X. *et al.* Sex differences between APPswePS1dE9 mice in A-beta accumulation and pancreatic islet function during the development of Alzheimer's disease. *Lab. Anim.* **50**, 275–285 (2016).
68. Wang, J., Tanila, H., Puoliväli, J., Kadish, I. & Groen, T. van. Gender differences in the amount and deposition of amyloidβ in APPswe and PS1 double transgenic mice. *Neurobiol. Dis.* **14**, 318–327 (2003).
69. Vozenilek, A. E. *et al.* AAV8-mediated overexpression of mPCSK9 in liver differs between male and female mice. *Atherosclerosis* **278**, 66–72 (2018).
70. Jarrett, K. E. *et al.* Somatic Editing of Ldlr With Adeno-Associated Viral-CRISPR Is an Efficient Tool for Atherosclerosis Research. *Arterioscler. Thromb. Vasc. Biol.* **38**, 1997–2006 (2018).
71. Leading causes of death, UK - Office for National Statistics. https://www.ons.gov.uk/peoplepopulationandcommunity/healthandsocialcare/causesofdeath/articles/leadingcausesofdeathuk/2001to2018.
72. Witteman, J. C., Grobbee, D. E., Kok, F. J., Hofman, A. & Valkenburg, H. A. Increased risk of atherosclerosis in women after the menopause. *BMJ* **298**, 642–644 (1989).
73. Sutton-Tyrrell, K. *et al.* Carotid Atherosclerosis in Premenopausal and Postmenopausal Women and Its Association With Risk Factors Measured After Menopause. *Stroke* **29**, 1116–1121 (1998).
74. Hodis, H. N. & Mack, W. J. Menopausal Hormone Replacement Therapy and Reduction of All-Cause Mortality and Cardiovascular Disease: It's About Time and Timing. *Cancer J. Sudbury Mass* **28**, 208–223 (2022).
75. Andersson, K.-E. PDE5 inhibitors – pharmacology and clinical applications 20 years after sildenafil discovery. *Br. J. Pharmacol.* **175**, 2554–2565 (2018).
76. Nortley, R. *et al.* Amyloid β oligomers constrict human capillaries in Alzheimer's disease via signaling to pericytes. *Science* **365**, eaav9518 (2019).
77. Li, B. *et al.* Atherosclerosis is associated with a decrease in cerebral microvascular blood flow and tissue oxygenation. *PLOS ONE* **14**, e0221547 (2019).

78. Shen, L. *et al.* Effects of Intracranial Pressure Monitoring on Mortality in Patients with Severe Traumatic Brain Injury: A Meta-Analysis. *PLoS ONE* **11**, e0168901 (2016).
79. Santiago, J. A. & Potashkin, J. A. The Impact of Disease Comorbidities in Alzheimer's Disease. *Front. Aging Neurosci.* **13**, 631770 (2021).
80. Rungta, R. L. *et al.* Diversity of neurovascular coupling dynamics along vascular arbors in layer II/III somatosensory cortex. *Commun. Biol.* **4**, 1–11 (2021).
81. Michelson, N. J., Vanni, M. P. & Murphy, T. H. Comparison between transgenic and AAV-PHP.eB-mediated expression of GCaMP6s using in vivo wide-field functional imaging of brain activity. *Neurophotonics* **6**, 025014 (2019).
82. Minogue, A. M. *et al.* Age-associated dysregulation of microglial activation is coupled with enhanced blood-brain barrier permeability and pathology in APP/PS1 mice. *Neurobiol. Aging* **35**, 1442–1452 (2014).
83. Ahn, K.-C. *et al.* Characterization of Impaired Cerebrovascular Structure in APP/PS1 Mouse Brains. *Neuroscience* **385**, 246–254 (2018).
84. de Oliveira, J. *et al.* High Cholesterol Diet Exacerbates Blood-Brain Barrier Disruption in LDLr–/– Mice: Impact on Cognitive Function. *J. Alzheimers Dis.* **78**, 97–115 (2020).